THE ROLE OF CALCIUM STORES IN CALCIUM SIGNALLING IN HUMAN SPERM

By

JENNIFER TONI MORRIS

A thesis submitted to

The University of Birmingham

for the degree of

DOCTOR OF PHILOSOPHY

School of Biosciences

College of Life and Environmental Sciences

The University of Birmingham

January 2014

Abstract

Calcium (Ca^{2+}) signalling is implicated in the regulation of numerous sperm processes elemental for fertilisation including the acrosome reaction, hyperactivated motility (HA) and capacitation. A number of studies have identified components of Ca^{2+} storage organelles in human sperm, including inositol-1,4,5-triphosphate receptors IP_3Rs, secretory pathway calcium ATPases (SPCA), ryanodine receptors (RyR) and the store operated calcium entry (SOCE) channels STIM and Orai, all of which are associated with the acrosome and posterior head/neck region of the sperm (PHN). In 2005, Herrick *et al.*, characterised the Ca^{2+} storage capacity of mammalian acrosomes; however the identity of the PHN Ca^{2+} store is less clear. The aim of this study was to characterise the PHN Ca^{2+} store to determine the relationship between store mobilisation and HA in human sperm. We observed localisation of high $[Ca^{2+}]$ at the PHN and midpiece of human sperm. Treatment with mitochondrial uncouplers CCCP and DNP elevated $[Ca^{2+}]_i$ and depolarised the mitochondrial membrane potential (MMP) consistent with mobilisation of mitochondrial Ca^{2+} stores. However pre-treatment with mitochondrial uncouplers had no significant effect on the characteristic biphasic $[Ca^{2+}]_i$ increase associated with progesterone. Conversely prior mobilisation of stored Ca^{2+} with thimerosal (IP_3R activator) or pre-treatment with SKF-96365 (SOCE inhibitor) significantly reduced the sustained component of the biphasic $[Ca^{2+}]_i$ response, whilst treatment with 2-APB or SKF (SOCE modulators) enhanced the progesterone induced $[Ca^{2+}]_i$ transient. In addition treatment with novel Orai targeted bioportides results in a significant prolongation of the progesterone-induced $[Ca^{2+}]_i$, apparently due to non-reversible SOCE activation, initiated during the transient. These results indicate the presence of at least two discrete Ca^{2+} stores at the PHN which contribute separately to the biphasic progesterone $[Ca^{2+}]_i$ increase and a role for STIM/Orai mediated SOCE in both transient and sustained components of the progesterone-induced $[Ca^{2+}]_i$ signal in human sperm.

For Mum

Acknowledgements

Throughout my PhD I have had the support of numerous colleagues, friends and family without whom the last five years would have felt considerably longer!

First and foremost I would like to thank my supervisor Dr Stephen Publicover for his advice, support and patience; without which this thesis would not have been possible. Your mentorship and guidance encouraged me to develop a plethora of skills that have been elemental in both my research and further career progression. Furthermore I believe you are responsible for a certain singing/dancing cat which sat on my desk throughout this process. Secondly I would like to thank the Department of Biosciences at the University of Birmingham and Birmingham Women's Hospital for providing both the funding and samples to conduct the research required for this thesis. I am grateful that you could see my potential.

To Dr Linda Lefievre and Dr Kate Nash, thank you for your time, advice and friendship. You taught me many things during your time in biosciences, including the benefits of eBay and my unconscious tendency to talk to myself. In addition I am grateful for the support and camaraderie of all members of the Publicover Lab past and present including, Sarah, Aduen, Ruben, Joao, Venkata and for a short time Leonor. I would also like to thank everyone on the 8th floor and the science geeks, in particular Lizzie, Sarah, Rich, Rach, Yui and Yousra for eating the many cake creations that I subjected them to during my time in Biosciences, for the disasters I apologise.

Finally I would like to thank my friends and family for their unwavering support even when it appeared that my write up would take forever! (I hope you're pleased it's finished Nan, don't

worry I won't make you read the rest). Dad, thank you for your understanding and annual man and a van removals service, without which I would have to downsize considerably! To my sister Alana, thank you for six months of experimental cuisine three times a day though my appreciation for the compulsory satellites of salad was not always evident. Last but not least and most importantly I would like to thank my mum whose drive, determination and mentorship has always inspired me to achieve my full potential. Your continued unwavering support, encouragement and 'Cocktail hour' have been fundamental throughout my life and for this I am eternally grateful.

Presentations and Publications of Research

Publications

Alasmari, W., Costello, S., Correia, J., Oxenham, S.K., **Morris, J.,** Ferandes, L., Santos, J.R., Kirkman-Brown, J., Michelangeli, F., Publicover, S. and Barratt, C.L.R. (2013). Ca^{2+} signalling through CatSper and Ca^{2+} stores regulate different behaviour in human sperm. *The Journal of Biological Chemistry*. **288**, 6248-6258.

Costello, S., Michelangeli, F., Nash, K., Lefievre, L., **Morris, J.**, Machado-Oliveira, G., Barratt, C., Kirkman-Brown, J. and Publicover, S.J. (2009). Ca^{2+} stores in sperm: their identities and functions. *Reproduction*. **138(3)**, 425-437.

Lefièvre, L., Nash, K., Mansell, S., Costello, S., Punt, E., Correia, J., **Morris, J.,** Kirkman-Brown, J., Wilson, S.M., Barratt, C.L.R. and Publicover, S. (2012). 2-APB-potentiated channels amplify CatSper-induced Ca^{2+} signals in human sperm. *Biochem. J.* **448,** 189–200.

Nash K, Lefievre L, Peralta-Arias R, **Morris J**, Morales-Garcia A, Connolly T, Costello S, Kirkman-Brown JC, Publicover SJ (2010) Techniques for imaging Ca^{2+} signalling in human sperm. *J. Vis. Exp*. **40**, pii 1996.

Presentations

Morris J, Publicover SJ (2010) Identifying the role of calcium stores in flagellar motility**.** Oral presentation at the **SRF Annual Meeting, Nottingham, UK.**

Morris J, Publicover SJ (2011) Identifying the role of calcium stores in flagellar motility. Poster presentation at the **BGRS Symposium, Birmingham , UK.**

Morris J, Publicover SJ (2011) Identifying the role of calcium stores in flagellar motility. Poster presentation at the **Gordon Research Conference on Activation and Development, Boston, United States of America.**

TABLE OF CONTENTS

CHAPTER ONE: INTRODUCTION

CHAPTER TWO: MATERIALS AND METHODS

CHAPTER FOUR: PHARMACOLOGICAL MANIPULATION OF Ca^{2+} STORES AT THE PHN WITH THIMEROSAL

LIST OF FIGURES

LIST OF TABLES

LIST OF ABBREVIATIONS

2-APB	2-aminoethyldiphenyl borate
4AP	4-aminopyridine
ACU	Assisted Conception Unit
ADP	adenosine diphosphate
AKAP	A kinase anchor protein
ALH	amplitude of lateral head displacement
ANOVA	analysis of variance between groups
AR	acrosome reaction
ATP	adenosine triphosphate
BCF	beat frequency
BM	basement membrane
BSA	bovine serum albumin
BTB	blood testis barrier
Ca^{2+}	calcium ions
$[Ca^{2+}]_i$	intracellular calcium concentration
$[Ca^{2+}]_e$	extracellular calcium concentration
CAD	CRAC activation domain
CaM	calmodulin
cADPR	cyclic adenosine diphosphate receptor
cAMP	cyclic adenosine monophosphate
CCE	capacitative Ca^{2+} entry
CASA	computer aided semen analysis
CCCP	carbonyl cyanide 3-chlorophenylhydrazone
CCE	capacitative Ca^{2+} entry
CIF	Ca^{2+} influx factor
Cl^-	chloride ions

CNBD	cyclic nucleotide binding domain
CNG	cyclic nucleotide gated
CO_2	carbon dioxide
COREC	Central Office for Research Ethics Committees
CPM	counts per minute
CPP	cell penetrating peptide
CRAC	Ca^{2+} release activated Ca^{2+} channels
DCB	3,4-dichlorobenzamil hydrochloride
ddH_2O	double distilled water
DHT	5α-hydrotestosterone
DIDS	4,4-diisothiocyanostilbene-2,2-disulphonic acid
DMSO	dimethylsulphoxide
DNA	deoxyribonucleic acid
DNP	2,4-Dinitrophenol
DTT	dithiothreitol
EBSS	earles balanced salt solution
EGTA	ethylene glycol-bis (2-aminoethylether) tetra acetic acid
ER	endoplasmic reticulum
ERM	erzin-radixin-moesin
ES	equatorial segment
ETC	electron transport chain
FCCP	carbonyl cyanide p-(trifluoromethoxy) phenylhydrazone
FRET	Forster Resonance Energy Transfer
FSH	follicle stimulating hormone
FSP	fucose sulfate polymer
GADPDS	Glyceraldehyde-3-phosphate dehydrogenase-S
GDP	guanosine diphosphate

GFP	green fluorescent protein
GnRH	gonadotrophin-releasing hormone
Gq	G-protein
HA	Hyperactivation
HBS	HEPES buffered saline
HBSS	HEPES buffered sucrose solution
HCO_3^-	bicarbonate ions
$[HCO_3^-]$	bicarbonate ion concentration
HEPES	N-(2-Hydroxyethyl) piperazine-N'-(2-ethanesulfonic acid)
HFEA	Human Fertilization and Embryology Authority
HIV	Human Immunodeficiency Virus
HVA	high voltage activated
Hz	Hertz
IAM	inner acrosomal membrane
IBC	IP_3 binding core
I_{CRAC}	CRAC channel current
ICSI	intracytoplasmic sperm injection
IMM	inner mitochondrial membrane
IP_3	Inositol-1,4,5-triphosphate
IP_3R	Inositol-1,4,5-triphosphate receptor
IS	interstitial space
IVF	*in vitro* fertilization
K^+	potassium ions
KCl	potassium chloride
kDa	kilo Daltons
KOH	potassium hydroxide
LC	Leydig cells

LH	luteinizing hormone
LIN	linearity
LVA	low voltage activated
MCU	mitochondrial uniporter
MF	Mag-Fluo-4AM
$MgCl^{2+}$	magnesium chloride
min	minutes
ml	millilitres
mm	millimetres
mM	millimolar
MMP	mitochondrial membrane potential
Mg^{2+}	magnesium ions
mOsm	milli Osmole
mRNA	messenger ribonucleic acid
mV	millivolts
N	nucleus
Na+	sodium ions
NADH	Nicotinamide adenine dinucleotide
NBC	Na^{+}/ HCO_3^{-} co-transporters
NCX	Na+-Ca^{2+} exchanger
NE	nuclear envelope
nm	nanometre
nM	nanomolar
NNC	NNC-55-0396
NO	nitric oxide
NPC	nuclear pore complexes
OAM	outer acrosomal membrane

OGB Oregon Green-BAPTA-1AM

Orai CRAC PM Channel

PAS post acrosomal sheath

PBS phosphate buffered saline

pH_i intracellular pH

PHN Posterior head/neck

PKA protein kinase A

PKC protein kinase C

PKG protein kinase G

PM plasma membrane

PLC phospholipase C

PM plasma membrane

PMCA plasma membrane Ca^{2+} ATPase

PSA prostate specific antigen

PT peri-nuclear theca

PTK protein tyrosine kinase

PTP Mitochondrial Permeability Transition Pore

PUFA polyunsaturated fatty acids

RMCE receptor mediated Ca^{2+} entry

RNAi ribonucleic acid interference

RNE redundant nuclear envelope

ROI region of interest

ROS reactive oxygen species

R_{tot} fluorescence intensity mean

RyR ryanodine receptor

S seconds

SACY soluble adenylate cyclase

SAM	sterile alpha motif
SC	Sertoli cells
SCID	severe combined immune deficiency
SD	suppressor domain
sEBSS	supplemented EBSS
sec	seconds
S.E.M	standard error of the mean
Ser/Thr	serine/threonine
SERCA	sarcoplasmic-endoplasmic Ca^{2+} ATPase
$_{Si}$RNA	small interfering RNA
SKF	SKF-96365
SLO	Streptolysin-O toxin
SOAR	STIM1 Orai activating region
SOC	store operated Ca^{2+} channel
SOCE	store operated Ca^{2+} entry
SPCA	secretory pathway Ca^{2+} ATPase
Src	serine kinase
ST	seminiferous tubules
STIM	stromal interaction molecule
STR	straightness
TCA	tricarboxylic acid cycle
TIRF	Total internal reflectance fluorescence
TMD	transmembrane domain
TRPC	transient receptor potential cation channels
VAP	path velocity
VCL	curvilinear velocity
VSL	progressive velocity

VOCC	voltage-operated Ca^{2+} channels
WHO	World Health Organization
w/v	weight per volume
YFP	yellow fluorescent protein
Zn^{2+}	Zinc ions
ZP	zona pellucida
ΔF_{mean}	fluorescence intensity mean
ΔF_{max}	maximum fluorescence intensity
ΔF	fluorescence intensity
ΔF_{sus}	sustained fluorescence intensity
µm	micrometre
µM	micromolar
$\Delta \Psi_m$	mitochondrial membrane potential

CHAPTER ONE: INTRODUCTION

CHAPTER ONE: INTRODUCTION

1.1 Fertilization – overcoming the odds!

Human procreation like in all mammalian species is the product of sexual reproduction ultimately requiring the fusion of two complementary haploid gametes to produce a competent diploid zygote (Sutovsky & Manandhar, 2006). The intricate differentiation of spermatogonal stem cells into highly specialised mature sperm requires strict geographical organisation, tight hormonal regulation and the sophisticated processes of spermatogenesis, spermiogenesis and epididymal maturation. Subsequently cells undergo hyperactivation and capacitation; a transformation only achieved by entering the female tract (Gadella & Visconti, 2006).

1.2 Sperm morphology

Mammalian sperm are organised into two distinct regions; the head and flagellum, which are encompassed by an external plasma membrane (Figure 1.1; Bellve & O'Brien, 1983). The compartmentalised anatomy of sperm is an important contributing factor in the specialised cytology of the cell. Unlike the oocyte, which stockpiles proteins, molecules and organelles to sustain the fertilised zygote, sperm forfeit all superfluous contents reducing cell size to facilitate survival outside the male reproductive tract. This compact, elongated structure has favourable hydrodynamics for both motility and oocyte penetration ensuring structural conservation across species. However considerable size variation is observed from the 356µm sperm of the Australian honey possum to the archetypal human spermatozoon ~55µm in length (Cummins & Woodall, 1985).

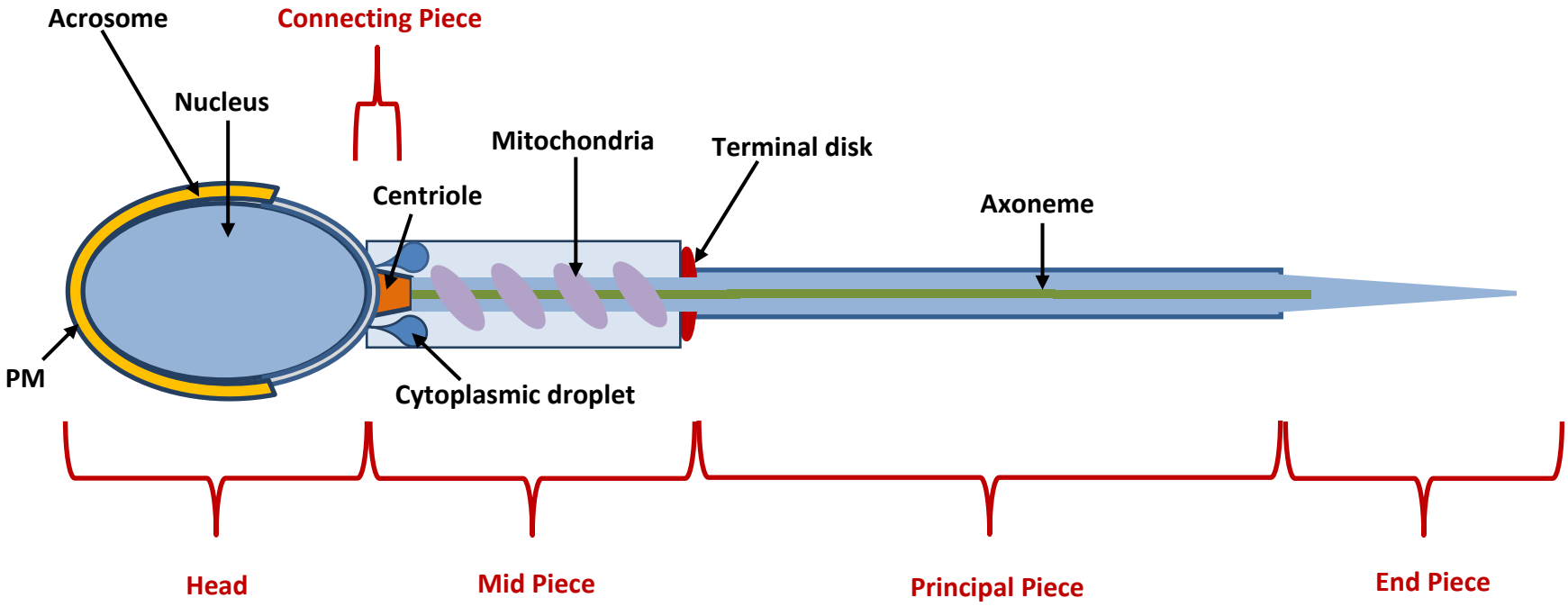

Figure 1.1 Overview of mammalian sperm structure. The mature spermatozoon has a highly compartmentalised structure and can be divided into several discrete regions: the head, connecting piece, mid piece, principal piece and end piece. Each region has distinct characteristics and roles in sperm function. The entire cell is encompassed by a plasma membrane (PM) whose composition changes during capacitation.

1.2.1 The Head

In all mammalian species the sperm head consists of a highly condensed haploid nucleus, a small amount of cytosol and the overlying acrosome. There is also clear species variation, the rodent sperm head is falciform or hook shaped, whilst the head of ungulate, carnivore and primate sperm are spatulate or spatula shaped (Sutovsky & Manandhar, 2006).

1.2.1.1 The Nucleus

The sperm nucleus is hyper-condensed; histones have been partially replaced by positively charged protamines to reduce volume. The nuclei of both human and mouse sperm contain two arginine rich protamines; a typical type-I protamine present in all mammalian species and the predominant unique type-II protamine with a high histidine content (Bellve & O'Brien, 1983). The nucleus is surrounded by a reduced nuclear envelope which is apparently devoid of nuclear pore complexes (NPCs). Studies by Ho & Suarez (2003) detected NCPs in an area of excess membrane termed the redundant nuclear envelope (RNE), which accumulates at the base of the nucleus. This structure is surrounded by the peri-nuclear theca; a rigid matrix of disulphide bond stabilized structural proteins associated with proteins imperative in intracellular signalling and acrosomal anchoring (Sedo *et al*., 2009). The acrosome forms a cap over the peri-nuclear theca, encasing the anterior pole of the nucleus (Sutovsky & Manandhar, 2006).

1.2.1.2 The Acrosome

The acrosome subdivides the sperm head into two distinct segments; the acrosomal and post-acrosomal regions. The acrosome is a Golgi-derived vesicle-like organelle which covers approximately two thirds of the sperm head. This vesicle contains proteolytic enzymes such as acrosin, proteases, esterases, peptidases and phospholipases enclosed by inner and outer membranes anchoring the acrosome to the nucleus (Herrick *et al.,* 2005). Prior to fertilization the outer acrosomal membrane fuses with the overlying plasma membrane in an exocytotic process called the 'acrosome reaction' (AR; section 1.8). Subsequently cell fusion can occur between the sperm equatorial segment; an area rich in oocyte fusion receptors fertilin-β and cyritistin, and the oocyte oolemma (Evans, 2002; Kaji & Kudo, 2004; Toshimori *et al.,* 1992; Toshimori & Ito, 2003).

1.2.2 The Flagellum

Adjoined to the sperm head is a single flagellum which provides the motile force that allows the cell to traverse the female tract and ultimately reach the oocyte. The flagellum contains a core axoneme and prominent accessory structures (Hamilton & Waites, 1990). In humans the flagellum is approximately 50μm long, 0.5μm in diameter and can be topologically subdivided into four major segments based on external substructure: the connecting piece; midpiece; principal piece and end piece each sharing a common innermost axonemal structure (Cummins & Woodall, 1985; Ford, 2006).

1.2.2.1 The Axoneme

Like cilia and flagella of all species the sperm axoneme has a distinctive 9+2 radial symmetry arrangement of microtubule doublets, surrounded by unique sperm-specific accessory

structures (Fawcett & Porter, 1954). The 9+2 arrangement consists of nine symmetrical peripherally arranged microtubule doublets connected via dynein arms and two central microtubules. The central microtubules are sounded by a helical sheath and connected to the peripheral doublets by radial spokes. Each peripheral doublet comprises of a circular A-tubule attached to a larger C-shaped B-tubule through two arm projections, nexin bridges and radial links (Bellve & O'Brien, 1983). The outer doublets are paralleled by nine outer dense fibres and it is these and not the central pair that provide flexible support during flagellar movement.

1.2.2.2 The Connecting Piece

The connecting piece is ~0.5µm in length and the most proximal of the flagellar regions. In most mammals except rodents the connecting piece contains the proximal centriole an essential male contribution to the zygote. Located in the dense mass of capitculum caged by nine striated or segmented columns the proximal centriole is a continuation of the outer dense fibres (Johnson & Everitt, 2000).

1.2.2.3 The Midpiece

The midpiece, 3.5µm long in human sperm links the connecting piece to the principal piece. Covered by a sheath of 75-100 helically arranged mitochondria the midpiece contains the apparatus essential for ATP production to drive motility (Suarez, 2008). Diffusion of mitochondrial ATP production has questionable ability to deliver ATP to the distal end of the flagellum rapidly enough to support active sliding of dynein molecules. However sperm-

specific glycolytic isoenzymes have been identified throughout the flagellum indicating a crucial role for glycolysis in the regulation of motility (Piomboni *et al.,* 2012).

1.2.2.4 The Principal Piece

The principal piece is separated from the midpiece by the annulus or Jensen's ring (Barratt *et al.,* 2009). At 55µm long, the principal piece constitutes the majority of the sperm flagellum and is characterized by a scaffold of protective fibrous sheath parallel to the outer dense fibres and connected by a series of cross linked disulphide bonds (Eddy *et al.,* 2003; Turner, 2003). In addition to mechanical support the fibrous sheath has been found to provide the scaffolding essential for a number of protein kinases required for capacitated and hyperactivated motility, including A-kinase anchor proteins (Carrera *et al.,* 1994), phosphodiesterases, Protein Kinase G (PKG; Moss & Gerton, 2001; Storey & Kayne, 1975; Travis *et al.,* 1998). The principal piece also plays an import role in glycolysis with many glycolytic enzymes important in sperm ATP production localized to this region.

1.4.2.5 The End Piece

Unlike the rest of the flagellum the end piece is not surrounded by outer dense fibres. Instead the axonemal doublets which comprise the core flagellum slowly begin to regress resulting in tapering of the inner microtubules (Ford, 2006).

1.3 Anatomy of the testis

Testicular organization is crucial in the highly regulated process of sperm production. Post-pubertal testis has two main functions: (1) the creation of mature sperm which transmit genetic information to the zygote, and (2) the synthesis of hormones essential in maintaining reproductive function (Johnson, 2013). The testis has a complex compartmentalised structure consisting of two discrete regions; numerous seminiferous tubules or intratubular compartments and the surrounding interstitial space or extratubular compartment (Figure 1.2). Both compartments are structurally distinct; the Sertoli cells (SC) of the tubules are closely associated with the development of sperm while the Leydig cells (LC) synthesise hormones (mainly androgens) in the interstitial space containing the blood vessels, nerves, white blood cells and lymph vessels associated with all tissues (Franca *et al.,* 1998).

Antigens present on the sperm surface are not tolerated by the body's immune system; presence of sperm in either the systemic or lymphatic circulation can lead to an autoimmune response and subfertility (Johnson, 2013). Consequently during the peri-pubertal period, before the onset of spermatogenesis a cellular barrier develops physiologically separating the intratubular and extratubular compartments. This barrier known as the blood-testis barrier (BTB) consists of multiple layers of adherens, gap and tight junctions firmly adhering each SC to its' adjacent neighbours (Sutovsky & Manandhar, 2006). The BTB is a selective, semi-permeable barrier that prevents immune system infiltration, sperm leakage and limits the exchange of water soluble materials between the basal and adluminal compartments of the seminiferous epithelium (Cheng & Mruk, 2010). As a result, the architecture and environment of the seminiferous tubules is fundamental in sperm development.

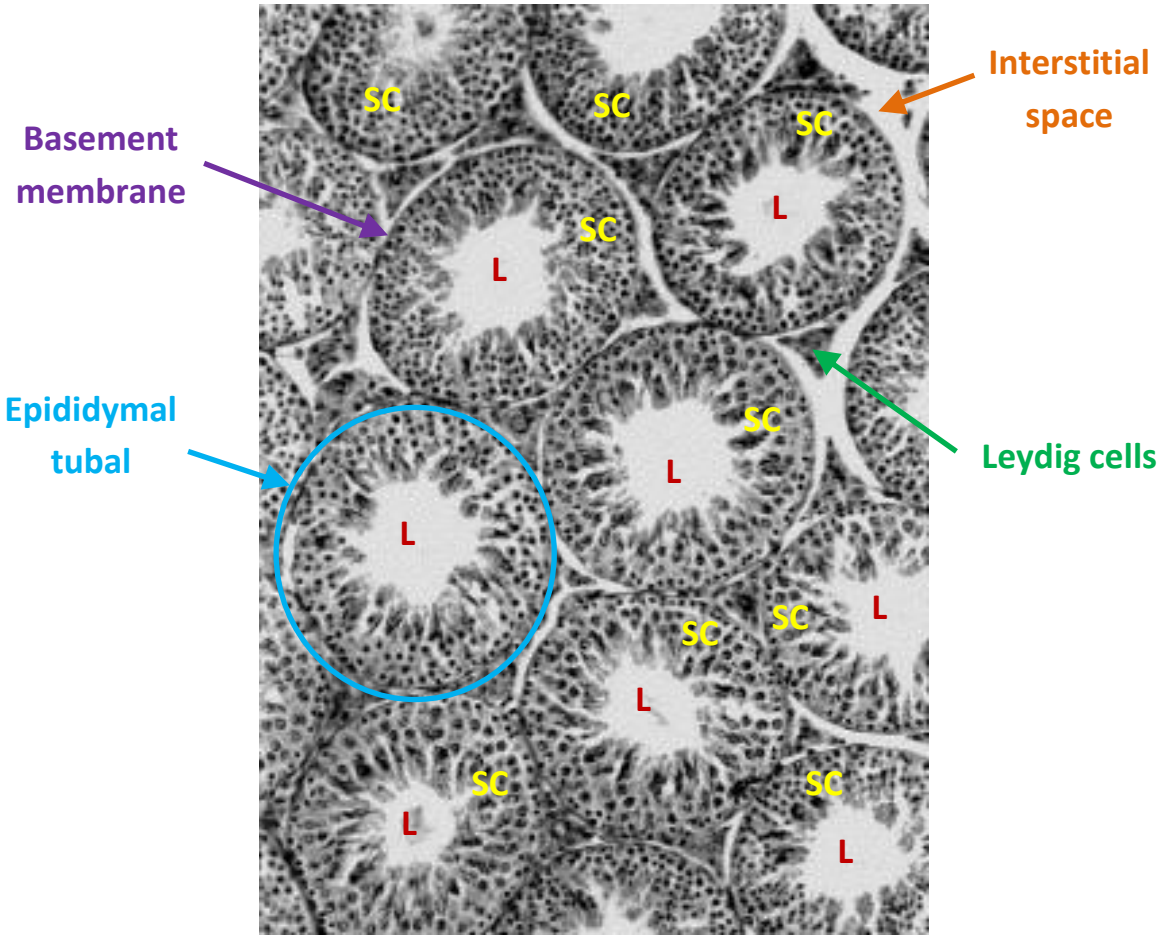

Figure 1.2 Mammalian testis composition. A cross section of the mammalian testis displaying, the seminiferous tubules (ST), Sertoli cells (SC), Leydig cells (LC), basement membrane, (BM), interstitial space (IS) and seminiferous tubal lumen (L) (adapted from Kang *et al.*, 2002).

1.3.1 Seminiferous tubule organisation

Configuration of the testicular seminiferous tubules is vital for continuous germ cell development, permitting selective uptake of paracrine factors and preventing immune cell infiltration. Composed predominantly of SCs which extend from the tubule periphery to the lumen, the seminiferous tubules are separated into basal and adluminal compartments by the BTB; vital for preventing an autoimmune response to sperm antigens produced long after self-tolerance is established (Kopera *et al.,* 2010). The basal compartment constitutes the outermost layer of the seminiferous tubule, enveloped by the basement membrane where type-A spermatogonia (sperm progenitors) reside. The basement membrane itself is closely associated with the circulatory system enabling the uptake of nutrients vital for gamete production (Shalet, 2009). Beyond the BTB, in the adluminal compartment, are the SCs which act as "nurse cells" to synthesize and secrete proteins, cytokines, steroids, tubular fluids and growth factors essential for germ cell development (Alves *et al.*, 2013).

Spermatogenesis the process of sperm differentiation consists of three distinct stages: mitotic proliferation, meiotic division and cytodifferentiation (Johnson, 2013). As spermatogonia begin to proliferate they migrate from the basal compartment across the BTB into the adluminal compartment of the seminiferous tubules. Sperm progenitors are able to cross the BTB by temporarily disrupting the dynamic SC-SC interactions and passing between the cells to the adluminal surface. It is here where terminally differentiated sperm are first embedded in the luminal surface of the SC before being released into the seminiferous tubule lumen in a process known as spermiation (Kopera *et al.,* 2010).

To maintain sperm production throughout the reproductive lifespan of eutherian mammals, spermatogenesis must provide a continuous supply of mature sperm. Due to the time

constraints of the differentiation process (sixty-four days in human) this would be impossible without the cyclical arrangement of the seminiferous epithelium which enables the synchronous development of each stage of spermatogenesis, occurring in discrete segments of the seminiferous epithelium over time (Russell *et al.,* 1990). This continuous cycle of sperm production maintains a constant output of ~1000cells per heartbeat during the reproductive lifespan of an individual (Griswold & Oatley, 2013).

1.3.2 Hormonal regulation of sperm cell differentiation

In humans, endocrine control of spermatogenesis begins in utero with the differentiation of mesenchymal stem cells into foetal LCs. At this point in development the endocrine regulatory hypothalamus-pituitary-testicular axis is established (Figure 1.3). The initial LCs secrete androgens required for development of male genitalia, disappearing 3-6 months after birth, accompanied by a drop in testosterone levels (Shalet, 2009). At puberty, pulses of gonadotrophin-releasing hormone (GnRH) are secreted by the hypothalamus triggering the pituitary to produce luteinising hormone (LH) and follicle stimulating hormone (FSH; McLachlan, 2000; Alves *et al.,* 2013). LH is primarily responsible for stimulating the synthesis of testosterone from lactate and cholesterol in the smooth endoplasmic reticulum of LCs, secreting approximately 4-10mg per day in humans (Johnson, 2013). Testosterone contributes to the development of secondary sexual characteristics whilst its metabolites such as 5α-hydrotestosterone (DHT) can bind the SC androgen receptors on the cell surface initiating entry into meiosis, spermatogenesis and BTB maintenance (Alves *et al.,* 2013). Concurrently FSH accelerates SC proliferation in spermatogenesis and the production of intracellular androgen receptors thus increasing responsiveness to testosterone (Shalet, 2009). This synergistic relationship between LH and FSH is reinforced by negative feedback effects

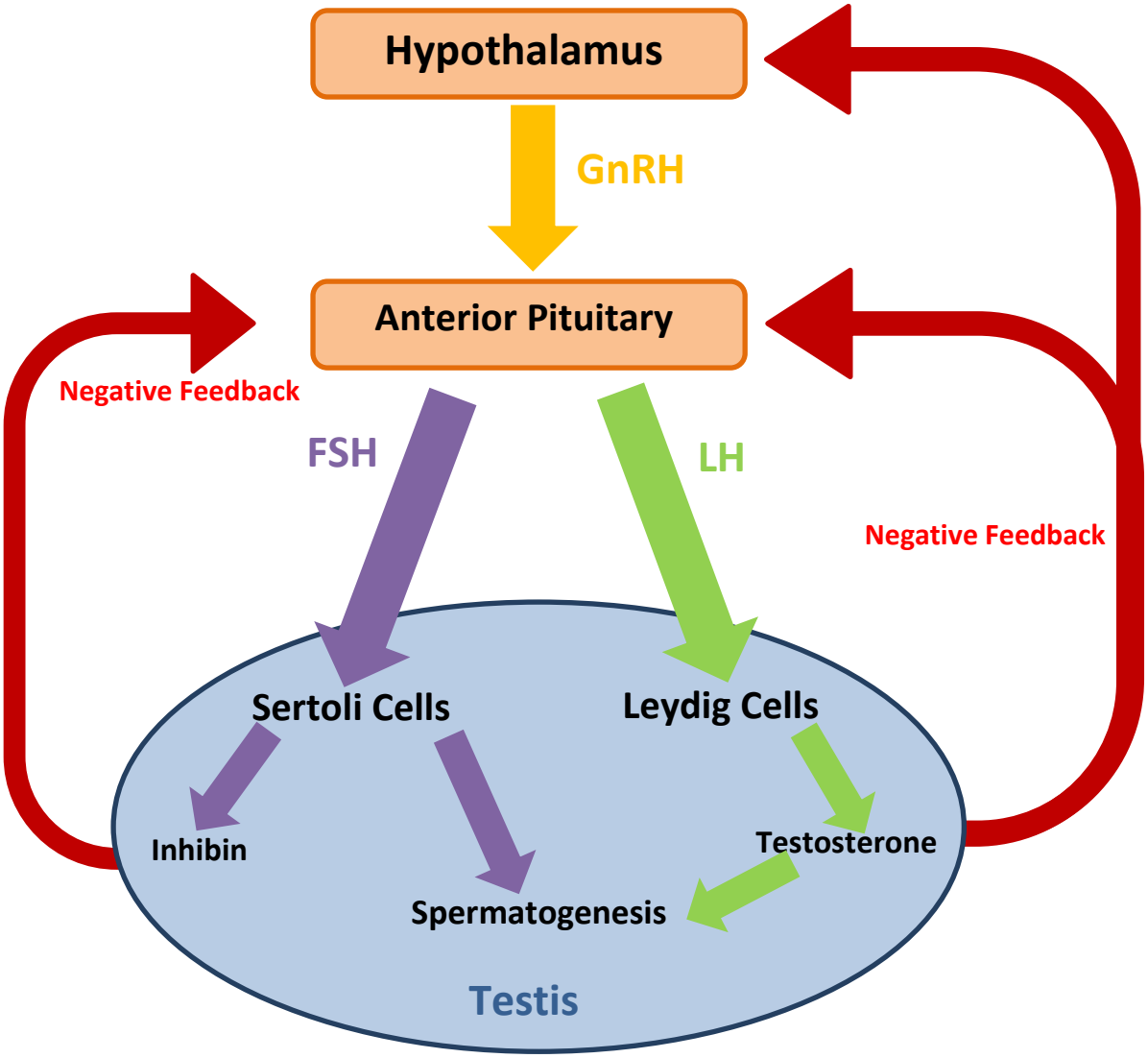

Figure 1.3 Hormonal regulation of spermatogenesis. The hypothalamus produces Gonadotrophin Releasing Hormone (GnRH) which stimulates the anterior pituitary to produce follicle stimulating hormone (FSH) and luteinising hormone (LH). LH in turn stimulates the Leydig cells of the testis to produce testosterone involved in spermatogenesis. FSH induces Sertoli cells to undergo spermatogenesis whilst simultaneously producing inhibin. High levels of both Inhibin and testosterone form negative feedback loops with the pituitary and hypothalamus to maintain homeostasis.

on the secretion of GnRH by the hypothalamus preventing downstream effects and maintaining continuous spermatogenesis (Figure 1.3).

1.4 Sperm cell differentiation

Male gametogenesis begins during the fourth week of gestation; primordial germ cells migrate from the yolk sac to the genital ridge in the undifferentiated gonad (Shalet, 2009). Murine germ cells proliferate during migration and for a few days after colonizing the gonad differentiating into quiescent non-proliferative type-A pro-spermatogonia. Approximately one week after birth the first wave of male germ cells will initiate spermatogenesis a process essential later in life to maintain the daily output of fully differentiated sperm (McLaren *et al.*, 1984; McLaren, 2003).

1.4.1 Spermatogenesis

Spermatogenesis, the production of mature haploid sperm from primordial germ cells, can be subdivided into three distinct stages; an initial mitotic proliferation producing cell quantity; a second meiotic division that generates diversity; and spermiogenesis the process of cytoplasmic differentiation (Johnson & Everitt, 2000; Chocu *et al.*, 2012). Duration of spermatogenesis is crucial; each stage has precise and regular timings to ensure periodic renewal of both the stem cell pool and sperm output (Johnson, 2013).

In humans primordial germ cells differentiate into type-A spermatogonia at birth, spermatogenesis is then arrested until the peri-pubertal period (Sutovsky & Manandhar, 2006). An increase in both testosterone and GnRH production during the onset of puberty induces spermatogenesis to resume in the seminiferous tubules of the testis (section 1.3.2). Here the highly compartmentalised structure of the seminiferous tubule epithelium create a

favourably organised environment for germ cell development, permitting staggered production of fully mature sperm according to the cycle of the seminiferous epithelium. In short different regions of the seminiferous tubule are able to enter spermatogenesis independently.

In humans a new wave of type-A spermatogonium enter the spermatogenic cycle every sixteen days, these cells stagger their pattern of development to ensure maintenance of reproductive potential (Griswold & Oatley, 2013). Increased testosterone and GnRH levels induce the initial mitotic proliferation cascade of type-A spermatogonia into either additional type-A spermatogonia to maintain the reproductive lifespan or differentiate into type-B spermatogonia competent to enter meiosis (Figure 1.4). These mitotic events occur at approximately forty-two hour intervals, with the number of mitotic divisions before meiosis characteristic of the species (Johnson & Everitt, 2000). All subsequent mitotic divisions of type-B spermatogonia from a single type-A spermatogonium produce diploid primary spermatocytes joined by thin cytoplasmic bridges. These cytoplasmic connection forms a 'syncytium' allowing synchronous development of all daughter cells, sharing of mRNA and proteins throughout spermatogenesis (Johnson & Everitt, 2000).

In preparation for meiosis primary spermatocytes undergo chromosome duplication. At this time random separation of homologous chromosomes and chromosome crossover (chiasma) ensures that each spermatocyte is genetically discrete (Shaman & Ward, 2006). During the two meiotic divisions the spermatids move from the basal intratubular compartment of the testis to the adluminal intratubular compartment by transiently disrupting the BTB. Upon completion of the second meiotic division each diploid spermatid spermatids must

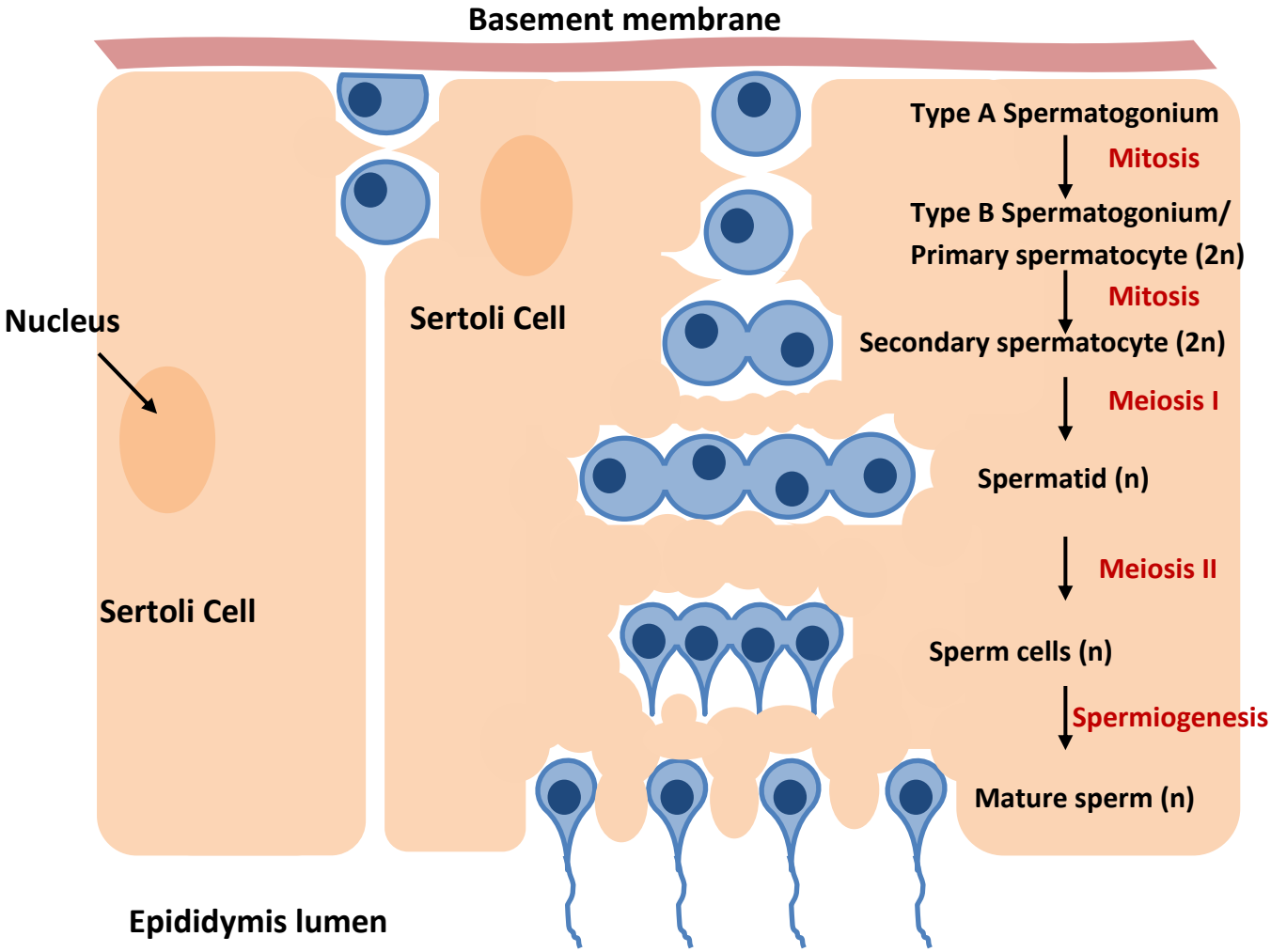

Figure 1.4 Geographical overview of spermatogenesis. Spermatogensis begins with the differentiation of type A diploid (2n) spermatogonium into type B spermatogonium (2n) at the junction of the adluminal compartment and basement membrane in the epididymal tubule. Type B spermatogonia undergo a species specific number of mitotic proliferations before finially differentiating into diploid secondary spermatocytes between the gap junctions of neighbouring sertoli cells. The first meiotic division of secondary spermatocytes produces haploid spermatids joined via thin cytoplasmic bridges which remain through meiosis II. Haploid sperm cells undergo spermiogenesis before separating into individual mature sperm, that are released into the lumen of the epididymal tubules.

subsequently undergo drastic structural remodelling during spermiogenesis to produce mature sperm (Kopera *et al.,* 2010).

1.4.2 Spermiogenesis

At cessation of meiosis II round haploid spermatids undergo spermiogenesis, a series of morphological and functional changes required to produce polarised sperm with fertilizing potential. In humans the process takes twenty-two days, however further maturation in the male tract is required to make the cells competent (section 1.5; Sutovsky & Manandhar, 2006). Spermiogenesis can be separated into four distinct stages, elongation, acrosomal cap formation, flagellum and centriole formation and spermiation, the process of cytoplasmic rejection and cell release (Johnson & Everrit, 2000).

Haploid round spermatids entering spermiogenesis are similar in structure to somatic cells. The first characteristic changes of elongation involve repackaging of nuclear DNA. In somatic cells nuclear DNA is associated with histones, however these are replaced by smaller protamines in sperm. Basic charged proteins, protamines allow hypercondensation of the haploid chromatin by coiling 50-kb segments of DNA into 60nm toroidal subunits, thus forming the hydrodynamic shape essential for motility; simultaneously causing the termination of transcription and translation processes (Brewer *et al.,* 2003). Subsequently the spermatid Golgi apparatus fuses to form a single acrosomal vesicle in humans important in the process of fertilization, which then migrates to the proximal hemisphere of the sperm head where it forms a cap (Johnson, 2013). The final structure vital for sperm cell function is the flagellum, a complex structure composed of many individual components the central axoneme forms from the cells' centrioles. The centrioles migrate to opposite poles of the cell; one takes a radial position forming the axoneme, while the second lies perpendicular to form

the connecting piece (Sutovsky & Manandhar, 2006). Approximately one half of the mitochondria present in the immature spermatid acquires a reinforced mitochondrial capsule (Cataldo *et al.,* 1996) and organise helically around the axoneme to form the mitochondrial sheath of the midpiece. The remaining mitochondria are ejected with the superfluous cytoplasm (~70%) and surplus organelles via the residual body, which is phagocytosed by the SCs leaving only a small cytoplasmic droplet adjacent to the connecting piece. The resulting terminally differentiated cells are then released into the lumen of the seminiferous tubule for further maturation in the male tract.

1.5 Sperm maturation in the male tract

Sperm released into the lumen of the seminiferous tubule are fully differentiated but they are in a state of quiescence. For successful fertilization these sperm must undergo a series of post-gonadal modifications in the epididymis, followed by capacitation in the female tract (Tulsiani & Abou-Haila, 2011).

1.5.1 Epididymal Maturation

After being released into the lumen of the seminiferous tubules sperm are transported through the rete testis and efferent ducts into the epididymis (Cornwall, 2009). Migration from the tubules to the rete testis is due to peripheral myoid cell contraction in the tubules and testicular capsule, along with an increase in testicular pressure from subsequent sperm production. In addition both SCs and the rete testis epithelium actively secrete fluid to encourage flow (Ilio & Hess, 1994). At the vasa efferentia ciliated epithelial cells prevent cellular aggregation and facilitate passage of sperm from the rete testis into the proximal epididymis. Here absorptive cells with long microvilli reabsorb testicular fluid through

sodium and chloride ionic exchange resulting in an increase in sperm concentration (Johnson & Everritt, 2000).

Differentiated sperm are for the most part synthetically inactive; as a result epididymal maturation requires interaction of sperm with epididymal proteins and secretions (Cornwall, 2009). In humans the epididymis is grossly divided into three regions: caput (the most proximal), corpus (central) and cauda (the most distal). Passage through all three regions of the epididymal duct takes approximately one-two weeks in most species (Cooper, 2011), in humans this averages eleven days (Cooper & Yeung, 2006). The majority of sperm maturation events occur in the caput and corpus regions with the cauda region primarily acting as a temporary storage site for mature sperm until transfer to the vas deferens and ejaculation (Cornwall, 2009; Cooper, 2011). However, the storage capacity of the human epididymis is relatively small, after approximately two weeks abstinence sperm will start to appear in the urine (Barratt & Cooke, 1988).

The epithelium of each region possesses distinctive gene expression profiles that result in segment specific protein secretion into the luminal fluid, creating maturation microenvironments. These changes in luminal fluid content include the addition of L-carnitine, taurine, myo-inositol, glycerophophorylcholine, lactate, fructose, glycoproteins, dihydrotestosterone, chloride, cholesterol (Saez *et al.,* 2011) and HCO_3^- (Johnson & Everitt, 2000). Exposure to these molecules cause the stepwise biochemical changes in sperm that influence the acquisition of motility potential, transforming cell movement form juvenile to mature form (Cornwall, 2009). Samples taken from the cauda epididymis display an observably greater percentage of motile cells compared to the caput (Cooper, 2011). Increased velocity, forward progression and straightness of swimming path are all properties

of normal swimming behaviour acquired in the epididymis, which will change again upon hyperactivation (Smith *et al.,* 2008).

1.5.2 Ejaculation

Ejaculation is the final stage of sperm processing in the male tract and can be separated into two distinct phases; emission, where sperm are exposed to accessory gland secretions and ejected into the posterior urethra; and expulsion, the ejection of sperm from the urethra at the glans meatus into the female tract (Giuliano & Clement, 2005). Both stages are tightly controlled by the sympathetic, parasympathetic and somatic divisions of the nervous system (Peeters & Giuliano, 2008). However it is during emission that the final stages of sperm maturation occur.

Accumulation of sperm in the cauda epididymis initiates progression of the cells into the vas deferens. A storage reservoir, cells entering the vas deferens are densely packed, a build up here can result in the passage of sperm into the urine. It should be noted that *in vitro* sperm taken from the vas deferens are fully capable of oocyte fertilization (Silber, 1997). *In vivo* sperm must first be suspended in seminal plasma to facilitate transport to the female tract. Seminal plasma is a product of the accessory sex glands; seminal vesicles, prostate, Bulbourethral and Littre glands all contribute (Bronson, 2011). The seminal vesicles provide the majority of ejaculate volume (~3ml per ejaculate in humans). These sac-like glands produce plasma rich in bicarbonate prostaglandins, antioxidants, fructose, semenogelin and ascorbic acid. The ejaculate provides nutritional factors, pH buffering capacity, reducing agents to give the best chance of survival upon entering the female tract (Juyena & Stelletta, 2012). Antioxidants, such as superoxide dismutase, glutathione, catalase and vitamins C and E are thought to protect sperm from oxidative stress following exposure to atmospheric

oxygen and subsequent loss of motility (Johnson, 2013). In addition seminal plasma can contain large numbers of leucocytes and is the vehicle for a number of infectious agents.

The Bulbourethral and Littre glands contribute approximately 5% of the total ejaculate volume. The prostate provides zinc, choline, citric acid, prostasomes and prostate specific antigen (PSA) responsible for liquefaction of the seminal plasma semenogelin proteins (Burden *et al.,* 2006). Prostasomes were first discovered in 1978 by Ronquist *et al.,*; membranous micro-vesicles, they are secreted by the prostate gland acinar epithelium (Ronquist, 2012) and considered to be a contributing factor in the maturation of sperm due to their ability to fuse to the cell membrane (Burden *et al.,* 2006). Prostasomes vary greatly in size from 40-500nm and can be separated into two distinct groups, larger electron light and smaller more dense vesicles. In 2003 proteomic analysis of prostasomes revealed 139 proteins (Utleg *et al.,* 2003), numerous small molecules and several ions including Ca^{2+}, Zn^{2+}, GDP, ADP and ATP were also present in these vesicles (Arienti *et al.,* 1997). Unlike other vesicles the lipoprotein membranes of prostasomes are composed of an unusually high proportion of cholesterol (~45%), resulting in their unique ability to fuse with other cells (Burden *et al.,* 2006). Cholesterol composition is particularly important as it believed to contribute significantly to stabilisation of the acrosomal cap preventing premature acrosome reaction (AR; Saez *et al.,* 2011). Further studies have identified pH sensitivity of the sperm/prostasome fusion process with acidic pH similar to the vaginal environment optimal. At pH 5.0 fusion events occurred in the neck/midpiece region of the sperm, which would be beneficial for triggering changes in motility associated with capacitation (Arienti *et al.,* 1997; 2004). Subsequent studies identified an increase in percentage motility in swim up preparations performed in the presence of prostasomes (Arienti *et al.,* 1999).

1.6 Sperm navigation in the female tract

In humans and other internal fertilizers, sperm are deposited in the female genital tract at coition. Sperm must then traverse the female tract overcoming a series of obstacles in order to penetrate the oocyte (Harper & Publicover, 2005). As a result only a small proportion of the ejaculate successfully navigates to the fertilization site. Some species variation exists at point of entry. The pig, dog, horse, mouse and rat ejaculate sperm directly into the cervix and/or uterus (Rath *et al.,* 2008) whereas human, sheep and cow ejaculates are deposited in the vagina and onto the cervical os. In most species the semen coagulates forming a plug which may be temporary or permanent depending on the species. Human semen coagulation begins when semenogelins are introduced to the seminal plasma by the seminal vesicles and lasts for approximately 1hr (Suarez & Pacey, 2006). Thought to maximise sperm transmission, the coagulate provides protection from the harsh vaginal environment.

In humans the first vital stage for sperm survival is quick progression through the cervix to avoid attack by the female immune system and damage due to vaginal acidity (pH5.7). Sobrero and MacLeod (1962) observed that human sperm leave the seminal pool and begin to enter the cervix within minutes of deposition. The cervix presents its own challenges to the sperm, as the epithelium of the cervical canal produces highly hydrated mucus. Entry to the uterus is dependent solely on ability to penetrate and survive the mucus. Only when progesterone is absent does the cervix produce mucus with a favourable consistency for morphologically normal sperm penetration (Suarez & Pacey, 2006; Johnson, 2013). The mucus also contains leukocytes and neutrophils with the capability of engulfing sperm cells. It has been demonstrated that both serological-complement and complement-fixing anti-sperm antibodies must be present for neutrophils to engulf sperm (D'Cruz *et al*., 1992).

Sperm successful in reaching the uterus must then travel the relatively short distance through the uterine cavity to the uterotubal junction. In humans, this is only a couple of centimetres in length and can be easily accomplished in 10-20min with a swimming speed of approximately 5mm/min. Studies on sperm transport through the uterus are difficult to conduct and contractions of the uterine myometrium would aid the rapid progression through the uterus and away from leukocyte attack (Suarez & Pacey, 2006). Nevertheless it appears that sperm are likely to enter the uterotubal junction by their own propulsion. Upon passage of the narrow uterotubal junction sperm enter the Fallopian tube isthmus, which in humans may act as a temporary sperm reservoir until ovulation. Human sperm have been shown to transiently interact with the endometrium of the Fallopian tube that would affect the sperm progress towards in the ampulla (Pacey *et al*., 1995). Increased complexity of the mucosal folds of the tube lining reduces the risk of polyspermy and ensures the advancement of only the most 'fit' sperm to the oocyte (Holt & Fazeli, 2010). To successfully transmit through the female reproductive tract and fertilize the oocyte all sperm must also undergo a series of alterations in synchrony with the environmental changes they encounter, termed *Capacitation* (Austin, 1952). Moreover sperm must make the transition from forward progressive motility acquired in the male tract to hyperactivated motility capable of penetrating the outer oocyte vestements.

1.6.1 Capacitation

Despite a period of maturation in the epididymis mammalian sperm are unable to fertilize oocytes immediately after ejaculation. Instead a period of time is required in the female tract, during which a series of biochemical changes activate the fertilization potential of sperm (Gadella & Visconti, 2006). This phenomenon was discovered independently by Austin and Chang in 1951 (Gadella & Visconti, 2006; Shivaji *et al.*, 2007). Termed *capacitation*, it was

defined as the minimum period of female tract interaction required for sperm to gain fertilizing capability and is only considered complete by the ability to AR in response to the ZP (Shivaji *et al.,* 2007). These initial observations spawned many subsequent lines of enquiry into the precise nature of the biochemical processes occurring in the female tract. It is now known that capacitation induces a number of physiological changes in sperm including an increase in plasma membrane fluidity (Wolf *et al.,* 1986; Benoff *et al.,* 1993), reorganisation of sperm surface molecules, $[Ca^{2+}]_i$ increase (Singh *et al.,* 1978; Gonzalez-Martinez *et al.,* 2002; Xie *et al.,* 2006), membrane hyperpolarization (Zeng *et al.,* 1995), intracellular pH increase (pH_i; Babcock & Pfieffer, 1987) and increased phosphorylation, particularly on tyrosine residues (Moseley *et al.,* 2005;Visconti, 2009). The molecular basis for these changes has identified the involvement of a number of regulatory second messengers; but a unified model for all capacitative changes is still in its infancy (Gadella & Visconti, 2006).

It should be noted that unlike other processes governing sperm maturation and development, capacitation is not a step-wise process. Instead it appears to be the product of a matrix of sequential and parallel processes, each requiring different conditions for completion (Visconti, 2009). Some changes instigated at deposition in the female tract may be instantaneous (fast events) while others require oviduct entrance to terminate (slow events) (Figure1.5). Many of the studies on capacitation have been conducted *in vitro* due to ethical constraints; as a result there may be some disparity with *in vivo* events (De Jonge, 2005).

1.6.1.1 Fast events of capacitation

Sperm of the cauda epididymis are predominately immotile, requiring high levels of HCO_3^- and Ca^{2+} present in the seminal plasma for motility activation. *In vitro* studies have shown

contact with an isotonic solution containing HCO_3^- and Ca^{2+} is sufficient to induce vigorous flagellar movement necessary for progressive forward motility (Tajima *et al.,* 1987). There are several candidates for HCO_3^- transport across the plasma membrane. Recent studies suggest contribution from Cl^-/ HCO_3^- exchangers (Chen *et al.,* 2009) and CatSper channels in the flagellum (Carlson *et al.,* 2003). The most well documented theory is PM Na^+/ HCO_3^- co-transporters (NBC). These channels would explain the electrogenic, Na^+ dependent nature of the response to HCO_3^- consistent with an increase in pH_i. In addition treatment with DIDS (4,4-diisothiocyanostilbene-2,2-disulphonic acid) a known inhibitor of NCB prevents the aforementioned effects (Demarco *et al.,* 2003). Upon entering the cell the increased [HCO_3^-] simultaneously increases pH_i and stimulates the production of cAMP (~60secs; Harrison & Miller, 2000; Visconti, 2009) by an atypical soluble adenylyl cyclase (SACY) that is thought to orchestrate capacitation (Carlson *et al.,* 2007). cAMP in turn activates PKA which phosphorylates serine/threonine residues on target proteins in the flagellum (~90sec from HCO_3^- activation) leading to an increase in beat frequency and motility activation, as well as contributing to numerous other signalling processes (Xie *et al.,* 2006; Visconti, 2009).

1.6.1.1 Slow events of capacitation

Although both fast and slow events of capacitation are mediated by a HCO_3^-/SACY/cAMP/PKA pathway, slow events require additional cholesterol efflux and tyrosine phosphorylation for completion. Initiation of slow capacitation events commences with cholesterol efflux from the PM. *In vitro* this is achieved through the addition of bovine serum albumin (BSA) or as β-cyclodextrins to the capacitation media (Visconti *et al.,* 1999). Both molecules are believed to function as a cholesterol sink, removing cholesterol from the PM. However as in the early events of capacitation, HCO_3^- and Ca^{2+} are both essential contributors to the intracellular signalling cascade underlying phospholipid membrane

reorganisation (Bailey, 2010). In mouse K^+ influx, Na^+ and Cl^- permeability are believed to contribute to PM hyperpolarisation increasing cholesterol efflux and membrane fluidity for lipid raft reassembly (Xin *et al.,* 2006; Cross, 2004). It is uncertain how much hyperpolarisation occurs in human cells. PM cholesterol removal stimulates PKA phosphorylation of serine/threonine residues initiating a much larger signalling cascade. Though a mechanism remains to be elucidated, upon cholesterol efflux PKA causes an increase in protein tyrosine phosphorylation, which is maintained in the presence of BSA, HCO_3^- or Ca^{2+} (Visconti, 2009). Recent studies suggest a serine kinase (cSrc) may be responsible for the phosphorylation of tyrosine observed at capacitation in mice (Visconti *et al.,* 2011) as cSrc inhibitors block capacitation and significantly reduce sperm motility parameters (Baker *et al.,* 2006; Lawson *et al.,* 2008; Mitchell *et al.,* 2008). Conversely studies on cSrc-null mice demonstrated no significant effect on tyrosine phosphorylation suggesting there is an additional kinase present capable of maintaining function (Krapf *et al.,* 2010). Despite the absence of a clearly defined mechanism of action it should be noted that the contribution of tyrosine phosphorylation to capacitation is essential, particularly in the final events before oocyte fusion and the switch to hyperactivated motility.

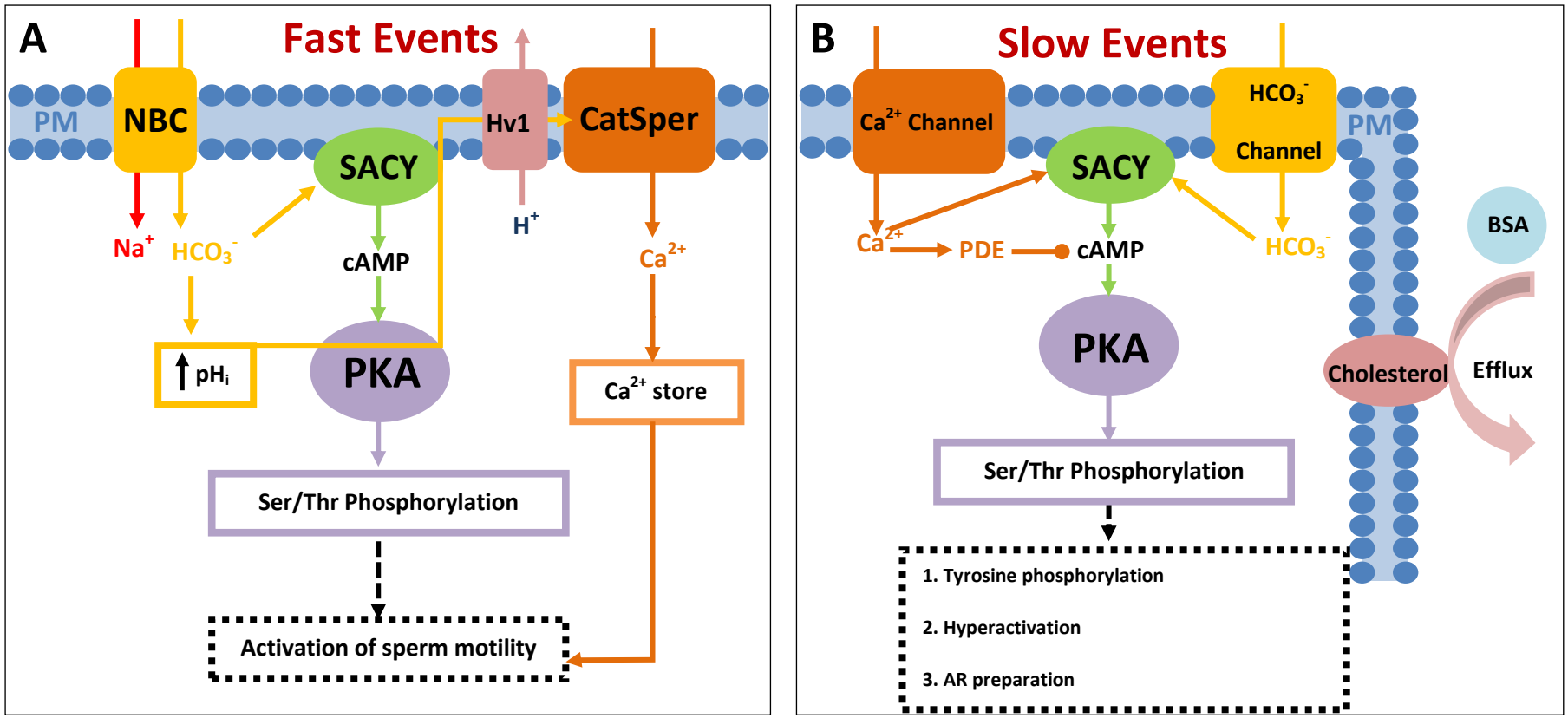

Figure 1.5 The biochemical pathways governing fast and slow capacitation events. (A) Fast events of capacitation. Sodium/bicarbonate cotransporters (NBC) in the plasma membrane (PM) transport sodium and bicarbonate ions into the cell causing an increase in intracellular pH (pH_i) and soluble adenylate cyclase Y (SACY) activation. In addition CatSper channels allow an increase in $[Ca^{2+}]_i$ further activating SACY, which produces cAMP a known activator of protein kinase A (PKA), an enzyme responsible for the phosphorylation of serine and threonine residues on target proteins. Furthermore excessive levels of calcium activate PDE which hydrolyses cytoplasmic cAMP. (B) Slow events of capacitation. Cholesterol efflux from the plasma membrane by serum albumin (BSA) induces reorganisation of the plasma membrane which alters the outcome of bicarbonate and calcium ion influx associated with slow capacitation events.

1.6.2 Hyperactivation

At ejaculation sperm activate progressive forward motility where beat frequency is high but the angle of flagellar bending is low (Suarez, 2008)**.** However this pattern of motility alone is insufficient to enable navigation of the female tract and penetration of the oocyte vestements. In 1970, Yanagimachi first reported a visible change in the swimming behaviour of hamster sperm before and after capacitation. Experiments involving exposure of sperm to the oviductal fluid of the oestrous female showed cells develop a distinctive 'activated' swimming pattern not observed at ejaculation. Subsequent studies of several mammalian species have revealed similar capacitation induced motility changes, which despite subtle species variation all show common elements (Gadella & Visconti, 2006).

This hyperactivated motility is characterised by vigorous, asymmetrical flagellar bending at the mid-piece causing high amplitude lateral head displacement but non-progressive movement (Gagnon & de Lamirande, 2006; Ohmuro & Ishijima, 2006; Figure 1.6). Hyperactivated motility has been observed at both the site and time of fertilization in mammals (Ho & Suarez 2003) and aids in cumulus dispersal thus allowing the sperm to reach the oocyte and undergo the acrosome reaction (Kaji & Kudo, 2004). Experiments co-culturing sperm and Fallopian tube epithelium reveal hyperactivation enables sperm to detach from the 'sticky' walls of the oviduct and progress towards the oocyte (Pacey *et al.*, 1995).

$[Ca^{2+}]_i$ has the most significant contribution to the regulation of hyperactivation. The primary secondary messenger associated with flagellar asymmetry, Ca^{2+} plays a pivotal role in many sperm processes (Ho & Suarez, 2001). Studies conducted on immobile demembranated sperm, show restoration of normal motility in medium containing ~50nM of Ca^{2+} with some cells hyperactivating at ~100nM, while the majority will hyperactivate when Ca^{2+} reaches

~400nM (Ho *et al*., 2002). Removal of calmodulin (CaM) from demembranated bovine cells eradicated the ability to hyperactivate; reintroduction of CaM into the medium restored this. In humans CaM kinase inhibitors reduced motility over time, thought to correlate with reduced ATP production (Suarez, 2008). Harper *et al.,* 2004 demonstrated a direct correlation between cyclical Ca^{2+} oscillations in the posterior head/neck (PHN) region and flagellar beat pattern.

Several other avenues of evidence to support the existence of a Ca^{2+} store in the PHN. Inositol 1,4,5 receptors (IP_3R) have been localised to the region and could facilitate a mechanism for cyclical store emptying and refilling (section 1.10.3.1). Studies using 4-aminopyridine and thapsigargin, (known to deplete Ca^{2+} stores) show that both can induce hyperactivated motility resulting from Ca^{2+} store depletion in bovine, murine and human sperm (Suarez, 2003). Ryanodine (section 1.10.3.2) and CatSper (section1.10.1.4) receptors have also been identified in close proximity to the PHN, which would enable rapid response to the external environment. The presence of a Ca^{2+} store in the base of the flagellum could facilitate Ca^{2+} interaction with the axoneme and initiation of hyperactivated motility.

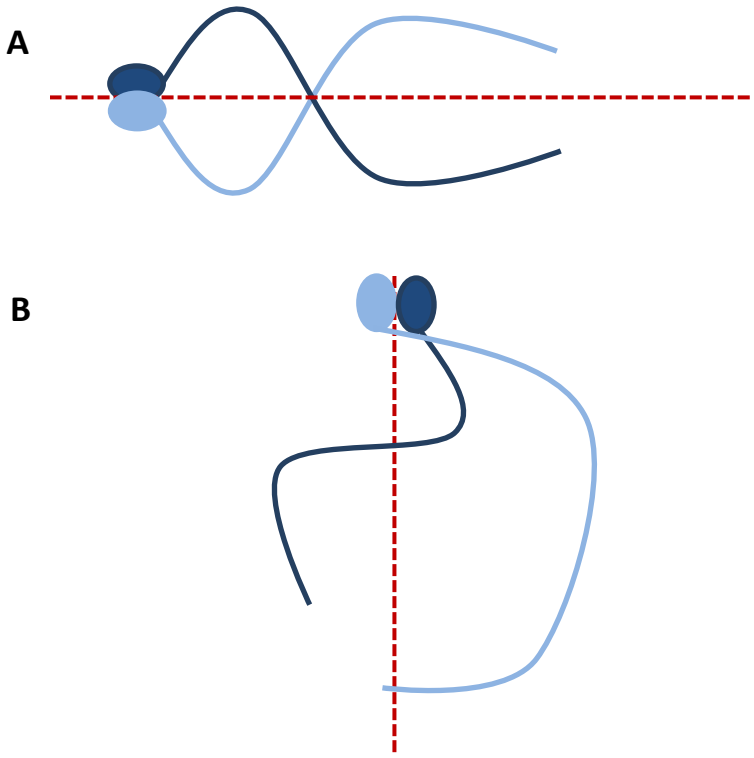

Figure 1.6 Comparison of normal and hyperactivated modes of sperm motility. Sperm position at 2 time points imposed on top of each other to reveal characteristics of (A) normal forward progressive motility of uncapacitated sperm and (B) hyperactivated asymmetrical motility, with distinctive large amplitude of lateral head displacement.

1.7 The Oocyte

It is traditionally accepted that females are born with a finite reserve of primary oocytes arrested at the first meiotic prophase. Several recent studies have claimed to identify functional oogonial stem cells in post pubertal females of several species including humans (Stoop *et al.*, 2005; Oatley & Hunt, 2012). However the methodologies and reproducibility are questioned by the scientific community resulting in little impact on the conventional model of oocyte production (Ghazal, 2013).

Oocyte maturation in females occurs on a monthly cycle (~28 days), hormonally controlled by levels of oestrogen, progesterone, GnRH, LH and FSH. Each cycle several primary oocytes resume oogenesis in the primordial follicle, resulting in the extrusion of a mature oocyte from the ovary at ovulation (Sanchez & Smitz, 2012). The ovulated oocyte is considerably larger than sperm, contributing cytoplasm, mitochondria, organelles, essential genetic material and additional external membrane structures involved in both the fertilization process and blockage of polyspermy (Figure 1.7). The PM (oolemma) of all mammalian species is surrounded by the Zona Pellucida (ZP). A glycoprotein matrix, human ZP is composed of four proteins (Lefievre *et al.*, 2004), while murine oocytes possess only three (Greve & Wassarman, 1985). The ZP is accredited with a number of crucial roles in fertilisation including oocyte protection, species-specific sperm binding and blockage of polyspermy (Conner *et al.*, 2005). On the outermost layer the oocyte is surrounded by the cumulus oophorus, a hyaluranon-rich matrix consisting of granulosa derived cumulus cells separated into an inner cell mass (corona radiata) and outer cell mass (cumulus). Cells of the corona radiata contain numerous gap junctions to permit the transport of essential growth factors to the oocyte (Rienzi *et al.*, 2012), while the outer cumulus forms a physical barrier to abnormal sperm.

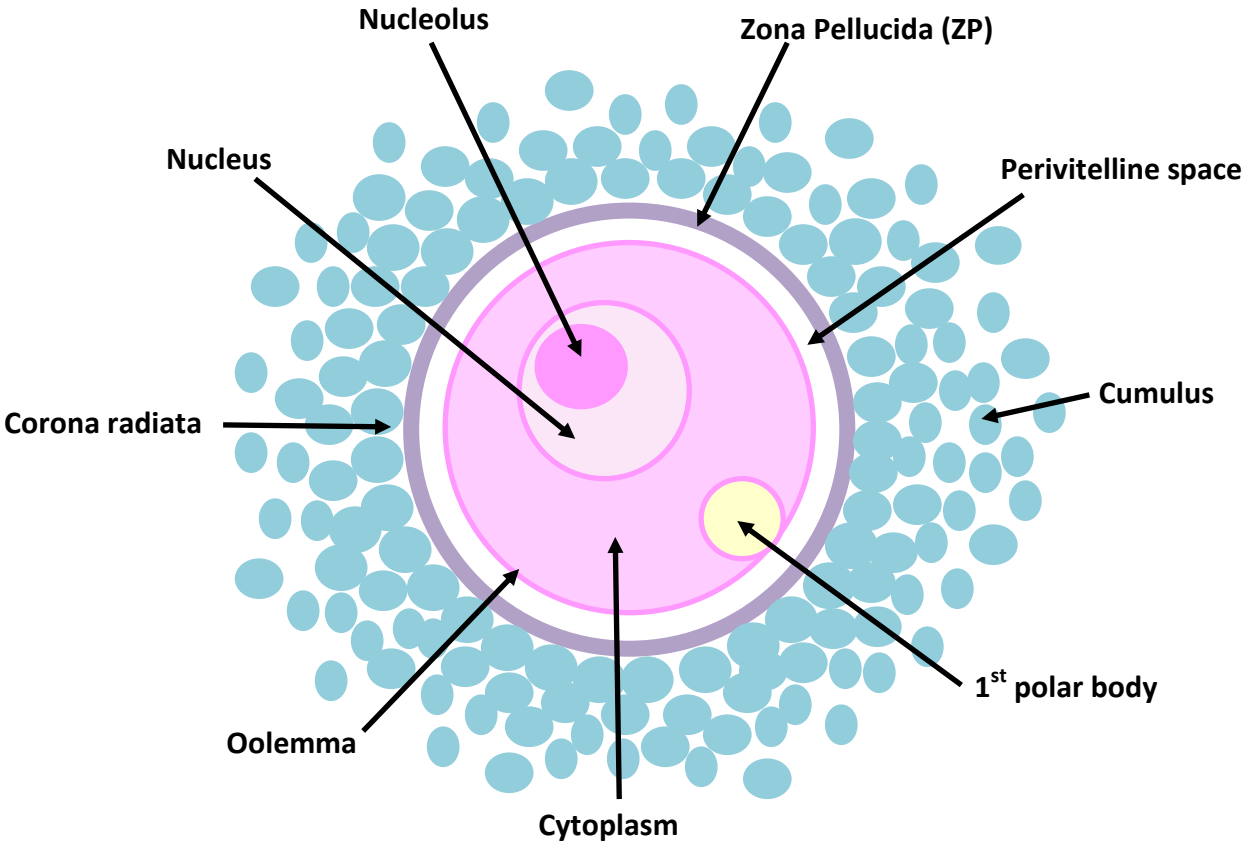

Figure 1.7 Organisation of the mammalian cumulus- oocyte complex. At the centre the oocyte contains a haploid nucleus, surrounded by a large amount of cytoplasm to support initial stages of cell division. The specialised plasma membrane (oolemma) is surrounded by the zona pellucida (ZP) a glycoprotein matrix, which provides initial contact from sperm-oocyte binding. The outermost layer of the complex is the cumulus, a hyaluranon rich cell layer that secretes progesterone necessary for chemotaxis.

1.7.1 The chemotactic role of the cumulus

Chemotactic guidance of sperm along the Fallopian tube towards the ampulla and oocyte has long been disputed (Yoshida & Yoshida, 2011). However in 2008 Oren-Benaroya *et al.*, established cumulus secreted progesterone (~1-10µM) as the chemoattractant in humans. Progesterone is a renowned regulator of mammalian sperm function and effective indicator of fertilizing ability; being shown to affect motility (Hyne *et al.,* 1978; Calogero *et al.,* 2000; Munire *et al.,* 2004), AR (Meizel & Turner 1991; Parinaud *et al.,* 1992) and $[Ca^{2+}]_i$ (Kirkman Brown *et al.,* 2003; Harper *et al.,* 2004). Therefore, it was a logical assumption that sperm cells would possess a progesterone specific receptor. Unlike somatic cells the transcriptionally and translationally inactive sperm would be unable to mediate stereotypical steroid signalling. Instead progesterone would need to regulate sperm function non-genomically through the use of intracellular second messengers (Blackmore, 1993). Recently a candidate was discovered and a mechanism of action elucidated (section 1.10.1.4; Arnoult *et al.,* 2011).

1.8 Acrosome Reaction

Capacitated sperm have the potential to undergo the AR, an exocytotic event that modifies the outer acrosomal membrane resulting in proteolytic enzyme release from the acrosomal vesicle (Figure 1.8; DasGupta *et al.,* 1994). AR is an irreversible Ca^{2+}-dependent process providing two key functions: penetration of the ZP, through the release of hyaluronidase and acrosin; and oocyte binding, through the exposure of the IAM (Harper *et al.,* 2008). *In vitro* AR has been induced by exposure to progesterone (Turner *et al.,* 1994; DasGupta *et al.,* 1994) and ZP (Bailey & Storey 1994; Shirakawa & Miyazaki, 1999). Consequently *in vivo* it is believed that progesterone produced by the female tract primes the sperm for AR permitting oocyte fusion.

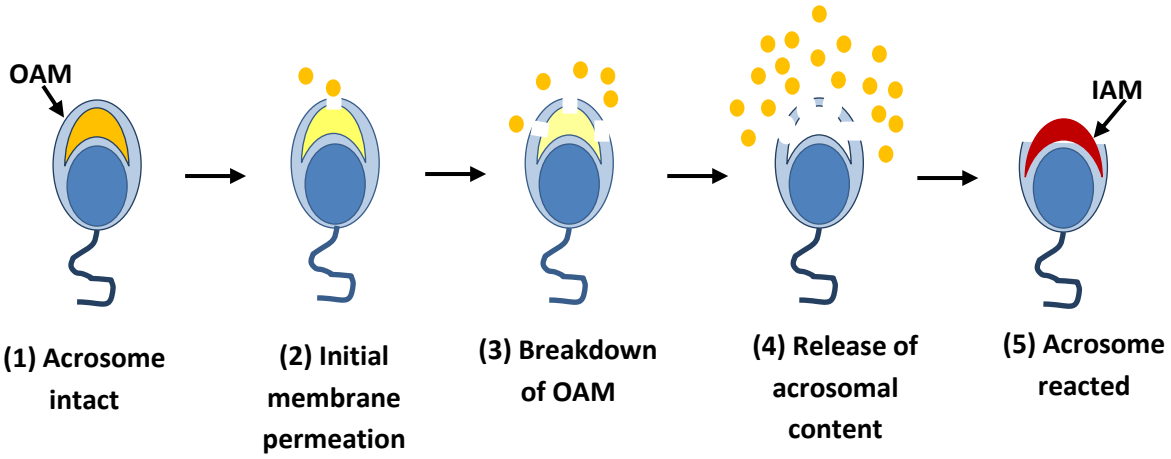

Figure 1.8 Dynamic resolution of acrosomal exocytosis involved in the acrosome reaction (AR). Under normal conditions the outer acrosomal membrane (OAM) is intact forming a cap over the anterior pole of the sperm head (1). Exposure of the cells to an AR inducing stimulus causes initial OAM permeation (2), closely followed by the breakdown of the OAM (3). Loss of the OAM results in the release of acrosomal content (hyaluronidase, acrosin and Ca^{2+}) into the immediate vicinity resulting in an acrosome reacted cell (5) with the capabililty to bind the ZP (based on a figure from Harper *et al.*, 2008).

1.8.1 Zona pellucida structure and the AR

The zona pellucida (ZP) surrounds all mammalian oocytes, an extracellular glycoprotein coat it is essential in oogenesis, fertilization and preimplantation development (Wasserman *et al.,* 2004; Wasserman & Litscher, 2013). Initial studies conducted on murine oocytes identified three distinct proteins in the ZP matrix, ZP1-3 (Bleil & Wasserman, 1980). Structural analysis revealed an interconnected matrix of all three proteins, with ZP2 and ZP3 forming "beads on a string" like filaments joined in a three dimensional assembly by ZP1 (Greve & Wasserman, 1985). A series of fertilization experiments on ZP-null mice revealed an essential role for ZP3 and ZP2 in sperm binding. Loss of ZP3 leads to ZP malformation and female factor infertility (Wasserman & Litscher, 2008). The carboxyl-terminus of ZP3 was shown to perform as a primary sperm receptor and inducer of AR, while ZP2 functions as a secondary sperm receptor in sperm-oocyte fusion (Rankin *et al.,* 1996; 1998; Rankin & Dean, 1996).

Initial characterisation of the human ZP identified three ZP protein homologues of murine ZP1-3 (Shabanowitz & O'Rand, 1988; Chamberlin & Dean, 1990). Subsequent studies of other mammalian systems revealed species specific disparities in ZP structure. An SDS-PAGE study of human ZP composition initially identified four ZP protein populations, ZP1, ZP2 and two ZP3 subpopulations ZP3H (high Mr) and ZP3L (low Mr; Bercegeay *et al.,* 1995). Lefievre *et al.,* 2004 was the first to use a proteomic based approach to definitively identify the presence of four distinct ZP glycoproteins in the human. Christened ZP1, ZP2, ZP3 and ZPB (now ZP4, this discovery called for a change in the nomenclature of ZP glycoproteins) human ZP1 (low abundance) and ZP4 show 47% sequence similarity (Gupta *et al.,* 2012).

In mouse and human models ZP proteins induce AR and the associated biphasic calcium influx, best characterised in the mouse (Bailey & Storey 1994; Shirakawa & Miyazaki, 1999; Cross *et al.,* 1988; Patrat *et al.,* 2000). In acrosome intact sperm of the mouse, ZP3 receptors on the OAM bind oocyte ZP3, inducing the opening of T-type VOCCs and a transient influx of calcium. During this initial phase $[Ca^{2+}]_i$ rises rapidly (50sec) from nanomolar to micromolar levels (Arnoult *et al.,* 1996; O'Toole *et al.,* 2000). Subsequently the transient phase recedes followed by a slower and sustained $[Ca^{2+}]_i$ elevation maintained by continued ZP3 contact. Sperm interaction with ZP3 activates a PLC signalling cascade generating IP_3, which in turn mobilises Ca^{2+} from the acrosome (Roldan & Shi, 2007; Walensky & Snyder, 1995). Sperm-ZP3 binding causes an intracellular pH elevation mediated via a G-protein dependent pathway that when inhibited can prevent fertilization (Rockwell & Storey, 2000; Arnoult *et al.,* 1996).

In experiments conducted using both affinity purified native or recombinant human ZP proteins, ZP1, ZP3 and ZP4 have all bound capacitated sperm independently inducing AR in a manner analogous to that described above (Cross *et al.,* 1988; Fraken *et al.,* 2000; Chakravarty *et al.,* 2005; 2008). However multiple possible sperm-ZP binding sites in the human suggest a more complex ZP structure (Gupta & Bhandari, 2011). Both mouse and human ZP2 only bind the IAM of acrosome reacted sperm, supporting a role for ZP2 in sperm-oocyte fusion, (Kerr *et al.,* 2002; Gupta *et al.,* 2012). Recent studies by Avella *et al.,* 2013 have identified cleavage of ZP2 as a definitive block to polyspermy; however the cognate sperm receptor is still unknown.

1.8.2 Progesterone induced AR

The biphasic $[Ca^{2+}]_i$ response associated with sperm-ZP induced AR is also observed when sperm are exposed to progesterone (Blackmore, 1993). A steroid hormone, progesterone is produced throughout the female reproductive tract; however it is surrounding the oocyte that progesterone concentration peaks (~1-10μM; Benaroya *et al.,* 2008). Ultimately it is the role of granulosa cells of the oocyte cumulus to secrete progesterone and maintain a chemotactic gradient along the Fallopian tube, providing sperm with a mechanism for navigating the female tract (section 1.7.1).

In vitro 3μM progesterone produces a biphasic Ca^{2+} response and induction of AR characteristic of ZP3-sperm interaction (Kirkman-Brown *et al.,* 2000). As with ZP induced AR there is an initial rapid transient increase in $[Ca^{2+}]_i$ succeeded by a slower sustained response with observable oscillations, maintained by the presence of progesterone in the extracellular medium (Meizel & Turner, 1991; Kirkman-Brown *et al.*, 2000). Application of progesterone in this manner is incongruous with models of chemotactic gradient exposure *in vivo*. A more authentic methodology involving the application of progesterone in a logarithmic gradient failed to induce the initial Ca^{2+} transient but activated heterogeneous oscillatory responses (Harper *et al.,* 2004). These variable Ca^{2+} oscillations observed during the sustained phase were present in ~45% of the cell populations and mirror those observed by cyclical refilling of somatic cell stores (Harper *et al.,* 2004; Bedu-Addo *et al.,* 2007). Overlaying of calcium fluorescence and phase contrast images revealed a correlation between the Ca^{2+} spikes and asymmetrical bending of the midpiece, a characteristic of hyperactivated motility which would aid penetration of the outer egg vestments (Harper *et al.,* 2004; 2005). Dynamic resolution of the AR induced by A23187 revealed that cells which undergo the AR prematurely loose their capacity for functional motility (Harper *et al.,* 2008). These

observations emphasize the importance of Ca^{2+} stores in sperm. Oscillations observed by Harper *et al.,* 2004 originated at the PHN not the acrosome (a known Ca^{2+} store). They are believed to be the result of a second Ca^{2+} store predominantly involved in the regulation of motility having particular consequence during hyperactivation (Costello *et al.,* 2009). Unlike ZP induced AR the intracellular mechanism responsible for the Ca^{2+} response is acutely debated. Recent advances have isolated a PM progesterone receptor CatSper, however how this functions in conjunction with intracellular Ca^{2+} stores remains to be elucidated (Strunker *et al.,* 2011; Brenker *et al.,* 2012).

1.9 Key stages of Fertilization

The ultimate goal of each sperm is oocyte fusion. Only a single spermatozoon from the millions present in an ejaculate can achieve this objective. Navigation of the female tract removes the least worthy competitors from the race; typically morphologically abnormal these cells are phagocytosed by leukocytes. Those cells with capacitation potential traverse the maze-like crevices of the oviduct to locate the oocyte (Holt & Fazeli, 2010).

Once at the oocyte sperm still have five more obstacles to overcome before successful fertilization (Figure 1.9); (1) dispersal of the cumulus oophorus, where hyperactivated activity enables passage, (2) The acrosome reaction, exposing the inner acrosomal membrane (Jagannathan *et al.,* 2002). (3) Penetration of the ZP aided by hyaluronidase and acrosin released from the acrosome where (4) the successful sperm will bind to the oolemma and (5) fuse with the membrane depositing its nuclear material into the oocyte. It has been noted that the oocyte has regions rich in microvilli where fusion almost always occurs (Evans, 2002). The detailed molecular mechanism is still yet to be elucidated but a number of molecules

have been identified in binding and fusion processes. On oocytes CD9, GPI-anchored proteins and integrins have all been investigated as possible fusion molecules with sperm fertilin-β and cyritestin acting as points of attachment (Evans, 2002; Kaji & Kudo, 2004). It is likely that fusion occurs simultaneously at multiple points; but further research is needed to determine the exact nature of the attachment and fusion process (Zhao *et al.*, 2008).

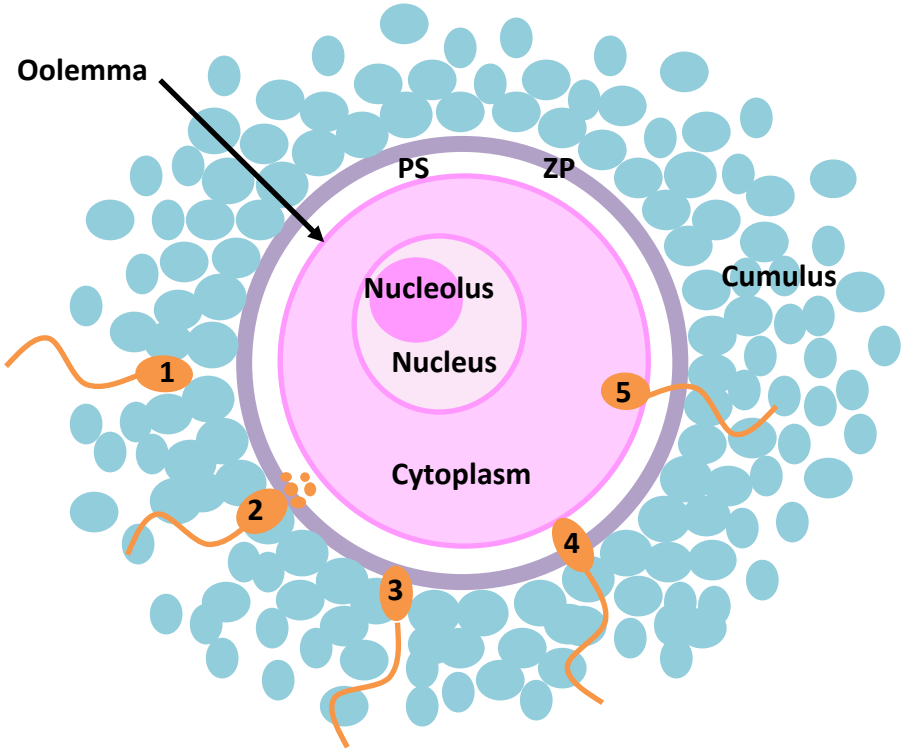

Figure 1.9 The five stages of fertilization. For successful fertilization sperm must first navigate the cumulus complex (1) then undergo the acrosome reaction (AR) (2). This in turn aid penetration of the zona pellucida (ZP) (3) binding of the oolemma (4) and finally fusion of the two gametes (5). (PS) Perivitelline space.

1.10 The Essential role of Ca^{2+}

$[Ca^{2+}]_i$ is an essential modulator of cell function and as a result, stringent regulation of $[Ca^{2+}]_i$ is imperative. Intracellular Ca^{2+} stores are integral in the management of cytoplasmic $[Ca^{2+}]$ and contribute significantly to the generation of complex $[Ca^{2+}]$ signals such as oscillations and waves in somatic cells (Costello *et al*., 2009).

A highly specialised 'minimalist' cell, the mature spermatozoon has removed all superfluous cytoplasm and intracellular organelles including ER during spermatogenesis discussed previously (Lefievre *et al.,* 2007). Although some evidence of mRNA presence has been reported in the mature sperm cell it is generally accepted that nuclear DNA translation or transcription does not take place due to its highly condensed nature rendering it inactive. Therefore sperm are dependent on manipulation of second messenger concentrations for the management of intracellular inherited proteins (Jimenez-Gonzalez *et al*., 2006). Ca^{2+} is a second messenger found abundantly in sperm and Ca^{2+} signalling regulation is crucial in fundamental sperm behaviours including hyperactivation, chemotaxis, AR and various capacitation events (Kirkman-Brown *et al*., 2003; Publicover *et al*., 2007). With responsibility for a vast range of cellular processes in sperm it is essential that Ca^{2+} signalling be tightly controlled. Several studies have identified Ca^{2+} signalling impairment in sperm as the source of male sub-fertility (Hildebrand *et al*., 2012; Nomikos *et al*., 2011; Khattri *et al*., 2012). Here I shall discuss intracellular and PM Ca^{2+} channels and evidence for their presence in human sperm and Figure 1.10 is included as a system overview.

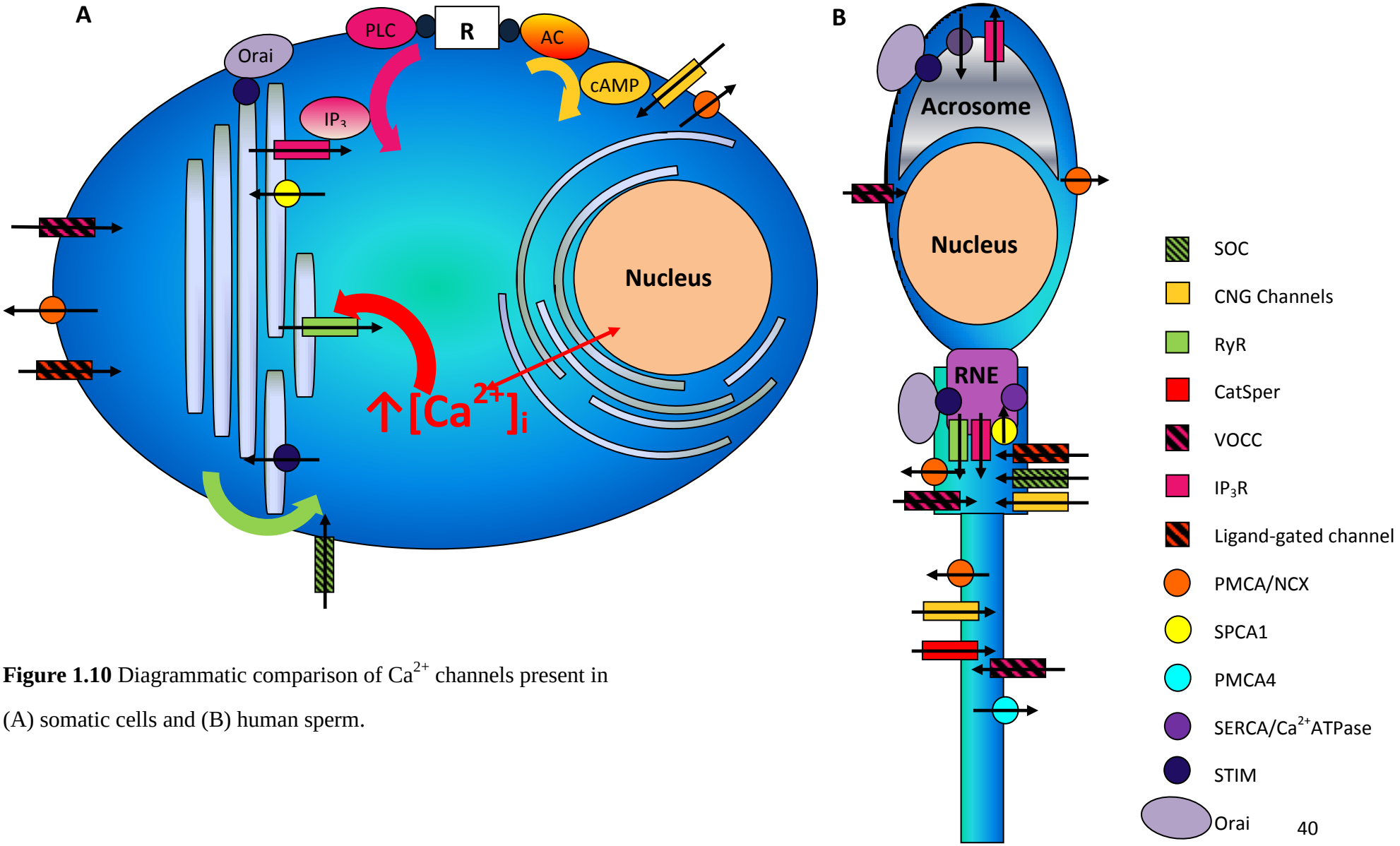

Figure 1.10 Diagrammatic comparison of Ca^{2+} channels present in (A) somatic cells and (B) human sperm.

1.10.1 Calcium channels located at the plasma membrane

At present four calcium channel candidates responsible for PM Ca^{2+} influx have been detected in human sperm. Storage operated Ca^{2+} channels (SOCs), including STIM, Orai and TRPC, voltage operated Ca^{2+} channels (VOCCs), cyclic nucleotide gated channels (CNG) and the sperm specific CatSper channel have all been identified in mature sperm. All have the potential to induce an increase in cytoplasmic $[Ca^{2+}]_i$ upon activation, the result of extracellular Ca^{2+} influx.

1.10.1.1 Storage Operated Ca^{2+} Channels (SOCs)

Cytosolic $[Ca^{2+}]_i$ elevation is the result of PM Ca^{2+} influx or Ca^{2+} release from intracellular stores. Typically both mechanisms are required to facilitate cyclical Ca^{2+} store mobilisation and sustained Ca^{2+} signalling (Putney, 2011). In order to achieve this cells require Ca^{2+} channels responsible for intracellular Ca^{2+} store mobilisation and activation of external Ca^{2+} influx otherwise known as store operated Ca^{2+} entry (SOCE) or capacitative Ca^{2+} entry (CCE). SOCs are Ca^{2+} permeable channels localised to the PM of human sperm (Costello *et al*., 2009). Recent studies in somatic cells have also suggested a role for SOCs in the initiation of downstream signalling cascades in spatially restricted areas close to Ca^{2+} entry points (Putney, 2011).

SOC activation is caused by depletion of an intracellular Ca^{2+} store, typically the ER (Berridge *et al*., 2000). In somatic cells SOCE can be induced through the application of agonists that initiate intracellular Ca^{2+} store depletion including Thapsigargin, IP_3 and incubation in Ca^{2+} free media (Putney, 2011). The SOCE associated transport of Ca^{2+} across the plasma membrane and direct deposition into the cytoplasm causes a small electrical current. Identified in 1992 by Hoth and Penner, I_{CRAC} or Ca^{2+} release activated Ca^{2+} current is

the best characterised SOC current. The CRAC channel is distinguishable as a non-voltage gated, highly Ca^{2+} selective SOC with both low conductance and low permeability to large ions. CRAC channels have been identified in T-cells, mast cells and haematopoietic cells (Lewis, 2011; McNally & Prakriya, 2012; Smyth *et al*., 2006).

An integral component in the SOC activation pathway is communication between intracellular Ca^{2+} stores and PM CRAC channels. Initial findings suggested transient receptor potential channels (TRP) were the membrane channel responsible for I_{CRAC} (Liu *et al*., 2000; Rosado & Sage, 2000; Parekh & Putney 2005). Initial hypotheses for CRAC channel activation relied on the production of an essential diffusible second messenger. Termed CIF (Ca^{2+} influx factor) this second messenger was produced by the Ca^{2+} store in response to decreased $[Ca^{2+}]_i$, instigating both $iPLA_2\beta$ and liposolid production, to induce CRAC activation (Cahalan *et al*., 2009). Although $iPLA_2\beta$ and liposolids have both been identified their presence was proven redundant by these recent results. However with the identification of two interactive transmembrane protein groups consecutively in 2005 and 2006 a new model has developed. Stromal interaction molecules (STIM) and Orai are located in the ER membrane and plasma membrane respectively (Liou *et al.,* 2005; Feske *et al*., 2006) together they form a conformational coupling mechanism enabling successful SOCE.

1.10.1.1.2 Stromal Interaction Molecule (STIM)

STIM is a type-I transmembrane protein localised to the ER of resting somatic cells. In humans two homologues STIM1 and STIM2 were identified in a HeLa cell screen (Liou *et al.,* 2005), demonstrating 61% sequence similarity between each other and 60% sequence similarity with Drosophila Stim proteins (Cahalan, 2009). At present STIM homologues have been identified in most species, however an increase in number of homologues present in

vertebrates has led to the assumption that the Stim gene duplicated about 500 million years ago during the invertebrate-vertebrate transition (Cahalan, 2009).

STIM1 was originally characterized in somatic cells as a glycosylated phosphoprotein constituting ~25% of the PM. The primary polypeptide sequence of STIM proteins reveals a modular structure consisting of two protein-protein interaction domains. Further structural analysis revealed the STIM1 N-terminus resides in the ER lumen, encompassing a single EF-hand Ca^{2+} binding motif that acts as a luminal Ca^{2+} sensor (Zhang, 2005; reviewed by Frischauf 2008). A sterile alpha motif (SAM) containing two N-linked glycosylation sites link the N-terminus and EF-hand to the transmembrane region. A single pass transmembrane protein the STIM1 polypeptide emerges on the cytoplasmic face. Here the C-terminus extends into the cytoplasm with three coiled-coil domains (CC1, CC2 and CC3) overlapping an erzin-radixin-moesin (ERM)-like domain terminating with glutamate, serine/proline, serine/threonine and lysine-rich regions (Kim & Muallem, 2011; Frischauf, 2008).

Identified concurrently by two independent groups, STIM was the result of siRNA screens aiming to identify SOCE proteins. The Drosophila S2 cells used in one study possessed CRAC channels similar to those observed in human T lymphocytes (Roos *et al*., 2005), while the second study identified the human isoforms STIM1 and STIM2 from HeLa cells (Liou *et al*., 2005). In both studies the SERCA (sarcoplasmic-endoplasmic reticulum Ca^{2+}-ATPase) inhibitor Thapsigargin was administered in order to deplete the intracellular Ca^{2+} stores (Zhang *et al*., 2005; Cahalan, 2009). Furthermore Liou *et al*., 2005 created STIM1 and STIM2 knockout mice to observe the effect on SOCE, in both instances decreased SOCE was observed implicating STIM in CCE regulation.

Current CRAC channel activation models propose that in the basal state when ER Ca^{2+} store is filled Ca^{2+} is bound to the low affinity EF-hand and STIM exists as a dimer stabilised by C-terminal coiled-coil domains (Baba *et al*., 2006; Stathopulos *et al*., 2006; Williams *et al*., 2001). When the ER Ca^{2+} store is depleted, Ca^{2+} disassociates from the EF-hand initiating unfolding of the SAM domain and STIM oligomerization. Both natural and chemically induced oligomerization triggered redistribution close to the plasma membrane and CRAC channel activation, without any obvious changes to ER structure expected by a marked redistribution of STIM (Cahalan *et al*., 2009; Stathopulos *et al*., 2006). FRET (Forster Resonance Energy Transfer) imaging has identified predetermined foci for STIM translocation, these region are located in the ER periphery where close contact with the plasma membrane can be formed (Muik *et al.*, 2008). Upon contact with the PM STIM triggers SOCE but does not contribute to the CRAC channel itself, instead STIM relocates rapidly following signal termination believed to be the consequence of a negative feedback loop (Liou *et al.*, 2007; Cahalan *et al*., 2009).

1.10.1.1.3 Orai

The PM component of SOCE, Orai was initially identified by three groups in 2006 (Feske *et al*., 2006; Vig *et al*., 2006; Zhang *et al*., 2006). The product of RNAi Drosophila S2 screens, Orai1 was categorised as a critical component in store SOC entry downstream of STIM proteins (Prakriya *et al*., 2006). TRPC channels have also been shown to interact with STIM proteins, but do not show CRAC channel characteristics. Identification of Orai as the pore-forming subunit of CRAC channels came after a series of mutation studies on essential Orai structural residues, with one group identifying a role for Orai in severe combined immune deficiency (SCID; Feske *et al*., 2006; Prakriya *et al*., 2006; Yeromin *et al*., 2006). To date three Orai isoforms have been classified in mammalian systems (Orai 1-3). Believed to reside

solely in the PM Orai isoforms consist of four hydrophobic transmembrane spanning domains with both the N and C termini situated in the cytoplasm (Feske *et al*., 2006; Muik *et al*., 2012; Soboloff *et al*., 2012). There is a proline/arginine-rich region at the N-terminus and an N-glycosylation site within the extracellular loop between transmembrane segments 3 and 4 (Frischauf, 2008). In addition four glutamic residues are highly conserved between species and are fundamental in the formation of effective PM Ca^{2+} channels (Prakriya *et al*., 2006).

Current evidence establishes a relationship between STIM and Orai1 proteins in CRAC channel formation. In mammalian systems STIM1, unlike STIM2 has been shown to strongly activate all three Orai homologues producing I_{crac} currents in patch-clamp studies (Mercer *et al*., 2006; Feske *et al*., 2006; Muik *et al*., 2012; Soboloff *et al*., 2012). In addition Orai point mutations (Prakriya *et al*., 2006; Vig *et al*., 2006) and photo-bleaching GFP (green fluorescent protein tagged)-tagged Orai subunits revealed an Orai tetramer is the predominant activated CRAC channel (Ji *et al*., 2008; Penna *et al*., 2008, Maruyama *et al*., 2009; Roberts-Thomson *et al*., 2010).

STIM1 oligomerization is triggered through EF-hand-SAM domain interactions and stabilised by coiled-coil interactions at the C-terminus upon intracellular Ca^{2+} store depletion. Multimerisation of stable STIM1 oligomers is sufficient to induce translocation adjacent to the plasma membrane and organise neighbouring Orai subunits into plasma membrane clusters, where CRAC channel Ca^{2+} influx occurs (Luik *et al*., 2008; Soboloff *et al*., 2012). Preliminary STIM and Orai co-immunoprecipitation studies coupled with FRET and electron microscopy measurements demonstrated increased interaction strength after Ca^{2+} store depletion over a 10-25nm ER-PM gap providing evidence for direct physical interaction between the proteins (Yeromin *et al*., 2006; Muik *et al*., 2008; 2012; Calloway *et al*., 2009).

The CRAC activation domain (CAD) or STIM1 Orai activating region (SOAR) of the STIM1 C-terminus is responsible for the recruitment and activation of Orai (Park *et al*., 2009; Yuan *et al*., 2009; Huang *et al*., 2006). Composed of 98 amino acids CAD/SOAR contains the conserved STIM1 amino acid fragment 344-442 encompassing CC2 and CC3; thus SOAR has dual roles in STIM1 oligomerization and as the minimal sequence required to fully activate all Orai channels through binding to both the N- and C-termini (Soboloff *et al*., 2012; Yuan *et al*., 2009). In addition combination of SOAR with STIM1 amino acid region 450-485 permits regulation of the interaction strength (Yuan *et al*., 2009).

The biphasic $[Ca^{2+}]_i$ response of human sperm to progesterone is well characterised (Kirkman-Brown *et al*., 2000; Harper *et al*., 2004) but the mechanism of action is little understood. Recent detection of the presence of STIM and Orai analogues in human sperm acrosome and PHN/midpiece region has identified a role for SOCE in extending the transient $[Ca^{2+}]_i$ caused by agonist induced store mobilisation, such as those observed with progesterone (Lefievre *et al*., 2012). Studies using somatic cells have localised STIM proteins to the membrane of intracellular Ca^{2+} stores (Liou *et al*., 2005; Roos *et al*., 2005). In human sperm the acrosome acts as an ER-like Ca^{2+} store and shows a strong association with IP_3R (Herrick *et al*., 2005). In addition localisation of IP_3R to the PHN region provides evidence for a second Ca^{2+} store possibly associated with motility; however this second store has yet to be characterised in depth (Naaby-Hansen *et al.*, 2001; 2010).

1.10.1.1.3 Canonical transient receptor potential channels (TRPC)

Transient receptor potential canonical channels are six pass transmembrane cation channels. Initially identified in Drosophila photoreceptors, *TRP* have been reported to act as molecular sensors of environment, which is an essential initiator of CCE (Kumar & Shoeb, 2011). Mammalian homologues of TRP include TRPC, TRPV and TRPM. TRPC has been found in a wide range of mammalian tissues including the human testis and mature sperm cells (Trevino *et al*., 2004; Castellano *et al*., 2003). Castellano *et al*., 2003 identified RNA messengers for TRPC1, 3, 6 and 7 in human spermatogenic cells by reverse transcription polymerase chain reaction (RT-PCR). Confocal immunofluorescence localised TRPC1, 3, 4, and 6 to the cell surface of the sperm head and all TRPCs to the flagellum suggesting a contributing role in motility which looked promising. When STIM proteins were discovered in 2005 TRPCs were initially considered to be the plasma membrane CRAC channel component. Like Orai TRPCs form multimeric complexes which allow cation entry in response to depleted calcium or agonist stimulation and have been shown to interact with STIM (Liao *et al*., 2008; Salido *et al*., 2011). However the discovery of Orai as the CRAC channel in 2006 placed less significance on TRPC contribution to SOCE.

.

1.10.1.2 Voltage Operated Ca^{2+} Channels (VOCCs)

VOCCs are the most well defined Ca^{2+} channel family characterised by their ability to induce increases in $[Ca^{2+}]_i$ in response to membrane depolarization (Catterall, 2000; Darszon *et al*., 2011). Also known as Ca_V channels, VOCCs are categorised as either high voltage activated (HVA) or low voltage activated (LVA). HVA channels are distinguished by the requirement for strong depolarisations to stimulate followed by a slow inactivation; initially subdivided into L, N, P/Q, and R types dependent on electrophysiological properties current nomenclature gives two subfamilies Ca_V1(L) and Ca_V2(N, P/Q & R; Catterall, 2000;

Jimenez-Gonzalez *et al*., 2006). Unlike HVA, LVA channels require small membrane depolarisations to activate and inactivate quickly; termed T type VOCCs due to their transient nature they now form the Ca_V3 family (Darszon *et al*., 2011).

All VOCCs are transmembrane proteins which exhibit strong structural similarity and result from a complex of proteins. At the VOCC centre is the pore-forming α1 subunit ~190-250kDa comprised of four homologous domains (I-IV) joined by cytoplasmic linker regions. Each α1 domain contains six transmembrane helices (S1-S6) with a non-helical P-loop between S5-S6, which determines ion conductance and selectivity in the channel pore (Jimenez-Gonzalez *et al*., 2006). In addition the α1 subunit is surrounded by a transmembrane, disulphide linked complex of α2 and δ subunits and an intracellular β subunit, in some family members a transmembrane γ subunit is also associated (Catterall, 2000).

Multiple studies provide evidence for VOCC expression in mammalian mature and immature sperm cells (Arnoult *et al*., 1996; Lievano *et al*., 1996). Although patch-clamping only identified LVA currents in human sperm (Jagannathan *et al*., 2002), antibody immunostaining techniques have identified the presence and localisation of T, L (Goodwin *et al*., 2000), R, P/Q (Trevino *et al*., 2004) and N type (Wennemuth *et al*., 2000) channels. In human sperm VOCCs occupy distinct regions for example T-type channel $Ca_V3.3$ is localised at the midpiece and $Ca_V3.2$ in the principal piece and posterior sperm head (Serrano *et al*., 1999). VOCCs are believed to participate in mediation of bicarbonate-cAMP signal in a process regulated by PKA and CaM causing Ca^{2+} influx and hyperactivation, however their role has been overshadowed by the discovery of CatSper (Darszon *et al*., 2011).

1.10.1.3 Cyclic Nucleotide Gated Channels (CNG)

CNG channels are PM non-selective cation channels activated by the binding of cyclic nucleotides cGMP or cAMP (Biel & Mikelakis, 2007; 2009). Originally identified in vertebrate photoreceptor cells the channels are important cellular switches that trigger cation influx in response to increases in cGMP or cAMP concentration (Wang *et al*., 2007). As a result CNG channels can contribute to increased levels of intracellular [Ca^{2+}] and have been identified in numerous mammalian cell types; most notably in sensory neurons involved in vision and olfaction where they are the terminus of photon absorption and odorant binding signal transduction (Biel & Mikelakis, 2009). CNG channels consist of a complex heteromeric structure; the core contains six α-helical segments (S1–S6) with an ion-conducting pore loop between S5 and S6. Segment 4 carries an overall positive charge with regularly spaced arginine and lysine residues, both termini are located on the cytoplasmic face with the cyclic nucleotides binding the C- terminus at a CNBD domain (Biel, 2009).

CNG have been identified in mammalian sperm (Cisneros-Mejorado & Sánchez, 2011; Weyand *et al*., 2004) along with cAMP, conversely cGMP and its associated pathway components (PDE and PKG) are low or absent (Lefievre *et al*., 2000). The cAMP/ sAC/ PKA pathway has proved essential in sperm function and is implicated in capacitation processes, however Brenker *et al.*, 2012 identified GPCR's and cAMP were unnecessary for odorant induced Ca^{2+} signalling through CatSper channels, see below.

1.10.1.4 CatSper Channels

Sperm-associated cation channels, CatSper are a pH sensitive family of proteins expressed exclusively in the principal piece PM of sperm (Ren *et al*., 2001; Shukla *et al*., 2012). Their ideal position proposes CatSper participation in motility regulation; moreover disruption of

CATSPER1 induced sperm motility defects resulting in male infertility (Ren *et al*., 2001). Four highly homologous six transmembrane spanning CatSper proteins have been identified CatSper1 (Ren *et al*., 2001), CatSper2 (Quill *et al*., 2001), Catsper3 and Catsper4 (Lobley *et al*., 2003), all are believed to participate equally in ion channel formation (Shukla *et al*., 2012). Current models suggest the functioning ion channel is a multiple protein complex containing tetramer pore forming subunit composed of CatSper (1-4), associated with a 2-TM CatSperB (also known as CatSperβ; Li *et al*., 2007), the single-TM CatSperγ and CatSperδ (Qi *et al*., 2007; Wang *et al*., 2009; Chung *et al*., 2011) isolated via protein purification. It is suggested that more auxiliary proteins may have a weak association with the channel but were unable to withstand the abrasive detergents used in the purification process.

In human studies CatSper (1-4) mRNA has been localised exclusively to testicular tissues (Jin *et al*., 2005; Qi *et al*., 2007; Quill *et al*., 2001; Ren *et al*., 2001). In mouse CatSper2 transcription in pachytene spermatocytes precedes CatSper1, 3 and 4 transcription in spermatids (Ren *et al*., 2001; Jin *et al*., 2005; Qi *et al*., 2007). Li *et al*., 2007 showed a correlation between frequency of CatSper transcripts in human semen samples and sample motility. Initial studies conducted in CatSper null mice identified loss of a single CatSper subunit did not inhibit motility; however transition to hyperactivation was prevented rendering the mice infertile (Ren *et al.*, 2001; Quill *et al.*, 2003; Jin *et al.*, 2007; Qi *et al.*, 2007); reinforced by a clinical case of hereditary infertility caused by CatSper2 deletion (Avidan *et al*., 2003).

Recent results from two studies have identified a role for CatSper as the elusive non-genomic progesterone receptor in human sperm (Lishko *et al*., 2011; Strunker *et al*., 2011). To date

CatSper is the sole Ca^{2+} permeable channel detected by patch clamp studies of mature sperm (Kirichok & Lishko, 2011). Both groups utilised patch clamping to demonstrate nanomolar progesterone concentrations and alkaline pH activate a rapid Ca^{2+} influx through CatSper channels (Lishko *et al.,* 2011; Strunker *et al.,* 2011). NNC-55–0396 (2μm) and mibefradil (30μm & 40μm) abolished CatSper currents but although they significantly inhibited the progesterone-induced Ca^{2+} response they did not eliminate the response entirely (Jensen & Publicover, 2012; Strunker *et al.,* 2011; Sagare-Patil *et al.* 2012). These results suggest that although CatSper undoubtedly contributes to the Ca^{2+} influx associated with progesterone a further source of Ca^{2+} must also be responsible. A further study has reported CatSper activation as a result of several small organic molecules including bourgeonal (a chemotactic agent) suggesting a promiscuous receptor that may function as a polymodal, chemosensory Ca^{2+} channel via a mechanism that does not involve metabotrophic receptors, cAMP or it's analogues (Brenker *et al*., 2012).

1.10.2 Calcium clearance mechanisms

The process of maintaining $[Ca^{2+}]_i$ and returning$[Ca^{2+}]_i$ to basal levels post-stimulation is important in all eukaryotic cells. This stringent control of $[Ca^{2+}]_i$ is achieved through the process of calcium clearance either into intracellular Ca^{2+} stores or the extracellular environment. In somatic cells the ER has been clearly identified as the Ca^{2+} store but since the ER is notably absent from human sperm the acrosome (Herrick *et al*., 2005), mitochondrion and remnants of the nuclear envelope (RNE; Ho & Suarez, 2003) are believed to fulfil this role. Presently three mechanisms for calcium clearance have been identified in human sperm and are discussed below.

1.10.2.1 Calcium ATPases (Ca^{2+} ATPases)

Ca^{2+} ATPases belong to the P-type family of ATPases, which utilize ATP to transport Ca^{2+} across membranes. During this process the ATPases are transiently phosphorylated causing a conformational change from low affinity E1 structure to a high affinity E2 structure proposed by de-Meis and Vianna (1979). Currently three classes of Ca^{2+} ATPases have been identified in somatic cells; the plasma membrane Ca^{2+} ATPase (PMCA), the sarcoplasmic-endoplasmic reticulum Ca^{2+} ATPase (SERCA) and the secretory pathway Ca^{2+} ATPase (SPCA; Michelangeli *et al*., 2005). Structurally PMCA, SERCA and SPCA are analogous with approximately 30% sequence similarity (Gunteski-Hamblin *et al*., 1992). The elucidation of SERCA1A crystal structure in 2004 and subsequently SERCA2 and 3 gave a basis for Ca^{2+} ATPase structure and function of the P-type family. SERCA1A was shown to comprise of 10 TM domains (also known as the M domain) and three cytoplasmic domains A, N and P responsible for ATP binding; phosphorylation and an actuator domain which contributes to transmembrane helices re-arrangement, allowing the Ca^{2+} translocation (Brini & Carafoli, 2011; Toyoshima, 2009).

Schatzmann (1966) initially identified PMCA in erythrocytes, since then PMCA have been characterised in numerous cell types including mammalian sperm. PMCA are the largest Ca^{2+} ATPase subgroup due to an additional auto-inhibitory calmodulin binding site at the C-terminus (Brini & Carafoli, 2009; 2011); when bound calmodulin decreases the Ca^{2+} affinity of the pump whilst acidic phospholipids have the opposite effect (Brini & Carafoli, 2009). Several studies employing western blotting and immuno-localisation techniques have identified PMCA4 as the main isoform present in both testis and sperm, identifying the principal piece as its primary location (Wennemuth *et al*., 2003; Okunade *et al*., 2004; Schuh *et al*., 2004). PMCA4 knockout mice exhibited normal ejaculates which failed to respond to

capacitative conditions and induce hyperactivated motility resulting in male infertility (Okunade *et al*., 2004). Detection of $[Ca^{2+}]_i$ showed elevated $[Ca^{2+}]_i$ levels in PMCA4 null mice (370nM) compared the WT (157nM) after an hours incubation in capacitation medium, effects mirrored by the application of PMCA inhibitor 5-(and-6)-carboxyeosin diacetate succinimidyl ester (Schuh *et al*., 2004). These observed effects imply a role for PMCA's in capacitation.

Conflicting evidence for the presence of SERCA in sperm has made their impact on calcium clearance controversial. Rossato *et al*., 2001 revealed application of 10-100nM thapsigargin (a potent SERCA-specific inhibitor) induced both Ca^{2+} mobilisation and AR in sperm. In addition SERCA were localised to the acrosome and mid-piece of sperm using a fluorescent thapsigargin analogue (BODIPY-FL-thapsigargin). More recent studies using SERCA specific antibodies have failed to detect the presence of SERCA1 in human sperm (Harper *et al*., 2005). However SERCA2 has been identified in the acrosome and midpiece of human sperm (Lawson *et al*., 2007) and SERCA3 mRNA has been identified in mature sperm cells (Hughes *et al*., 2000) in addition to a thapsigargin response similar to that observed by Rossato *et al*., 2001 in round rat spermatids. Together these findings implicate a role for SERCA in $[Ca^{2+}]_i$ control.

SPCA1 and 2 are mammalian homologues of Pmr1 initially identified in *S. cerevisiae* (Gunteski-Hamblin *et al*., 1992). In somatic cells SPCA are associated with membrane bound organelles predominantly the Golgi apparatus (Wuytack *et al*., 2002; Vandecaetsbeek *et al*., 2012). Thought to participate in both Ca^{2+} and Mn^{2+} regulation within the Golgi network, the use of microscopy was unable to distinguish an association with the *cis* or *trans* network exclusively (Michelangeli *et al*., 2005; Wuytack *et al*., 2002). Unlike SERCA and PMCA

there is no known SPCA1 specific inhibitor. However bisphenol has been shown to be equally potent at inhibiting both SPCA1 and SERCA (Harper *et al*., 2005). SPCA1 has been identified and localised to the anterior midpiece analogous with the PHN region in human sperm (Harper *et al*., 2005; Ho & Suarez, 2003). Here, Harper and Collegues demonstrated that bisphenol treatment mobilises Ca^{2+} stored at the PHN of human sperm. In addition bisphenol treatment inhibits the Ca^{2+} oscillations induced by 3μM progesterone application and characterised by Harper and collegues in 2004 (Harper *et al.*, 2005).

1.10.2.2 Na^{+}-Ca^{2+} Exchanger (NCX)

In somatic cells NCX has been associated with mediating cytoplasmic $[Ca^{2+}]_i$ decrease through both mitochondrial uptake (Palty *et al*., 2012) and external extrusion across the PM (Berridge *et al*., 2003). NCX are bidirectional dependent on the electrochemical gradients of both Ca^{2+} and Na^{+}; in forward mode the NCX typically exports one Ca^{2+} ion for the uptake of three Na^{+} ions, in reverse the opposite occurs facilitating Ca^{2+} influx (Jimenez-Gonzalez *et al*., 2006). NCX belongs to the cation-Ca^{2+} exchanger superfamily due to the presence of two highly conserved α repeats in the TM domain. NCX is composed of a single α-helical TM spanning region with a long cytosolic loop containing a high affinity Ca^{2+} binding domain (residues 371-509; Hildge, 2012). Two NCX sub-families exist NCX and NCXK (K^{+}-dependent NCX), NCX has three known isoforms NCX(1-3) and multiple splice variants (Hildge, 2012; Jimenez-Gonzalez *et al*., 2006).

The presence of NCX in mammalian sperm was first identified in the rat by Bradley and Forrester 1980, who reported inhibition of plasma membrane vesicle NCX by verapamil, (Jimenez-Gonzalez *et al*., 2006). Since then RT-PCR studies have confirmed the presence of NCX1 splice variants in rat testis (NCX1.3 and NCX1.7) and NCKX3 in mouse testis

(Quednau *et al*., 1997; Kraev *et al*., 2001). NCX was first identified in human sperm in 1987 by Babcock and Pfeifer. Application of novel NCX inhibitors bepridil, DCB (3,4-dichlorobenzamil hydrochloride) and KB-R7943 on human sperm resulted in both $[Ca^{2+}]_i$ elevation and $[Na^+]_i$ reduction that coincided with loss of motility (Krasznai *et al*., 2006). Evidence from Su and Vacquier, 2002 supports a crucial role for NCX in $[Ca^{2+}]_i$ homeostasis maintenance in sea urchin sperm.

1.10.2.3 Mitochondrial Uniporter (MCU)

Mitochondrial contribution to Ca^{2+} homeostasis is well established, with mitochondria now recognised as one of the main intracellular Ca^{2+} storage organelles under normal physiological conditions. Undeniably mitochondria efficiently adapt oxidative phosphorylation to nutrient availability, ATP requirement and in response to extracellular microclimate fluctuations (Scorziello *et al*., 2013). It is not an anomaly then to acknowledge the impact of Ca^{2+} uptake on mitochondrial function, in addition to mitochondrial involvement in Ca^{2+} signal generation (Jimenez-Gonzalez *et al*., 2006). Mitochondria consist of an intracellular matrix, an inner and outer membrane. The outer membrane is permeable to ions and small molecules; however Ca^{2+} transport across the inner membrane where it is sequestered in the matrix requires a specific transporter (MCU; Patron *et al*., 2013). MCU contains two TM helices joined by a linker containing highly conserved acidic residues essential for function and two EF-hand domains (in the mitochondrial inter-membrane space). A functioning uniporter is the result of oligomerisation of MCU in the inner mitochondrial membrane and regulated by MICU1 an associated protein under basal conditions (Figure 1.14; Baughman *et al*., 2011; Mallilankaraman *et al*., 2011). Ca^{2+} uptake through MCU is an electrogenic process mediated by changes in membrane potential (Ψ_m), MICU1 establishes a threshold for Ca^{2+} uptake by binding to the EF-hands of MCU, thus preventing uptake when

$[Ca^{2+}]_{cyt}$ is low. Mutations resulting in loss of MICU1 leads to constitutive activation of MCU in somatic cells and mitochondrial Ca^{2+} uptake inducing cell death, (Mallilankaraman *et al*., 2011; Raffaello *et al*., 2012).

Mitochondria in human sperm are spatially restricted to the midpiece and believed to form a helical arrangement around a central axon as discussed previously. Isolation of mitochondria at the anterior of the flagellum potentially forms an important calcium source. Multiple studies have identified accumulation of Ca^{2+} in sperm mitochondria *in situ,* although more recent studies on intact mammalian sperm at a plethora of developmental stages suggest a variation in mitochondrial Ca^{2+} accumulation and regulation, notably bovine (Schoff, 1995; Vijayaraghavan & Hoskins, 1990) and murine where mitochondrial contribution to Ca^{2+} clearance increased when other mechanisms of uptake were inhibited (Wennemuth *et al*., 2003). A Recent study in Sea Urchin sperm reported that application of several mitochondrial inhibitory agents including CCCP (a proton gradient uncoupler) increase $[Ca^{2+}]_i$ with at least two different profiles dependent on extracellular Ca^{2+} (Darzon *et al*., 2011). Furthermore SOCC blockers (including SKF96365) and Ca^{2+}ATPase inhibitors (thapsigargin and bisphenol) antagonise Ca^{2+} influx induced by mitochondrial inhibitors, indicating an essential role for mitochondria in Ca^{2+} entry regulation through SOC's at the PM (Ardon *et al*., 2009). Nevertheless Ca^{2+} imaging of human sperm demonstrates application of mitochondrial uncoupler DNP (2,4-dinitrophenol) does not affect the mobilisation of intracellular stores responsible for progesterone induced Ca^{2+} oscillations (Harper *et al.*,

2004). Consequently mitochondrial contributions to agonist induced Ca^{2+} responses in human sperm is limited but they play a role in maintaining resting $[Ca^{2+}]_i$ homeostasis (Jimenez-Gonzalez *et al.*, 2006).

1.10.3 Ca^{2+} mobilisation from intracellular stores

Intracellular Ca^{2+} storage organelles are ubiquitous across eukaryotic cells with the most prevalent the best characterised. The ER, SR, mitochondria and nuclear envelope have all been identified as calcium stores in somatic cells. Their responsibility; to sequester superfluous Ca^{2+} and maintain basal $[Ca^{2+}]_i$ under physiological conditions and amplification of Ca^{2+} signals through the release stored Ca^{2+} upon stimulation. At present two somatic cell channels capable of mobilising stored Ca^{2+} have been identified in human sperm, the inositol 1,4,5-trisphosphate receptor (IP_3R) and the ryanodine receptor (RyR) both demonstrate localised distribution at the PHN of human sperm.

Conversely mature human sperm contain none of the intracellular organelles associated with the majority of somatic cell Ca^{2+} storage (Harper *et al*., 2004). However there is evidence for the existence of at least two unique Ca^{2+} stores. The acrosome has been shown to store Ca^{2+} proven elemental in exocytosis and ZP binding; exhibiting localised IP_3R expression on the outer surface (Herrick *et al*., 2005). The identity of the second Ca^{2+} remains controversial, localised to the PHN region and mitochondria has been implicated (Wennemuth *et al*., 2003). However it is the RNE and/or the cytoplasmic droplet situated around the sperm neck that seems a more likely candidate (Naaby Hansen *et al*., 2001; Harper *et al*., 2004; 2005).

1.10.3.1 Inositol 1,4,5-trisphosphate receptors (IP_3Rs)

Inositol 1,4,5-trisphosphate (IP_3) is a global second messenger produced in most cell systems. A small water-soluble molecule, IP_3 diffuses easily into the cytosol allowing communication of extracellular signals at the PM to intracellular organelles (Berridge, 2003; Michelangeli *et*

al., 1995; Parys & De Smedt, 2012). It's receptor IP_3R is an intracellular Ca^{2+} channel with the ability to release Ca^{2+} from intracellular stores (typically the ER) in response to IP_3 binding (Lencesova & Krizanova, 2012). IP_3R's affinity for IP_3 is modulated by $[Ca^{2+}]_{cyt}$, in isolated systems IP_3 affinity lies in the nanomolar range, however Ca^{2+} is a co-agonist of IP_3R, when $[Ca^{2+}]_{cyt}$ is low ~300nM IP_3R activity is increased (Parys & De Smedt, 2012). In mammalian systems there are three IP_3R isoforms (IP_3R 1-3), all possess a similar structure and function with ~74% sequence similarity but orchestrate the formation of different Ca^{2+} signals due to variability in associated protein interactions, organelle localisation, agonist and co-agonist affinity (Parys & De-Smedt, 2012; Taylor *et al*., 1999).

Each IP_3R gene encodes a single polypeptide composed of approximately 3000 residues, containing four major domains. The N-terminal suppressor domain (SD) encompasses the 223 amino acids at the amino terminal and is thought to contribute to the conformational change induced by IP_3 binding to the IBC domain (IP_3 binding core). The IBC itself amino acids 224-604 consists of an α and β subunit connected to SD by two flexible linkers L1 and L2 with both subdomains contributing to IP_3 binding. At the carboxy-terminus the six-time spanning transmembrane domain (TMD) makes up the Ca^{2+} channel pore (Darszon *et al.*, 2011). In between IBC and TMD is the modulatory domain. It is here that the recently identified IRBIT (Bultynck *et al*., 2003; Rossi *et al*., 2012) protein binds, interestingly it does not activate IP_3Rs but but dissociates the receptor when IP3 binds, thus regulating Ca^{2+} signalling (Darszon *et al*., 2011). In addition the modulatory domain also contains numerous phosphorylation and ATP binding sites are integral in regulation of protein function (Bosanac *et al*., 2002; da-Fonseca *et al*., 2003).

mRNA for all three IP_3R isoforms have been detected in mammalian sperm throughout differentiation and maturation and the evidence reviewed in Jimenez-Gonzalez *et al*., 2006. In addition proteins essential for agonist induced IP_3 production the G-protein (Gq) and phospholipase-α (PLCα) have both been detected in mammalian sperm, (Walensky & Snyder, 1995; Kuroda *et al*., 1999). Localisation studies have identified IP_3R1 in the acrosomal region and IP_3R3 in the RNE/PHN and midpiece region of human sperm (Walensky & Snyder, 1995; Kuroda *et al*., 1999; Naaby-Hansen *et al*., 2001). These studies also identify the presence of two separate IP_3 binding profiles consistent with variations in IP_3R isoform IP_3 affinity (Wojcikiewicz & Luo, 1998; Dyer & Michelangeli, 2001). In 2005, Herrick *et al*., used thimerosal (a known IP_3R activator) to illustrate a role for IP_3R in the acrosome reaction, demonstrating an important physiological role for IP_3R. Calreticulin (a low affinity, high capacity Ca^{2+}-buffering protein) associated with somatic cell IP_3R associated stores has also been localised to Ca^{2+} storage regions in the human spermatozoon (Naaby-Hansen *et al*., 2001; Ho & Suarez, 2003). Furthermore Ca^{2+} stored in the PHN region of human sperm is apparently mobilised by both progesterone stimulation (Harper *et al*., 2004) and 5μM thimerosal treatment which induces sustained $[Ca^{2+}]_i$ elevation and hyperactivation insensitive to NNC-55-0396 (CatSper inhibitor; Alasmari *et al*., 2013). Recent findings propose a model where CatSper and 2-APB sensitive intracellular Ca^{2+} stores contribute to the biphasic progesterone response (Lefievre *et al*., 2012).

1.10.3.2 Ryanodine Receptors (RyR)

Ryanodine is a plant alkaloid isolated from *Ryania speciosa.* Originally identified for its insecticidal properties ryanodine was found to associate with a eukaryotic membrane protein termed the ryanodine receptor (RyR; Van-Petegem, 2012). RyRs have since been identified

as an intracellular Ca^{2+} induced Ca^{2+} release channel located in the ER/SR membrane (Lanner, 2012). There are three RyR isoforms in mammalian systems sharing ~70% sequence homology (Brini, 2004), RyR1 identified in skeletal muscle, RyR2 established in cardiac muscle and RyR3 discovered in brain but since found to have the widest tissue distribution (Jimenez-Gonzalez *et al.*, 2006). All isoforms form homotetrameric assemblies making them the largest characterised ion channels (Kimlicka & Van-Petegem, 2011; Van-Petegem, 2012). Each RyR monomer contains approximately 5000 amino acid residues split into two major domains; the cap or cytoplasmic N-terminus accounts for ~80% of the protein, while the remaining 20% form the stalk traversing the membrane constituting the channel pore and projecting into the Ca^{2+} store lumen (Darszon *et al*., 2011). Currently only ~11% of RyR structure has been analysed in detail using cryo-electron microscopy but the receptor is thought to contain 6-8 transmembrane helices (Van-Petegem, 2012). What is known is that the cytoplasmic region contains multiple binding sites for small molecules and protein binding partners including Ca^{2+}, Calmodulin and calsequestrin (Kimlicka & Van-Petegem, 2011). In somatic cells RyR on intracellular Ca^{2+} stores are believed to be activated by changes in $[Ca^{2+}]_i$, although the degree of response is dependent on the RyR isoform, accessory proteins and secondary messenger (cADPR) binding. For example at high $[Ca^{2+}]_i$ CaM inhibits RyR1 and RyR2 however at low $[Ca^{2+}]_i$ it activates RyR1 but inhibits RyR2 (Ikemoto *et al*., 1995).

Evidence for RyR in mammalian sperm has shown that both RyR1 and RyR2 are present in spermatocytes and spermatids of rat (Giannini *et al*., 1995) mouse (Trevino *et al*.,1998) and cow (Minelli *et al*. 2000); however only RyR3 could be detected in the acrosomal region of mature sperm using RT-PCR and isoform specific RyR antibodies (Trevino *et al*., 1998). Harper *et al*., 2004 was the first to identify RyR in the PHN region of human sperm, using a

fluorescent ryanodine analogue (BODIPY-FL-X-ryanodine) RyRs were shown to co-localize with SPCA1 predominantly in PHN with a proportion in the acrosome. In addition RyR locality corresponds with progesterone induced $[Ca^{2+}]_i$ oscillations which were abolished upon tetracaine application (RyR inhibitor) (Harper *et al*., 2004). Chiarella *et al*., 2004 indicated a role for RyR in sperm development, high doses of ryanodine were shown to decrease spermatogonial proliferation and increase cell meiosis emphasising the importance of their physiological role. Most recently Park *et al*., 2011 conducted a series of prostasome fusion experiments, in which RyR2 depleted sperm had both reduced sperm motility and low fertilization success. These findings demonstrate an essential role for RyR in cADPR-mediated Ca^{2+} mobilization at the PHN with particular significance when exposed to progesterone.

1.11 Research aims

The core objective of this research thesis was to characterise mobilisation of stored Ca^{2+} at the PHN of human sperm, to determine the presence, identity and regulation of intracellular Ca^{2+} store/s in the region. This was tackled by the following research aims:

- Confirmation of the presence and localisation of areas of high $[Ca^{2+}]_i$ in humans sperm.
- Investigate Ca^{2+} storage capability of sperm mitochondria, the potential contribution of this Ca^{2+} store to shaping the biphasic progesterone $[Ca^{2+}]_i$ response and hyperactivation.
- Characterise the effect of IP_3R stimulation with thimerosal on $[Ca^{2+}]_i$ at the PHN.
- Analyse the effects of SOCE modulators 2APB and SKF on PHN $[Ca^{2+}]_i$ and the characteristic biphasic progesterone response.
- Investigate the effect of novel KIKKK containing STIM1 bioportides on $[Ca^{2+}]_i$ at the PHN and SOCE associated with formation of the $[Ca^{2+}]_i$ progesterone transient.
- Study the effects of inducers of hyperactivated motility and $[Ca^{2+}]_i$ elevation on mitochondrial membrane potential in human sperm.

CHAPTER TWO: MATERIALS AND METHODS

2.0 Foreword

This chapter describes the general methods used and will be referred to throughout the following results chapters. Examples are included for clarification purposes.

2.1 Materials

2.1.1 Chemicals

All chemicals were cell culture tested grade where available (for suppliers see Appendix I). Mag-Fluo-4AM and Oregon-Green-BAPTA-1AM were supplied by Molecular Probes (distributed by Invitrogen Life Technologies Ltd. Paisley). JC-1 mitochondrial dye was purchased from Enzo Life Sciences (Exeter). DMSO-Pluronic F-127 and Poly-D-Lysine were procured from Invitrogen Life Technologies Ltd. SKF-96365 Hydrochloride was acquired from Merck Millipore (Watford). 2-aminoethoxydiphenyl borate (2-APB) was obtained from Calbiochem (distributed by Merck Biosciences, Beeston, Nottingham, UK) and Bis(2-hydroxy-3-tert-butyl-5-methyl-phenyl) methane (bisphenol) was generously donated by Dr Michelangeli (University of Birmingham, UK).

STIM peptides KIKKK(STIM$^{371-392}$), a scrambled control and KIKKK(STIM$^{371-392}$) analogue (alanine at position 10 substituted with α-aminoisobutyric acid) were developed by Pantechnia, University of Wolverhampton.

All media including sucrose buffered saline, Earle's balanced salt solution (EBSS) and Ca^{2+} free EGTA-buffered EBSS (~$3x10^{-7}$M Ca^{2+}) were prepared in the laboratory using chemicals obtained from Sigma-Aldrich Ltd. (Appendix II) and were supplemented immediately prior to use with 0.3% (w/v) fatty acid free bovine serum albumin (BSA) acquired from United States Biological distributed by SAFC Biosciences Inc. (Andover, Hampshire), unless otherwise stated. Streptolysin-O toxin (SLO) was purchased from Professor Bhakdi at the Institute of Microbiology and Hygiene (Guttenberg Universitat Mainz). SLO was dissolved as a concentrated stock solution in DTT and diluted in PBS before activation.

All other chemicals including carbonyl-cyanide-4-(trifluoromethoxy)-phenyl-hydrazine (CCCP), NNC-55-0396 hydrate (NNC), Progesterone, 2,4-Dinitrophenol (DNP), Dimethyl sulfoxide (DMSO), Dithiothreitol (DTT), 4-Aminopyridine (4AP), Thimerosal, EGTA, HEPES and PBS were acquired from Sigma Aldrich Company Ltd. (Dorset). Agonists were dissolved as a concentrated stock solution in DMSO where necessary and diluted in supplemented Earle's balanced salt solution (sEBSS, 0.3% (w/v) BSA, HEPEs, pH 7.3-7.35, osmolarity 285mOsm) before application.

2.1.2 Apparatus and consumables

Samples were collected in 100ml specimen pots from Alpha Laboratories (Hampshire) and transferred to 5ml round bottom, 15ml and 50ml polystyrene Falcon tubes supplied by Starlabs UK Ltd (Milton Keynes, UK). Cells were imaged using a perfusion chamber seated in a platform produced by the Biosciences Workshop (University of Birmingham, UK) based on Warner Instruments RC-20 chamber and P-5 platform (Figure 2.1). Each chamber was fitted with a 12mm round coverslip from Warner Instruments (distributed by Harvard Apparatus). All imaging experiments were performed on a Nikon TE300 inverted fluorescence microscope, fitted with a Cairn Opto LED light source using either a Rolera-XR cooled CCD camera or an Andor Ixon 897 EMCCD camera controlled by a PC running iQ software (Andor Technology, Belfast, UK; Figure 2.2). CASA was performed using a Hamilton Thorne CASA system running IVOS v.10 (Massachusetts, USA).

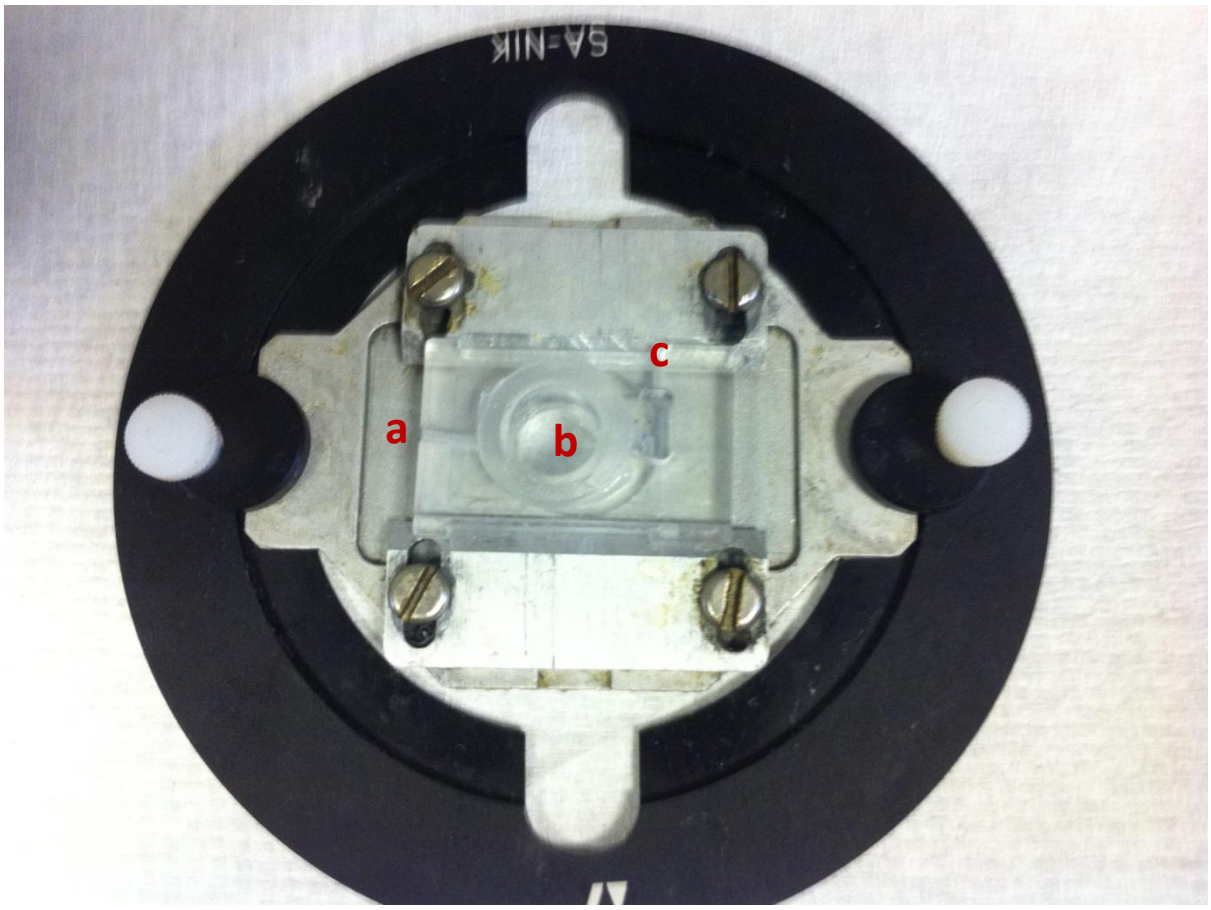

Figure 2.1 The imaging perfusion chamber based on Warner Instrument RC-20 chamber seated in a Warner Instruments P-5 platform. (**a**) Perfusion chamber inlet, (**b**) cells adhered to poly-D-lysine coverslip, covered with a 12mm round coverslip and secured with cap, (**c**) perfusion chamber outlet.

A

B

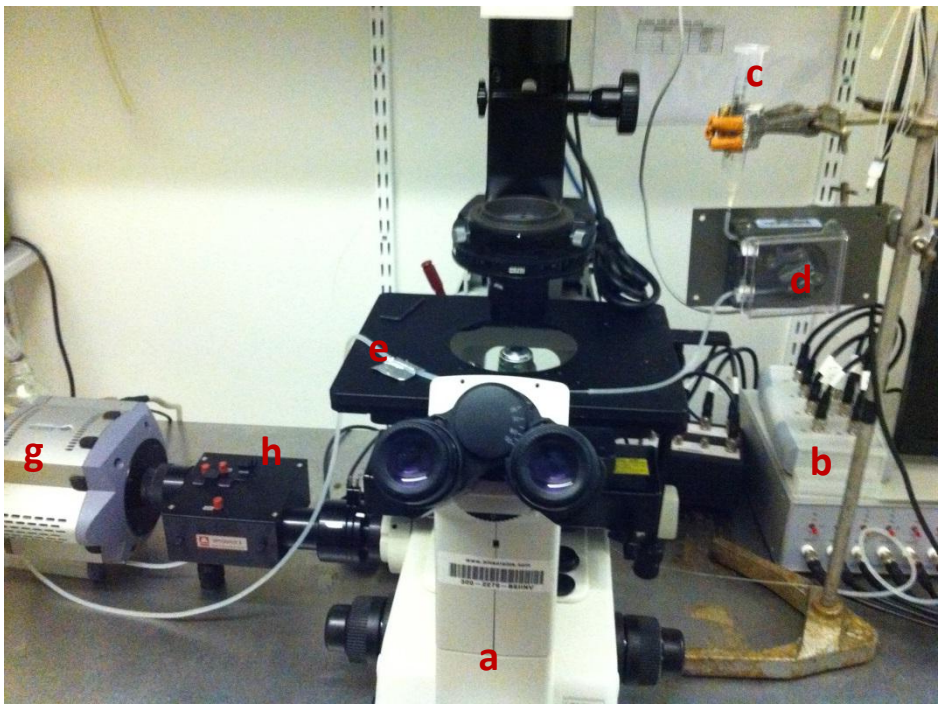

Figure 2.2 Photograph of imaging and perfusion system set up, both systems feature a Nikon TE300 inverted fluorescence microscope (**a**), fitted with a Cairn Opto LED light source (**b**), perfusion header (**c**), peristaltic pump (**d**) and waste disposal suction (**e**), (**A**) uses a Rolera-XR cooled CCD camera (**f**), (**B**) uses an Andor Ixon 897 EMCCD camera (**g**) and Optosplit by Cairn Research (**h**) all controlled by separate PC's running iQ software.

2.2 Donor recruitment

Human research sample donors were recruited at Birmingham Women's Hospital, Birmingham, U.K. (Human Fertilization and Embryology Authority (HFEA) Centre number 0119) or the Department of Biosciences at the University of Birmingham, Birmingham, U.K., in accordance with the HFEA Code of Practice (Version 7). Ethical approval was obtained from both the Life and Health Sciences Ethical Review Committee ERN_ 12-0570 and the Central Office for Research Ethics Committees (COREC): all donors gave informed written consent to the research.

2.3 Preparation of sperm

Human semen was collected from healthy donors by masturbation after 2-3 days of sexual abstinence and allowed to liquefy for 30 minutes at 37^{o}C (95:5 air/CO_2). Highly motile sperm were harvested using a direct swim up procedure as described previously by (Harper *et al.*, 2003, Nash *et al.*, 2010). Polystyrene round-bottomed Falcon tubes (2045) containing 1ml of sEBSS medium (with 0.3% BSA and 15mM HEPES unless otherwise stated) were underlayed with 0.2ml of liquefied semen, (Figure 2.3). Tubes were then incubated at a 45^{o} angle for 1hr at 37^{o}C and 5% CO_2. The top 750µl was then removed from each tube, pooled together and concentration calculated using an improved Neubauer haemocytometer in accordance with the WHO methods 1999 (Figure 2.4). After counting, cells were adjusted to 6 x10^6 cells/ml and left to capacitate at 37^{o}C in 5% CO_2. For single cell imaging and CASA cells were adjusted to 3x10^6cells/ml after capacitation prior to experimentation.

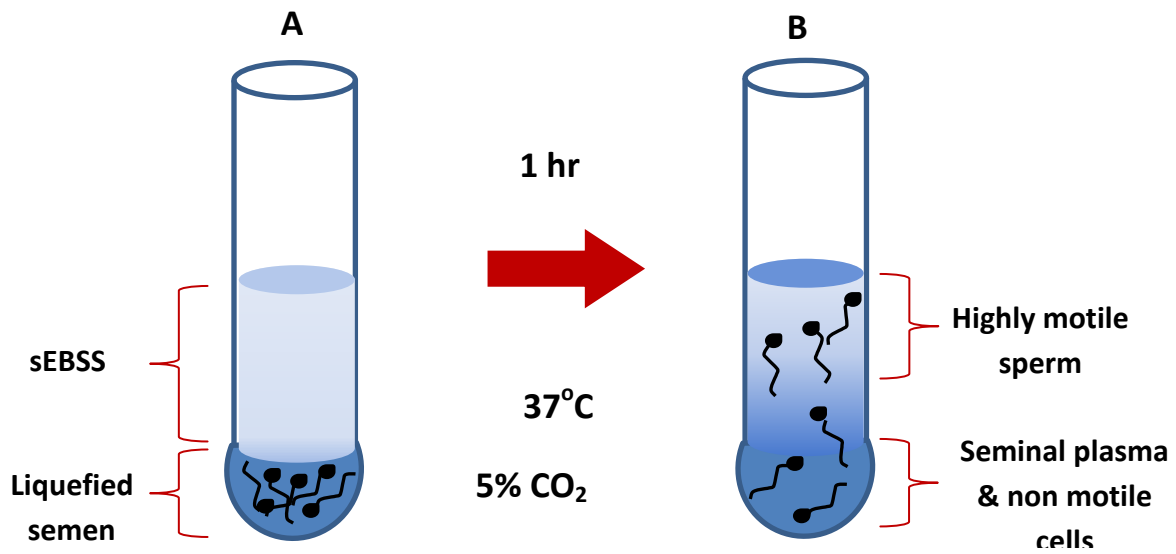

Figure 2.3 Separation of sperm cells from semen using direct swim-up procedure, (**A**) liquefied semen is deposited at the bottom of the falcon tube under sEBSS, (**B**) Highly motile sperm are removed from the top portion of the resulting column.

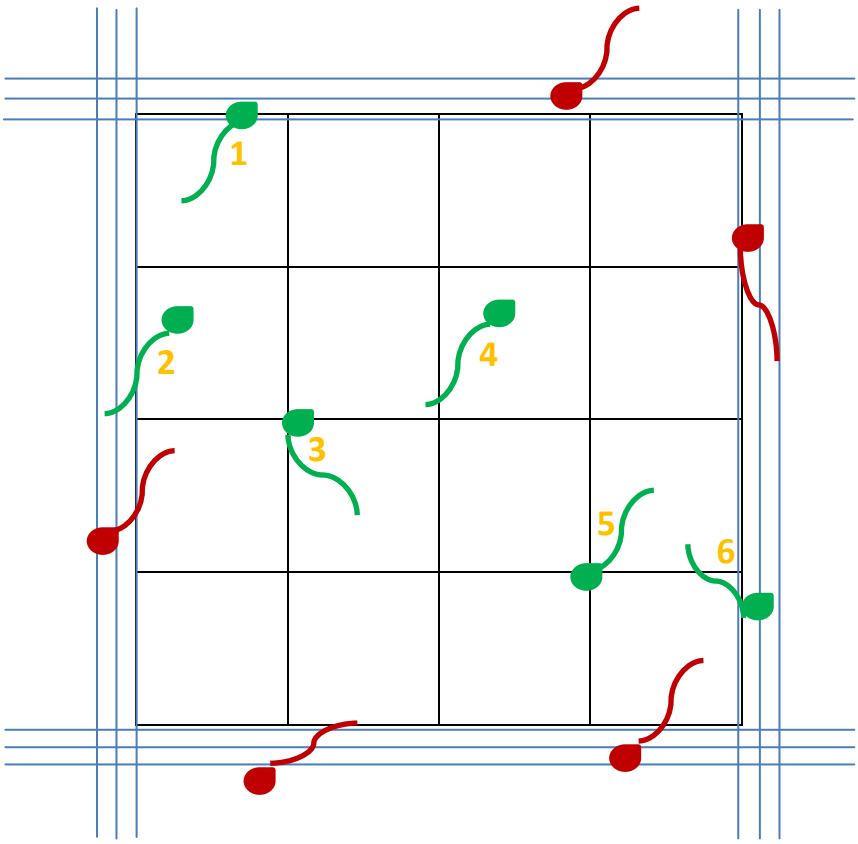

Figure 2.4 Haemocytometer cell counting method. The haemocytometer used was 0.1mm deep and the 25 large squares represent an area of 1 square mm. Each of the 25 large squares is broken down into 16 smaller squares; the red sperm were not counted because these sperm were more than halfway outside the counting area. Green cells were counted as more than 50% of the entire cell was present in the large square.

2.4 Sperm incubation and capacitation

Sperm harvested by swim up procedure were suspended in sEBSS prepared in the laboratory (Appendix II**)**. The osmolarity and pH of all the laboratory prepared media were checked and adjusted to 285 – 295 mOsm/kg (using NaCl and an Advanced Instruments Inc. osmometer) and pH 7.3-7.35 (using HCl/NaOH). Media was subsequently filtered, sterilised and aliquoted into 100ml sterile containers stored at 4^{o}C until use. Capacitating media (sEBSS) was incubated at 37^{o}C and 5% CO_2 in air for at least one hour prior to use to allow equilibration. 0.3% BSA was added prior to use and pH confirmed to be 7.3-7.35. After adjustment to 6 x10^{6}cells/ml cells harvested by swim up were allowed to capacitate in sEBSS for a minimum of 6 hours unless otherwise stated, (Kirkman-Brown *et al*., 2000).

2.5 Computer Assisted Semen Analysis (CASA)

For CASA studies, capacitated cells at 6 x10^{6}cells/ml in sEBSS 0.3% BSA were adjusted to a concentration of 3-4x10^{6}cells/ml. 100µl aliquots were then treated with or without agonist stimulants and 10ul of the resulting sperm suspension was immediately introduced to either side of a pre-warmed 20µm depth 2X-CEL sperm analysis chamber (Hamilton Thorne Biosciences). Experiments were performed using a Hamilton Thorne CASA system running IVOS v.10 at 37^{o}C to assess physiological sperm motility parameters. At least 20 regions were selected for analysis of each sample with a minimum of 100 cells observed in total. For human sperm analysed at 60Hz using a 20x objective hyperactivated sperm were defined by Mortimer *et al.*, (1998) as track velocity (VCL) >150µm/s, linearity (LIN) <50µm/s and lateral head amplitude (ALH_{max}) >7µm/s.

2.5.1 Data processing

Path velocity (VAP), progressive velocity (VSL), track velocity (VCL), lateral head amplitude (ALH), beat frequency (BCF), straightness (STR), linearity (LIN), elongation and hyperactivation (HA) values were automatically generated and registered by the CASA machine while performing the experiments. Treatment influenced changes in motility parameters were compared in Microsoft excel using two-tailed students paired t-tests. Treated cells were compared with both untreated cells and in some instances progesterone treatment where experiments were conducted on the same cell population. Results were believed statistically significant if $P<0.05$.

2.6 Single cell imaging

In all single cell imaging protocols, unless otherwise stated, cells were incubated for 6 hours to allow capacitation at a concentration of 6 $x10^6$cells/ml. The preparation was then diluted to $3x10^6$cells/ml with sEBSS containing 0.3% BSA prior to imaging experiments.

2.6.1 Calcium imaging with Oregon Green BAPTA-1AM

200µl aquilots of capacitated sperm were loaded with 1.2µl 12µM Oregon Green BAPTA-1AM (0.6% dimethyl sulfoxide (DMSO) dispersed with 0.12% pluronic F-127) and incubated for 30 min at 37^{o}C and 5% CO_2. Following this incubation the entire aliquot was transferred to a continually perfusable imaging chamber, in which the lower surface consisted of a 1% poly-D-lysine coated coverslip (Figure 2.5). A further 30 minute incubation of the imaging chamber at 37^{o}C and 5% CO_2 allowed labelled cells to adhere to the coverslip. After incubation the chamber was mounted above a 40x air objective on a Nikon TE300 inverted fluorescence microscope, fitted with a Cairn Opto LED light source and filters for

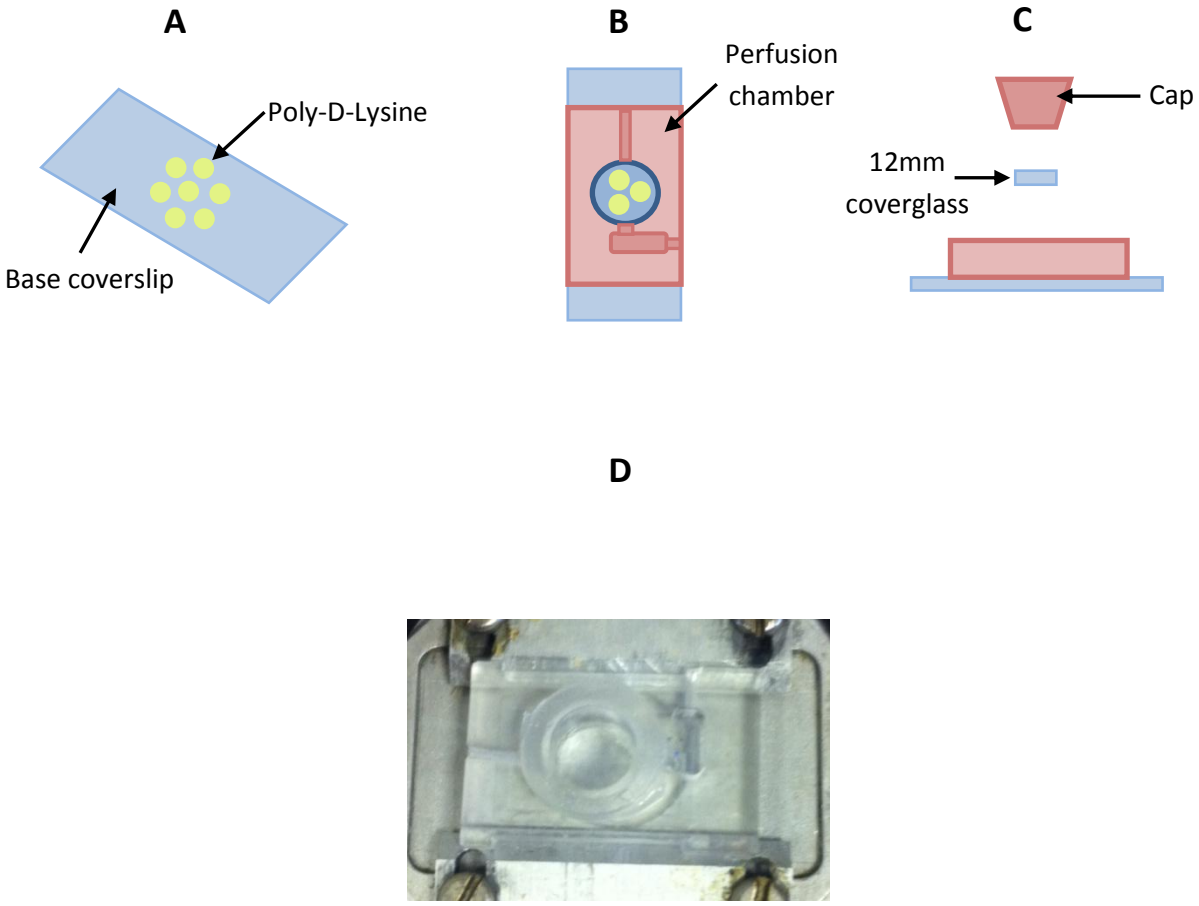

Figure 2.5 Perfusion chamber preparation. (**A**) Poly-D-lysine is applied to coverslips in small spots, (**B**) the perfusion chamber is attached to a poly-D-lysine coated coverslip using vacuum grease, (**C**) a 12mm circular coverslip is secured on the anterior surface of the chamber with a cap, (**D**) a complete perfusion chamber.

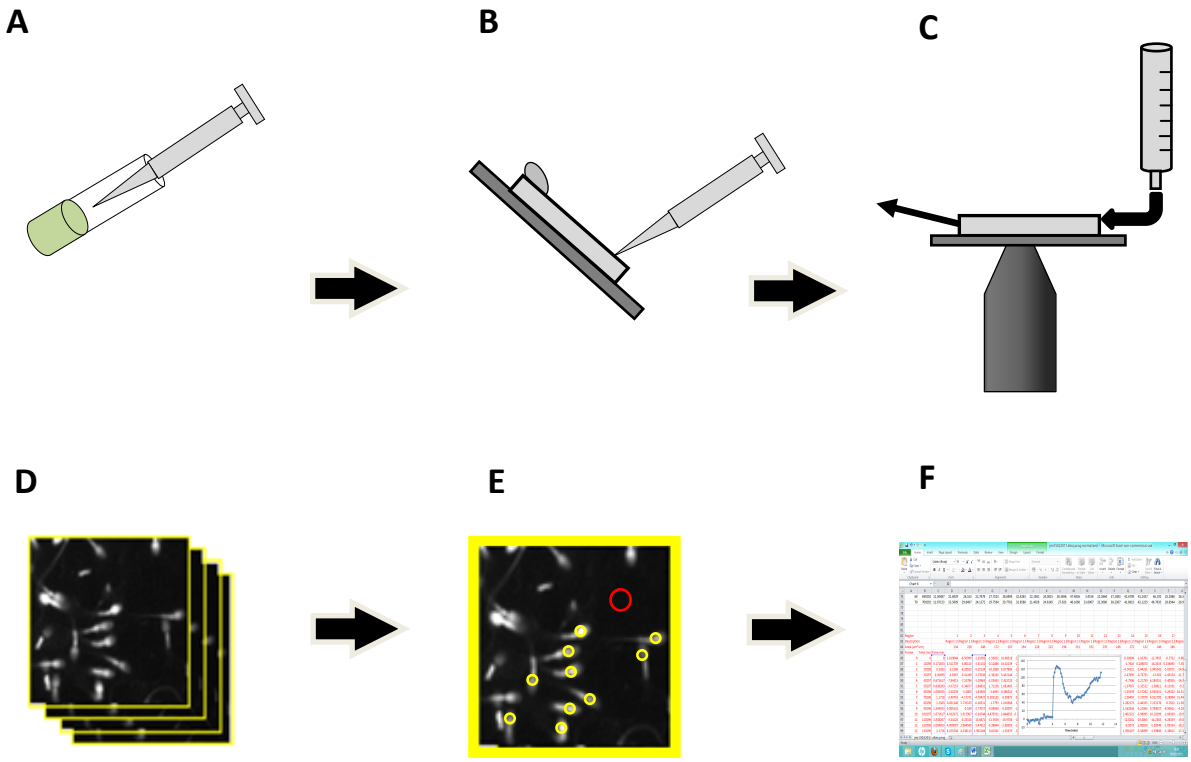

Figure 2.6 Summary of key steps in single cell imaging. (**A**) Following a 4-6 hour capacitation 200µl of cells are incubated with fluorescent dye and (**B**) transferred to a perfusable imaging chamber. (**C**) The imaging chamber was then inserted above a 40x objective and perfused with sEBSS containing various pharmacological agonists. (**D**) A series of time lapse images are acquired, (**E**) ROI's were selected and (**F**) data analysed offline in Microsoft Excel.

excitation 488nm and emission 540nm (Cairn Research, Kent, UK). The chamber was then connected to a perfusion system (Figure 2.2), consisting of a peristaltic pump with perfusion rate of approximately 0.4ml/min. Prior to experiment commencement at least 10ml of fresh sEBSS medium was washed through the chamber to remove excess dye and unattached cells. Following a 3-5min recorded control period sEBSS was removed and pharmalogical agents applied directly by addition to the perfusion header (Nash *et al.,* 2010; Figure 2.6). There is an approximate 30sec delay of any cellular response recorded due to the travel time through the perfusion tube and is taken into account when calculating response times. This was determined by observing the travel time of an air bubble introduced into the perfusion tubing from the perfusion header to the imaging chamber. All experiments were undertaken at 25±1^{o}C with a continuous flow of medium, unless stated otherwise. Cells were illuminated and fluorescence images were taken every 10 seconds using the 40x objective and Q Imaging Rolera-XR cooled CCD camera or an Andor Ixon 897 EMCCD camera controlled by a PC running iQ software. Data storage and acquisition were controlled by a PC running the iQ software.

2.6.1.1 Single cell data processing

Data were processed offline using the iQ software as previously described by Nash *et al.*, (2010). In brief a region of interested (ROI) was drawn around the posterior head/neck region (PHN) of each spermatozoon visible in the image field, unless otherwise stated. The image series was then replayed numerous times to allow close inspection of individual cells by eye. Inspection allowed identification of any cells which drifted out of the ROI or if the fluorescence faded to zero within the control period (assumed dye loss due to cell death), these cells were removed from analysis. An additional background ROI was also selected to enable automatic background subtraction by the iQ software. The raw intensity values

generated were imported into Microsoft Excel and normalized to pre-stimulus values using the equation:

$$R = [(F - F_{rest})/ F_{rest}] \times 100 -100$$

Where R is the normalized fluorescence intensity, F is fluorescence intensity at time *t* and F_{rest} is the mean of at least 20 determinations of *F* taken during the control period.
Normalised fluorescence intensity values (R) at each time point were compiled to generate a mean value for normalised head fluorescence from all cells in the experiment (R_{tot}). The resulting values were then plotted on a time-fluorescence intensity graph (Figure 2.7).

2.6.1.1.1 Cell population statistics – peak amplitude

For the following cell population statistics all values were determined using the R_{tot} trace, an average of all the cell responses in a given experiment. The amplitude of $[Ca^{2+}]_i$ transients (ΔF_{mean}), were determined by subtracting the 'control' period average from the average of the three points spanning the peak of the normalised R_{tot} trace (typically the highest point and the points either side). In biphasic responses such as progesterone the amplitude of the $[Ca^{2+}]_i$ sustained component, ΔF_{sus}, was calculated by averaging three consecutive points three minutes after agonist application, unless otherwise stated (Figure 2.8). In experiments where a steady rise in $[Ca^{2+}]_i$ was observed peak amplitude was calculated by averaging the three highest consecutive points within four minutes of agonist application. Experiments involving an initial exposure of cells to one treatment followed by an additive exposure to a second treatment were first processed as described above. The incremental increase in fluorescence induced by exposure to a second treatment was calculated by defining a second 'control'

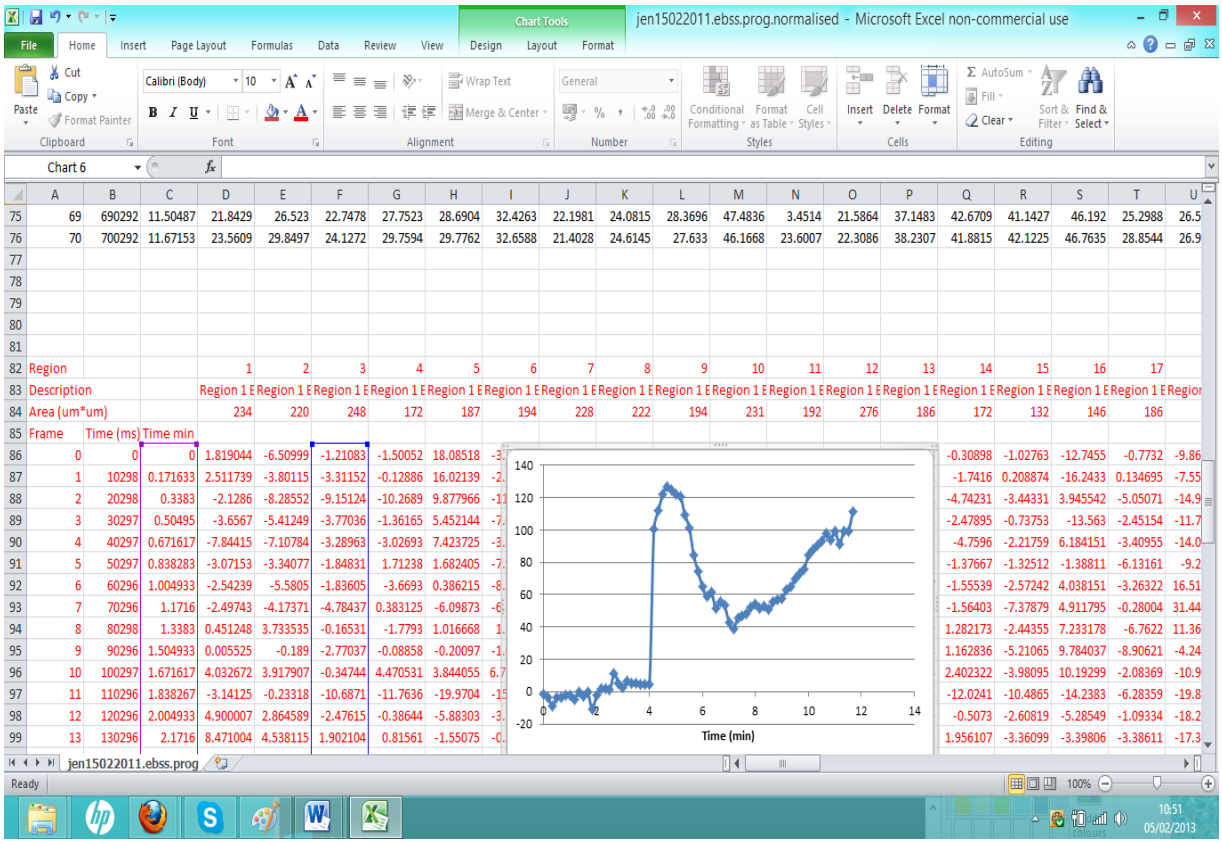

Figure 2.7 Image demonstrating offline data analysis in Microsoft Excel. The graph shows the fluorescence intensity trace against time of a single cell's response to progesterone, (cell 3). Numbers in black, (top) are the raw intensity values obtained from Andor IQ software. The red numbers (below) are the fluorescence intensity values normalised using the formula stated in section 2.6.1.2. In this example progesterone treatment results in the characteristic peak followed by a sustained transient.

A

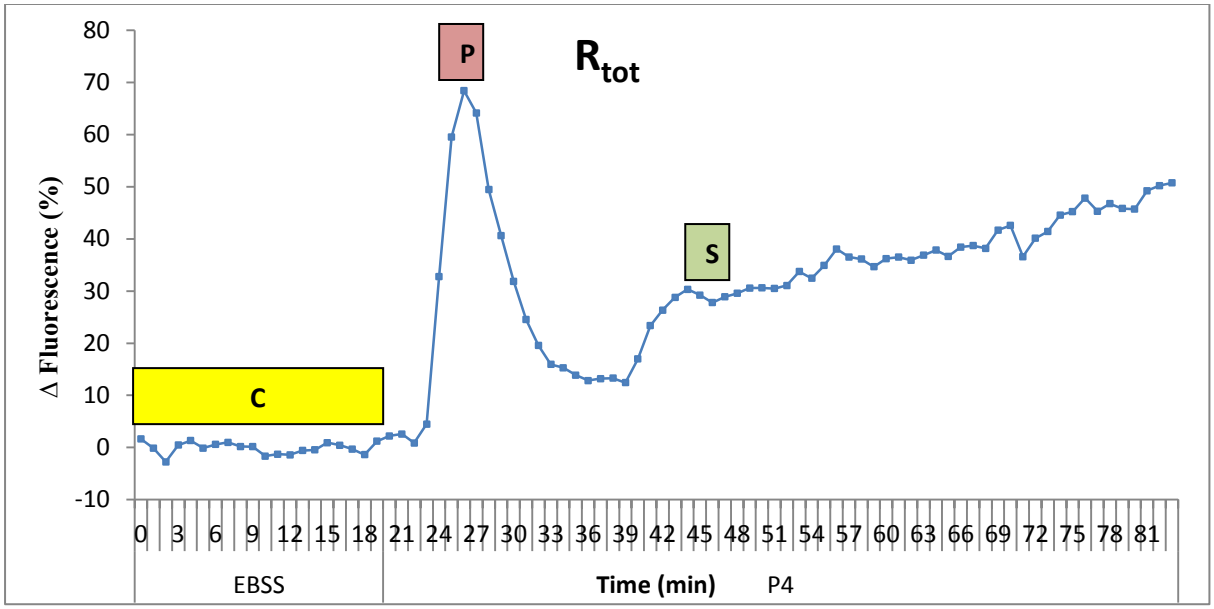

B

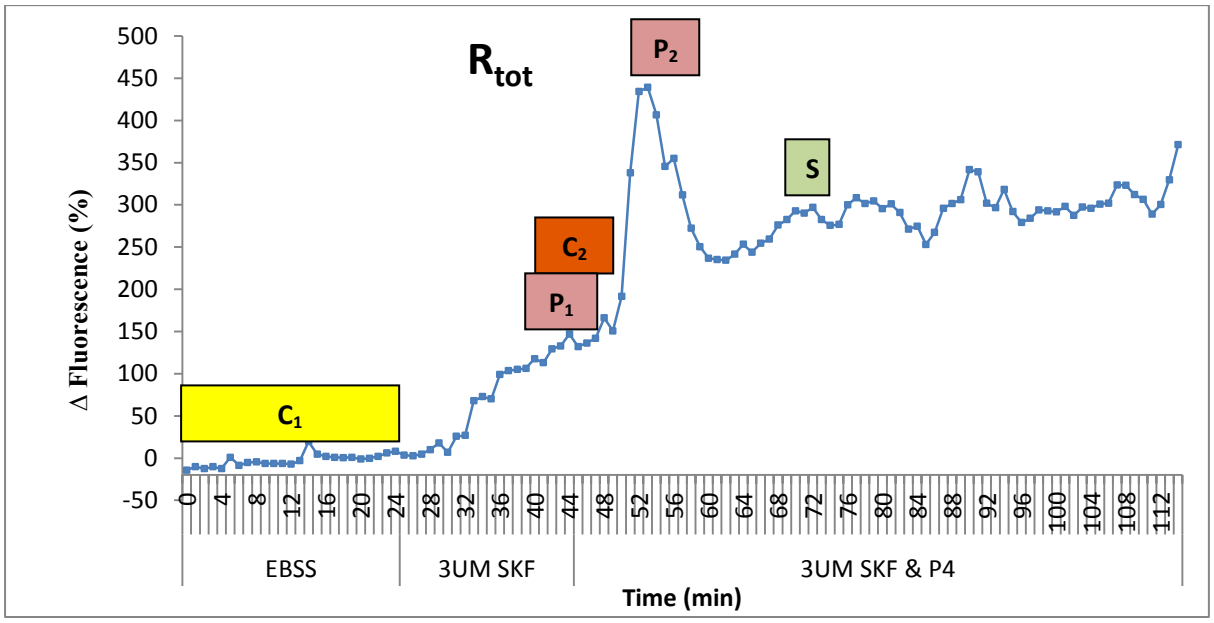

Figure 2.8 Illustration of key loci in determining response amplitude for R_{tot} in single cell imaging experiments (A) Cells exposed to a single progesterone treatment, where C is control period, P is peak amplitude and S is sustained amplitude response (B) Cells exposed to sequential treatments of 3μM SKF and progesterone, where C_1 is initial control period, P_1 is peak amplitude for first treatment, C_2 is second 'control' period, P_2 is peak amplitude for second treatment amplitude and S is sustained response for treatment 2.

period composed of the four images captured immediately prior to second treatment application. The second treatment amplitude was then calculated by subtracting the R_{tot} values during the second control period from those recorded at both peak and sustained responses, where necessary. Paired t-tests were performed using Microsoft Excel, statistical significance was set at $P<0.05$. Time to peak was determined as time of peak response to stimulus (determined by R_{tot}) minus control period before treatment application.

2.6.1.1.2 Individual cell response frequency statistics

Individual cell $[Ca^{2+}]_i$ responses to treatment were analysed using Microsoft Excel Logic to determine the percentage population of cells eliciting the observed response and contributing to R_{tot}. For each cell the amplitude of the $[Ca^{2+}]_i$ transient or in experiments were a steady rise in $[Ca^{2+}]_i$ was observed, peak amplitude (ΔF_{max}), was determined by subtracting the 'control' period average from the average of the highest point within 20 frames of treatment application (unless otherwise stated) and the points either side. In addition time to ΔF_{max} was also determined for each individual cell in a manner analogous to that described for R_{tot} in section 2.6.1.1.1. In biphasic responses the amplitude of the $[Ca^{2+}]_i$ sustained component (ΔF_{sus}) was also calculated for each individual cell by averaging three consecutive points three minutes after agonist application, unless otherwise stated.

2.6.1.1.2.1 Significance of individual cell responses

To determine the significance of individual cell $[Ca^{2+}]_i$ responses to treatment the mean and 95% confidence interval were calculated for 'control', 'peak' and 'sustained' responses as determined by R_{tot} amplitude calculations (section 2.6.1.1.1) and 'second control', 'peak' and

'sustained' where necessary. A response was categorised as a significant increase, a significant decrease or no significant response. An increase was deemed significant if it satisfied the equation:

$$(T_m - T_{con}) > (C_m + C_{con})$$

Where T_m is the treatment peak mean (frames determined by R_{tot}), T_{con} is the treatment 95% confidence interval, C_m is the control mean and C_{con} is the control 95% confidence interval. A decrease was deemed significant if it satisfied both the following equations:

$$(T_m - T_{con}) < (C_m + C_{con}) \ \& \ T_m < C_m$$

If a response was negative to both these statements then it was categorised as no significant response. In experiments when a second treatment was used then the second control period was used to compare the fluorescence increment to.

2.6.2 Calcium imaging with Mag-Fluo-4AM

For Ca^{2+} imaging with a low affinity calcium dye 200µl aquilots of capacitated sperm were loaded with 0.6µl Mag-Fluo-4AM (0.6% dimethyl sulfoxide (DMSO) dispersed with 0.12% pluronic F-127). Mag-Fluo-4AM loaded cells were incubated, and imaged as Oregon Green BAPTA-1AM (section 2.5.1).

2.6.2.1 Single cell data processing

Mag-Fluo-4AM loaded cells display localised areas of calcium fluorescence, (Figure 2.9B). ROI's on the iQ software enable the production of average fluorescence intensities per pixel as opposed to per cell to facilitate analysis of $[Ca^{2+}]_i$ in discreet areas of the cell. Data was processed offline using the iQ software and peak amplitudes determined as with Oregon

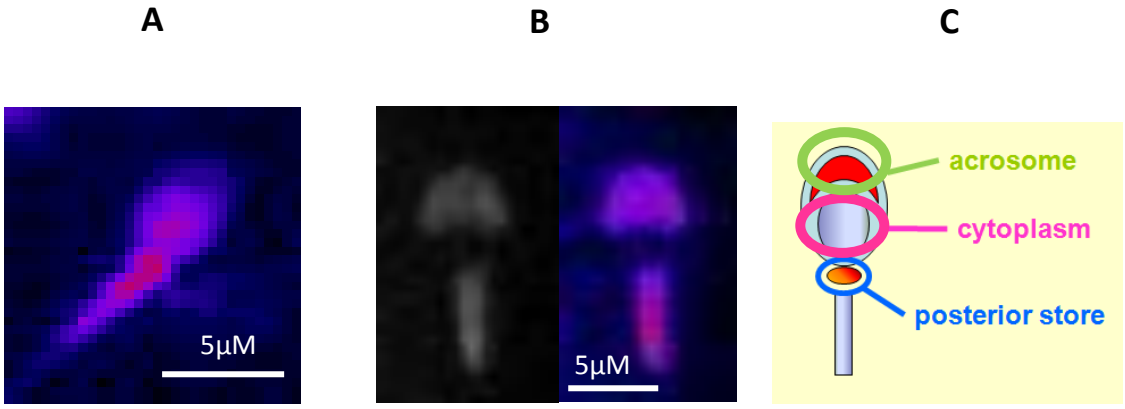

Figure 2.9 Visualisation of calcium stores with fluorescent dyes (**A**) Fluorescence observed Oregon Green BAPTA 1AM treated cell (**B**) Fluorescence observed in Mag-fluo-4AM treated cell, both stores clearly visible, (**C**) Identification of three ROI's in Mag-Fluo-4AM data analysis.

Green BAPTA-1AM treated cells (section 2.6.1.2.1). However each Mag-Fluo-4AM loaded cell had three distinct ROI's, one encompassing each the acrosome, cytoplasm (posterior head region) and PHN of each spermatozoon visible in the image field, (Figure 2.9C). As a result Peak amplitudes and decreases were compiled for each ROI separately as in section 2.6.1.1.1 and 2.6.1.1.2 for population statistics and individual cell statistics respectively.

2.7 Mitochondrial imaging with JC-1

For mitochondrial membrane potential studies 200µl aliquots of capacitated cells at $3x10^6$/ml were initially loaded into the continually perfusable imaging chamber (Figure 2.1) as with calcium imaging studies. Cells were then allowed to adhere to the poly-D-lysine coverslip on the base of the chamber for 30 minutes at 37^{o}C and 5% CO_2. Once cells had adhered 200µl of JC-1 at a concentration of 5µg/ml, (in sEBSS) was washed through the chamber replacing the capacitating sEBSS. Cells were then incubated in the chamber for a further 20 minutes at 37^{o}C and 5% CO_2 to allow the JC-1 to penetrate the mitochondrial membrane. The chamber was then attached to the perfusion system, excess JC-1 dye washed off with sEBSS and a control period of minimum 30 frames recorded before exposure to agonists and stimulants as with calcium imaging section 2.6.1 (Figure 2.2B). All JC-1 experiments were conducted at 25±1^{o}C with a continuous flow of medium. Images were taken every 10 seconds using a Cairn Optosplit containing red and green filters and Andor Ixon 897 EMCCD camera, 40x oil objective on a Nikon TE300 inverted fluorescence microscope, fitted with a Cairn LED light source controlled by a PC running iQ software (Andor Technology, Belfast, UK). The cells were excited using a 470nm LED, red emissions were collected at 590nm and green emissions collected at 529nm.

2.7.1 Single cell data processing

JC-1 loaded cells display areas of localised fluorescence dependent on the mitochondrial membrane potential (MMP). At depolarised MMP JC-1 exists as a green fluorescent monomer readily diffusible in the cytoplasm. Hyperpolarised MMP result in the formation of red fluorescent J-aggregates localised to the mitochondria. The emission shift from green to red is indicative of mitochondrial hyperpolarisation. A red: green fluorescence intensity ratio allows the observation of membrane potential irrespective of mitochondrial size, shape and density. Data from JC-1 experiments were processed offline using the iQ software similarly to Nash *et al.,* (2010). However first Optosplit red and green fluorescence images were merged and aligned to produce a single representation of the experimental cell population, (Figure 2.10). A single ROI encompassing the head and midpiece was drawn around each individual cell visible in the image field. Due to the physiology of the mature sperm cell it was essential that both the head and midpiece be included in the ROI to monitor levels of the cytoplasmic green JC-1 monomer. The resulting image series was replayed to remove cells where dye loss was evident in the control period, (an indicator of cell death) or had migrated out of the ROI. In addition a free background ROI was selected to enable automatic background subtraction by the iQ software. The raw intensity values generated were imported into Microsoft Excel and a ratio generated using the following formula:

$$R = F_R / F_G$$

Where R is the ratio of fluorescence intensity, F_R is the red fluorescence intensity of a single cell at time t and F_G is the green fluorescence intensity of the same cell at time t. The ratio of red: green fluorescence intensities (R) at each time point were compiled generate a mean ratio

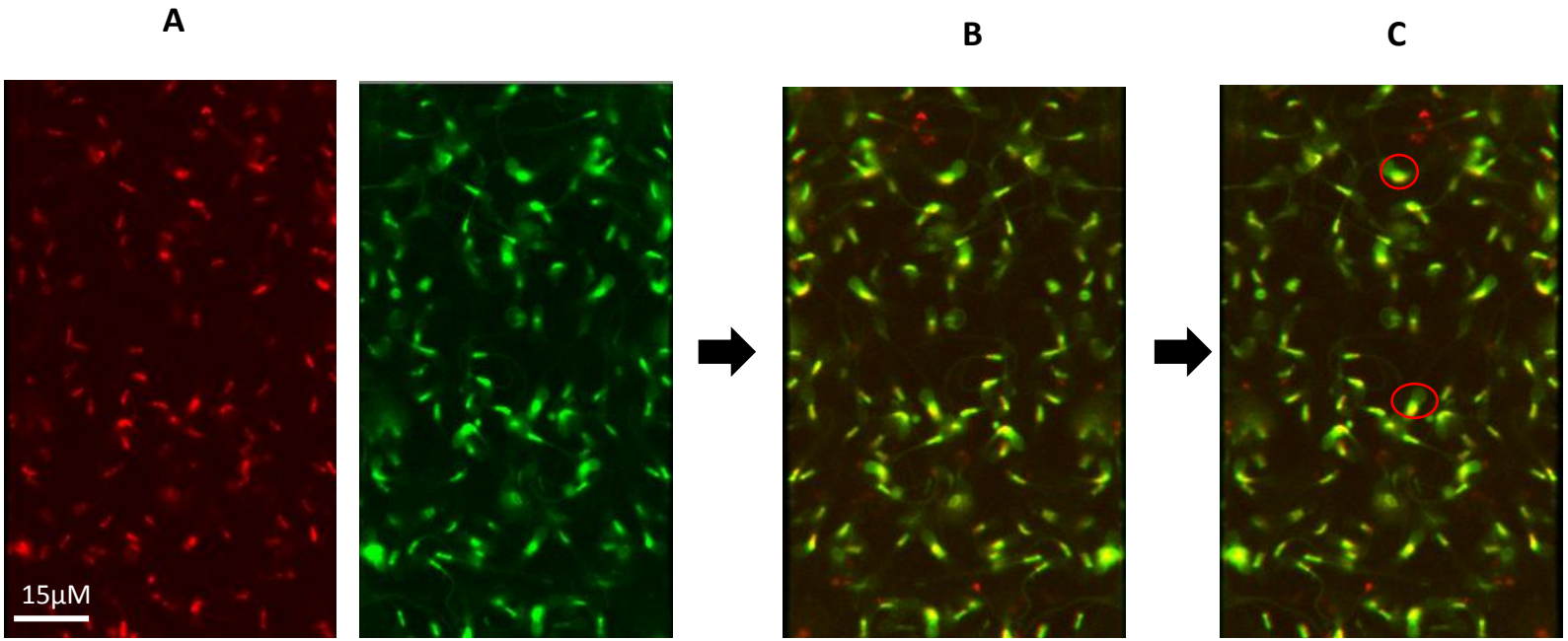

Figure 2.10 Illustration of the data analysis process for cells treatment with JC-1 (**A**) Separate images obtained for red and green channels, (**B**) red and green images merged together, (**C**) ROI's drawn around each cell (red).

for red: green fluorescence from all cells in the experiment (R_{tot}). The resulting values were then plotted on a time-fluorescence intensity graph.

2.7.1.1 Mitochondrial membrane potential cell population statistics

For cell population statistics all values were determined using the fluorescence intensity R_{tot} trace calculated as the average F_R/F_G ratio response of all cells in a given experiment. Effect of treatment on MMP was determined in a manner analogous to effect on $[Ca^{2+}]_i$. Change in F_R/F_G ratio was determined by subtracting the 'control' period average from the average of the three points spanning the peak increase or decrease of the R_{tot} trace within 24 frames, unless otherwise stated. In experiments were cells were exposed to a second additive treatment immediately following the first, the incremental effect on MMP was calculated by defining a second 'control' period composed of the four images captured immediately prior to second treatment application. The effect of the second treatment on MMP was then calculated by subtracting the second control period F_R/F_G ratio from that of the maximum observed effect whether this be an increase or decrease in MMP. Time taken to see observable changes in MMP were determined as time to maximum response minus the control period before treatment application. Paired t-tests were performed using Microsoft Excel, statistical significance was set at $P<0.05$, all values are shown as mean ± S.E.M.

2.7.1.2 Mitochondrial membrane potential individual cell responses

Analysis of individual cell MMPs were conducted using Microsoft Excel Logic. As a result we were able to determine the percentage population of cells eliciting the observed response and contributing to R_{tot}. For each cell the amplitude of change in F_R/F_G ratio was determined by subtracting the 'control' period average from the average of the highest/lowest point

within 24 frames of treatment application (unless otherwise stated) and the points either side. In addition time to maximum F_R/F_G ratio response was also determined for each individual cell as described in section 2.7.1.1.

2.7.1.2.1 Significance of individual cell responses

The significance of MMP responses was determined using the same formula used for Ca^{2+} imaging experiments with one alteration. Instead of using Ca^{2+} response values for the treatment peak T_m, the maximum change in F_R/F_G ratio was used instead, see section 2.6.1.1.2.1.

2.8 Single cell calcium imaging of Streptolysin-O permeabilisation

Single cell calcium imaging was set up as in chapter 2.6.2. Permeabilization was performed using Streptolysin-O from *Streptococcus pyrogenes* adapted from methods previously described (Diaz *et al.*, 1996; Yunes *et al.*, 2000). 200µl aquilots of sperm capacitated for 2-3 hours were loaded with 0.6µl Mag-Fluo-4AM and incubated for an hour at 37^{o}C and 5% CO_2. Cells were then incubated for 30 minutes in a continuously perfusable imaging chamber to allow adherence to the poly-D-lysine on the base of the chamber. After a control period of 20 frames where cells were washed with sEBSS, SLO was applied in phosphate buffered saline, pH 7.4 and filtered to give an end activity of 0.4U/mL after washing through the system with a sucrose buffer (containing 20mM HEPES-KOH, 250Mm sucrose, 0.5mM EGTA, 2mM DTT, 1.5mM $MgCl_2$ and 50mM KCl). Permeabilisation was determined successful visually by the loss of cytoplasmic dye but the retention of dye in both the acrosomal and PHN regions. Following successful permeabilisation agonists were applied to the cells and the calcium signalling response observed.

2.8.1 Streptolysin-O permeabilisation analysis

Data was processed as per section 2.6.2.1. with one alteration. As treatment was applied to cells after initial exposure to the toxin causing a decrease in posterior acrosomal fluorescence, the initial control period for these cells was taken as the four images prior to treatment. Amplitude for decrease in fluorescence during the permeabilisation process was determined by subtracting the average of three consecutive points before agonist application from the initial control period.

CHAPTER THREE: Ca^{2+} LOCALISATION AND MITOCHONDRIAL Ca^{2+} STORAGE POTENTIAL AT THE PHN

3.1 Abstract

Human sperm are transcriptionally inactive; therefore cellular processes must be mediated via tightly modulated second messenger systems. Regulation of $[Ca^{2+}]_i$ has been implicated in many processes essential for sperm function including AR, hyperactivated motility and capacitation (chapter 1). However mature cells do not contain the organelles normally associated with somatic cell Ca^{2+} storage. Previous studies have identified the presence of Ca^{2+} pumps and channels associated with somatic Ca^{2+} stores (chapter 1.10) and evidence for functional Ca^{2+} stores in human sperm (Costello *et al.,* 2009). Current evidence suggests the presence of two discrete Ca^{2+} stores in human sperm, one in the acrosomal region (Herrick *et al.,* 2005) and at least one at the posterior head/neck region (PHN) (Lefievre *et al.,* 2012), each with distinct mechanisms of filling and mobilisation. Preliminary data has identified the posterior store as a key regulator of sperm motility and hyperactivation. In mammalian sperm mitochondria have been proposed as a Ca^{2+} store, due to their contribution to Ca^{2+} homeostasis in somatic cells (Storey & Keyhani, 1975; Babcock *et al,* 1976; Vijayaraghavan & Hoskins, 1990). In this chapter we found that application of mitochondrial uncouplers (CCCP and DNP) increased $[Ca^{2+}]_i$ at the PHN, acrosome and mitochondrial regions, with some effects on subsequent progesterone response kinetics. These effects were greatly reduced in the absence of extracellular Ca^{2+}, indicative of both Ca^{2+} uptake and intracellular release. Furthermore, pre-treatment with bisphenol (ATPase inhibitor) reduced the increase in Ca^{2+} influx associated with CCCP and DNP application. Analysis of mitochondrial membrane potential (MMP) confirmed both mitochondrial inhibitors cause depolarisation of the MMP. However subsequent application of 3μM progesterone can cause MMP hyperpolarisation partially reversing the response observed with application of mitochondrial inhibitors. Together this data indicates the existence of at least two discrete calcium storage compartments in this already highly specialised cell.

3.2 Introduction

A fundamental component of cell function is the capacity to respond to environmental cues. In somatic cells regulation of cellular activity can be controlled via two distinct mechanisms, gene expression and post-translational modification. Regulation via gene expression occurs over periods of hours requiring changes in either transcription, translation, mRNA transcripts or protein turnover. In contrast post-translational modification is a much faster process involving subtle changes to proteins already present in the cell; typically via a cascade of second messengers. In mature human sperm the machinery involved in DNA transcription and protein translation are either absent (ER) or highly condensed (nucleus) and although some evidence has been found for mRNA presence (Meikar *et al.,* 2011) it is not considered to play an essential role in cellular function. As a result the mechanisms underlying sperm specific behaviour must be reliant on post translational modifications by other small cellular messengers, which are either endogenous or abundant in the extracellular environment during the ejaculation and fertilization process.

Ca^{2+} is believed to be responsible for the regulation of a number of processes elemental for sperm function, including hyperactivation, chemotaxis, capacitation and AR (Publicover *et al.,* 2007). Indeed, impaired Ca^{2+} signalling has been associated with subfertility in an increasing number of studies (Baldi *et al,* 1999; Espino *et al,* 2009). A multitude of individual signalling cascades are modulated by Ca^{2+} signalling, which requires tight regulation of $[Ca^{2+}]_i$. Quiescent cells maintain low $[Ca^{2+}]_i$, which can change rapidly with the release of Ca^{2+} from intracellular stores or influx from the extracellular environment upon agonist stimulation. The presence of plasma membrane Ca^{2+} channels on the mature human spermatozoon is well established (Publicover *et al.,* 2007).The properties of some channels

are well documented in somatic cell physiology (SOC's, Ca^{2+}-ATPases) while others are specific to the sperm cell (CatSper; Strunker *et al.,* 2011). Numerous Ca^{2+} channels and pumps associated with somatic Ca^{2+} stores have been identified in human sperm, including but not limited to SERCA, SPCA and RYR (chapter 1.10). It was the localisation of somatic Ca^{2+} storage channels that initially suggested the presence of an anterior Ca^{2+} store in the human spermatozoon. In 2005, Herrick *et al.,* characterised the first Ca^{2+} storage organelle in human sperm; the acrosome is a membranous vesicle situated on the anterior sperm head and essential in AR and other processes fundamental for sperm function. Increasing evidence also suggests the presence of a second store in the PHN region of the sperm (Ho & Suarez, 2001; 2003). Several somatic Ca^{2+} store channels have been localised to the region including STIM and Orai isoforms (Lefievre *et al.,* 2012). Evidence suggests that a store in this region could contribute to motility regulation of each sperm cell (Marchetti *et al.,* 2002; Gallon *et al.,* 2006; Sousa *et al.,* 2011). However the identity of the posterior store, its characterisation and contribution to important cellular processes remains elusive. Previous studies have identified at least two potential candidates for a Ca^{2+} storage organelle in the PHN of mammalian sperm; the redundant nuclear envelope and the mitochondria (Costello *et al.,* 2009). Both have the potential for Ca^{2+} storage however in this chapter we will be focusing on the potential for mitochondrial contribution to intracellular Ca^{2+} responses.

Mitochondria are the ATP producing powerhouses of the cell; they also contribute to reactive oxygen species (ROS) production, lipid oxidation and Ca^{2+} homeostasis (Amaral *et al.,* 2013). In somatic cells mitochondria generate ATP via oxidative phosphorylation; a process that involves transportation of reduced electron carriers across the inner mitochondrial membrane (IMM) via the electron transport chain (ETC) complexes. This process generates a

proton gradient across the IMM consisting of a pH component and an electrostatic component or mitochondrial membrane potential (MMP; Amaral *et al.,* 2013), which is used to drive ATP synthesis. It is this charged nature of the MMP that ultimately enables the mitochondria to sequester Ca^{2+} ions through an electrogenic Ca^{2+} uniporter (MCU), thus acting as a potential intracellular Ca^{2+} store (Nichol1s & Ferguson, 2002). At present there is mounting evidence that agonist stimulation can lead to mitochondrial Ca^{2+} accumulation in a number of healthy cell lines (Ardon *et al.,* 2009; Duchen, 1999). The mitochondria of sea urchin sperm have been shown to both sequester and release $[Ca^{2+}]_i$ in response to pharmacological manipulation by mitochondrial uncouplers (CCCP). Furthermore Ca^{2+} ATPase inhibitors (including bisphenol; Ardon *et al.,* 2009) have been shown to antagonise mitochondrial inhibitor induced $[Ca^{2+}]_i$ increases and activate SOCs. These findings support a role for stored mitochondrial Ca^{2+} human sperm $[Ca^{2+}]_i$ homeostasis, however the contribution, if any, of mitochondrial Ca^{2+} to the Ca^{2+} responses observed in response to agonists and impact on motility parameters is unknown.

3.3 Aims

The aim of this chapter was to determine whether mitochondria act as a Ca^{2+} store and contribute to shaping progesterone induced Ca^{2+} signals in human sperm.

3.4 Material and Methods

3.4.1 Materials

Carbonyl-cyanide-4-(trifluoromethoxy)-phenyl-hydrazine (CCCP), 2,4-Dinitrophenol (DNP), and progesterone were all purchased from Sigma Aldrich Company Ltd. (Dorset). Bis(2-hydroxy-3-tert-butyl-5-methyl-phenyl) methane (bisphenol) was generously donated by Dr Michelangeli (University of Birmingham, UK). For all other materials see chapter 2.1.1.

3.4.2 Methods

3.4.2.1 Cell preparation

Human semen was collected and prepared as in chapter 2.3.

3.4.2.2 Cell incubation and capacitation

Sperm were incubated and capacitated for a minimum of 5 hours as in chapter 2.4.

3.4.2.3 CASA

Capacitated cells were treated with 10μM DNP, 10μM CCCP or an untreated parallel control and their motility parameters were digitally assessed by CASA as described in chapter 2.5.

3.4.2.4 Single cell imaging

Cells were allowed to capacitate for 5 hours at 6 $x10^6$cells/ml in sEBSS before dilution to $3x10^6$cells/ml prior to treatment with fluorescent dyes for single cell imaging. All imaging experiments for this chapter were conducted at 25 $\pm1^oC$.

3.4.2.4.1 Oregon Green BAPTA-1AM (OGB)

Cells were loaded and imaged as in chapter 2.6.1. After a 20 frame control period cells were exposed to either10µM CCCP, 1µM, 5µM, 10µM or 100µM DNP in the presence and absence of extracellular Ca^{2+} for a minimum of 30 frames. In addition some cells were pre-treated with 15µM Bisphenol for 30 frames before exposure to mitochondrial uncouplers and their responses compared to untreated controls.

3.4.2.4.2 Mag-Fluo-4AM (MF)

Cells were loaded and imaged as in chapter 2.6.2. After a 20 frame control period cells were exposed to either10µM CCCP, 10µM DNP or 3µM progesterone for 30 frames. Cells exposed to 10µM CCCP or 10µM DNP were subsequently additively treated with 3µM progesterone and the individual cell responses observed.

3.4.2.4.3 Streptolysin-O permeabilisation

Cells were loaded and imaged as in chapter 2.8.

3.4.2.5 Mitochondrial imaging with JC-1

All mitochondrial imaging experiments were conducted following the protocol outlined in chapter 2.7. After an initial control period of 30 frames cells were exposed to either 10µM CCCP, 10µM DNP, 100µM DNP or 3µM progesterone for 30 frames (5mins). In addition cells exposed to 10µM CCCP, 10µM DNP or 100µM DNP were then treated with 3µM progesterone (5mins) and the MMP response observed.

3.4.3 Analysis

3.4.3.1 CASA

Experiments were performed in duplicate on four days. As a result a daily average was determined and compared between treated samples and the parallel untreated control using a paired t-test. Response was significant if $P<0.05$.

3.4.3.2 Single cell imaging

In this chapter response to CCCP, DNP or Bisphenol treatment was determined within 4 minutes of treatment application (24 frames) for all imaging protocols, (Ca^{2+} and mitochondrial membrane potential). Transient progesterone responses were determined within 20 frames of application; with the sustained progesterone component occurring 3 minutes after application (frames 18-20). Results from calcium imaging with Oregon Green BAPTA1-AM and Mag-Fluo-4AM results were analysed as in chapter 2.6.1. and chapter 2.6.2 respectively. Cells permeabilised with Streptolysin-O were analysed as in chapter 2.8.1.

3.4.3.3 Mitochondrial imaging with JC-1

Effects of agonists on mitochondrial membrane potential were analysed as in chapter 2.7.

3.5 Results

3.5.1 Mitochondrial inhibitors depolarise the mitochondrial membrane potential

Mitochondrial inhibitors CCCP and DNP are uncouplers which affect mitochondrial function by disrupting the mitochondrial membrane potential (MMP; $\Delta\Psi_m$). To confirm that mitochondrial inhibitors reduce the MMP in human sperm we measured the MMP of resting cells and used time lapse fluorescence imaging to observe the effects in real time. Cells were loaded with JC-1; a dual emission MMP sensitive dye. At low MMPs the dye exists as a green monomer throughout the cytoplasm of sperm cells, high MMPs cause aggregation of the monomers into red J-aggregates in the mitochondria itself (chapter 2.7). At rest cells typically exhibit high levels of red mitochondrial fluorescence and low levels of green cytoplasmic fluorescence resulting in an F_R/F_G ratio of typically 0.5-1.5 (Figure 3.2A). It should be noted that although control F_R/F_G ratio's vary amongst experiments MMP did not fluctuate significantly during the initial 200s control period. At rest MMP oscillated in >90% of the cell population (Figure 3.1A, C, E&G). Oscillations were small, insignificant and followed no distinctive pattern in each experimental population, indicating they are individual to each cell.

After a control period of 20 frames cells were treated with either 1µM, 10µM, 100µM DNP or 10µM CCCP and the response monitored for a further 30 frames (5min). All four treatments caused the F_R/F_G ratio (MMP) to fall between 0.05 and 0.7 in 70-90% of the cell population (Figure 3.1). In cells loaded with JC-1, application of mitochondrial inhibitors induces a clearly visible increase in cytoplasmic green fluorescence in both 10µM CCCP and 100µM DNP experiments (Figure 3.1B&H); for examples of mean experimental red and

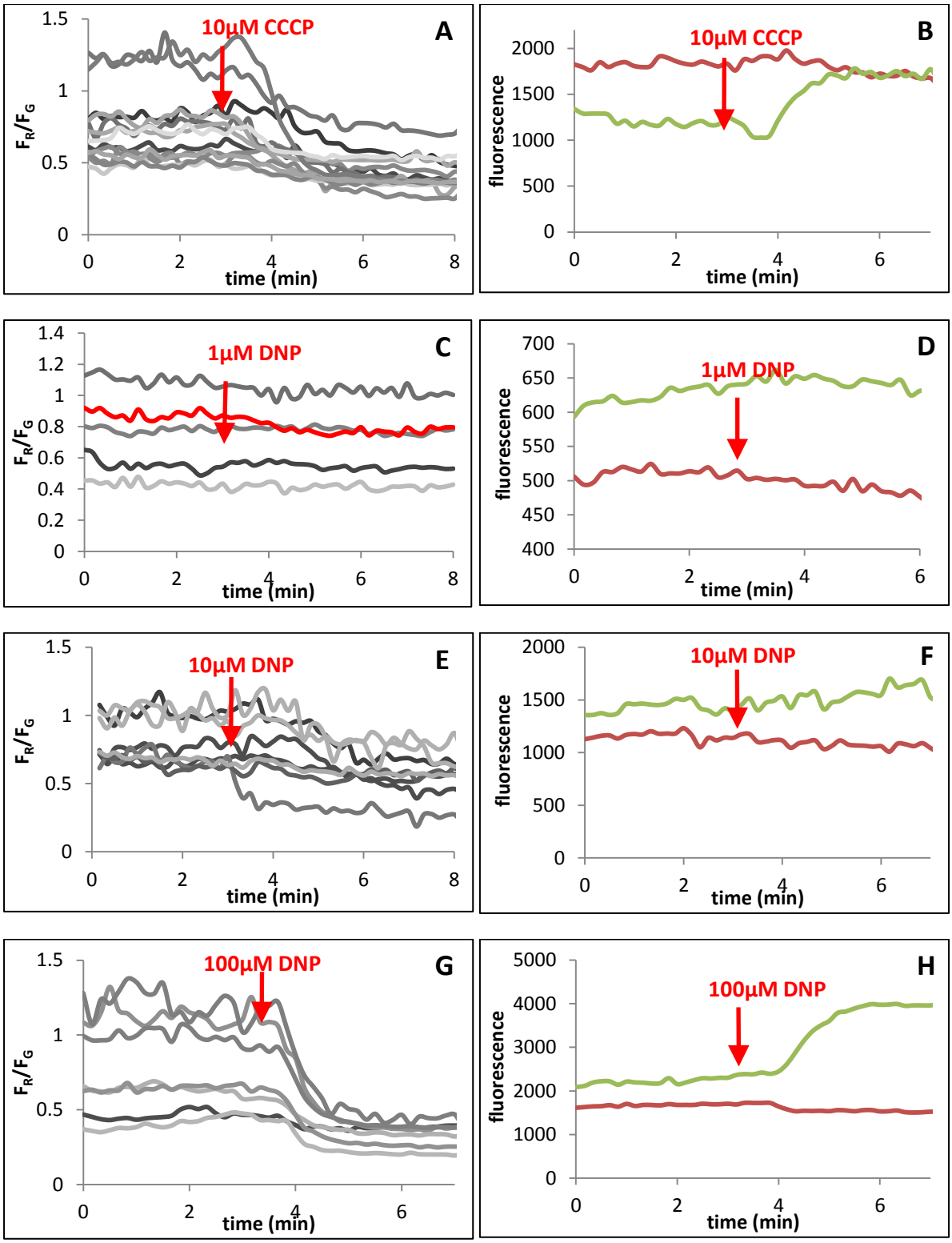

Figure 3.1 Effect of mitochondrial inhibitors on MMP of human sperm. Mitochondrial membrane potential can be determined by the ratio of red: green fluorescence (F_R/F_G) as determined by JC-1 dye application. In the following graphs cells were treated with JC-1 and monitored in sEBSS for 300s before 10µM CCCP, 1µM, 10µM or 100µM DNP application (red arrow). A, C, E & G show individual cell PHN F_R/F_G responses (greys traces) for 10µM CCCP, 1µM, 10µM or 100µM DNP treatment respectively. B, D, F & H show representative F_R and F_G traces for a single cell.

green fluorescence traces see Figure 3.1B, D, F & H. In cells treated with 1µM or 10µM DNP the MMP depolarisation was significantly less than that induced by both 10µM CCCP (*P*=0.0003, *P*=0.0009 respectively; t-test; n=3, n=15 respectively) or 100µM DNP (*P*=0.004, *P*=0.009 respectively; t-test; n=3 n=15 respectively; Figure 3.2D) application. These results suggest a dose dependent effect of DNP on MMP. Analysis of individual cell responses reinforces DNP dose response relationship with an increased proportion of cells exhibiting depolarisation with increasing DNP concentration (Figure 3.2E). 10µM CCCP appears to have a similar impact on MMP as 100µM DNP exhibiting similar population response kinetics (Figure 3.2D&E). In summary both CCCP and DNP induce mitochondrial depolarisation, in human sperm cells.

3.5.1.1 Effect of mitochondrial uncouplers on progesterone induced hyperpolarisation of the mitochondrial membrane potential

In human sperm the most well characterised $[Ca^{2+}]_i$ response is the biphasic signal induced by progesterone and this is often used as a positive control in Ca^{2+} imaging experiments. In JC-1 loaded cells 3µM progesterone induced a sustained F_R/F_G increase (MMP hyperpolarisation) of 0.2 in ~80% of cells (Figure 3.3D). To test the effects of mitochondrial inhibitors CCCP and DNP on the progesterone induced MMP hyperpolarisation, experiments were conducted in pairs, where cells from the same semen sample were treated with 3µM progesterone with and without mitochondrial inhibitor pre-treatment. For pre-treatment cells were exposed to 10µM DNP, 100µM DNP or 10µM CCCP prior to progesterone application. In all experimental pairs those cells pre- treated with mitochondrial inhibitors exhibited the MMP depolarisation previously described (section 3.5.1; Figure 3.3 A-C).

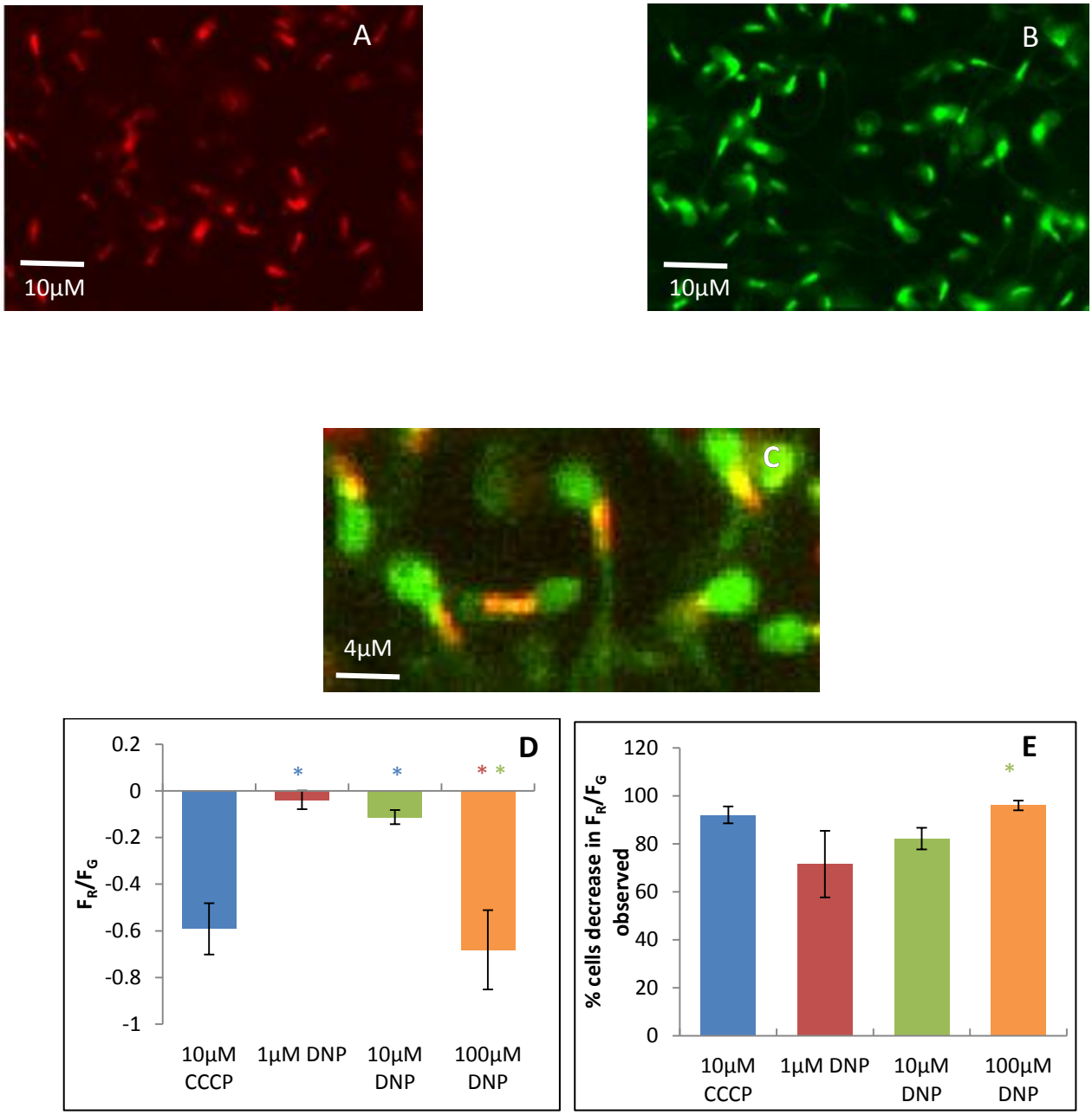

Figure 3.2 Mitochondrial inhibitors depolarise the MMP of human sperm. JC-1 loaded cells demonstrate red mitochondrial fluorescence (A) and green cytoplasmic fluorescence (B). (C) Red/green fluorescence overlay of sperm cells loaded with JC-1. (D) Minimum F_R/F_G ratio responses within 3min of inhibitor application. (E) Proportion of cells with an observable decrease in F_R/F_G. Results are means ± S.E.M. * $P<0.05$ compared to1µM DNP, * $P<0.05$ compared to 10µM DNP,* $P<0.05$ compared to CCCP; paired t-test; n=11, n=5, n=9 & n=8 respectively).

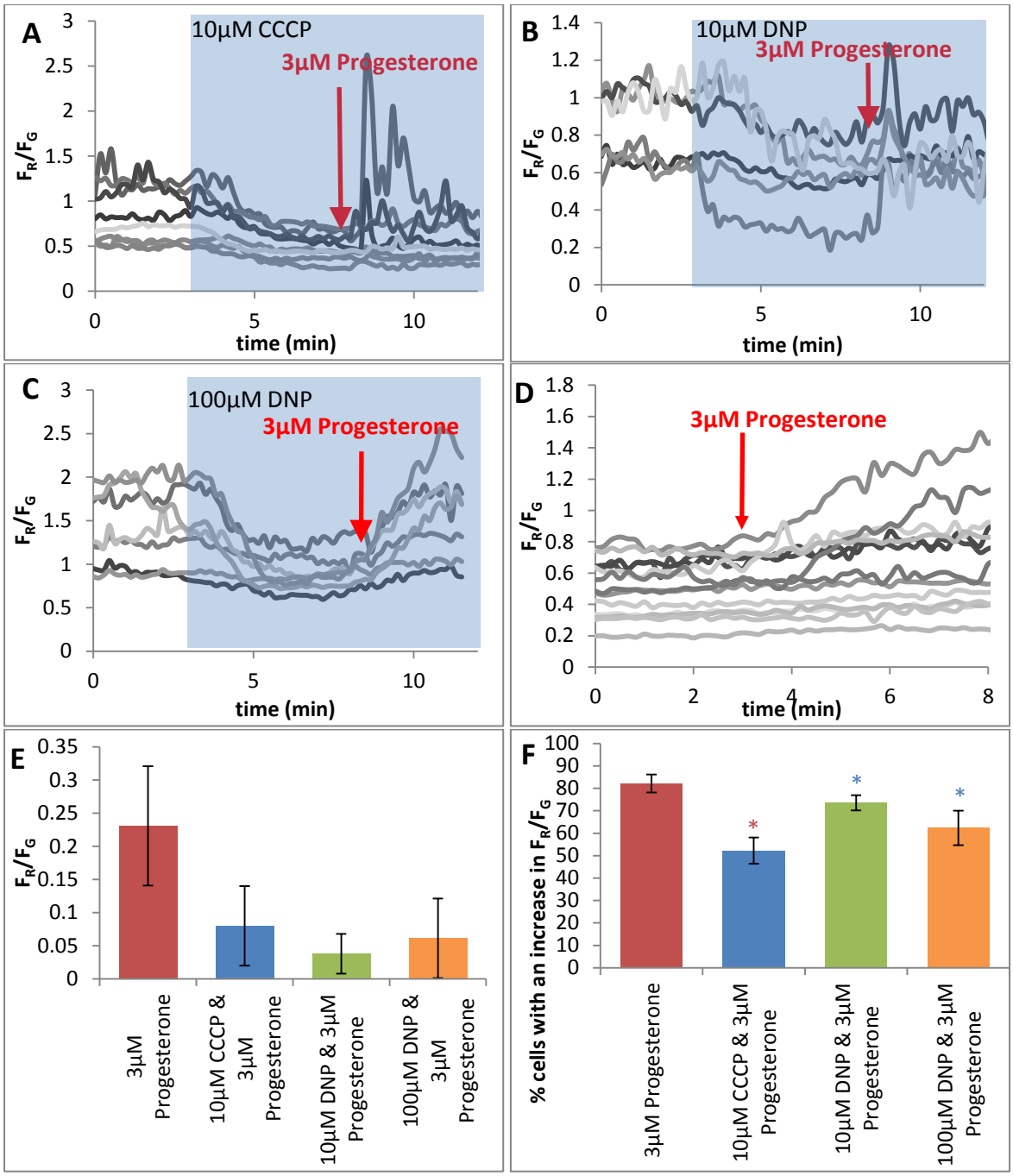

Figure 3.3 Effect of mitochondrial inhibitors on progesterone induced MMP hyperpolarisation. In the following graphs cells were treated with JC-1 and monitored in sEBSS for 300s before 10µM CCCP (A), 10µM (B), 100µM DNP (C) application (red arrow) prior to stimulation with 3µM progesterone (D). (A-D) Show individual cell PHN F_R/F_G responses (grey traces). (E) Maximum F_R/F_G ratio responses within 3min of inhibitor application. (F) Proportion of cells with an observable increase in F_R/F_G. Results are means ± S.E.M. * $P<0.05$ compared to progesterone control, * $P<0.05$ compared to CCCP; paired t-test; n=11, n=11, n=9 & n=8 respectively.

Subsequent addition of 3µM progesterone to the perfusion media resulted in hyperpolarisation of the MMP in a subset of cells (3.3E&F). In 10 out of 11 experimental pairs pre-treatment with 10µM CCCP (300s) reduced the level of progesterone induced mitochondrial hyperpolarisation by F_R/F_G 0.15 compared to that seen without pre-treatment (n=11; *P*=0.14; paired t-test; Figure 3.3A&E). Thus reducing the number of significant F_R/F_G responses observed by 25% (Figure 3.3F). DNP pre-treated cells respond similarly with 8 out of 9 and 7 out of 8 experimental pairs treated with 10µM DNP and 100µM DNP respectively showing a smaller MMP hyperpolarisation compared to progesterone alone (Figure 3.3B&C). 10µM DNP pre-treatment induced a significant reduction in the percentage of cells that showed hyperpolarisation of MMP in response to progesterone application (*P*=0.02; n=11; paired t-test), however this was not observed with other mitochondrial inhibitors.

3.5.2 Mitochondrial inhibitors raise resting $[Ca^{2+}]_i$ at the PHN

Initially we examined the effect of mitochondrial inhibitors CCCP and DNP on resting $[Ca^{2+}]_i$ at the PHN of human sperm samples loaded with OGB. Treatment with 10µM, 100µM DNP or 10µM CCCP increased PHN $[Ca^{2+}]_i$ (Figure 3.4A-D). Cell populations treated with 10µM CCCP or 10µM DNP exhibited similar Ca^{2+} response kinetics, each producing a sustained rise then plateau in $[Ca^{2+}]_i$ of ~8% (Figure 3.4D), in 60-70% of the cell population (Figure 3.4F). However cells treated with 100µM DNP produced a transient increase $[Ca^{2+}]_i$ of ~10% (Figure 3.4C&D) which lasted ~1min and remained elevated above control levels thereafter. Figures 3.4A-D illustrate individual cell PHN $[Ca^{2+}]_i$ traces that are representative of the population CCCP and DNP responses observed. Individual cell response kinetics reveal a bell shaped distribution of peak amplitude response increments for both mitochondrial inhibitors with most cells exhibiting a peak of 10-20% (ΔF; Figure 3.4E).

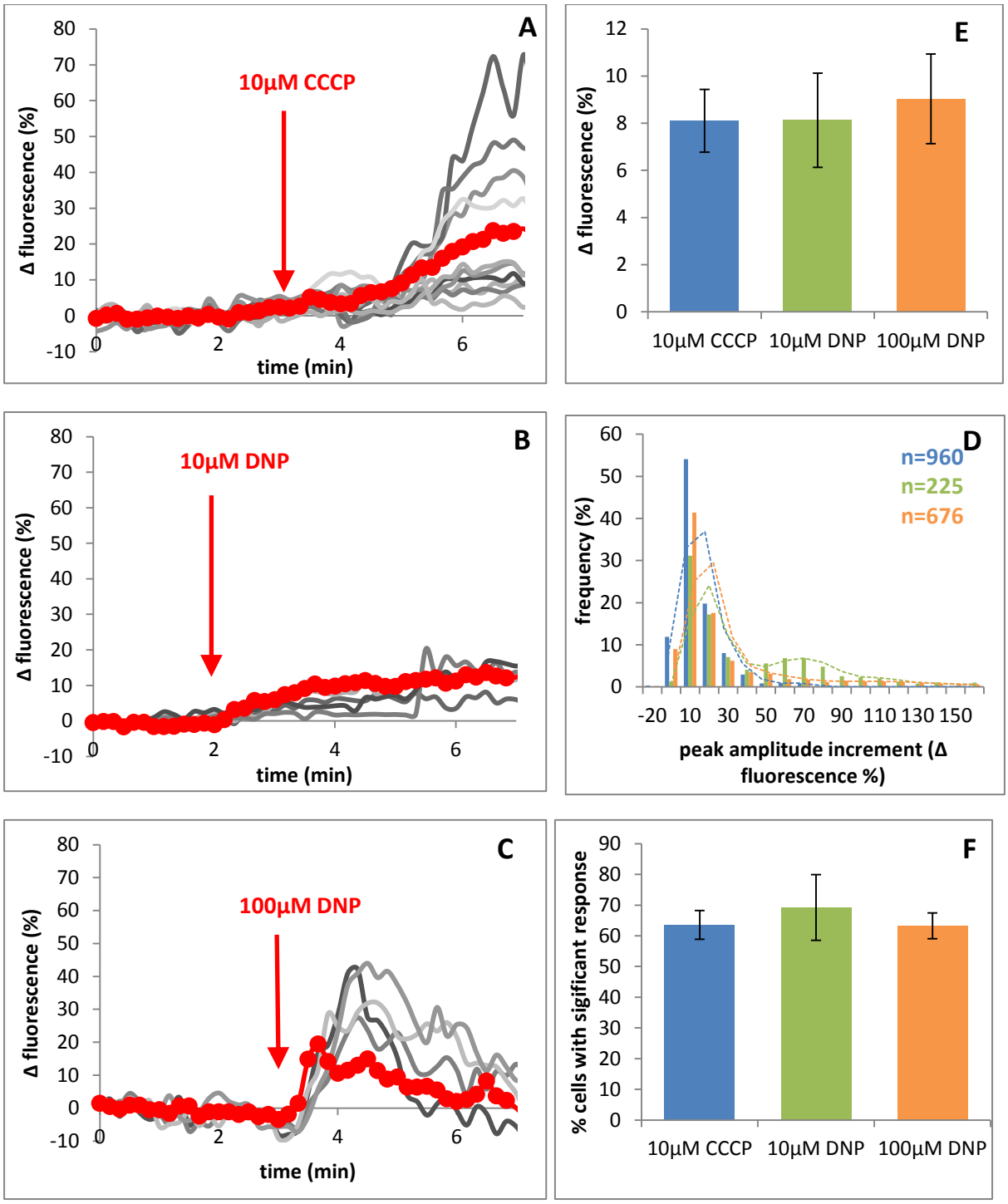

Figure 3.4 Mitochondrial inhibitors elevate $[Ca^{2+}]_i$ at the PHN. Graphs A-C show representative individual cell responses (grey traces) and a ΔF_{mean} for a single experiment (red trace) treated with (A) 10µM CCCP (B) 10µM DNP and (C) 100µM DNP. (D) Maximum increase in ΔF_{mean} within 4min of inhibitor application. (E) Frequency distribution of ΔF_{max} amplitude amongst the cell population. (F) Proportion of cells displaying significant ΔF_{max} response amplitude. Results are means ± S.E.M. * P<0.05 compared to CCCP; paired t-test; n=11, n=9 & n=8 respectively.

3.5.2.1 Mitochondrial inhibitors $[Ca^{2+}]_i$ responses are dependent on external Ca^{2+}

To determine the origin of Ca^{2+} responsible for the increase in $[Ca^{2+}]_i$ at the PHN induced by mitochondrial inhibitors experiments were conducted in Ca^{2+} free sEBSS ($[Ca^{2+}]$~$3x10^{-7}$M). Sperm were loaded with OGB in the presence of extracellular Ca^{2+} and monitored for a period of at least 20 frames under these conditions. Subsequently the cells were exposed to Ca^{2+} free sEBSS ($[Ca^{2+}]$~$3x10^{-7}$M) for 100s before the mitochondrial inhibitors were added in the absence of extracellular Ca^{2+}. Figure 3.5A-B show several representative $[Ca^{2+}]_i$ responses to mitochondrial inhibitor stimulation in the absence of extracellular Ca^{2+}. In these experiments it is important to note that some interesting observations get lost in the population averages. As Figure 3.5C demonstrates, introduction of EGTA buffered saline $[Ca^{2+}]_i$ decreased over a period 5-6 minutes. Application of 10µM DNP, 10µM CCCP or 100µM DNP during this period induced only a small, transient increase in population $[Ca^{2+}]_i$. As Figures 3.5A-B demonstrates a subset of cells display a small significant transient increase or sustained $[Ca^{2+}]_i$ increase in response to inhibitor application under these conditions, consistent with Ca^{2+} release from intracellular stores (Figure 3.5D). It is apparent that this release of stored Ca^{2+} does not equal the increase in $[Ca^{2+}]_i$ observed in the presence of extracellular Ca^{2+} suggesting that mitochondrial inhibitor $[Ca^{2+}]_i$ increases observed in Ca^{2+} containing media include a significant component dependent upon influx of extracellular Ca^{2+}.

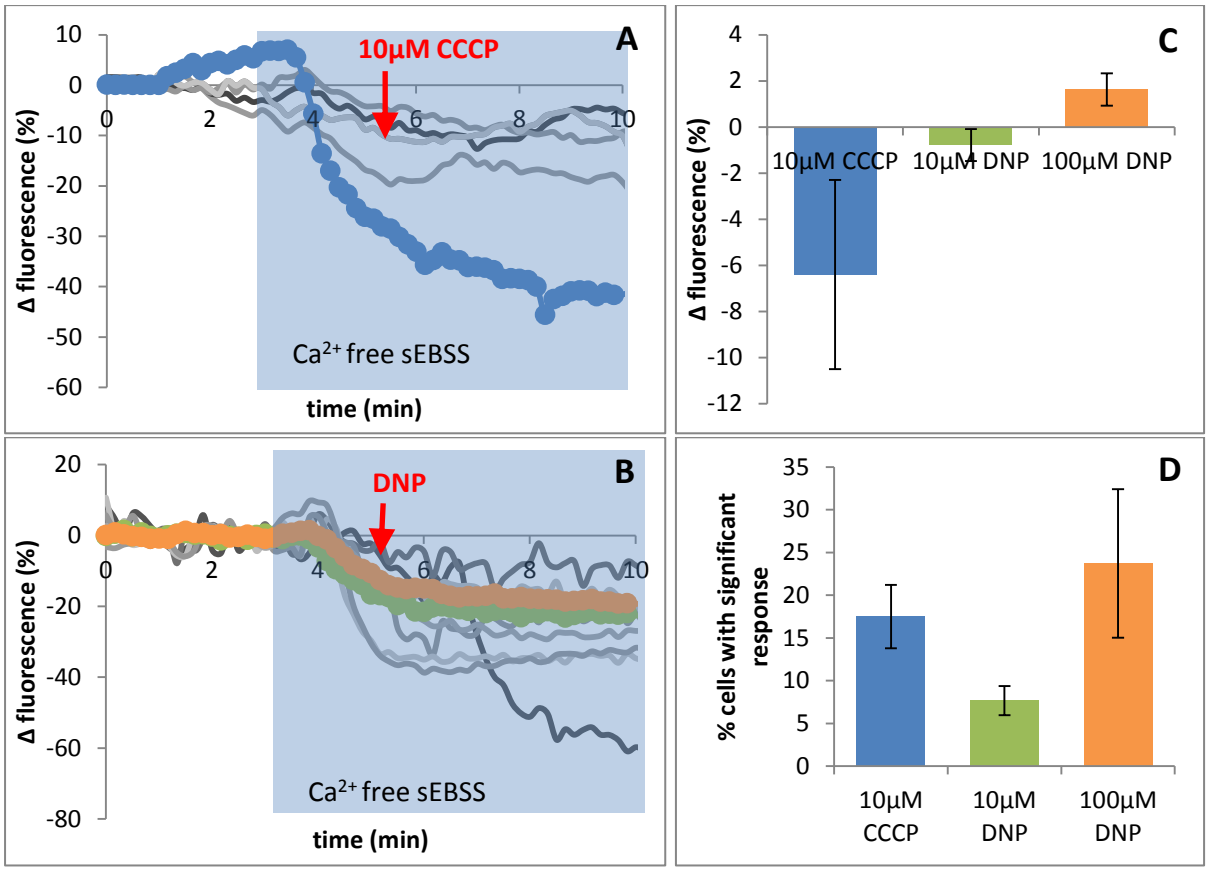

Figure 3.5 Effect of mitochondrial inhibitors on $[Ca^{2+}]_i$ at the PHN in the absence of extracellular Ca^{2+}. Representative individual cell $[Ca^{2+}]_i$ traces in response to addition of CCCP (A, 10µM blue trace), DNP (B, 10µM green trace, 100µM orange trace) with ΔF_{mean} expressed as coloured traces. (C) Maximum increase in ΔF_{mean} within four minutes of inhibitor application. (D) Proportion of cells displaying significant ΔF_{max} response amplitude. Results are means ± S.E.M. n=6, n=6 & n=6 respectively.

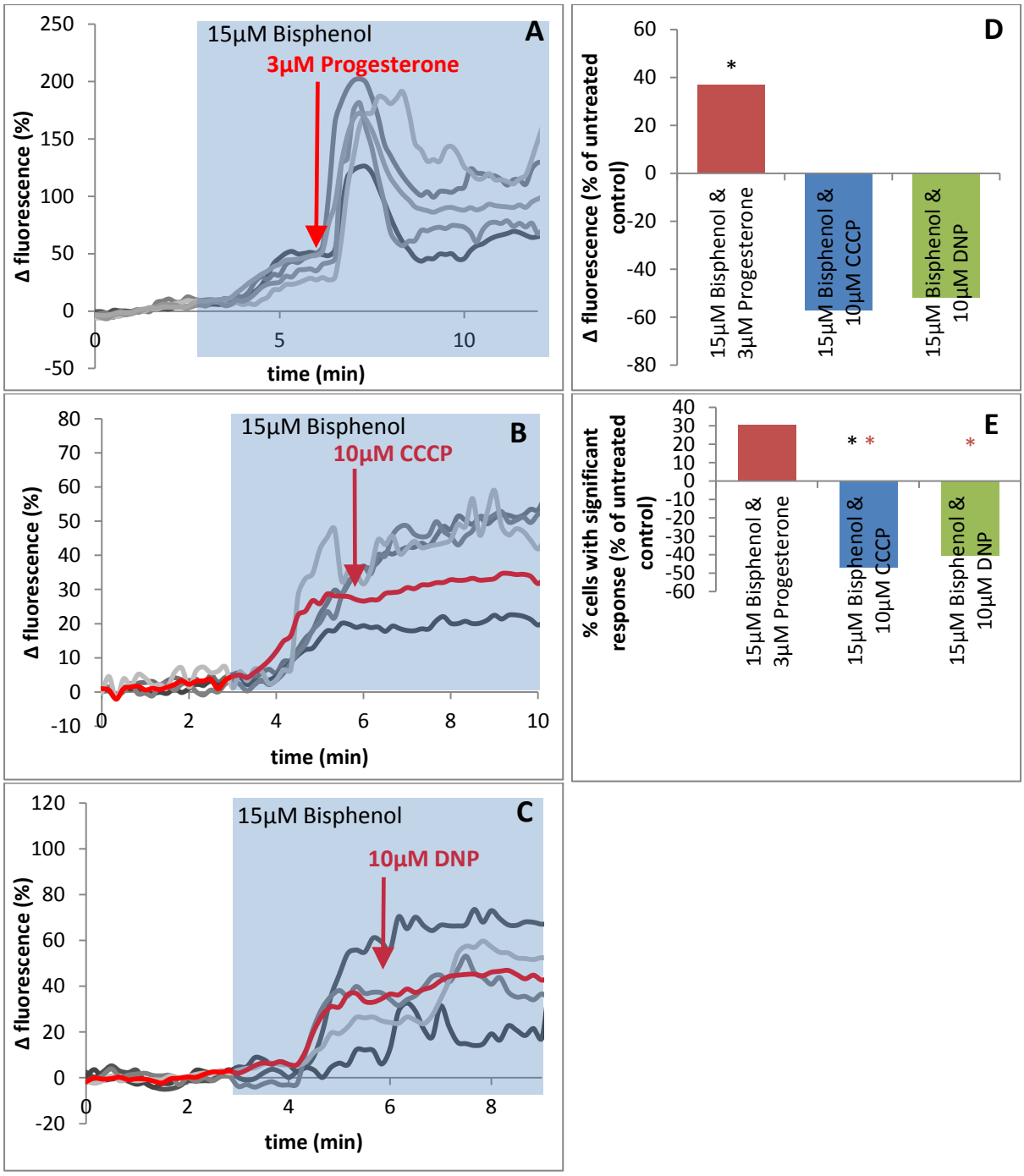

Figure 3.6 Bisphenol reduces the mitochondrial inhibitor induced $[Ca^{2+}]_i$ increase at the PHN. In the following graphs cells were loaded with OGB and monitored in sEBSS for 300s before stimulation with 15µM Bisphenol and subsequent treatment with (A)3µM progesterone (B) 10µM CCCP or (C)10µM DNP (red arrow). A-C show individual cell responses (greys traces) and ΔF_{mean} for a single experiment. (D) Maximum ΔF_{mean} responses within 3min of inhibitor application. (F) Proportion of cells with a significant increase in ΔF_{mean}. Results are means ± S.E.M. * $P<0.05$ compared to progesterone control, * $P<0.05$ compared to parallel untreated controls; paired t-test; n=7, n=7 & n=8 respectively).

3.5.2.2 Bisphenol effect on $[Ca^{2+}]_i$ increases induced by mitochondrial inhibitors

Bisphenol is a specific Ca^{2+}-ATPase inhibitor, in sea urchin sperm 15μM bisphenol mobilises stored Ca^{2+} leading to activation of SOCs and Ca^{2+} influx (Ardon *et al.,* 2009). In human sperm SPCA1 and SERCA Ca^{2+}-ATPase pumps have been detected at the PHN/midpiece. These pumps are believed to contribute significantly to Ca^{2+} uptake at the PHN Ca^{2+} store, possibly even contributing to Ca^{2+} accumulation into the mitochondria. Here we wanted to determine whether treating cells with 15μM bisphenol (to prevent store Ca^{2+} uptake) prior to mitochondrial inhibitor application affected the increase in $[Ca^{2+}]_i$ observed at the PHN.

Application of 15μM bisphenol induced a sustained increase of in $[Ca^{2+}]_i$ of ~30% followed by a plateau in ~85% of cells (Figure 3.6A-C). To determine the effect of bisphenol treatment on the mitochondrial inhibitor $[Ca^{2+}]_i$ response all experiments were carried out in pairs. Cells from the same semen preparation were exposed to 10μM CCCP, 10μM DNP or 3μM progesterone with and without pre-exposure to 15μM bisphenol. Pre-treatment with bisphenol decreased the $[Ca^{2+}]_i$ responses induced by both CCCP and DNP (57% and 51% respectively; P=0.15, P=0.26 respectively; paired t-test; n=7, n=5; Figure 3.6D). In contrast treatment with 3μM progesterone after bisphenol application caused a significant increase in the $[Ca^{2+}]_i$ response observed (P=0.03; n=7; Figure 3.6D). The proportion of cells producing a significant increase in $[Ca^{2+}]_i$ in response to mitochondrial inhibitors was significantly decreased in both CCCP and DNP treated cells pre-exposed to bisphenol (P=0.013 and P=0.02 respectively; paired t-test; n=5, n=7; Figure 3.6E).

3.5.3 Mitochondrial inhibitors raise resting $[Ca^{2+}]_i$ at the acrosome, PHN and midpiece

Our initial observations on the effects of mitochondrial inhibitors CCCP and DNP on resting $[Ca^{2+}]_i$ at the PHN utilised the high affinity Ca^{2+} dye OGB, which displayed Ca^{2+} distribution throughout the cell (Figure 3.7A). To clearly distinguish areas of high Ca^{2+} concentration we over loaded cells with the low affinity Ca^{2+} dye Mag-Fluo-4AM (MF), subsequent permeabilisation with Streptolysin-O enabled loss of cytoplasmic Ca^{2+} and visualisation of two discrete regions of Ca^{2+} localisation at the acrosome and PHN/midpiece (Figure 3.7C). It should be noted that successful Streptolysin-O permeabilisation was inconsistent and in some cases contributed to premature AR and loss of Ca^{2+} fluorescence consistent with cell death, which prevented observation of subsequent agonist induced $[Ca^{2+}]_i$ responses. However cells loaded with MF for shorter periods enabled clear observation of separate Ca^{2+} stores without the need for permeabilisation (Figure 3.7B), which facilitated analysis of $[Ca^{2+}]_i$ at discrete intracellular regions to determine localised agonist effects at the acrosome, PHN and midpiece of human sperm (defined in Figure 2.9C). As a result all of the following experiments in this section where conducted in intact cells labelled with MF.

3.5.3.0.1 Progesterone induces biphasic $[Ca^{2+}]_i$ responses at the acrosome, PHN and midpiece

Stimulation with 3μM progesterone induces a characteristic biphasic increase in $[Ca^{2+}]_i$ at the acrosome, PHN and midpiece in intact human sperm, which consists of an initial transient followed by a sustained plateau or series of oscillations. Figure 3.8A shows an example of representative $[Ca^{2+}]_i$ traces obtained at the acrosome, PHN and midpiece of a single cell. It

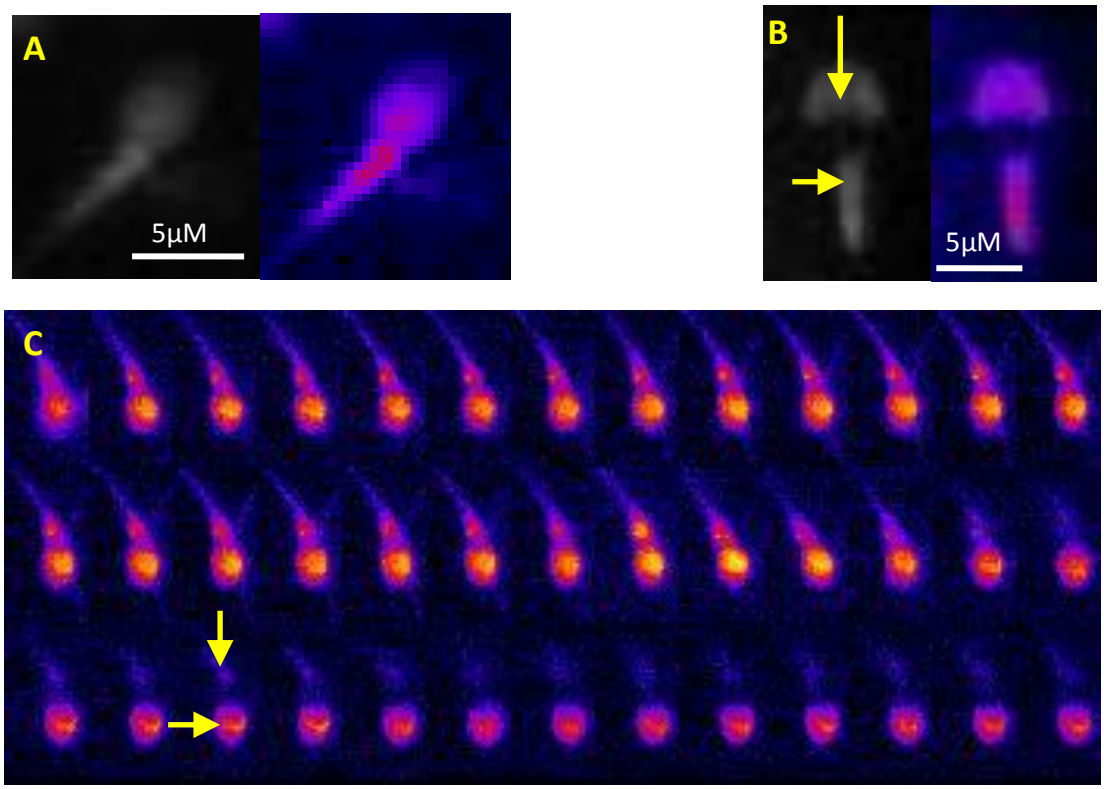

Figure 3.7 Visualisation of Ca^{2+} stores in human sperm. Grey scale and pseudo-colour image of $[Ca^{2+}]_i$ in cells loaded with Oregon Green BAPTA-2AM(A) or Mag-Fluo4-AM (B). (C) Sequential image series of a Mag-Fluo-4AM loaded cell permeabilised with SLO to clearly define the Ca^{2+} stores (yellow arrows). SLO is added to cells overloaded with MF in frame 4. Yellow corresponds to areas of high Ca^{2+} concentration and cold colours areas of low Ca^{2+} concentration.

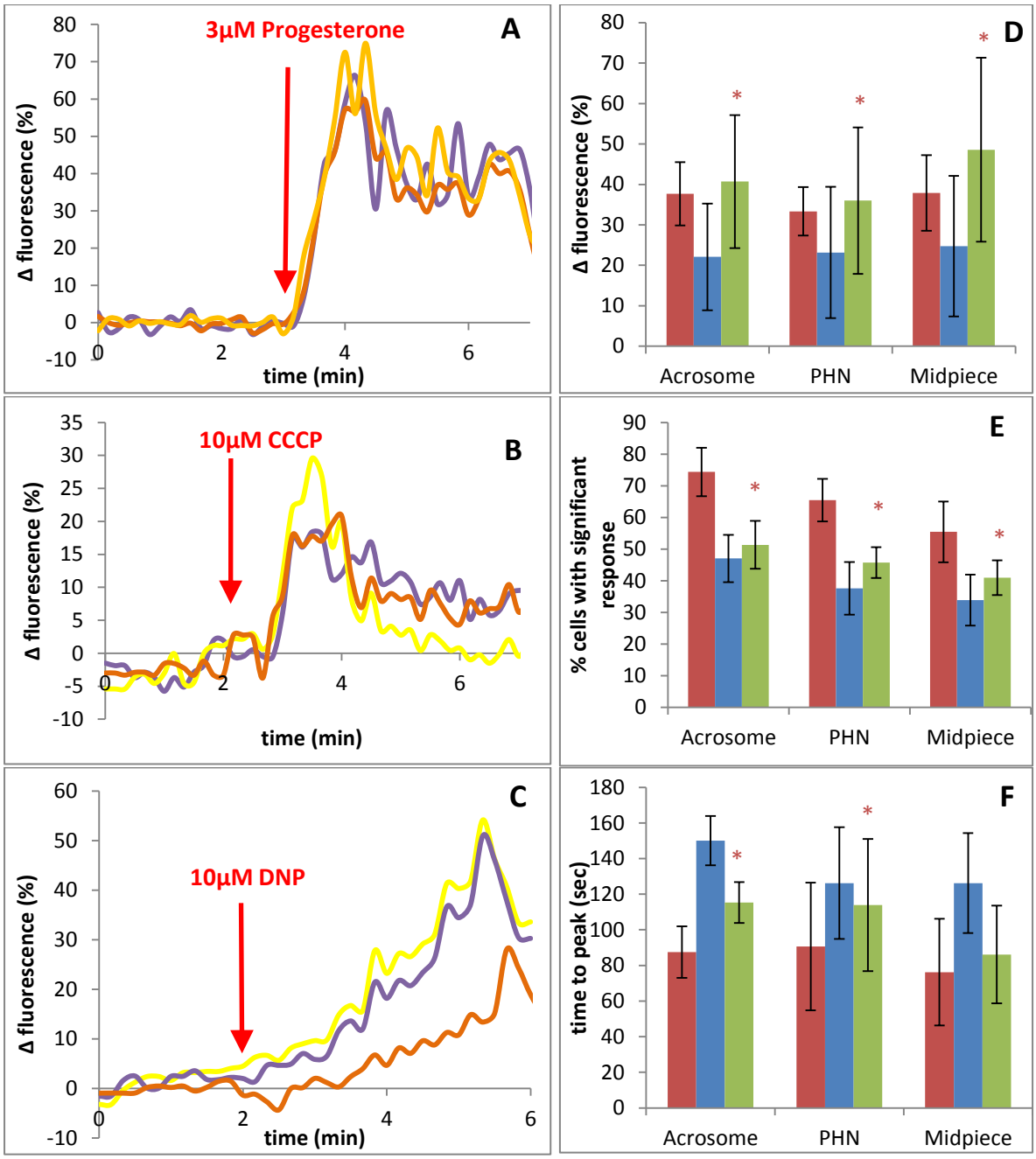

Figure 3.8 Mitochondrial inhibitors elevate resting $[Ca^{2+}]_i$ at the acrosome, PHN and midpiece. The increase in $[Ca^{2+}]_i$ observed at the acrosome (purple), PHN (orange) and midpiece (yellow) in representative cells treated with progesterone (A), CCCP (B) or DNP (C). In graphs D-F cells were treated with either 3µM progesterone (red) 10µM CCCP (blue) or 10µM DNP (green). (D) Maximum ΔF_{mean} amplitude within 3 min of progesterone application. (E) Proportion of cells displaying significant ΔF_{mean} response amplitude. (F) Time taken to achieve maximum increase in $\Delta F_{mean.}$ *P<0.05 compared to progesterone, *P<0.05 compared to DNP, n=16, n=8 & n=13 respectively where n equals the number of experimental repeats.

should be noted that the response amplitudes vary amongst the population however the trend observed in Figure 3.8A remains the same. The transient $[Ca^{2+}]_i$ elevation at all three regions began almost simultaneously within seconds of progesterone application (data were collected at 0.1 Hz and the ability to detect temporal differences was therefore limited) and decreased in a similar manner, followed by numerous oscillations. Peak $[Ca^{2+}]_i$ of 35-40% (Figure 3.8D) was achieved in >55% of cells (Figure 3.8E) within 75-90sec (Figure 3.8F) at all regions and showed no significant difference between regions (*P*=0.90, *P*=0.20 & *P*=0.73 respectively; ANOVA; n=16). Initial observations showed a greater proportion of cells exhibited a significant $[Ca^{2+}]_i$ response to progesterone at the acrosome, with the lowest proportion of significant responses observed in the midpiece (Figure 3.8E). However this was insignificant indicating progesterone induces similar $[Ca^{2+}]_i$ responses throughout human sperm.

3.5.3.0.2 CCCP similarly effects $[Ca^{2+}]_i$ at the acrosome, PHN and midpiece

In cells labelled with MF addition of 10μM CCCP induced a peak increase of ~25% in $[Ca^{2+}]_i$ at the acrosome, PHN and midpiece (Figure 3.8B&D) consistent with observations from OGB experiments (section 3.5.2). Like cells treated with progesterone, CCCP induces analogous $[Ca^{2+}]_i$ responses at the acrosome, PHN and midpiece of human sperm, which peaks 2-3min after application (*P*=0.99; ANOVA; n=8; Figure 3.8D). Furthermore the proportion of cells exhibiting a significant CCCP response and time taken to achieve peak $[Ca^{2+}]_i$ responses at the acrosome, PHN and midpiece did not differ significantly between the three regions (*P*=0.43 & *P*=0.85 respectively; ANOVA; n=8; Figure 3.8E&F).

3.5.3.0.3 DNP induced $[Ca^{2+}]_i$ increases measured with Mag-Fluo-4AM exceed those observed with progesterone treatment

10μM DNP increased $[Ca^{2+}]_i$ at the acrosome, PHN and midpiece of human sperm inducing a sustained rise or series of transients at each region (Figure 3.8D). Figure 3.8C shows a single cell response to DNP application which is representative of the cell population. Although the peak increase in $[Ca^{2+}]_i$ at the midpiece typically exceeds the increases observed at the acrosome and PHN by ~10%, ~30sec quicker (Figure 3.8D&F), there is no significant difference in the peak $[Ca^{2+}]_i$, proportion of cells exhibiting a significant response or time to peak between regions (*P*=0.84, *P*=0.52 & *P*=0.61 respectively; ANOVA; n=13). In MF loaded cells the peak $[Ca^{2+}]_i$ response induced by DNP significantly exceeds that induced by progesterone at all regions (*P*=0.03, *P*=0.003 & *P*=0.02 respectively; paired t-test; n=13; Figure 3.8D). Furthermore time taken to achieve DNP induced $[Ca^{2+}]_i$ peak takes ~20sec longer at the acrosome and PHN, which is significantly greater than parallel progesterone controls (*P*=0.027 & *P*=0.024; paired t-test; n= 13; Figure 3.8F). Interestingly analysis of individual cell responses reveals a significant decrease in the proportion of cells exhibiting a significant $[Ca^{2+}]_i$ response to DNP compared to progesterone at all three regions observed (acrosome *P*=0.009, PHN *P*=0.005 & midpiece *P*=0.04; paired t-test; n=13). Together these results indicate that DNP induced $[Ca^{2+}]_i$ elevations are not restricted to mitochondrial Ca^{2+} storage capacity and that they are significantly distinct from progesterone induced $[Ca^{2+}]_i$ changes.

3.5.3.1 Mitochondrial inhibitors differentially effect the biphasic progesterone $[Ca^{2+}]_i$ transient at the acrosome, PHN and midpiece

The biphasic $[Ca^{2+}]_i$ response induced by progesterone application is well characterised (Kirkman-Brown *et al.*, 2000; Harper *et al.*, 2004) with a distinctive dose effect relationship

between progesterone response and ΔF_{mean} amplitude. Alone the mitochondrial inhibitors CCCP and DNP raise $[Ca^{2+}]_i$ at the acrosome, PHN and midpiece. Here we wanted to determine the effects of mitochondrial inhibitors and therefore possible mitochondrial Ca^{2+} contribution to the biphasic progesterone induced $[Ca^{2+}]_i$ response at the acrosome, PHN and midpiece using the low affinity Ca^{2+} dye MF in intact cells. It should be noted that although $[Ca^{2+}]_i$ elevations observed at each region vary there is no significant difference between the acrosome, PHN or midpiece for any of the three treatments observed (P<0.05; ANOVA; n=15, 8 & 7 respectively).

3.5.3.1.1 Acrosome

Ca^{2+} mobilisation has been observed at the acrosome in response to a number of agonists but principally progesterone (Rodriguez-Peña *et al.,* 2013). 3μM progesterone induces a characteristic biphasic $[Ca^{2+}]_i$ increase in the majority of cells with the transient response peaking within 1-2 min (section 3.5.3.0.1; Figure 3.9A). Pre-treatment with 10μM mitochondrial uncouplers CCCP or DNP have differential effects on the $[Ca^{2+}]_i$ transient observed (Figure 3.9B&C), but neither significantly affect the amplitude (Figure 3.9D), time to peak (Figure 3.9F) or proportion of cells producing a significant progesterone transient compared to untreated controls (Figure 3.9E). However CCCP and DNP effects on the progesterone induced $[Ca^{2+}]_i$ transient amplitude (Figure 3.9D), time to peak (Figure 3.9F) and proportion of cells producing a significant progesterone transient significantly differ (P=0.009, P=0.018 & P=0.030; paired t-test; n=8).

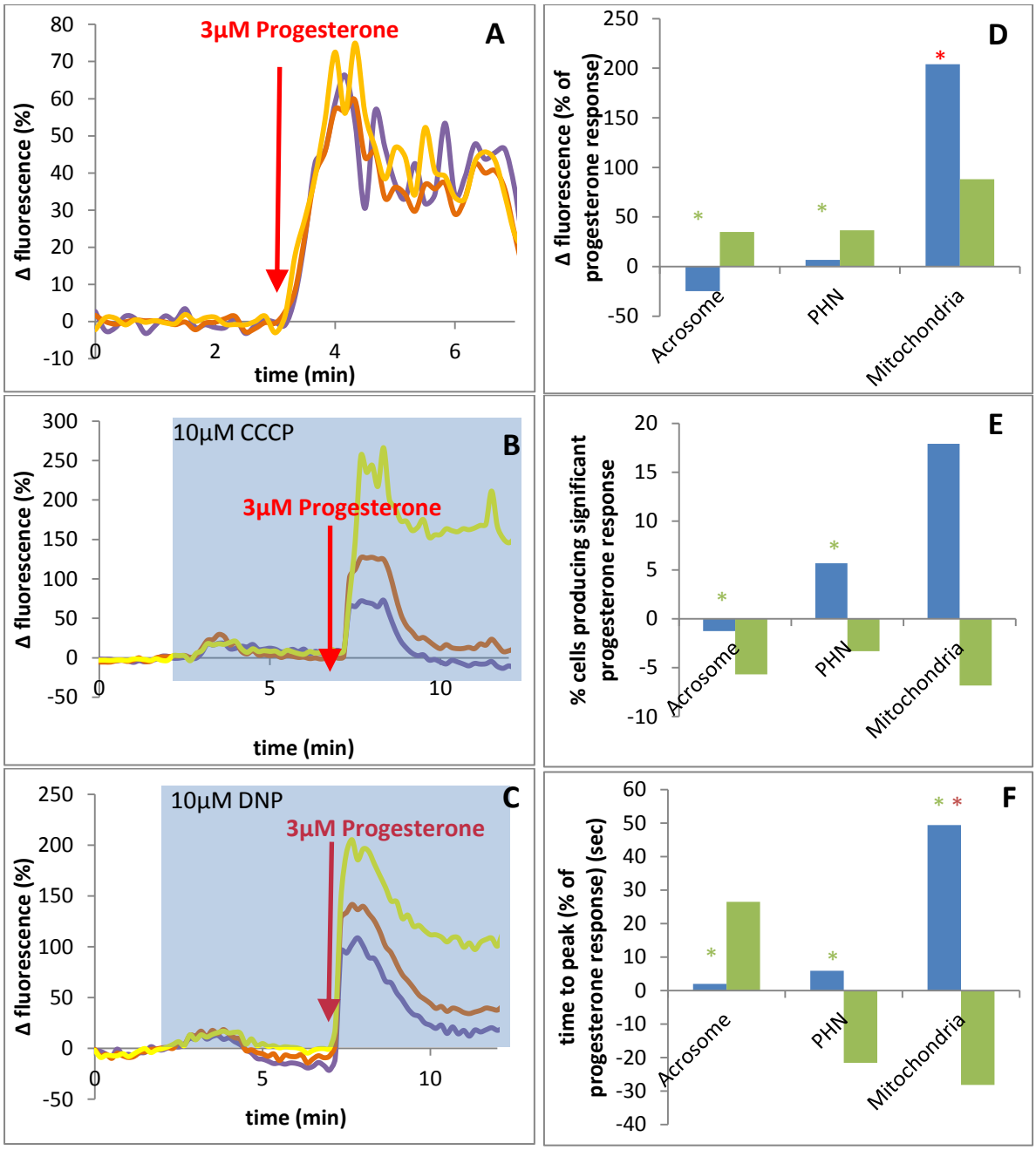

Figure 3.9 Effect of mitochondrial inhibitors on the progesterone induced $[Ca^{2+}]_i$ transient at the acrosome, PHN and midpiece. The increase in $[Ca^{2+}]_i$ observed at the acrosome (purple), PHN (orange) and midpiece (yellow) in representative cells treated with progesterone (A) after pre-treatment with CCCP (B) or DNP (C). Graphs D-F show mean results as percentage responses of the parallel progesterone control, bars represent cells pre-treated with 10µM CCCP (blue) and 10µM DNP (green). (D) Maximum ΔF_{mean} amplitude within 3 min of progesterone application. (E) Proportion of cells displaying significant ΔF_{mean} response amplitude. (F) Time taken to achieve maximum increase in ΔF_{mean}. *P<0.05 compared to progesterone, *P<0.05 compared to DNP. Results are mean responses for the population tested. n=8 where n equals the number of experimental repeats for all experiments.

3.5.3.1.2 PHN

At the PHN, mitochondrial uncouplers induced no significant effect on the transient $[Ca^{2+}]_i$ response induced by progesterone compared to parallel progesterone controls (P>0.05; paired t-test; n=8; Figure 3.9A-F). However there was a significant difference between CCCP and DNP effects on the progesterone transient amplitude (Figure 3.9D) and time to peak (Figure 3.9F; P=0.016 & P=0.0013 respectively; paired t-test; n=8). Cumulatively observations at the acrosome and PHN indicate that mitochondrial uncouplers have no significant effect on the transient $[Ca^{2+}]_i$ response induced by progesterone at regions where mitochondria are not present. This suggests that CCCP and DNP responses observed here are not the results of mitochondrial Ca^{2+}efflux but of an alternative Ca^{2+} store in the region.

3.5.3.1.3 Midpiece

Mitochondria of mammalian sperm are localised to the midpiece, as such it is likely that effects of mitochondrial inhibitors on $[Ca^{2+}]_i$ are most prominent here. At the midpiece, both 10μM CCCP and 10μM DNP induced an increase in the progesterone transient amplitude (Figure 3.9D). 10μM CCCP showed greater efficacy elevating the progesterone transient amplitude ~200% and time taken to achieve the peak ~50%, whilst the proportion of cells inducing a significant response also increased ~20% (Figure 3.9D, E&F; P=0.025 & P=0.02 respectively; paired t-test; n=8). In contrast the enhancement of the response to progesterone caused by pre-treatment with 10μM DNP, although consistent, was insignificant. Furthermore the time taken to achieve the peak and proportion of cells producing a significant peak was reduced compared to both progesterone controls (Figure 3.9E&F; P=0.08 & P=0.60 respectively; paired t-test; n=8) and 10μM CCCP (Figure 3.9E&F; P=0.002 & P=0.12 respectively; paired t-test; n=8). Taken together these results indicate that CCCP significantly increases the progesterone induced $[Ca^{2+}]_i$ at the midpiece, (seen mildly

at the PHN and acrosome) which implicates Ca^{2+} contribution from the mitochondria or an alternative Ca^{2+} store in the region.

3.5.4 Hyperactivated motility is not induced by mitochondrial inhibitors

Data from the literature (Costello *et al.,* 2009) suggests a role for a Ca^{2+} store in the PHN of human sperm in controlling motility in particular hyperactivated motility. Specifically we wanted to determine whether application of mitochondrial inhibitors CCCP and DNP reduced percentage hyperactivation in capacitated cell populations. In Ca^{2+} imaging experiments increases in $[Ca^{2+}]_i$ were observed after 1min application and persisted for at least 5min (as long as the inhibitor was still present). In the following experiments cells were exposed to either10μM CCCP, 10μM DNP or no treatment (control) in parallel at 37^{o}C for 4 minutes and then the motility parameters determined by CASA. Analysis revealed no significant difference between % hyperactivation observed in untreated controls compared to those samples exposed to either CCCP or DNP (Table 3.1). Interestingly DNP showed no significant differences in motility parameters compared to the untreated control population. However 10μM CCCP treated cells showed an increase in ALH and a significant reduction of STR compared to the control untreated cell population, which is indicative of a mild increase in hyperactivated motility. Overall this data suggests that mitochondrial inhibitors do not significantly affect the Ca^{2+} store that appears to be responsible for regulation of hyperactivated motility. This suggests that the mitochondria alone in human sperm is insufficient to store the levels of Ca^{2+} required to initiate hyperactivation and that it is likely there is a second Ca^{2+} store at the PHN responsible.

PARAMETER	CONTROL	S.E.M	10µM DNP	S.E.M	10µM CCCP	S.E.M	UNITS
Hyperactivation	7.13	1.94	6.42	2.36	8.38	2.75	%
Path velocity VAP	69.18	5.03	60.61	7.76	57.6*	5.30	µm/s
Prog. velocity VSL	59.75	5.43	49.68	7.92	43.53*	4.92	µm/s
Track Speed VCL	115.52	6.69	104.17	11.04	106.44***	7.95	µm/s
Lateral Amplitude ALH	5.25	0.26	5.31	0.24	5.85	0.22	µm
Beat Frequency BCF	23.90	1.40	23.98	0.81	20.19	0.50	Hz
Straightness STR	84.25	2.02	79.67	3.47	73.58**	1.82	%
Linearity LIN	52.33	2.84	47.13	3.22	40.58*	1.72	%
Elongation	66.46	1.09	65.83	1.24	66.25	0.78	%

Table 3.1 Effects of mitochondrial inhibitors on hyperactivated motility parameters as determined by CASA. Experiments were carried out in pairs, where cells from the same semen sample were analysed by CASA with and without treatment. Cells without treatment were prepared in sEBSS, control no treatment (lilac). Treated cells were exposed to either 10µM DNP (purple), 10µM CCCP (orange). For each condition path velocity (VCL), progressive velocity (VSL), track speed (VCL), lateral head amplitude (ALH), beat frequency (BCF), straightness (STR), linearity (LIN) and elongation were determined. * $P<0.05$, ** $P<0.02$, *** $P<0.01$, **** $P<0.005$; compared to CNT; paired t-test; n=3-7.

3.6 Discussion

Mitochondrial contribution to $[Ca^{2+}]_i$ homeostasis and signalling cascades is not well characterised in mammalian germ cells. In somatic cells the existence of a pathway enabling mitochondria to accumulate and store Ca^{2+} was established 40 years ago (Scarpa & Azzone, 1970; Tjioe *et al.,* 1970). In this model mitochondria facilitate Ca^{2+} uptake via the mitochondrial uniporter (MCU; chapter 1.10.2.3), which is dually mediated by the electrochemical membrane potential gradient ($\Delta\Psi m$, MMP) and $[Ca^{2+}]_i$ (Duchen, 2000). $\Delta\Psi m$ is primarily established by electron transport during oxidative phosphorylation. The result is a large negative potential gradient between the IMM and the cytosol, which enables mitochondrial Ca^{2+} accumulation under normal physiological conditions (Duchen, 2000). $[Ca^{2+}]_i$ also regulates mitochondrial storage capacity, at high $[Ca^{2+}]_i$ the modulatory protein MICU1 dissociates from the EF-hands of MCU enabling Ca^{2+} uptake, which is inhibited at low $[Ca^{2+}]_i$ (Mallilankaraman *et al.,* 2012; Figure 1.19). Mitochondrial Na^+-Ca^{2+} exchangers (NCX) modulate mitochondrial $[Ca^{2+}]_i$ ensuring that capacity reflects the $[Ca^{2+}]_i$ requirements of the cell (Palty *et al.,* 2012) and were identified in human sperm (Babcock & Pfeifer, 1987). In addition as the ATP producing powerhouses of the cell, mitochondria couple ATP production with increased Ca^{2+} flux and modulation of $[Ca^{2+}]_i$ (Rizzuto & Pozzan, 2006). This is of particular interest in mammalian sperm where mitochondrial inhibition has been shown to prevent hyperactivated motility; however hyperactivation potential was restored by the addition of Ca^{2+} (Ho & Suarez, 2003).

In mammalian sperm mitochondria display distinctive characteristics indicative of specialised cell requirements which set them apart from somatic cells. The highly polarised and compartmentalised structure of mature sperm ensures all superfluous organelles are eliminated at spermiogenesis and remaining organelles are localised according to function.

Mitochondria of human sperm are localised exclusively to the midpiece (Piomboni *et al.*, 2012) at the apical flagellum and are implicated in the initiation of flagellar motility. It should be noted that although the remaining flagellum (principal piece) is devoid of mitochondria, it is enriched in sperm specific glycolytic isoenzymes with the capacity to produce ATP and pyruvate required for mitochondrial oxidative phosphorylation that consequently influences mitochondrial Ca^{2+} accumulation (Vemuganti *et al.,* 2007). In addition mitochondria are tightly associated with both the axoneme and each other. Facilitated by disulphide bridges formed by a selenium rich protein, this close association makes mitochondrial isolation and extraction extremely difficult. As a result effects of mitochondrial function are historically assessed using pharmacological manipulation of known inhibitory compounds such as CCCP and DNP (Ho & Suarez *et al.,* 2003; Ardon *et al.,* 2009).

The basic findings presented here attempt to define the Ca^{2+} storage capability of human sperm mitochondria and their potential involvement in $[Ca^{2+}]_i$ increases associated with the characteristic progesterone induced Ca^{2+} transient. Since the characterisation of the Ca^{2+} storage capacity of the acrosome, its importance in AR and oocyte fusion in 2005, (Herrick *et al.,*) numerous studies have provided evidence for the existence of a second Ca^{2+} store at the PHN/midpiece region of mammalian sperm (Harper *et al.,* 2004; 2005; Ho & Suarez 2003). Due to its localisation, this store could potentially regulate flagella activity and subsequently hyperactivated motility; providing a useful target for asthenozoospermic treatments. Identification of the sperm specific progesterone receptor CatSper apparently reduced the potential importance of a second Ca^{2+} store at the PHN/midpiece. However inability to prevent the biphasic Ca^{2+} response at the region during CatSper inhibition with NNC-55-0396 emphasised the prevalence of a second Ca^{2+} store in mature cells (Strunker *et al.,* 2011).

At present evidence suggests that a Ca^{2+} store at the PHN/midpiece is either a remnant of the redundant nuclear envelope (RNE; Ho & Suarez 2001; 2003; Naaby-Hansen *et al.*, 2001) (whether this is an ER remnant or sperm specific membranous organelle) or the mitochondria which are localised to this region (Costello *et al.*, 2009). Here we report that in human sperm loaded with the low affinity Ca^{2+} dye Mag-Fluo-4AM and subsequently permeabilised with SLO to release cytoplasmic Ca^{2+} and dye, two regions of high [Ca^{2+}] are clearly identifiable, which must be membrane bound Ca^{2+}-storing organelles (Figure 3.7B). The first region covers the apex of the sperm head and corresponds with the acrosome, a known Ca^{2+} store. The second encompasses both the neck and midpiece region, and may indicate multiple Ca^{2+} stores at close proximity in the region. These images clearly indicate that the mitochondria accumulate Ca^{2+} in human sperm; additionally in some images individual mitochondria are clearly visible due to their helical arrangement around the axoneme. Sperm mitochondria have also been shown to accumulate Ca^{2+} in other mammalian species including rabbit (Storey & Keyhani, 1973; 1974), rat (Babcock *et al.*, 1976), bovine (Vijayaraghavan & Hoskins, 1990) and murine models (Wennemuth *et al.*, 2003) although the contribution to $[Ca^{2+}]_i$ regulation remains to be elucidated.

We have previously discussed a mechanism for Ca^{2+} uptake by the mitochondria in somatic cells. It should also be noted that contribution of mitochondrial Ca^{2+} to $[Ca^{2+}]_i$ and signalling is dependent on the stress imposed on the system. Under normal physiological conditions mitochondrial contribution to Ca^{2+} homeostasis is minimal, when exposed to pharmacological agents that induced an increase in $[Ca^{2+}]_i$ mitochondrial Ca^{2+} contribution increased also (Wennemuth *et al.*, 2003; Scorziello *et al.*, 2013). Indeed mitochondrial Ca^{2+} uptake has been implicated in some forms of apoptosis (Giacomello *et al.*, 2007). Here we

utilised the mitochondrial uncouplers CCCP and DNP to explore the consequence of preventing mitochondrial Ca^{2+} accumulation on $[Ca^{2+}]_i$ and $\Delta\Psi_m$.

In sea urchin sperm CCCP and DNP have been shown to induce $[Ca^{2+}]_i$ increases that are dependent on extracellular Ca^{2+} (Ardon *et al* ., 2009). In this study it is proposed that mitochondrial status influences Ca^{2+} entry and homeostasis, which is likely the result of close association between the mitochondrion and PM. In our studies reported here we demonstrate similar observations, $[Ca^{2+}]_i$ increases induced by mitochondrial inhibitors display partial dependency on external Ca^{2+} (Figure 3.5). Furthermore we show that basal $[Ca^{2+}]_i$ increases associated with CCCP and DNP stimulation occur at the acrosome, PHN and midpiece simultaneously with no significant difference in the ΔF_{mean} observed at each region in un-permeabilised cells labelled with MF (Figure 3.8). This is consistent with the idea that mitochondrial uncoupling induces Ca^{2+} entry into the cytoplasm at sites quite separate from the mitochondria, but it must be remembered that the slow image acquisition rate used in these experiments (0.1 Hz) may not allow identification of the origin of $[Ca^{2+}]_i$ signals. It should be noted that when applied prior to 3μM progesterone a significant increase in the progesterone-induced $[Ca^{2+}]_i$ signal was observed only at the midpiece. In addition there was no effect on $[Ca^{2+}]_i$ at the PHN indicative of a discrete $[Ca^{2+}]_i$ control mechanism in the region. Interestingly our results suggest that mitochondrial uncoupler induced $[Ca^{2+}]_i$ increases at the PHN are not the product of mitochondrial Ca^{2+} release (as mitochondrial $[Ca^{2+}]_i$ increased indicative of Ca^{2+} uptake) but the result of either PM Ca^{2+} influx or Ca^{2+} efflux from an alternative Ca^{2+} store at the region, which is echoed by Ardon and colleagues findings (Ardon *et al.,* 2009). Furthermore in cardiac cells Murgia *et al.,* 2009 has observed a close association between mitochondria (capable of Ca^{2+} accumulation) and the intracellular Ca^{2+} store the ER. Here they provide evidence for a number of close contacts <80nm between

the mitochondria and ER; thus strengthening the hypothesis that mitochondrial Ca^{2+} accumulation *in vivo* is dependent on their capacity to sense high $[Ca^{2+}]_i$ at IP_3 gated channels of the ER. These findings would support our suggestion of an additional IP_3 sensitive Ca^{2+} store at the PHN in close contact with the mitochondria, which contributes to the biphasic $[Ca^{2+}]_i$ response in human sperm.

Notably we have shown live visualisation of CCCP and DNP $\Delta\Psi_m$ depolarisation in human sperm. Due to the nature of mitochondrial Ca^{2+} uptake (MCU uniporter) movement is not countered by an opposing ion exchange, as such Ca^{2+} uptake can depolarise the $\Delta\Psi_m$ maintained by ATP production (Duchen, 2000; Rizzuto & Brini, 2004). In addition application of an IP_3-sensitive store agonist in astrocytes where $[Ca^{2+}]_i$ and $\Delta\Psi_m$ were measured simultaneously clearly demonstrates that $\Delta\Psi_m$ depolarisation clearly follows mitochondrial $[Ca^{2+}]_i$ elevation and causes hyperpolarisation when mitochondrial $[Ca^{2+}]_i$ is high (Duchen, 2000; Murgia *et al.,* 2009). Interestingly in cardiomyocytes the mitochondrial uncoupler FCCP, was shown to depolarise $\Delta\Psi_m$ in a manner similar to our observations, which correlated to mitochondrial Ca^{2+} uptake and subsequently induced mitochondrial Ca^{2+} release through PTPs (hyperpolarising the $\Delta\Psi_m$). Both these studies demonstrate a strong relationship between mitochondrial Ca^{2+} uptake and $\Delta\Psi_m$ depolarisation. However Zhao and colleagues also found that mitochondrial Ca^{2+} uptake and $\Delta\Psi_m$ depolarisation induced by mitochondrial uncouplers initiated spontaneous Ca^{2+} release from another closely associated IP_3 regulated Ca^{2+} store (Sarcoplasmic reticulum; Zhao *et al.,* 2013). If a similar relationship between Ca^{2+} stores also existed in human sperm this could account for increases in Ca^{2+} observed with CCCP or DNP application at the PHN and acrosome during $\Delta\Psi_m$ depolarisation, however further investigation is required. Furthermore progesterone induced $\Delta\Psi_m$ hyperpolarisation is indicative of NCX mitochondrial Ca^{2+} release in response to high

mitochondrial $[Ca^{2+}]_i$ and Ca^{2+} uptake (Zhao *et al.,* 2013). It has been suggested that the increase in mitochondrial $[Ca^{2+}]_i$ observed upon progesterone stimulation is the result of increased respiration and ATP production, which influences MMP and thus induces mitochondrial Ca^{2+} accumulation observed in MF labelled cells. However mitochondrial uncoupler pre-treatment has no significant effect on the progesterone induced $\Delta\Psi_m$ response and indicates a complex relationship between MMP, mitochondrial $[Ca^{2+}]_i$ and Ca^{2+} release from other intracellular Ca^{2+} stores exists in human sperm (Ho & Suarez 2003; Zhao *et al.,* 2013). It should also be noted that SPCA1 (Ca^{2+}-ATPase) has been localised to the PHN/midpiece of human sperm and could facilitate mitochondrial Ca^{2+} accumulation when MCU is inhibited (Harper *et al.,* 2004).

Interestingly $\Delta\Psi_m$ has been proposed as an accurate indicator of sperm fertilising potential. A number of studies have utilised $\Delta\Psi_m$ sensitive dyes such as JC-1 to compare the ejaculates of fertile and asthenozoospermic men (Evenson *et al.,* 1982). They have identified that high $\Delta\Psi_m$ is indicative of both hyperactivated motility and ability to fertilise the oocyte (Marchetti *et al.,* 2002; Gallon *et al.,* 2006; Sousa *et al.,* 2011). Indeed our own computer assisted semen analysis reveals that $\Delta\Psi_m$ depolarising agonists CCCP and DNP decreased the motility parameters associated with hyperactivation (Table 3.1). However effects on hyperactivated motility as defined by Mortimer *et al.,* 1998 were negligible, which could be the result of increased $[Ca^{2+}]_i$ from an alternative Ca^{2+} storage organelle in the vicinity. As in bovine models inhibition of hyperactivated motility by mitochondrial inhibitors was restored by Ca^{2+} addition without the requirement for ATP (Ho & Suarez 2003).

Our findings suggest that in human sperm mitochondria contribute to Ca^{2+} storage and homeostasis of $[Ca^{2+}]_i$. However the mechanisms are complex and dependent on a number of

factors. Association of $\Delta\Psi_m$ and mitochondrial Ca^{2+} accumulation seems apparent and suggests that an alternative Ca^{2+} store at the PHN is responsible for discrete $[Ca^{2+}]_i$ fluctuations observed there. Furthermore the increase in $[Ca^{2+}]_i$ associated with progesterone stimulation is complex and likely dependent on a number on $[Ca^{2+}]_i$ signalling pathways some of which are discussed in the following chapters.

CHAPTER FOUR: PHARMACOLOGICAL MANIPULATION OF Ca^{2+} STORES AT THE PHN WITH THIMEROSAL

4.0 Foreword

Data from this chapter contributed to the publication Alasmari *et al.*, 2013.

4.1 Abstract

Successful fertilisation requires sperm to tightly regulate $[Ca^{2+}]_i$ enabling hyperactivated motility and other essential behaviours. In somatic cells intracellular Ca^{2+} stores (ER) regulate $[Ca^{2+}]_i$ through Ca^{2+} mobilisation and store replenishment, requiring both PM channels and SOCE contribution. In human sperm the presence and identity of intracellular Ca^{2+} stores is debated. Herrick *et al.,* 2005 identified the capacity of the acrosome to act as a Ca^{2+} store. However, there is also increasing evidence to suggest presence of a Ca^{2+} store at the PHN (Ho & Suarez, 2003; Lefievre *et al.,* 2012). Localisation of a number of Ca^{2+} channels associated with the Ca^{2+} stores of somatic cells at the PHN including IP_3R supports this theory (Walensky & Synder, 1995). Identification of the progesterone-sensitive ion channel CatSper in human sperm has led to questioning of the contribution of intracellular stored Ca^{2+}, but pharmacological blocking of CatSper does not abolish the biphasic $[Ca^{2+}]_i$ increase associated with progesterone suggesting Ca^{2+} contribution from an alternative source. We used the IP_3R activator thimerosal to determine effects of treatment on $[Ca^{2+}]_i$ increases associated with progesterone. We show that treatment with thimerosal is temperature sensitive, with a more consistent $[Ca^{2+}]_i$ response observed in cells treated at 30^oC compared to 25^oC. Treatment with 5μM thimerosal induces a sustained increase in $[Ca^{2+}]_i$ at the PHN, which is not inhibited by the CatSper blocker NNC-55-0396. However initial treatment with 5μM thimerosal is sufficient to significantly occlude the sustained intracellular Ca^{2+} response observed upon subsequent stimulation with progesterone. Here we propose that IP_3R medicated Ca^{2+} flux from intracellular Ca^{2+} stores contribute to the sustained component of the progesterone response at the PHN and the regulation of hyperactivated motility in human sperm.

4.2 Introduction

The female reproductive tract is a hostile environment for non-self-cells and upon deposition in the anterior cervix sperm must overcome a series of obstacles to achieve fertilization (chapter 1.6). Unlike the sperm of external fertilisers mammalian sperm must first have the ability to enter and progress through the viscous and visco-elastic environments of the cervix and uterus to the oviductal tubule (Suarez, 2008). Here sperm must both bind and then successfully detach from the oviductal epithelium to achieve full fertilising potential (Pacey *et al*., 1995). Finally the sperm penetrates the outer gelatinous cumulus matrix and the fibrous ZP surrounding the oocyte before fusing with the oolemma. In all these circumstances there is a requirement for an alteration in flagellar beat which is crucial to successfully traverse the female tract. Yanagimachi was the first to identify the ability of sperm to modulate their motility through flagellar beat pattern in 1970. His studies identified that capacitation, (chapter 1.6.1) was an important regulator of hamster sperm motility, responsible for a switch from high frequency, low amplitude, and symmetrical flagellar beat to a more dynamic pattern of motility (Yanagimachi, 1970). Characterised by low frequency asymmetrical flagellar bends, hyperactivated motility (chapter 1.6.2) has been identified in several species (Hamster: Yanagimachi, 1970; Mouse: Cooper & Woolley, 1982; Human: Burkman, 1984) each with distinctive characteristics. In human samples these characteristics are essential in defining the parameters for CASA analysis of hyperactivated motility. However there is heterogeneity in hyperactivated behaviour observed amongst cells from the same population suggesting a number of possible distinctive sperm behaviours to increase the chance of successful fertilisation (Alasmari *et al.*, 2013).

The role of $[Ca^{2+}]_i$ signalling in the regulation of sperm flagellar beat has long been acknowledged (Morisawa, 1994; Publicover *et al.,* 2007) but a definitive mechanism of action remains to be elucidated. Identification of sperm specific CatSper Ca^{2+} channels in the sperm flagellum membrane in 2001 provided a correlation between flagellum location and $[Ca^{2+}]_i$ signalling (Quill *et al.,* 2003; Ren *et al.,* 2001). In addition, sperm of CatSper-null mice failed to undergo hyperactivation resulting in infertility (Ren *et al.,* 2001). CatSper is believed to act as a polymodal chemosensor sensitive to progesterone, prostaglandin E, neurotransmitters, chemokines and odorants in human sperm (Brenker *et al.,* 2012; Strunker *et al.,* 2011). As such CatSper is attributed with the ability to assimilate multiple environmental stimuli into regulation of motility.

IP_3R, ryanodine receptors (RyR) and Ca^{2+} storage organelles have also been identified in mammalian sperm, (Chiarella *et al.,* 2004; Naaby-Hansen *et al.,* 2001; Trevino *et al.,* 1998; Herrick *et al.,* 2005). Current evidence suggests the existence of two discrete Ca^{2+} stores in the human spermatozoon, the acrosome and a second store at the posterior head/ neck region (PHN; Costello *et al.,* 2009). When human sperm are loaded with low affinity Ca^{2+} dye Mag-Fluo-4AM and then permeabilised with Streptolysin O to allow escape of cytoplasmic dye both stores are clearly visible (Figure 4.1; Costello *et al.,* 2009). The acrosome was initially identified as a Ca^{2+} store due to the high density of IP_3R localised to the plasma membrane which have also been localised to the PHN (Walensky & Snyder, 1995; Publicover *et al.,* 2007). Fluorescence microscopy revealed that application of Ca^{2+}-ATPase inhibitor (SERCA) thapsigargin and IP_3R agonist thimerosal induced acrosomal exocytosis in the majority of cells (Herrick *et al.,* 2005) suggesting a role for a Ca^{2+}-IP_3 mobilization pathway in acrosomal exocytosis.

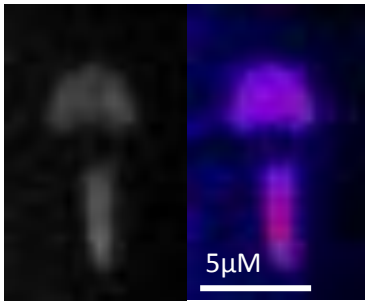

Figure 4.1 Location of Ca^{2+} stores in human sperm. Grey scale and pseudo-colour images (respectively) of a single human sperm cell treated with Mag-Fluo-4AM. Treatment clearly identifies two discrete Ca^{2+} stores where areas of white or warm colours (respectively) show areas of high Ca^{2+} concentration.

The identity of the Ca^{2+} store at the PHN is less well characterised. It has been suggested that the PHN store could be remaining endoplasmic reticulum, Golgi or a result of mitochondrial Ca^{2+} storage (Costello *et al.,* 2009). Multiple studies on rodent, bull (Ho & Suarez, 2001) and human (Bedu-Addo *et al.,* 2007) sperm have shown that Ca^{2+} can be mobilised from a store in the sperm neck region stimulating flagellar movement. Indeed CatSper null mice which are typically incapable of hyperactivated motility can be induced to undergo hyperactivation by the release of Ca^{2+} from intracellular stores (Marquez *et al.,* 2007). The current model proposes that CatSper acts as the membrane bound progesterone receptor in the sperm flagellum initiating $[Ca^{2+}]_i$ increase which is amplified and propagated forward by Ca^{2+} induced Ca^{2+} release at the PHN (Alasmari *et al.,*2013). A subset of cells generate Ca^{2+} oscillations by cyclic refilling of the PHN store upon progesterone stimulation, which co-insides with synchronous sperm neck flexure and flagellar bending (Harper *et al.,* 2004). If the aforementioned model is correct then Ca^{2+} signals generated by CatSper and those of Ca^{2+} stores should be capable of regulating different sperm behaviours in response to a single stimulus.

The effects of thimerosal on $[Ca^{2+}]_i$ at the PHN of human sperm has not been well characterised. In somatic cells thimerosal was initially identified as having two concentration dependent effects on IP_3Rs; subsequent analysis has also identified possible interaction with RyRs (Sayers *et al.,* 1993; Tanaka *et al.,* 1994). At low micromolar concentrations thimerosal sensitizes the IP_3 sensitive Ca^{2+} channel, causing the channel to open at lower concentrations of IP_3. Higher thimerosal concentrations have an inhibitory effect on IP_3 induced Ca^{2+} release. In addition this study also identified that 5mM DTT was sufficient to inhibit thimerosal effects on $[Ca^{2+}]_{i,}$ thus suggesting that thimerosal acts by modifying the cysteine residues present on the IP_3R. In external fertilisers incubation of sperm with thimerosal evoked sperm motility patterns consistent with hyperactivation which were insensitive to both reduced $[Ca^{2+}]_e$ and Ca^{2+} channel blockers (Butler *et al.,* 1999). Similarly upon thimerosal application bull sperm immediately switched from forward progressive to hyperactivated motility even in low Ca^{2+} media (Ca^{2+}<50nM) (Ho & Suarez, 2001). In addition Ho and Suarez (2001) identified that the acrosome reaction was not induced by low thimerosal concentrations suggesting a role for an alternative IP_3R gated Ca^{2+} store in the regulation of motility. Nevertheless further studies on the effects of thimerosal on $[Ca^{2+}]_i$ at the PHN are required to associate $[Ca^{2+}]_i$ increase at the PHN with hyperactivated motility in human sperm.

4.3 Aims

The aims of this chapter were to characterise the effects of thimerosal on basal $[Ca^{2+}]_i$ at the PHN in capacitated sperm. We wanted to determine the effects of IP_3R stimulation with thimerosal on the biphasic $[Ca^{2+}]_i$ response induced by progesterone. In addition we wanted to see if the CatSper channel blocker NNC-55-0936 influenced the $[Ca^{2+}]_i$ induced by thimerosal at the PHN.

4.4 Material and Methods

4.4.1 Materials

Thimerosal, 4-Aminopyridine (4AP), Progesterone and NNC-55-0396 hydrate (NNC) were all purchased from Sigma Aldrich Company Ltd. (Dorset). For all other materials see chapter 2.1.1.

4.4.2 Methods

4.4.2.1 Cell preparation

Human semen was collected and prepared as in chapter 2.3.

4.4.2.2 Cell incubation and capacitation

Sperm harvested by swim up procedure (chapter 2.4.2.1) were incubated and capacitated as in chapter 2.4 except for a subset of cells were length of capacitation effects on thimerosal $[Ca^{2+}]_i$ were observed. In these experiments cells were allowed to capacitate in normal capacitation media for 1, 4, 7 or 10 hours before imaging.

4.4.2.3 CASA

All cells were prepared for CASA as in chapter 2.5 and treated with 5μM thimerosal, 3μM progesterone, 2mM 4AP or with 5μM thimerosal and 3μM progesterone.

4.4.2.4 Single cell imaging

Cells were left to capacitate for 6 hours at 6 $x10^6$cells/ml in sEBSS, unless participating in the capacitation experiments were they were instead left to capacitate for 1, 4, 7 or 10 hours the human sperm cell preparation was then diluted to 3$x10^6$cells/ml with sEBSS prior to single cell imaging. All imaging experiments for this chapter were conducted at 30^oC (apart from

those marked at 25^{o}C) and followed the methodology outlined in chapter 2.6.1 Ca^{2+} imaging with Oregon Green-BAPTA-1AM. In those experiments undertaken in Ca^{2+} free sEBSS, cells were first monitored in sEBSS for a minimum of 20 frames, then perfused with Ca^{2+} free sEBSS for 10 frames before agonist application in Ca^{2+} free sEBSS.

4.4.3 Analysis

CASA experimental data were analysed as in chapter 2.5.2. Ca^{2+} imaging with Oregon Green-BAPTA-1AM results were analysed as in chapter 2.6.1. However for those experiments undertaken in low Ca^{2+} sEBSS the lowest 3 points in the 30 frames post Ca^{2+} free sEBSS application were used as a base level to monitor any subsequent increase in Δ fluorescence %.

4.5 Results

4.5.1Thimerosal, 4AP and Progesterone increase hyperactivation parameters in human sperm

In the following experiments the hyperactivation of all samples was assessed and determined by CASA. Experiments were conducted in pairs; all treated samples were performed with a parallel untreated control sample suspended in sEBSS. Treatment with 3µM progesterone had little effect on the proportion of cells showing hyperactivated motility. 5µM thimerosal caused a more marked increase but this effect was extremely variable and was not statistically significant (P=0.94, P=0.07; compared to control; paired t-test; Table 4.1). However stimulation with 2mM 4AP or simultaneous treatment with 5µM thimerosal and 3µM progesterone both caused a significant increase in the percentage of hyperactivated cells in the sample (P=0.007, P=0.03 respectively; n=5; compared to control; paired t-test; Table 4.1). The effect of 5µM thimerosal and 3µM progesterone combined treatment exceeds the additive effects of 5µM thimerosal and 3µM progesterone alone. Furthermore 5µM thimerosal, 5µM thimerosal and 3µM progesterone treatments have a significant increase in percentage hyperactivation compared to progesterone (P=0.04, P=0.01 respectively; compared to progesterone; paired t-test; Table 4.1).

In addition several key kinematic parameters measured by CASA including an increase in amplitude of lateral head displacement (ALH) track speed (VCL) and decreases in beat frequency (BCF) and linearity (LIN) show correlations with treatment trends observed by percentage hyperactivation (Table 4.1). In particular the effects of thimerosal on ALH were far greater than progesterone (P<0.05).

PARAMETER	No Treatment	S.E.M	2mM 4AP	S.E.M	5µM Thimerosal	S.E.M	5µM Thimerosal & 3µM Progesterone	S.E.M	3µM Progesterone	S.E.M	UNITS
Hyperactivation	4.6	0.81	26.39	2.85	25.37*	10.34	33.6**	8.68	4.8	2.02	%
Path velocity VAP	62.21	6.48	80.85	6.54	65.53	6.72	67.66	4.95	55.26*	4.71	µm/s
Prog. velocity VSL	53.34	7.07	63.07	7.82	44.93	3.68	44.20	3.57	43.19*	4.85	µm/s
Track Speed VCL	100.75	8.35	147.27	3.61	132.46*b	16.92	141.23**	14.73	96.48*	8.02	µm/s
Lateral Amplitude ALH	4.56	0.30	7.12*	0.43	6.92* *	0.74	7.34**	0.85	5.04	0.24	µm
Beat Frequency BCF	27.33	1.21	23.68	0.83	23.44*	1.48	22.85*	1.25	22.94*	1.67	Hz
Straightness STR	80.80	3.16	74.06	1.23	70.40	2.89	67.20	3.36	75*	2.53	%
Linearity LIN	51.50	3.24	41.33	0.88	37.1* *	2.50	33.8**	2.40	44.5*	2.30	%
Elongation	66.50	0.61	67.56	0.58	66.40	1.09	67.30	0.99	67.83	1.27	%

Table 4.1 Effects of thimerosal, progesterone and 4AP on motility parameters as determined by CASA. Experiments were carried out in pairs, where cells from the same semen sample were analysed by CASA with and without treatment. Cells without treatment were prepared in sEBSS, control no treatment (yellow). Treated cells were exposed to either 2mM 4AP (4AP, green), 5µM thimerosal (T, pink), 3µM progesterone (P, red), 5µM thimerosal & 3µM progesterone (T&P, purple). For each condition path velocity (VCL), progressive velocity (VSL), track speed (VCL), lateral head amplitude (ALH), beat frequency (NCF), straightness (STR), linearity (LIN) and elongation were determined. * $P<0.05$; compared to CNT; paired t-test; n=3-7. * $P<0.05$; compared to Progesterone; paired t-test; n=7, 7, 5, 5 &5 respectively.

4.5.2 Thimerosal raises resting $[Ca^{2+}]_i$ at the PHN in human sperm

At low micromolar concentrations thimerosal is reported to sensitize intracellular Ca^{2+} release (Sayers *et al.*, 1993). Herrick *et al*., 2005 utilised 100µM thimerosal to verify the Ca^{2+} storage capability of murine acrosomal vesicles. In the following experiments sperm were treated with a range of thimerosal concentrations at 25^{o}C and 30^{o}C, to observe both concentration and temperature sensitivity effects.

At 25^{o}C thimerosal significantly increased $[Ca^{2+}]_i$ in ~55-60% of cells at all concentrations, inducing a sustained elevation or series of transients within ~150 seconds (dependent on concentration; Figures 4.2, 4.3B&C). A concentration dependent increase in ΔF_{mean} is observed between 1µM, 5µM and 10µM thimerosal treatments however higher concentrations of thimerosal (>50µM) had similar effects or even an inhibitory effect compared to 10µM (Figure 4.3A). In addition the proportion of cells with a significant thimerosal response (section 2.6.1.2.3) did not vary significantly over the range 1µM to 50µM thimerosal, suggesting the increase in ΔF_{mean} is the result of dose sensitivity of the responsive cells and not recruitment of more cells into the responsive population.

Sperm stimulated with the same seven concentrations of thimerosal at 30^{o}C showed similar response kinetics to those seen at 25^{o}C, $[Ca^{2+}]_i$ inducing a sustained elevation or series of transients within ~150 seconds. The effect of thimerosal on $[Ca^{2+}]_i$ at 30^{o}C was significantly greater than at 25^{o}C and the proportion of cells producing a significant $[Ca^{2+}]_i$ response was increased by approximately 15% (Figure 4.3A&B) indicating temperature sensitivity consistent with previous observations (Figure 4.3A, B&C; P=0.008, P=0.0007, P=0.03

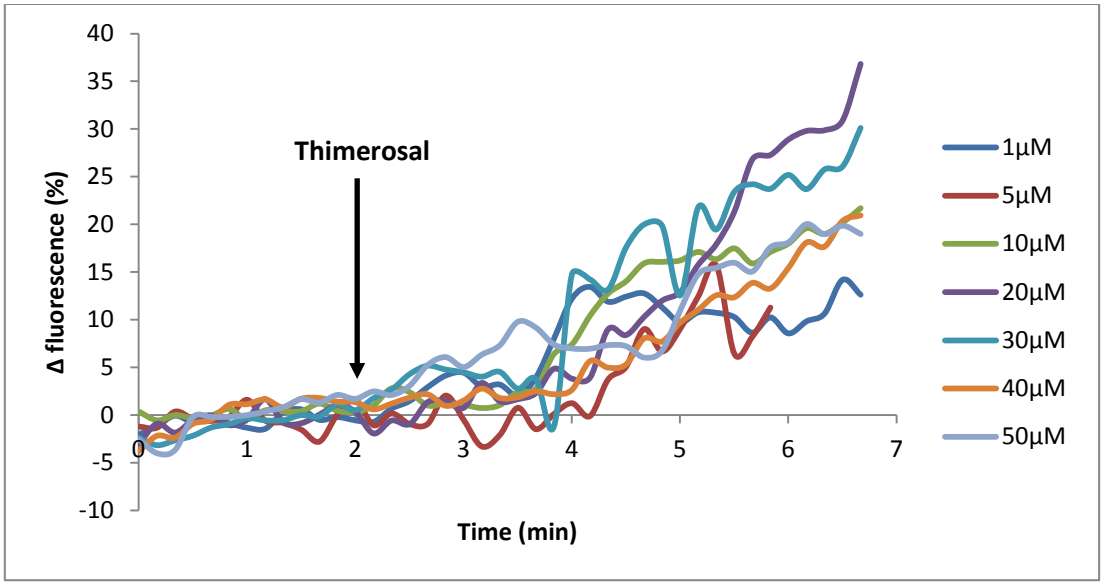

Figure 4.2 Effect of concentration on thimerosal induced increase in $[Ca^{2+}]_i$. (A) Each line shows ΔF_{mean} from a single experiment stimulated with thimerosal at 1μM (blue), 5μM (red), 10μM (green), 20μM (purple), 30μM (turquoise), 40μM (orange) & 50μM (pale blue).

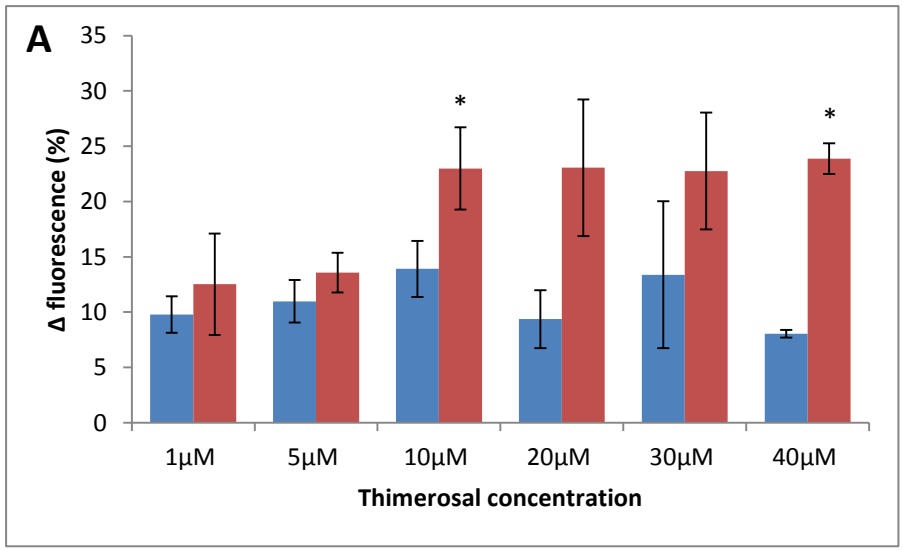

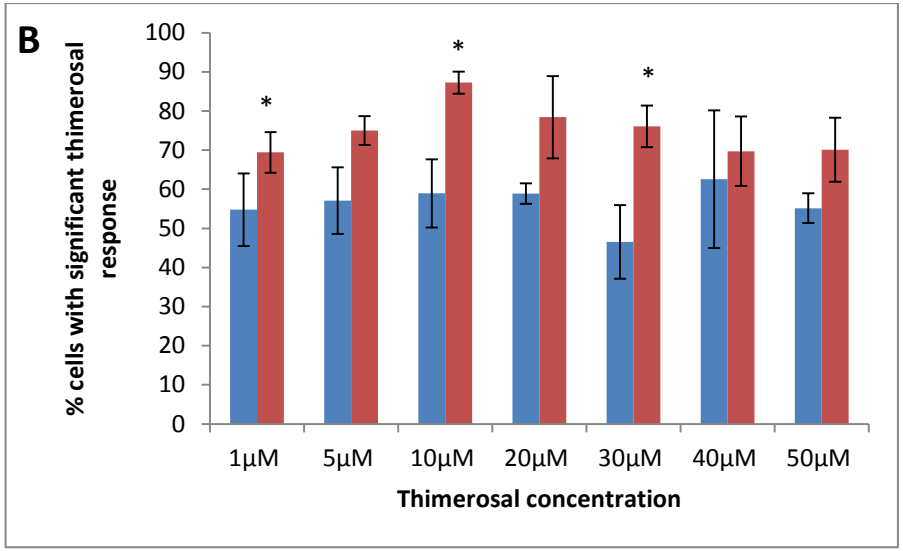

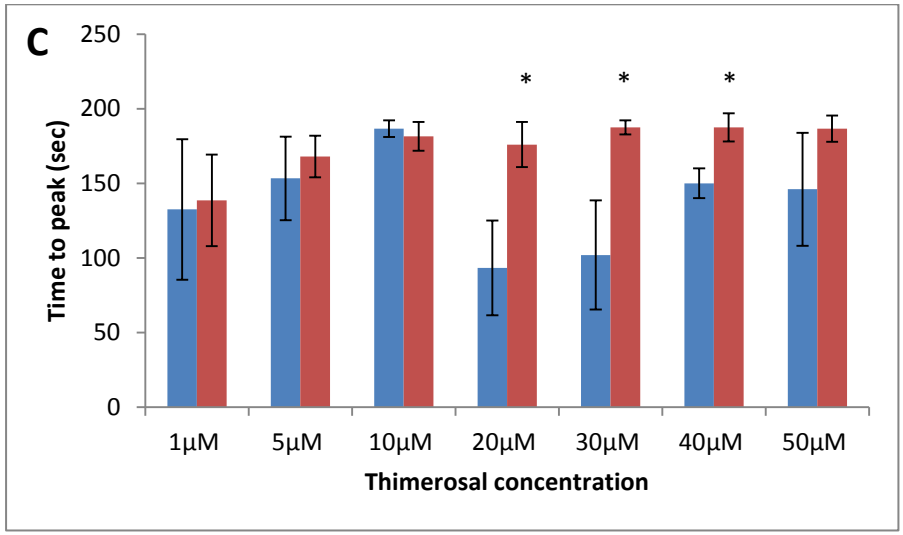

Figure 4.3 Effect of temperature on thimerosal induced increase in $[Ca^{2+}]_{i.}$ Cells were stimulated with 1μM, 5μM, 10μM, 20μM, 30μM, 40μM & 50μM thimerosal at 25°C (blue) and 30°C (red). (A) Increase in ΔF_{mean} 3 min after application of thimerosal. Results are means ± S.E.M for at least 3 sets of experiments, where aliquots of the sample were tested with each of the 7 concentrations 25°C (n=3-6), 30°C (n=4-7). (B) Proportion of cells exhibiting a significant thimerosal response as determined by ΔF_{max} peak. (C) Time to ΔF_{max} $[Ca^{2+}]_{i.}$ transient, mean time to thimerosal induced ΔF_{max} at each of the 7 concentrations. Each bar shows mean ± S.E.M of 3-7 sets of experiments, * P<0.05; compared to 25°C response; ANOVA; n=3-7.

respectively; ANOVA; Tanaka & Tashjian, 1994). As at 25°C, at 30°C there was a marked concentration sensitivity over the range 1-10μM (Figure 4.3A) with negligible effects on ΔF_{mean} at concentrations greater than 10μM. At 30°C the bimodal effect of thimerosal on IP_3R was most apparent in the proportion of responsive cells with sensitising effects in the 1-10μM range and inhibitory effects with thimerosal concentrations >10μM (Figure 4.3B). Temperature also has an impact on time taken to achieve ΔF_{max} (Figure 4.3C). At most thimerosal concentrations (except 10μM) responses observed at 30°C take significantly longer (*P*=0.03; ANOVA; Figure 4.3C), though this could be due to the increase in the amplitude of the $[Ca^{2+}]_i$ response. These observations identified that at 30°C 5μM thimerosal potently and consistently induces stimulatory effects on IP_3R such that increases in $[Ca^{2+}]_i$ are observed. As a result all subsequent thimerosal experiments were conducted at 30°C unless otherwise stated.

4.5.2.1 Thimerosal effect on $[Ca^{2+}]_i$ at the PHN in the absence of extracellular Ca^{2+}

Superfusion of capacitated cells with EGTA-buffered medium (~$3x10^{-7}$M Ca^{2+}) caused $[Ca^{2+}]_i$ to fall rapidly (Figure 4.4A). Application of 5μM thimerosal after 2 minutes exposure to this saline induced a small transient rise in $[Ca^{2+}]_i$ (ΔF_{mean} 5.81±1.08%; n=6) in a subset of cells (Figure 4.4). This is consistent with Ca^{2+} release from intracellular Ca^{2+} stores in response to thimerosal treatment. It should be noted that in the presence of extracellular Ca^{2+} thimerosal produced an increase in ΔF_{mean} approximately twice as large in five times as many cells (Figure 4.4). In the absence of extracellular Ca^{2+} it appears that a smaller proportion of cells are readily responsive to 5μM thimerosal treatment therefore extracellular Ca^{2+} contributes significantly to the responses observed *in vitro*.

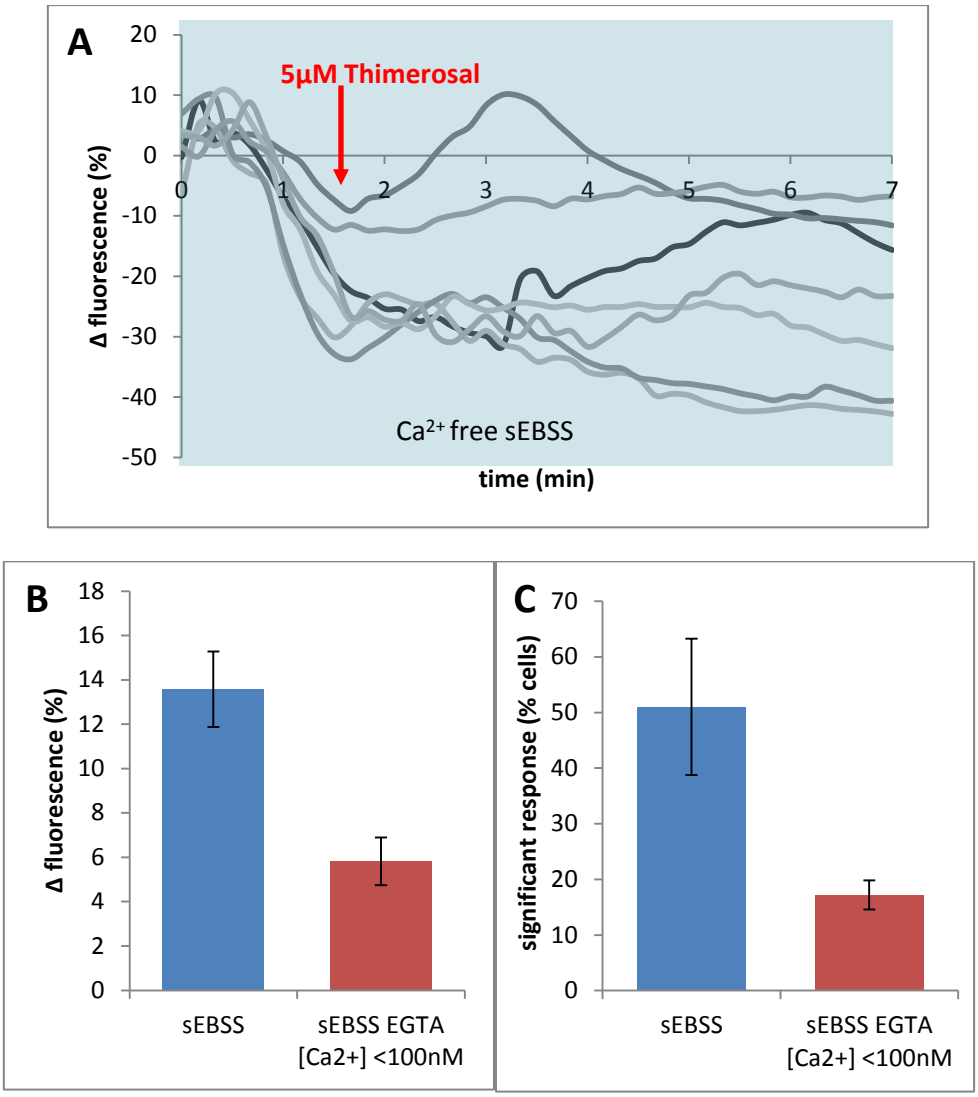

Figure 4.4 Thimerosal induced $[Ca^{2+}]_i$ response in the absence of extracellular Ca^{2+}. Cells were capacitated for 4-6 hours in sEBSS before stimulation with 5µM thimerosal in either Ca^{2+} free sEBSS (~$3x10^{-7}$M Ca^{2+}) (A) or normal sEBSS. (B)Increase in ΔF_{mean} after application of 5µM thimerosal, (C) proportion of cells exhibiting a significant thimerosal response as determined by ΔF_{max} response, results are means ± S.E.M. (n=4-6).

4.5.3 Capacitation time effects amplitude of thimerosal induced $[Ca^{2+}]_i$ response at the PHN

Capacitation is the sum of numerous intracellular processes that enable the sperm to achieve full fertilising potential that *in vivo* occur in the female reproductive tract (chapter 1.6.1). Under laboratory conditions semen samples are prepared and transferred to capacitating media in an attempt to induce these intracellular changes. For the following experiments all sperm samples were prepared under normal capacitating conditions (BSA and bicarbonate containing sEBSS; appendix II), for either 1, 4, 7 or 10 hours and the effect of 5 μM thimerosal was investigated. Treatment of sperm with 5μM thimerosal increased $[Ca^{2+}]_i$ in a subset of the cell population at all the capacitation periods initiating a sustained elevation or oscillating transients. Length of capacitation influenced the increase in $[Ca^{2+}]_i$ upon 5μM thimerosal stimulation and the proportion of cells in which a significant response was observed. In cells capacitated for 1, 4 and 7 hours there was an increase in ΔF_{mean} which began to decrease after 10 hours capacitation (Figure 4.5A). The increase in ΔF_{mean} observed after 7 hours capacitation was both the highest and most statistically significant from that observed after 1 hours capacitation (4hr P=0.21, 7hr P=0.035, 10hr P=0.544; paired t-test; n=4; Figure 4.5A). For each individual cell ΔF_{max} was determined during the 3 min interval required for most cells to stabilise at an increased level and the frequency distribution plotted (Figure 4.5 B&C respectively). Increment of ΔF_{max} amplitude shows a greater proportion of cells capacitated for 1 hour show either a small increase and decrease with a higher proportion of cells capacitated at 7 hours (~60%) exceeding 20% fluorescence (Figure 4.5C).

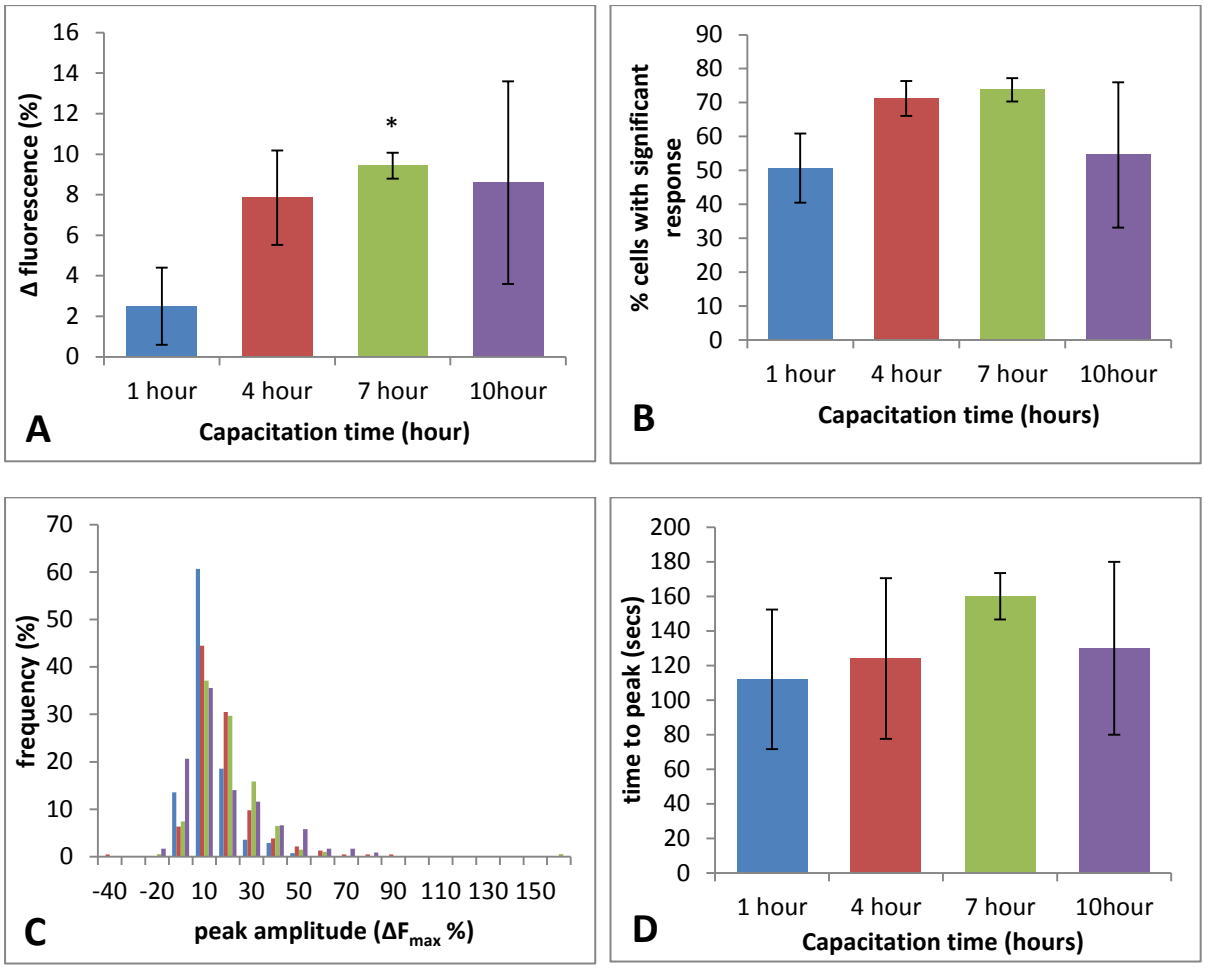

Figure 4.5 Capacitation effect on $[Ca^{2+}]_i$ response induced by 5µM thimerosal. Graphs show effects of 1 hour (blue), 4 hour (red), 7 hour (green) and 10 hour (purple) capacitation on (A) increase in ΔF_{mean} 3min after application of 5µM thimerosal. (B) Proportion of cells displaying significant response increase, (C) frequency distribution of ΔF_{max} amplitude amongst the cell population, (D) time taken to achieve maximum increase in ΔF_{mean}. Results are means ± S.E.M where appropriate for sets of four experiments in each of which aliquots from the same sample were tested at each of the four time points. (* P<0.05; paired t-test; compared to response at 1 hour; n=4).

The percentage of cells responding significantly to 5μM thimerosal treatment increases dramatically from 1 hour capacitation to 7 hours capacitation, decreasing at 10 hours (4hr *P*=0.21, *P*=0.10 & *P*=0.97; compared to 1hr capacitation; paired t-test; n=4; Figure 4.5B). Although a similar trend is observed with time to peak with an increase in time to peak climaxing at 7 hours capacitation (160s) large S.E.M means low statistical significance (4hr *P*=0.88, 7hr *P*=0.39 & 10hr *P*=0.80; compared to 1hr capacitation; paired t-test; n=4; Figure 4.5D). Overall this data indicates that the $[Ca^{2+}]_i$ response induced by thimerosal is regulated by capacitation; though the mechanism remains to be elucidated. Both insufficient and excessive capacitation time have detrimental effects on $[Ca^{2+}]_i$ response induced by thimerosal. As a result the prime time for thimerosal induced increases in $[Ca^{2+}]_i$ is between 5-8 hours capacitation.

4.5.4 The effect of thimerosal on the progesterone induced Ca^{2+} response

The non-genomic increase of $[Ca^{2+}]_i$ associated with progesterone is well characterised in human sperm (Kirkman-Brown *et al.*, 2000; 2003; Harper *et al.*, 2004). However a sperm specific progesterone receptor has only recently been identified; CatSper is a polymodal chemosensor which facilitates progesterone induced $[Ca^{2+}]_i$. Identified in 2011, CatSper is the only Ca^{2+} permeable channel to be detected by patch clamp studies in mature sperm, but inhibition of CatSper with NNC-55-0369 does not eliminate the biphasic response. It is therefore possible that the biphasic response is the result of two types of progesterone receptors with different binding profiles and intracellular Ca^{2+} responses, potentially including the release of stored intracellular Ca^{2+}.

4.5.4.1 Thimerosal pre-treatment significantly reduced the sustained progesterone induced Ca^{2+} response

At the PHN, application of 3μM progesterone triggers an initial transient increase in $[Ca^{2+}]_i$ (in ~90% cells) followed by a sustained plateau or series of smaller oscillatory transients (in ~85% cells) which subside when progesterone is removed, (Figure 4.6A). Cells treated with 5μM thimerosal for 300s had an initial sustained increase in $[Ca^{2+}]_i$ of ~15%. Subsequent application of 3μM progesterone induced a biphasic $[Ca^{2+}]_i$ increase at the PHN (Figure 4.6B&C). Similar responses were observed when cells were pre-treated with higher concentrations of thimerosal (up to 50μM; data not shown).

In cells pre-treated with thimerosal, the biphasic $[Ca^{2+}]_i$ response induced by 3μM progesterone has a transient amplitude of ~70% and occurred in ~80% of cells. Pre-treatment of cells with 5μM thimerosal (300s) had no significant effect on the transient amplitude (increase in ΔF_{mean}) or proportion of cells producing a significant $[Ca^{2+}]_i$ response compared to parallel controls (P=0.47& P=0.09 respectively; paired t-test; n=4; Figure 4.6D).

The sustained $[Ca^{2+}]_i$ response observed 3 minutes after progesterone application was observed in ~40% cells. The amplitude of this response was significantly reduced (>25%) in cells pre-treated with thimerosal (P=0.05; paired t-test; n=4; Figure 4.6E). This was clearly identifiable by the obvious shift in the distribution of cell response amplitudes to the left by 10-30% compared to the control population (Figure 4.6F). In addition there was a significant decrease in ~45% of the population producing a significant sustained response to progesterone (P=0.008; paired t-test; n=4; Figure 4.6G). The sensitivity of the sustained

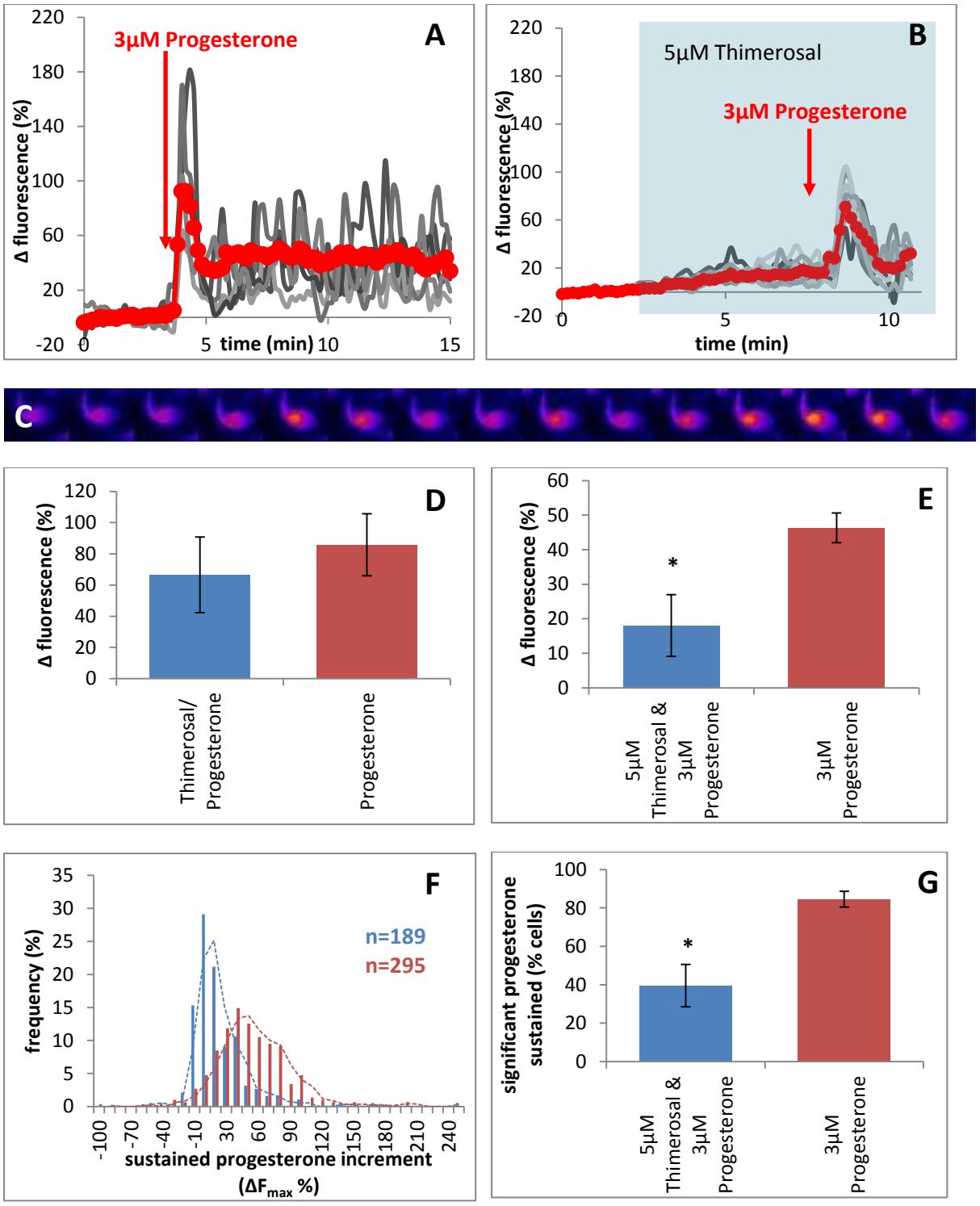

Figure 4.6 Effect of thimerosal pre-treatment on biphasic progesterone $[Ca^{2+}]_i$ response. All graphs display control no pre-treatment (red) and 5µM thimerosal pre-treated (blue). (A)&(B) show 6 individual cell PHN $[Ca^{2+}]_i$ responses (greys traces) and ΔF_{mean} (red trace) to 3µM progesterone application (red arrow) with and without 5µM thimerosal pre-treatment respectively. (C) Image series showing the increase in $[Ca^{2+}]_i$ associated with application of thimerosal and progesterone. (D) Transient increase in ΔF_{mean} (E) Sustained increase in ΔF_{mean} 3min post application of 3µM progesterone. (F) Proportion of cells exhibiting a significant sustained progesterone response (G) Frequency (%) of amplitude of ΔF_{sus} response amongst cell population. Results are means ± S.E.M. (n=4) (* P<0.05, paired t- test).

progesterone response to thimerosal highlights the potential contribution of intracellular Ca^{2+} stores to this part of the biphasic Ca^{2+} response. Previous studies have suggested different control mechanisms regulate the two components of the progesterone induced response. Here we show that the sustained response is inhibited by pre-treatment with thimerosal, which will deplete the intracellular Ca^{2+} store available and activate CCE, reducing the ability of these stores to contribute to subsequent progesterone response.

4.5.5 The effect of NNC-55-0396 on the thimerosal generated $[Ca^{2+}]_i$ increase at the PHN

Developed by Huang *et al.,* in 2004 as a non-hydrolysable, selective blocker of T type Ca^{2+} channels; NNC-55-0396 (NNC) is the most effective known blocker of CatSper channels; the sperm specific polymodal chemosensor and non-genomic progesterone receptor (chapter 1.10). At low concentrations NNC (<10μM) abolishes CatSper currents in human sperm, this reduces but does not eliminate progesterone induced $[Ca^{2+}]_i$ signal (Strunker *et al.,* 2011). Here we wanted to observe whether 10μM NNC significantly reduced the effect of thimerosal on $[Ca^{2+}]_i$ thus implicating CatSper channels in the modulation of the response.

4.5.5.1 Thimerosal induced $[Ca^{2+}]_i$ increase at the PHN is insensitive to NNC-55-0396

At low concentrations (≤ 10μM) thimerosal sensitizes IP_3 stimulated Ca^{2+} channels in somatic cells. In human sperm, application of 5μM thimerosal induced a ~15% increase in $[Ca^{2+}]_i$ at the PHN in ~65% of cells (Figure 4.7B & C), which is consistent with the release of

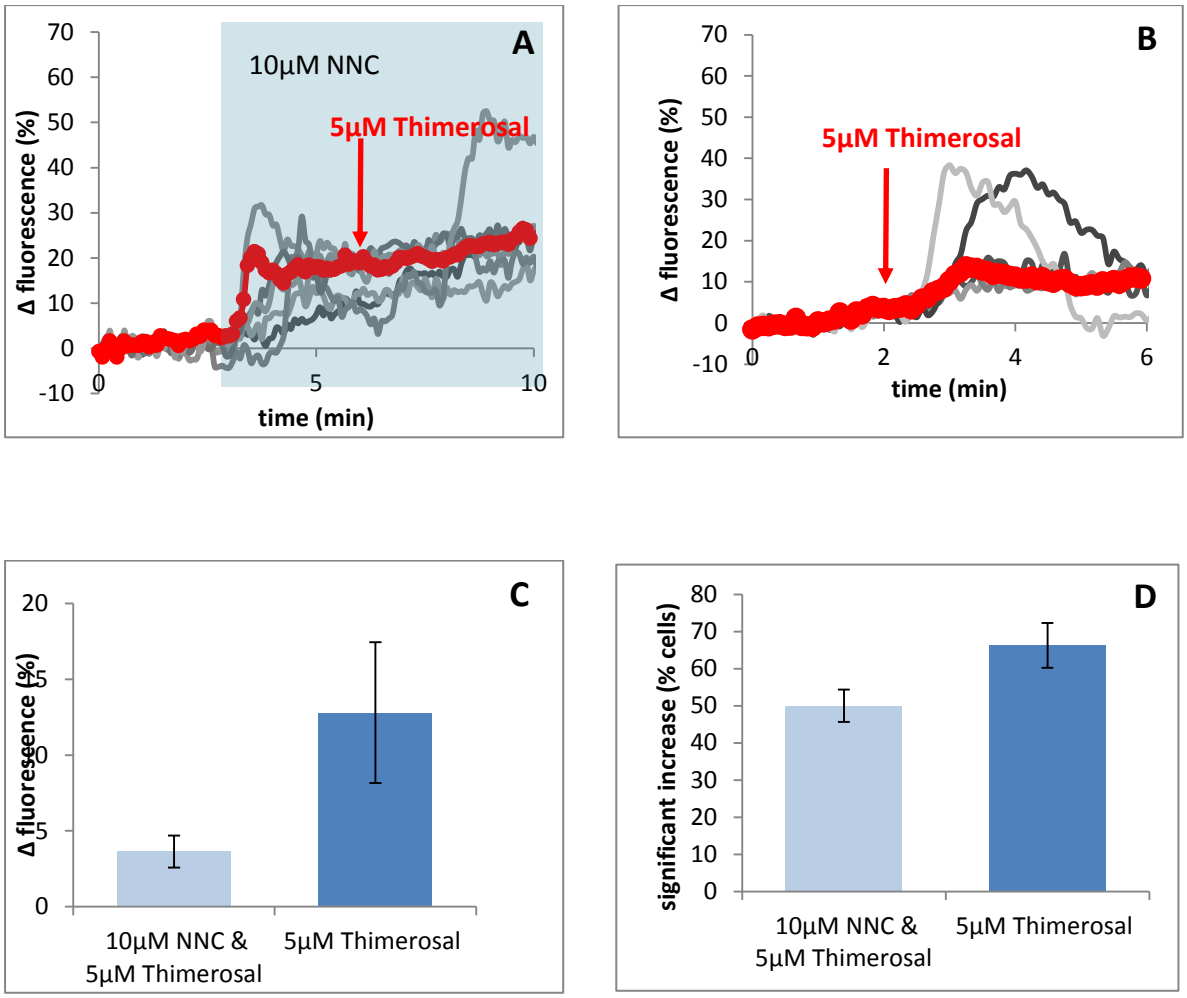

Figure 4.7 Effect of NNC55-0396 on thimerosal generated $[Ca^{2+}]_i$ response at the PHN. Graphs show 5 individual cell PHN $[Ca^{2+}]_i$ responses (greys traces) and ΔF_{mean} (red trace) to 5µM thimerosal application (red arrow) (A) with and (B) without 10µM NNC pre-treatment. (C) Increase in ΔF_{max}. (D) Proportion of cells exhibiting a significant thimerosal response as determined by ΔF_{max} response. (* P<0.05, compared to thimerosal, paired t-test, results are means ± S.E.M. n=11).

intracellular stored Ca^{2+}. When cells were first exposed to 10μM NNC then 5μM thimerosal the increase in $[Ca^{2+}]_i$ associated with thimerosal reduced (~10%) although this effect was variable and was not significant (*P*=0.107; n=11; paired t-test; Figure 4.8C). However NNC treatment alone increased $[Ca^{2+}]_i$ ~25% which may have affected the IP_3 sensitive Ca^{2+} stores of CCE channels involved in the thimerosal response.

Analysis of individual cell $[Ca^{2+}]_i$ responses showed that pre-treatment with 10μM NNC reduced the proportion of cells producing a significant $[Ca^{2+}]_i$ response to thimerosal only slightly, from ~65% without NNC pre-treatment to ~50% in those cells treated with 10μM NNC, (*P*=0.126; n=11; Figure 4.7D). Thus the thimerosal induced $[Ca^{2+}]_i$ influx includes a significant NNC-resistant component. To determine the nature of the relationship between NNC and thimerosal induced $[Ca^{2+}]_i$ responses, we also observed the effects of 5μM thimerosal on the effects of 10μM NNC.

4.5.5.2 Thimerosal pre-treatment does not affect the increase in $[Ca^{2+}]_i$ at the PHN associated with NNC

10μM NNC induced a significant increase of ~25% $[Ca^{2+}]_i$ at the PHN in >80% of cells, which then plateaued at an elevated level and was clearly visible in the ΔF_{mean} (Figure 4.8A). To observe any inhibitory effects of thimerosal on NNC induced $[Ca^{2+}]_i$ increases we pre-treated cells with 5μM thimerosal before exposure to 10μM NNC (Figure 4.8B). In those cells treated with thimerosal the subsequent increase in $[Ca^{2+}]_i$ associated with NNC application exceeded that observed by 10μM NNC (Figure 4.8C) by ~10% in 9 out of 11 experimental pairs, however this was insignificant (*P*=0.29; n=11; paired t-test; Figure 4.8D).

Analysis of individual cell responses revealed no significant effect on the proportion of cells exhibiting a significant $[Ca^{2+}]_i$ response to 10μM NNC with or without prior thimerosal treatment (*P*=0.77; n=11; paired t-test; Figure 4.8E) and no correlation between $[Ca^{2+}]_i$ responses to 5μM thimerosal and 10μM NNC (Figure 4.8F). Together these results indicate NNC does not significantly inhibit the thimerosal induced $[Ca^{2+}]_i$ response at the PHN suggesting that the increase in $[Ca^{2+}]_i$ observed is the result of Ca^{2+} release from intracellular stores not extracellular Ca^{2+} influx through CatSper.

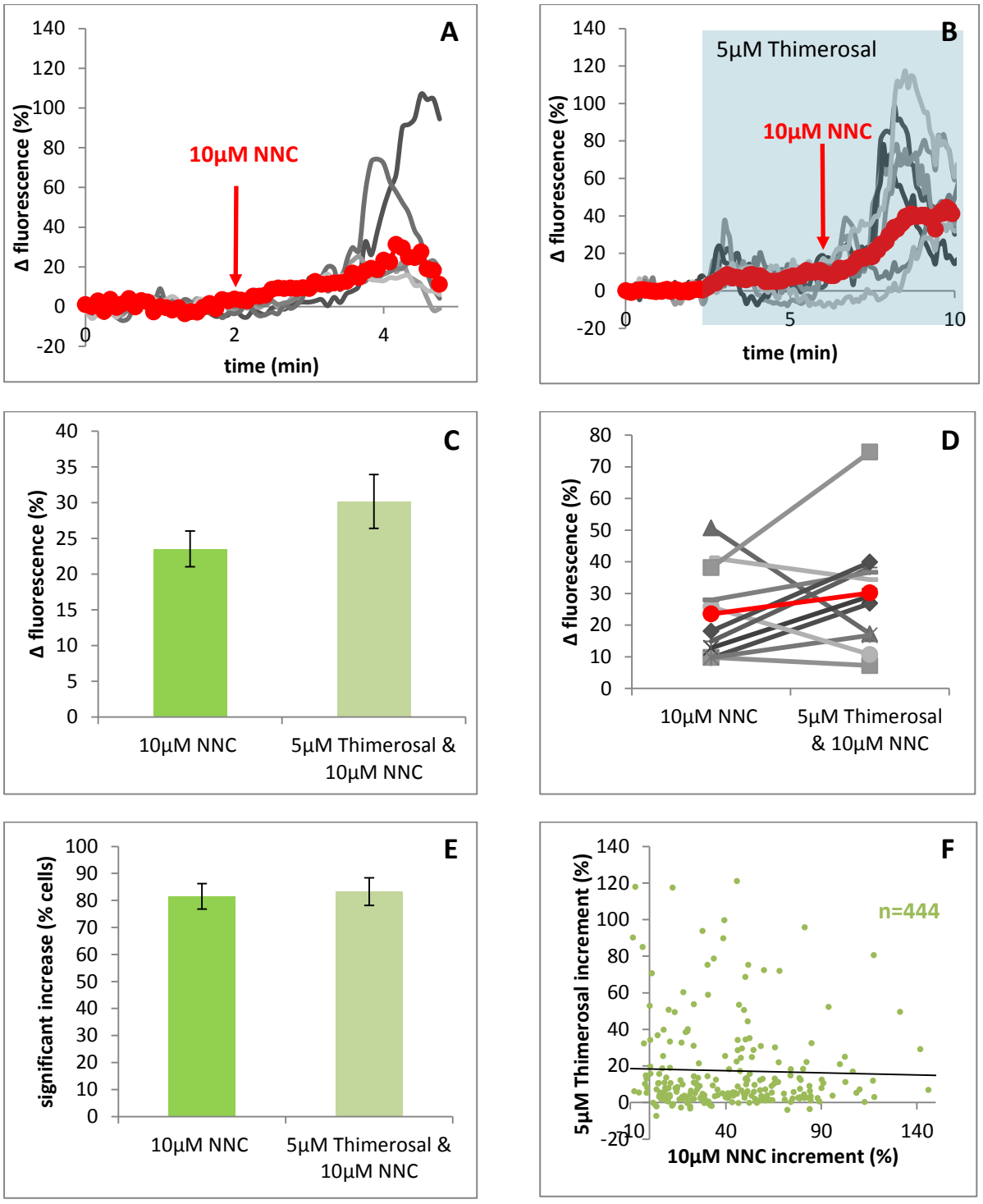

Figure 4.8 Effect thimerosal pre-treatment on NNC55-0396 $[Ca^{2+}]_i$ response at the PHN. Graphs show 5 individual cell PHN $[Ca^{2+}]_i$ responses (greys traces) and ΔF_{mean} (red trace) to 10µM NNC application (red arrow) (A) without and (B) with 5µM thimerosal pre-treatment. (C) Increase in NNC ΔF_{max}. (D) Comparison of NNC response treated/pre-treated experimental pairs. (E) Proportion of cells exhibiting a significant NNC response as determined by ΔF_{max} response. (F) Amplitude of thimerosal-induced resting $[Ca^{2+}]_i$ response (thimerosal increment x-axis) is not correlated with the amplitude of subsequent NNC-induced $[Ca^{2+}]_i$ increase (NNC increment y-axis), (* P<0.05, compared to NNC, paired t-test Results are means ± S.E.M, n=11).

4.6 Discussion

$[Ca^{2+}]_i$ signalling is an integral regulator of sperm function contributing to all physiological processes essential for ascension of the female tract and oocyte fertilisation including HA. In somatic cells complex Ca^{2+} signals such as oscillations and waves are generated through the manipulation of both Ca^{2+} flux across the PM and stored intracellular Ca^{2+}. Unlike somatic cells mature sperm lack the endoplasmic reticulum and other organelles that function as Ca^{2+} stores; however they do process Ca^{2+} channels essential for mobilisation of stored Ca^{2+} including IP_3R. In addition there is evidence for the existence of at least two discrete Ca^{2+} stores in human sperm; fluorescence imaging using low affinity Ca^{2+} dye Mag-Fluo-4AM clearly identifies two regions of Ca^{2+} accumulation one at the anterior acrosome and another at the PHN (Figure 4.1; Costello *et al.*, 2009). Interestingly despite some similarities between the two potential stores, distribution of the Ca^{2+} signalling receptors differ offering discrete mechanisms of store mobilisation and accumulation (Figure 1.16).

IP_3R are localised to the membrane of intracellular Ca^{2+} stores of somatic cells, external stimuli induce the production IP_3, which activates IP_3R to release stored Ca^{2+} into the cytoplasm thus increasing $[Ca^{2+}]_i$ (Berridge *et al.,* 2003; Michelangeli *et al.,* 1995). In addition the affinity of IP_3Rs for IP_3 is modulated by $[Ca^{2+}]_{cyt}$; low levels ~300nM IP_3R demonstrate increased affinity for IP_3 enabling tight regulation of $[Ca^{2+}]_{cyt}$ (Parys & De Smedt, 2012). Three mammalian IP_3R isoforms have been identified (1-3) and all have been detected in mature mammalian sperm (Jimenez-Gonzalez *et al.,* 2006); as well as both Gq and PLCα proteins essential in the IP_3 signalling cascade (Walensky & Snyder, 1995; Kuroda *et al.,* 1999). Immuno-localisation studies have isolated IP_3R1 expression to the acrosomal region and IP_3R3 to the RNE/PHN and midpiece, indicating the potential for two discrete

Ca^{2+} stores with separate regulatory mechanisms (Walensky & Snyder, 1995; Kuroda *et al.*, 1999; Naaby-Hansen *et al.*, 2001).

In 2005, Herrick *et al.*, identified the Ca^{2+} storage potential of the mammalian acrosome and recognised the high abundance of IP_3Rs and the associated protein PLC in the region. The group subsequently confirmed the presence of high Ca^{2+} levels in the acrosome maintained by an acrosomal Ca^{2+}-ATPase that was sufficient to induce acrosomal exocytosis. In addition the group utilised thimerosal (a known IP_3R activator) to illustrate a role for IP_3R in the mobilisation of stored intracellular Ca^{2+} in this region (Herrick *et al.*, 2005). The identity of a second Ca^{2+} store at the RNE/PHN region of mammalian sperm cells is less clear, although a store here would be in a prime location to facilitate Ca^{2+} induced modulation of motility. Localisation of IP_3R's to the PHN region of mature sperm has been identified in a number of mammalian species (Dragileva *et al.*, 1999; Kuroda *et al*., 1999; Naaby-Hansen *et al.*, 2001) including humans. In 2001, Naaby-Hansen *et al.*, reported expression of IP_3R in both the equatorial segment and membrane bound vesicles in the cytoplasmic droplet of human sperm consistent with the findings of Walensky and Snyder in murine models (1995). Additionally RyR 1&2, the Ca^{2+}-ATPase pump SPCA1 and Ca^{2+} store associated protein calreticulin have been detected at the PHN of mature sperm cells using immunofluorescent staining (Lefievre *et al.*, 2007; Harper *et al.*, 2004; 2005; Naaby-Hansen *et al.*, 2001). RyR are intracellular Ca^{2+} induced Ca^{2+} release channels located in the ER of somatic cells and are likely expressed in low numbers in human sperm due to low detected conductivity, (Costello *et al.*, 2009; Zalk *et al.*, 2007). The Ca^{2+}-ATPase pump SPCA1 utilises ATP to facilitate Ca^{2+} transport across membranes; localisation in the PHN is therefore beneficial for optimum performance as this is adjacent to the mitochondria containing midpiece and has the potential for interaction

(Harper *et al.*, 2005; chapter 1.10.3.1). Indeed, mitochondria are one of the candidates for intracellular Ca^{2+} storage at the PHN.

In somatic cells mitochondria are established Ca^{2+} storage organelles that contribute to the regulation of Ca^{2+} homeostasis and respond to elevated $[Ca^{2+}]_i$ levels by adapting oxidative phosphorylation and ATP production to the requirements of the cell (Scorziello *et al.*, 2013). Numerous studies have identified the Ca^{2+} uptake ability of mammalian sperm *in situ* (Storey & Keyhani, 1973; 1974; Babcock *et al.*, 1976; Vijayaraghavan & Hoskins, 1990), but the contribution of mitochondrial Ca^{2+} buffering on intracellular Ca^{2+} regulation has only been touched upon. Wennemuth *et al.*, 2003 were the first to identify the input of mitochondrial Ca^{2+} in murine sperm, here they noted that under normal physiological conditions mitochondrial Ca^{2+} buffering was small but when the system became stressed (through the inhibition of PM Ca^{2+} channels) mitochondrial Ca^{2+} contribution to $[Ca^{2+}]_i$ increased. In 2008 we reported that mitochondrial Ca^{2+} release does not contribute to the store operated Ca^{2+} oscillations induced by progesterone application in human sperm. In chapter 3 we identified that uncoupling of mitochondrial respiration with DNP or CCCP does not inhibit the progesterone induced Ca^{2+} response consistent with previous findings by Machado-Oliveira *et al.*, 2008. In fact DNP and CCCP alone can induce an increase in $[Ca^{2+}]_i$ at the PHN associated with a reduction in the mitochondrial membrane potential (MMP) observed with the MMP sensitive dye JC-1 (chapter 3).

An alternative candidate for storage of intracellular Ca^{2+} at the PHN is the RNE or an ER-like vesicle at the anterior midpiece. The RNE or excess nuclear membrane that accumulates upon nuclear condensation contains nuclear pore complexes (NPC) in addition to IP_3R. Suarez *et*

al., 2003 demonstrated localisation of IP_3R and calreticulin at the PHN of bovine and hamster sperm only partially correlated to NPC distribution suggesting that although the RNE had potential for Ca^{2+} storage there was also evidence for another Ca^{2+} storage organelle in the region. In addition we recently published evidence for the presence of SOCE components STIM and Orai in human sperm. These receptors enable Ca^{2+} store replenishment in somatic cells and are not required for mitochondrial buffering; furthermore in human sperm STIM and Orai isoforms show localised distribution at the acrosome and PHN enabling discrete modulation of Ca^{2+} store refilling (chapter 1.10.1.3.1).

In this chapter we identified the effects of thimerosal on IP_3Rs at the PHN of human sperm; low micromolar thimerosal concentrations sensitise IP_3Rs facilitating the release of Ca^{2+} from intracellular stores in a concentration dependent manner from 1-10μM. Concentrations of thimerosal greater than 10μM also induced an increase in $[Ca^{2+}]_i$ at the PHN although this did not exceed that observed at 10μM. At 25^{o}C the increases in $[Ca^{2+}]_i$ associated with thimerosal treatment were variable and significantly smaller than at 30^{o}C, consistent with the temperature sensitivity observed by Tanaka and Tashjian (2004; Figure 4.3) and the effects of thimerosal on motility measured at 37^{o}C in CASA experiments (Table 4.1). Through selective sensitisation of IP_3R with thimerosal we demonstrated the effect of stored Ca^{2+} mobilisation on motility parameters, with thimerosal producing much stronger hyperactivation than progesterone, which had relatively little effect on ALH. Furthermore dual application of thimerosal and progesterone increased hyperactivation in a manner that exceeded the sum of their individual effects.

The biphasic $[Ca^{2+}]_i$ response induced by progesterone at the PHN of human sperm is well characterised (Kirkman-Brown *et al.,* 2003; Harper *et al.,* 2004). However the identity of the PM progesterone receptor has only recently come to light. CatSper channels are sperm specific Ca^{2+} channels of a promiscuous nature (Strunker *et al.,* 2011; Brenker *et al.,* 2013) and absence of the channel results in infertility in murine models (Ren *et al.,* 2001; Quill *et al.,* 2003; Jin *et al.,* 2007). At present CatSper channels are the only progesterone sensitive Ca^{2+} channels that have been detected by patch clamp studies. Treatment with NNC-55-0396 completely abolishes this current and its potentiation by progesterone, but does not eliminate the increase in $[Ca^{2+}]_i$ associated with progesterone, although it should be noted that the response is reduced (Strunker *et al.,* 2011). This indicates the requirement for a second alternative source of Ca^{2+} which contributes to the progesterone induced intracellular Ca^{2+} response at the PHN, potentially an intracellular Ca^{2+} store in the region.

Initial analysis of the biphasic progesterone induced increase in $[Ca^{2+}]_i$ in mammalian sperm suggested two independent Ca^{2+} signalling pathways were responsible for the initial Ca^{2+} transient and sustained Ca^{2+} increase. In 2000, O'Toole proposed that the transient increase was the result of T-type Ca^{2+} channels, whilst the sustained response was the result of store operated Ca^{2+} entry (SOCE). Here we demonstrate that thimerosal reduces the sustained Ca^{2+} response induced by progesterone at the PHN. The simplest interpretation of this observation is that prior activation of SOCs by thimerosal-induced store mobilisation occludes the contribution of CCE to the sustained component of the progesterone-activated $[Ca^{2+}]_i$ signal. It must also be noted that NNC-55-0396 inhibition of CatSper channels did reduce the mean amplitude of the thimerosal-induced $[Ca^{2+}]_i$ at the PHN but this effect was not significant and the proportion of responsive cells was not reduced. Furthermore it is becoming clear that

NNC-55-0396, though an effective CatSper blocker, is far from specific. For instance it has recently been shown to inhibit sperm K^+ channels. Thus it appears that thimerosal acts primarily through a mechanism not involving CatSper but by mobilisation of stored Ca^{2+}.

In summary we report evidence for the presence of a thimerosal sensitive intracellular Ca^{2+} store at the PHN of human sperm, (distinct from the mitochondria); which contributes to the sustained increase in $[Ca^{2+}]_i$ induced by progesterone and functions independent of CatSper PM channels. This supports previous suggestions that the progesterone induced $[Ca^{2+}]_i$ response consists of two separate components regulated in part by separate intracellular signalling cascades and the presence of a Ca^{2+} store at the PHN with associated SOCE machinery (O'Toole, 2000).

CHAPTER FIVE: STORE-OPERATED Ca^{2+} ENTRY MODULATION USING 2-APB AT THE PHN OF HUMAN SPERM

5.0 Foreword

The data in this chapter contributed to the publication; 2-APB potentiated channels amplify CatSper-induced Ca^{2+} signals in human sperm, *Lefievre et al.,* 2012.

5.1 Abstract

In chapter 4, we reported evidence for the existence of a second Ca^{2+} store at the PHN in human sperm. Previous studies conducted by our research group have identified a correlation between intracellular Ca^{2+} stores and localisation of the SOCE proteins STIM and Orai, (Lefievre *et al.,* 2012). To date 2-aminoethyldiphenyl borate (2-APB) is the most well characterised modulator of SOCE, although its effect is rather unspecific. Initially identified as an IP_3R antagonist 2-APB has since been established as a bimodal modulator of SOCE. At high concentrations (>30μM) 2-APB inhibits the CRAC channel current associated with SOCE and conversely at low concentrations (<10μM) 2-APB activates SOCE (Goto *et al.,* 2010; Suzuki *et al.,* 2010; Lefievre *et al.,* 2012). In this chapter we aimed to determine the effects of 2-APB on both resting $[Ca^{2+}]_i$ and the biphasic $[Ca^{2+}]_i$ response observed upon 3μM progesterone application in human sperm. At 5μM, 50μM and 100μM 2-APB application showed an elevation in resting $[Ca^{2+}]_i$ in a dose dependent manner. Pre-treatment with 5μM 2-APB caused a significant increase in the transient $[Ca^{2+}]_i$ response induced by 3μM progesterone. 100μM and 50μM 2-APB also caused an elevation in the progesterone induced Ca^{2+} response but neither equalled the $[Ca^{2+}]_i$ response observed by 5μM 2-APB treatment. In addition cells treated with 50μM or 100μM 2-APB after 3μM progesterone showed a consistent decrease in the $[Ca^{2+}]_i$ response compared to parallel controls. Taken together these results suggest the presence of 2-APB sensitive Ca^{2+} channels with the ability to potentiate the $[Ca^{2+}]_i$ progesterone response at the PHN in human sperm.

5.2 Introduction

In the previous chapter we highlighted evidence for the presence of a second Ca^{2+} store in the PHN of human sperm. This Ca^{2+} store appears to contribute to the increase in $[Ca^{2+}]_i$ induced by progesterone though PM CatSper channel (Strunker *et al.,* 2011); which results in the switch from forward progressive to hyperactivated motility. To date only CatSper Ca^{2+} channels have been identified as a progesterone receptors in human sperm, although there is some debate as to whether CatSper mediated Ca^{2+} entry alone is sufficient to produce the characteristic biphasic Ca^{2+} response induced by progesterone (Lefievre *et al.,* 2012; Alasmari *et al.,* 2013).

In 1993 Blackmore proposed a role for Capacitative Ca^{2+} entry (CCE) in the increase in $[Ca^{2+}]_i$ associated with progesterone in human sperm. Central to his proposal was the need for an intracellular Ca^{2+} store, PM channel and an associated communication mechanism. In somatic cells CCE or SOCE is well established; STIM proteins reside in the ER, where they monitor the $[Ca^{2+}]_i$ of the storage organelle. Upon store mobilisation STIM molecules oligomerise and redistribute adjacent to the PM where they are visible as punctate structures (Cahalan, 2009; Stathopulos *et al*., 2006). Here STIM proteins activate PM SOCs (including Orai and TRPC) to induce influx of extracellular Ca^{2+} into the cell cytoplasm (chapter 1.10.3; Yuan *et al.,* 2007; Liao *et al.,* 2009). In mammalian sperm the identity and function of the PHN store is hotly debated however it is believed to possess many characteristics of the ER including the ability to induce CCE through PM channels. Recent findings by our group (Lefievre *et al.,* 2012) show a correlation between the SOCE system proteins STIM and Orai and Ca^{2+} store position. The study used immunofluorescence of SOCE proteins to reveal STIM and Orai distribution throughout the sperm cells (Lefievre *et al.,* 2012).

2-APB was identified by Maruyama *et al.,* 1997 as a membrane penetrable IP_3R inhibitor and is now well established as a dual mediator of SOCE channel function. At high concentrations 2-APB (>50µm) inhibits CCE channel current (I_{CRAC}), although a number of studies have shown that the degree of inhibition is dependent on the Orai isoform present (DeHaven *et al.*, 2008; Zhang *et al.,* 2008; Lis *et al.,* 2007). Conversely at low concentrations (~5µM) 2-APB activates SOCE (Goto *et al.,* 2010; Suzuki *et al.,* 2010; Lefievre *et al.,* 2012). There is also evidence for 2-APB activation of PM Ca^{2+} channels independent of intracellular Ca^{2+} store mobilisation at low doses (DeHaven *et al.,* 2008; Zhang *et al.,* 2008).

The biphasic $[Ca^{2+}]_i$ response induced by progesterone application is well characterised (Kirkman-Brown *et al.,* 2000; Harper *et al.,* 2004) with a distinctive dose effect relationship between progesterone response and amplitude of ΔF_{mean}. Due to the transcriptionally inactive nature of the mature spermatozoon progesterone induced $[Ca^{2+}]_i$ responses must be the result of a non-genomic mechanism. To date CatSper channels are the only progesterone receptor to be identified in human sperm however the progesterone induced Ca^{2+} response is not abolished by CatSper specific blockers. This proposes a model for two types of progesterone receptors present in human sperm, one high affinity initiating responses at low concentrations and one low affinity eliciting a response at high progesterone concentrations. Subsequently we wanted to investigate the stimulatory/inhibitory effects if any of 2-APB on SOCE contribution to the progesterone induced Ca^{2+} response in human sperm.

5.3 Aims

The aims of this chapter were to characterise the effects of 2-APB on basal $[Ca^{2+}]_i$ and the progesterone induced biphasic $[Ca^{2+}]_i$ response at the PHN in capacitated human sperm.

5.4 Material and methods

5.4.1 Materials

Progesterone and 2-aminothoxydiphenyl borate (2-APB) were purchased from Sigma Aldrich Company Ltd. (Dorset) and Calbiochem (distributed by Merck Biosciences, Beeston, Nottingham, UK) respectively. For all other materials see chapter 2.1.1.

5.4.2 Methods

5.4.2.1 Cell preparation

Human semen was collected and prepared as in chapter 2.3.

5.4.2.2 Cell incubation and capacitation

Sperm harvested by swim up procedure (chapter 2.4.2.1) were incubated and capacitated as in chapter 2.4.

5.4.2.3 Single cell imaging

Cells were left to capacitate for 6 hours at 6 $x10^6$cells/ml in sEBSS, the human sperm cell preparation was then diluted to $3x10^6$cells/ml with sEBSS prior to single cell imaging. All imaging experiments for this chapter were conducted at 25^oC with Oregon Green-BAPTA-1AM and followed the methodology outlined in chapter 2.6.1.

5.4.3 Analysis

Calcium imaging with Oregon Green BAPTA-1AM results were analysed as in chapter 2.6.1.

5.5 Results

5.5.1 2-APB elevates resting $[Ca^{2+}]_i$ at the PHN in human sperm

Application of 5µM, 50µM or 100µM 2-APB upon resting cells in the presence of extracellular Ca^{2+} significantly increased $[Ca^{2+}]_i$ at the PHN in ~ 65% cells, inducing a plateau or series of transients (Figure 5.1A). ΔF_{mean} typically showed $[Ca^{2+}]_i$ response to 2-APB treatment within 100s, with the response stabilising at an increased $[Ca^{2+}]_i$ level within 200s for all concentrations of 2-APB. Individual cell responses show some variation in response kinetics (Figure 5.1A) but no significant differences between stimulation with 5µM 2-APB, 50µM 2-APB and 100µM 2-APB. Indeed mean ΔF_{max} at the PHN was only slightly greater at higher doses of 2-APB (mean $\Delta F_{max:}$ 5µM 14.19±2.68%, 50µM 14.29±5.15%, 100µM 17.81±7.79%; n=15, n=6 & n=7 respectively; Figure 5.1B). The proportion of responsive cells and amplitude distribution of individual cell responses showed no great variation between the 2-APB concentrations (Figure 5.1C&D). In addition time taken to respond to 2-APB showed no significant dose sensitivity (Figure 5.1E&F).

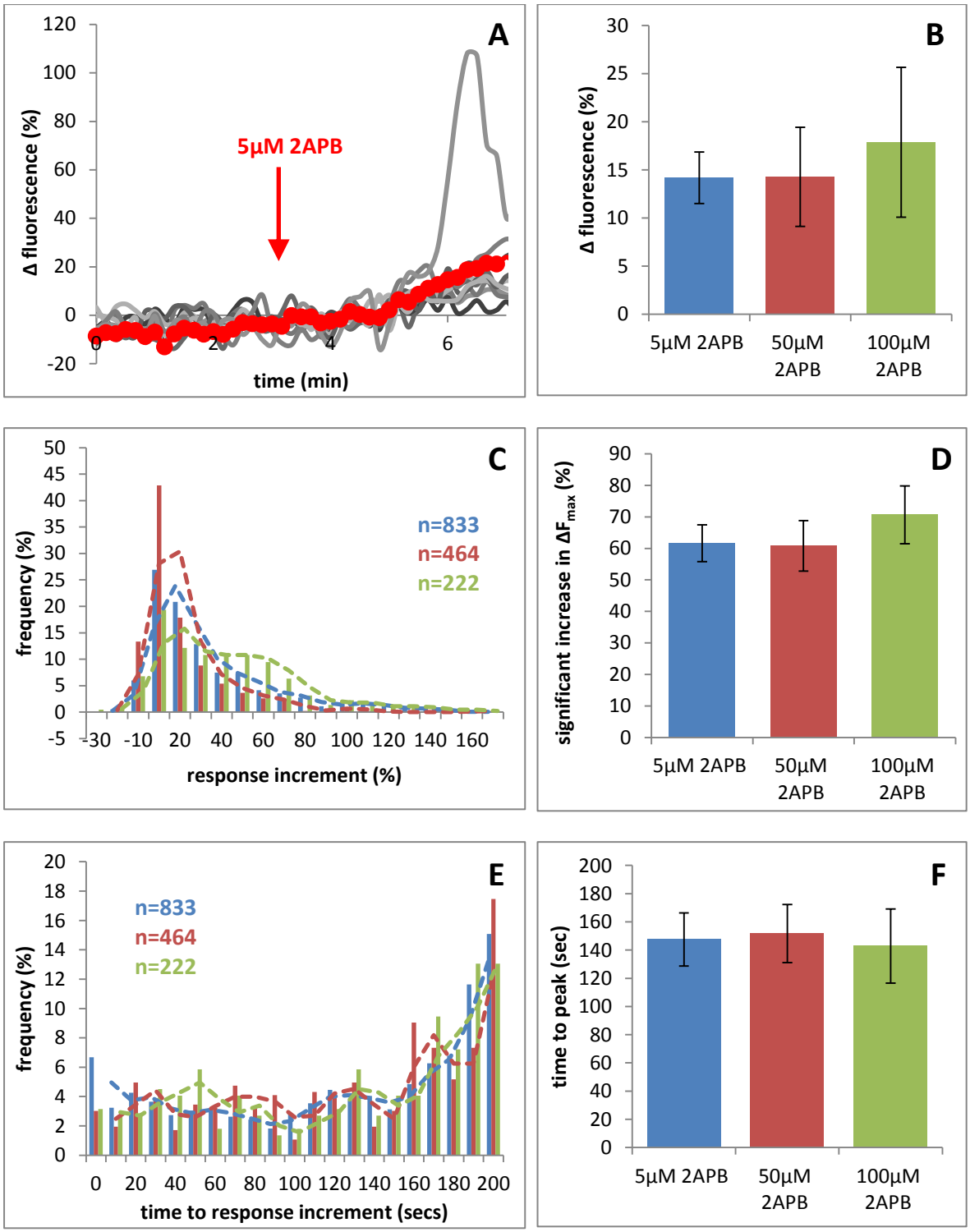

Figure 5.1 2-APB induced elevation of resting $[Ca^{2+}]_i$ at the PHN. (A) Individual ΔF cell responses to 5µM 2-APB (grey traces) and ΔF_{mean} (red trace) for all cells in that experiment, (n=88). In the following graphs capacitated cells were monitored for a minimum of 200sec before 5µM (blue), 50µM (red) or 100µM (green) 2-APB was applied. (B) Increase in ΔF_{mean} within 3min of 2-APB application. (C) Frequency distribution of ΔF_{max} amongst the cell population. (D) Proportion of cells displaying significant ΔF_{max} responses. (E) Frequency distribution of time taken to achieve ΔF_{max} amongst the cell population. (F) Time taken to achieve peak ΔF_{mean}. Results are means ± S.E.M. 5µM, n=15; 50µM, n=6; 100µM, n=7.

5.5.2 The progesterone induced $[Ca^{2+}]_i$ transient is enhanced by 2-APB pre-treatment

The archetypal $[Ca^{2+}]_i$ response to 3µM progesterone stimulation is a transient increase in $[Ca^{2+}]_i$ at the PHN which peaks within ~70s and is followed by a plateau (or a series of transients) in ~90% of cells and clearly visible in the ΔF_{mean} trace (Figure 5.2D). To observe the effects of 2-APB pre-treatment on progesterone induced $[Ca^{2+}]_i$ response, experiments were conducted in pairs. Aliquots of cells from the same semen sample were stimulated with 3µM progesterone both with and without pre-treatment with 5µM, 50µM or 100µM 2-APB. Pre-treatment with all concentrations of 2-APB caused an initial $[Ca^{2+}]_i$ increase (as described previously). In 6 experiments where cells were pre-treated with 5 µM 2-APB (300s) subsequent application of progesterone induced the characteristic biphasic $[Ca^{2+}]_i$ response but the amplitude was significantly enhanced compared to parallel 3µM progesterone control experiments (Figure 5.2, 5.3A; P=0.007). In most experiments pre-treated with 50µM and 100µM 2-APB responses were also greater than in parallel controls but these effects were variable and were not statistically significant (P=0.188 Figure 5.2, 5.3A). However only 4 out of 6 experimental pairs pre-treated with 50µM 2-APB showed an increase in ΔF_{mean} (P=0.188; paired t-test; Figure 5.3A).

Analysis of individual cell $[Ca^{2+}]_i$ transients showed that cells pre-treated with 2-APB (at all 3 concentrations) resulted in a shift of the progesterone response increment frequency distribution to the left with a higher proportion of cells displaying responses in the 20-80ΔF% range (Figure 5.3B). Interestingly 5µM, 50µM and 100µM 2-APB pre-treated cells all displayed bell shaped distribution of progesterone response increments (Figure 5.3B) despite only the ΔF_{mean} for 5µM 2-APB pre-treatment significantly differing from the control.

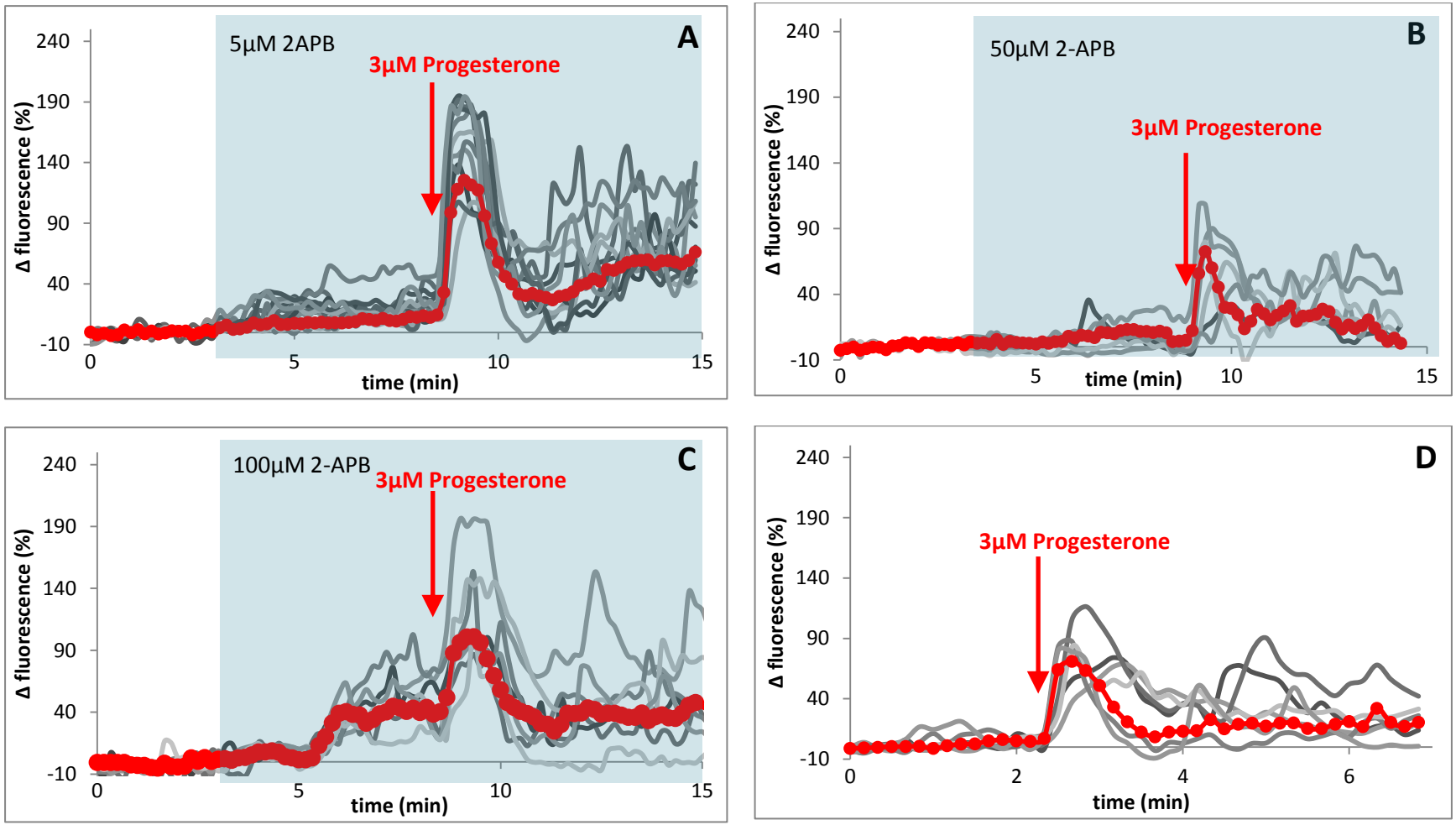

Figure 5.2 Effect of 2-APB on the transient progesterone response. Capacitated cells were pre-treated with (A) 5µM (B) 50µM (C) 100µM 2-APB or (D) no pre-treatment (grey box) for a minimum of 200s before 3µM progesterone stimulation. Each graph shows individual ΔF cell responses (grey traces) and ΔF_{mean} (red trace) for all cells in that experiment, (n=88, n=89 & n=39 respectively).

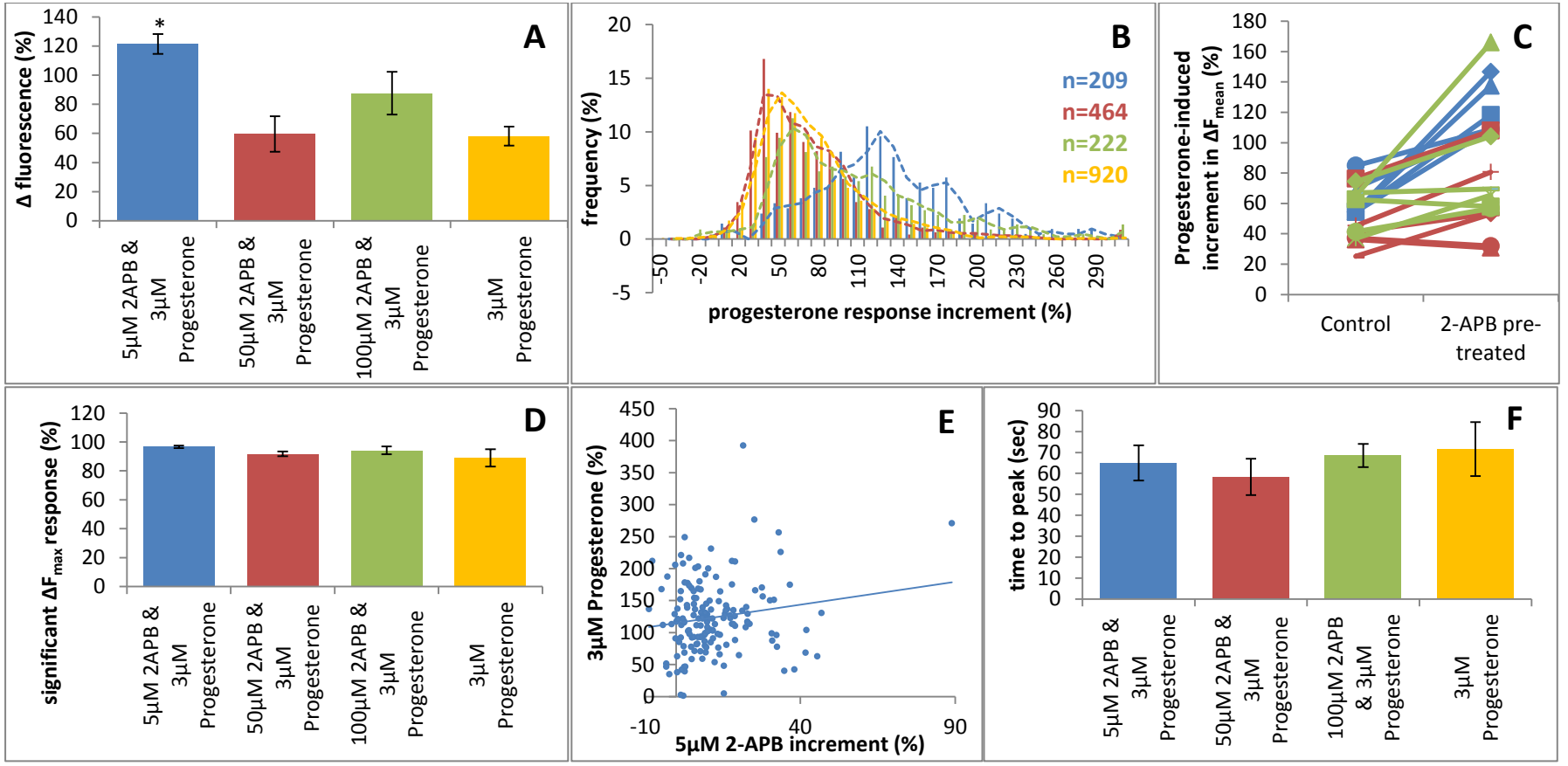

Figure 5.3 2-APB pre-treatment amplifies the progesterone induced Ca^{2+} transient at the PHN. In the following graphs cells were pre-treated with 5μM (blue) 50μM (red) 100μM (green) 2-APB or untreated control (yellow) for a minimum of 200s before 3μM progesterone stimulation. (A) Maximum increase in ΔF_{mean} within 3min of progesterone application, (B) frequency distribution of ΔF_{max} amplitude amongst the cell population, (C) comparison of (A) between treated/ 5μM pre-treated experimental pairs, (D) proportion of cells displaying significant ΔF_{max} response, (E) amplitude of 5μM 2-APB-induced resting $[Ca^{2+}]_i$ response (2-APB increment x-axis) is not correlated with the amplitude of subsequent progesterone-induced $[Ca^{2+}]_i$ increase (progesterone increment y-axis), (F) Mean time taken to reach progesterone $[Ca^{2+}]_i$ increase ΔF_{max}. All experiments were conducted with parallel untreated progesterone controls. Results are means ± S.E.M. * $P<0.05$; paired t-test; compared to progesterone response; 5μM (n=6) 50μM (n=6) 100μM (n=6).

The ΔF_{max} amplitude of the progesterone-induced $[Ca^{2+}]_i$ transient was determined for each individual cell response and classified as significant if the based on basal $[Ca^{2+}]_i$ levels and the 95% confidence interval. Cells pre-treated with 2-APB showed no significant increase in the percentage of cells exhibiting a significant response to progesterone application compared to the treated control (5µM *P*=0.40, 50µM *P*=0.45 & 100µM *P*=0.72; t-test; compared progesterone; Figure 5.3D) but as progesterone treatment alone typically induces a significant response in >90% cells the margin for increase is small. Comparison of 5µM 2-APB $[Ca^{2+}]_i$ response increment and subsequent 3µM progesterone induced $[Ca^{2+}]_i$ transient in pre-treated cells shows no correlation between the two elevations (Figure 5.3E) suggesting that 2-APB does not act via the mechanism responsible for the progesterone induced $[Ca^{2+}]_i$ transient. Time taken to achieve ΔF_{max} showed no significant change in 2-APB-pretreated cells at any dose (5µM *P*=0.22, 50µM *P*=0.84 & 100µM *P*=0.13; paired t-test; compared progesterone; Figure 5.3F).

5.5.3 Pre-treatment with 2-APB does not significantly modify the progesterone induced sustained $[Ca^{2+}]_i$ response

Treatment with 3μM progesterone initially produces a transient increase in $[Ca^{2+}]_i$ at the PHN which is followed by a sustained $[Ca^{2+}]_i$ plateau above basal levels. To investigate the effect of 5μM, 50μM and 100μM 2-APB pre-treatment on the sustained $[Ca^{2+}]_i$ elevation, the average of ΔF_{mean} was taken between 200 and 220 seconds after progesterone application and compared to treated cells. In 4 out of 6 experimental pairs pre-treated with 5μM 2APB the sustained $[Ca^{2+}]_i$ elevation at the PHN exceeded that of the progesterone control but this effect was highly variable (Figure 5.2D) and was not statistically significant (P=0.156; paired t-test; Figure 5.3A). Pre-treatment with higher concentrations of 2-APB (50μM and 100μM) were similarly inconsistent (P=0.470 & P=0.453 respectively; paired t-test; Figure 5.4A). Analysis of individual cell sustained $[Ca^{2+}]_i$ response traces shows a bell curve of sustained progesterone-induced response increments with and without pre-treatment (Figure 5.4B) only those cells pre-treated with 5μM 2-APB show a shift to the right indicative of elevated ΔF_{sus}. In addition pre-treatment with 5μM 2-APB shows an increase in the proportion of cells displaying a significant sustained response to progesterone at 220 seconds though this effect was again not significant (P=0.752; paired t-test; Figure 5.4C).

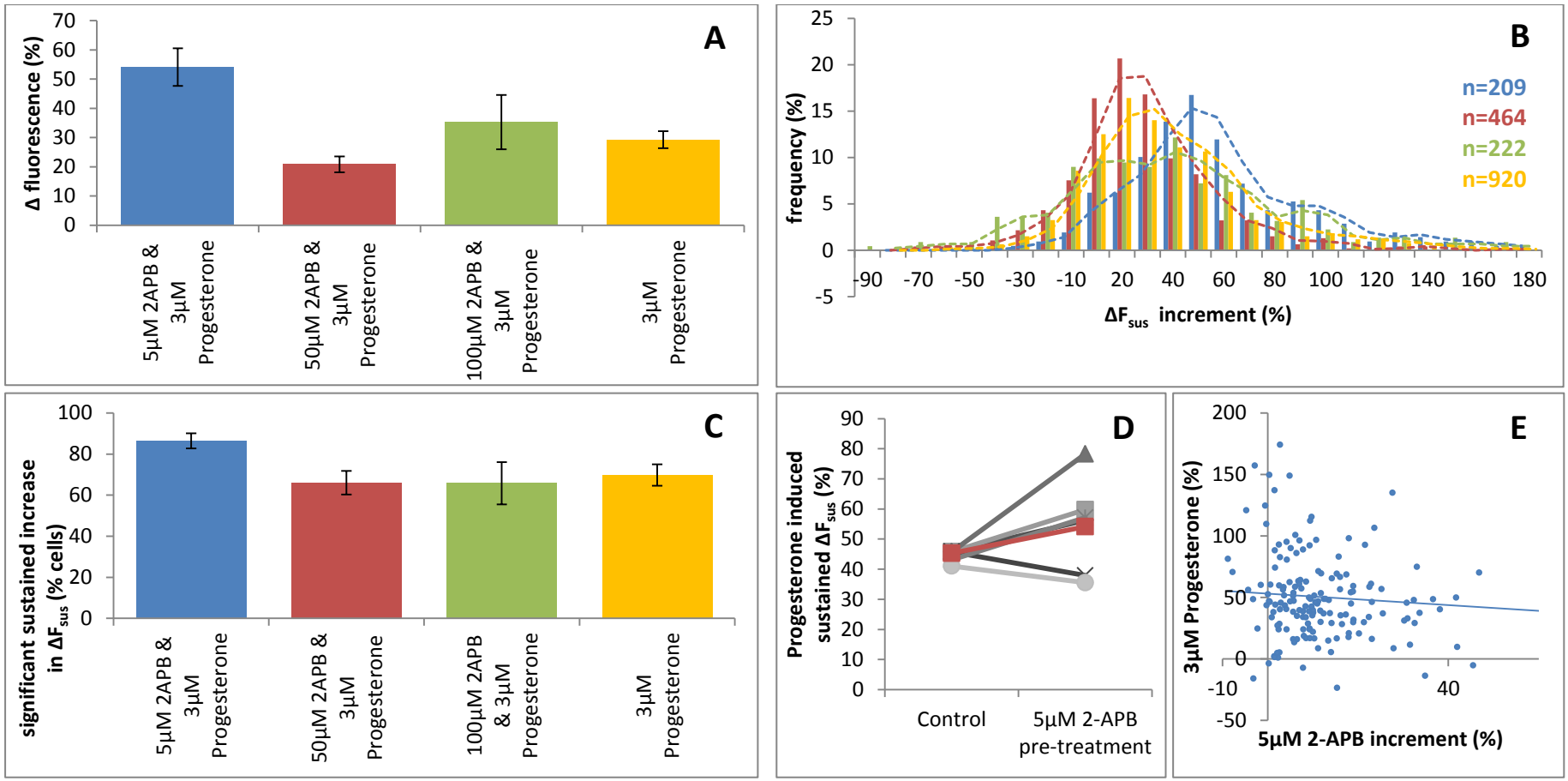

Figure 5.4 Effect of 2-APB pre-treatment on the sustained progesterone response at the PHN. In the following graphs cells were pre-treated with 5µM (blue) 50µM (red) 100µM (green) 2-APB or untreated control (yellow) for a minimum of 200s before 3µM progesterone stimulation, measurements were taken 3min after progesterone treatment. (A) ΔF_{mean} 3min after progesterone application, (B) frequency distribution of ΔF_{mean} amongst the cell population, (C) proportion of cells displaying significant sustained ΔF_{mean} responses (D) Comparison of (A) between untreated/pre-treated experimental pairs, (E) Amplitude of 5µM 2-APB-induced resting $[Ca^{2+}]_i$ response (2-APB increment x-axis) is not correlated with the amplitude of subsequent sustained progesterone-induced $[Ca^{2+}]_i$ increase (progesterone increment y-axis). All experiments were conducted with parallel treated progesterone controls for all 2-APB concentrations. Results are means ± S.E.M. 5µM (n=6) 50µM (n=6) 100µM (n=6).

5.5.3.1 Effects of 2-APB application on $[Ca^{2+}]_i$ after the progesterone induced $[Ca^{2+}]_i$ transient

To further investigate the effects of high 2-APB concentrations on the progesterone-induced sustained $[Ca^{2+}]_i$ plateau, 50µM and 100µM 2-APB were applied to cells 5-6 min after stimulation with 3µM progesterone when the $[Ca^{2+}]_i$ plateau was established. Upon 2-APB treatment an immediate transient fall in $[Ca^{2+}]_i$ was observed which then recovered to levels exceeding those before 2-APB application (~10% and ~20% increase in ΔF_{mean} in cells treated with 50µM and 100µM 2-APB respectively; Figure 5.5). The increase in ΔF_{mean} $[Ca^{2+}]_i$ (200-220s) that occurs when cells were exposed to 2-APB (section 5.5.1) was reduced when 2-APB was applied to cells previously stimulated with 3µM progesterone but this difference was not significant at either dose (Figure 5.6A). Frequency distribution profiles show similar bell shaped patterns of 2-APB response increment with and without initial progesterone treatment at both concentrations (Figure 5.6B). The proportion of cells displaying a significant response to 2-APB treatment was reduced by progesterone pre-treatment with both 50µM and 100µM, but again these effects failed to reach statistical significance (P=0.059 & P=0.816 respectively; Figure 5.6C).

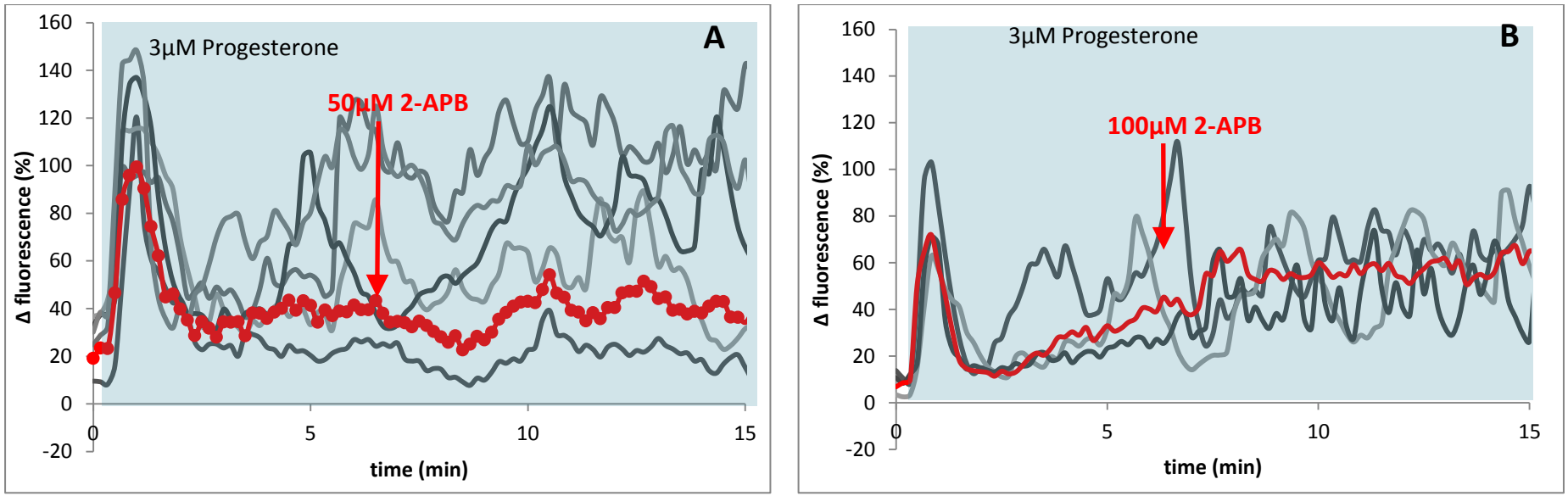

Figure 5.5 Effect of progesterone pre-treatment on 2-APB induced Ca^{2+} response at the PHN. Capacitated cells were pre-treated with 3µM progesterone for 300s (grey box) before application of (A) 50µM or (B) 100µM 2-APB (red arrow). Each graph shows individual ΔF cell responses (grey traces) and ΔF_{mean} (red trace) for all cells in that experiment, (n=39 & n=21 respectively).

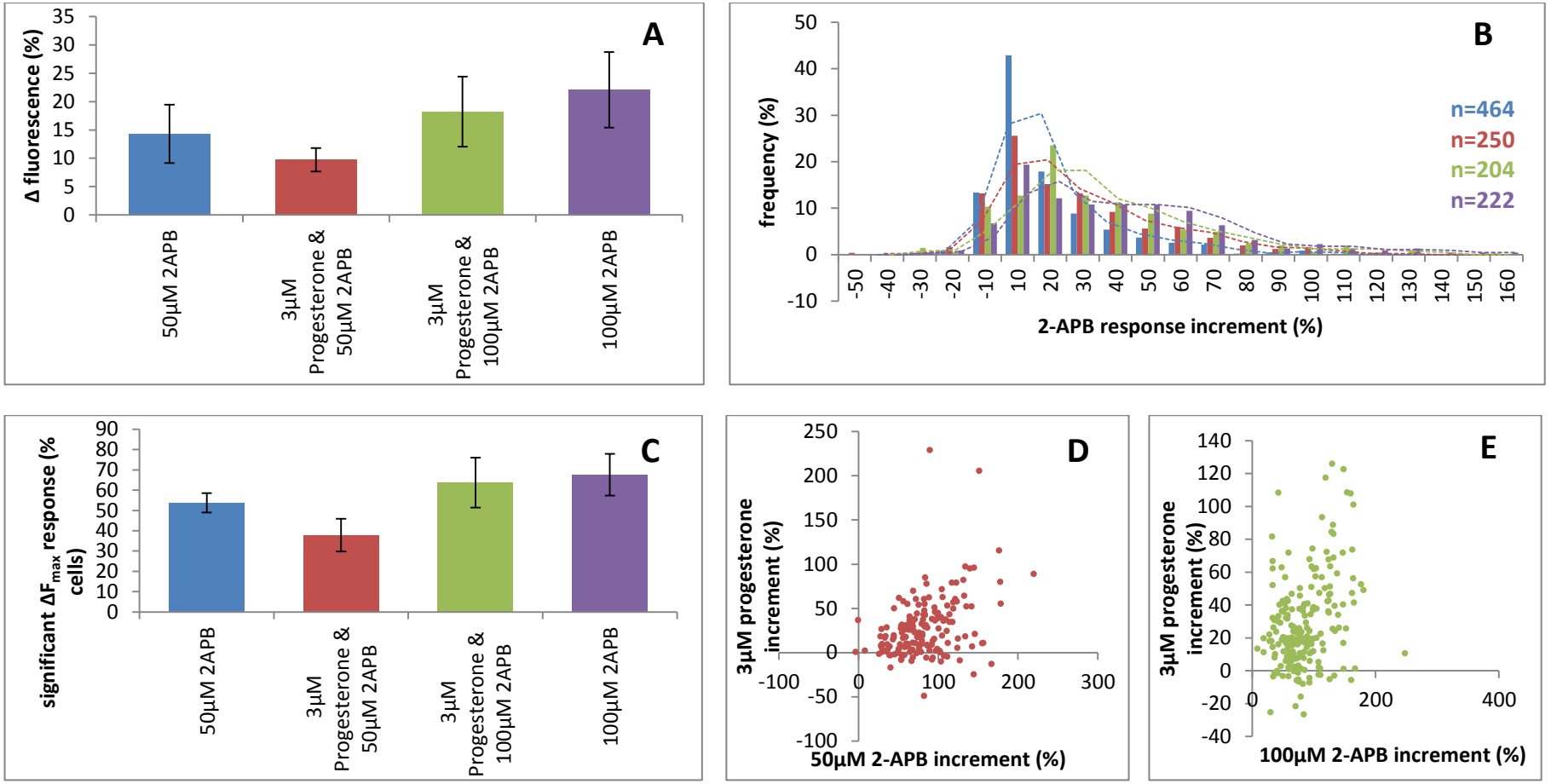

Figure 5.6 Progesterone pre-treatment does not prevent 2-APB induced Ca^{2+} elevation. Each graph shows the effects of 3µM progesterone pre-treatment on the 50µM (red) or 100µM (green) 2-APB induced Ca^{2+} response at the PHN compared to parallel samples exposed to only 50µM (blue) or 100µM (purple) 2-APB. (A)Maximum increase in ΔF_{mean} within 3min of 2-APB application, (B) frequency distribution of ΔF_{max} response amongst the cell population, (C) proportion of cells displaying significant ΔF_{max} response, (D) & (E) Amplitude of 2-APB-induced resting $[Ca^{2+}]_i$ response 50µM and 100µM respectively (2-APB increment x-axis) correlation with the amplitude of subsequent progesterone-induced $[Ca^{2+}]_i$ increase (progesterone increment y-axis). All experiments were conducted with parallel 2-APB controls and progesterone pre-treated experiments. Results are means ± S.E.M; 50µM (n=6) 100µM (n=6).

5.6 Discussion

The identification of CatSper channels through patch-clamp studies by Lishko *et al.*, 2011 and Strunker *et al.*, 2011 suggested a limited role for intracellular Ca^{2+} stores in the modulation of $[Ca^{2+}]_i$. Localised to the principal piece of the mammalian sperm flagellum, CatSper were identified as the primary progesterone receptor, in a prime location for modulating hyperactivated motility. However, treatment of cells with 10μM NNC-55-0396 (NNC) a known blocker of CatSper currents was unable to abolish the progesterone induced $[Ca^{2+}]_i$ response (Strunker *et al.*, 2011). The study by Strunker *et al.*, 2011 shows a 60% inhibition of the progesterone induced $[Ca^{2+}]_i$ response as a direct result of NNC application suggesting that the remaining 40% increase in $[Ca^{2+}]_i$ could result from intracellular Ca^{2+} store mobilisation.

To support a model for involvement of intracellular Ca^{2+} stores in human sperm $[Ca^{2+}]_i$ regulation a mechanism for replenishing depleted stores must also be present. In 1993 Blackmore identified the essential components for contribution from intracellular Ca^{2+} stores to the progesterone induced $[Ca^{2+}]_i$ response. In addition to the intracellular Ca^{2+} store the cell would require a plasma membrane Ca^{2+} channel and a mechanism of interaction between the two which he termed capacitative Ca^{2+} entry (CCE). Multiple candidates were considered as possible contributors to CCE in somatic cells (otherwise known as store-operated Ca^{2+} entry (SOCE) including but not limited to TRP channels. However it was the discovery of two interactive transmembrane protein groups in 2005 and 2006 respectively that led to the most convincing model for SOCE to date. The first potential SOCE component to be identified was stromal interaction molecules (STIM); residing in the ER membrane of somatic cells these receptors act as a Ca^{2+} sensor inducing a conformational change when ER $[Ca^{2+}]$ is low

resulting receptor translocation and interaction with a PM CRAC channel inducing Ca^{2+} influx (Liou *et al.,* 2005). The following year three groups consecutively identified the pore-forming CRAC channel component of SOCE as Orai (Feske *et al*., 2006; Vig *et al*., 2006; Zhang *et al*., 2006). Subsequent analysis proposes activated CRAC channels are composed of Orai tetramers which interact with oligomerised STIM molecules on the ER. Together STIM and Orai have been shown to form a conformational coupling mechanism that enables successful SOCE in somatic cells (Muik *et al*., 2012; Soboloff *et al*., 2012).

To date two STIM (STIM1 and STIM2) and three Orai (1-3) isoforms have been detected in human somatic cells (Cahalan, 2009). In addition, using immunofluorescence, we observed STIM1, STIM2 and all three Orai (1-3) isoforms in mature human sperm, though Orai 2 detection was not confirmed by Western blot (Lefievre *et al.,* 2012). We found that all mammalian homologues were present in the PHN region of human sperm, with Orai 3 only present in the most anterior segment. STIM2, Orai1 and Orai3 were also detected in the acrosomal region, whilst STIM2 and Orai3 were expressed along the entire flagellum (Figure 5.7). Localisation of these facilitators of SOCE predominantly to the PHN suggest a role for Ca^{2+} stores at the PHN of human sperm; their contribution to hyperactivated motility is unknown however it is likely enhanced by CatSper channels in close proximity in the PM.

The bimodal action of 2-APB on the CCE channel current (I_{CRAC}) is well documented, at high concentrations (>50 μm) 2-APB inhibits CCE current (DeHaven *et al.,* 2008; Zhang *et al.,*

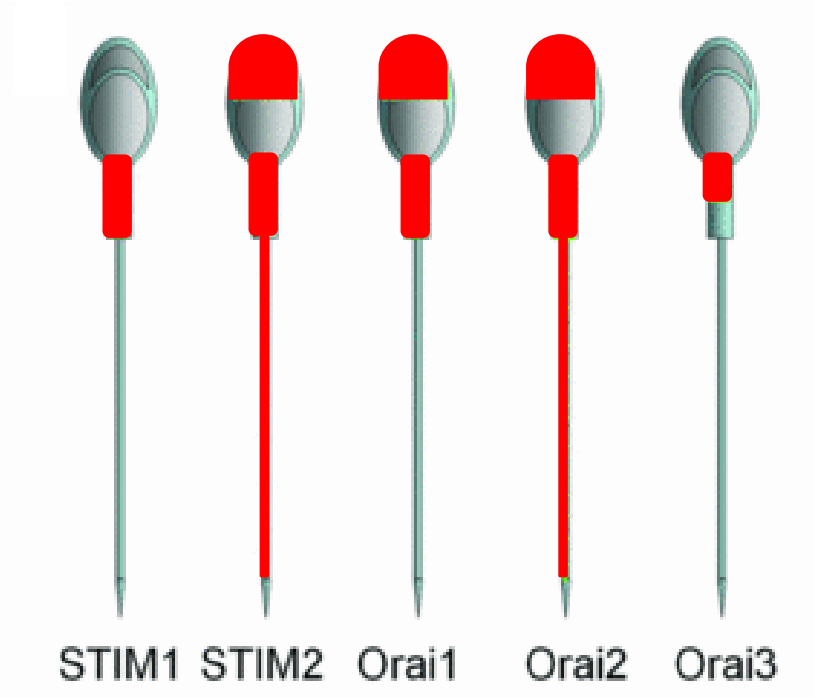

Figure 5.7 Distribution of STIM & Orai homologues in human sperm, modified from Lefievre *et al.*, 2012. Diagrammatic representation of immunofluorescence localisation of mammalian SOCE homologues (red), STIM1, STIM2, Orai1-3; all homologues were observed to be present in the PHN/midpiece of capacitated human sperm. STIM2, Orai1 & Orai2 were discovered in the acrosomal region, with STIM2 and Orai2 also detected in the flagellum.

2008; Lis *et al.,* 2007) whilst at low concentrations (~5μM) 2-APB activates SOCE (Goto *et al.,* 2010; Suzuki *et al.,* 2010; Lefievre *et al.,* 2012). As a result 2-APB has formed the basis for the development of a number of new SOCE modulatory compounds (Goto *et al.,* 2010; Suzuki *et al.,* 2010); however their potency remains to be tested thoroughly. Current models propose that at high concentrations 2-APB molecules bind to Orai subunits simulating STIM molecules and subsequently directly inhibit I_{CRAC} (DeHaven *et al.,* 2008; Zhang *et al.,* 2008; Lis *et al.*, 2007; Goto *et al.*, 2011). At low concentrations it is believed that 2-APB stimulates I_{CRAC} by increasing pore size and promoting the interaction of STIM and Orai proteins (Schindl *et al*., 2008). Here we demonstrate that 2-APB demonstrates a dose dependent elevation on $[Ca^{2+}]_i$ at the PHN of human sperm without mobilising the intracellular Ca^{2+} store (Figure 5.1A, B&C). An observation that was also documented in Hek cells by Schindl *et al*., 2008. Higher concentrations of 2-APB result in a greater proportion of the cell population eliciting a significant Ca^{2+} response (Figure 5.1D); this effect is abolished in EGTA buffered saline demonstrating that the 2-APB response is dependent on extracellular Ca^{2+} (data not shown; published in Lefievre *et al.,* 2012). This suggests that Orai molecules at the PHN participate in the increase in $[Ca^{2+}]_i$ at the region associated with 5μM 2-APB application.

We have identified that 2-APB alone elevates $[Ca^{2+}]_i$ at the PHN in the presence of extracellular Ca^{2+}. This effect was abolished and even reversed when $[Ca^{2+}]_i$ was heavily buffered (Lefievre *et al.*, 2012), confirming that 2-APB activates Ca^{2+} permeable channels in the plasma membrane of human sperm. Next we wanted to observe the effect of 2-APB treatment on the well characterised biphasic progesterone induced Ca^{2+} response. The recent identification of CatSper channels as the primary progesterone receptor in mammalian sperm has caused some controversy over the involvement of intracellular Ca^{2+} stores in human

sperm (Strunker *et al.*, 2011; Brenker *et al.*, 2012). However the inability of the CatSper inhibitor NNC to abolish the biphasic progesterone induced Ca^{2+} response suggests a secondary progesterone sensitive mechanism is present. As a dual action SOCE inhibitor/activator we compared the effects of a range of 2-APB concentrations on the biphasic progesterone induced $[Ca^{2+}]_i$. We observed that at stimulatory concentrations (5μM) 2-APB caused a significant elevation in the progesterone induced Ca^{2+} transient (Figure 5.3A). In addition higher inhibitory concentrations of 2-APB (50μM and 100μM) also enhanced the transient in 4 out of 6 experiments (Figure 5.4C). It should be noted that only those samples treated with 5μM 2-APB displayed an increase in the proportion of cells eliciting a significant response such that the distribution profile moved noticeably to the right Figure 5.3B&D). These results support those obtained in other cell types treated with stimulatory 2-APB concentrations suggesting a role for SOCE in the progesterone induced Ca^{2+} response (Goto *et al.*, 2010).

To determine the effect of 2-APB pre-treatment on the sustained progesterone response we measured the $[Ca^{2+}]_i$ 4 minutes after 3μM progesterone application. Our results mirrored those observed for the progesterone transient (Figure 5.5). Cells pre-treated with 5μM 2-APB displayed elevated $[Ca^{2+}]_i$ compared to parallel controls although these differences were not significant. In addition the proportion of cells producing a significant $[Ca^{2+}]_i$ was greater in those samples pre-treated with 5μM 2-APB causing a slight shift to the right in the population distribution statistics (Figure 5.4B). In cells treated with higher concentrations of 2-APB (50μM and 100μM) greater variability was exhibited amongst the cell population with a high proportion of the cells displaying an inhibitory effect on the sustained Ca^{2+} response (Figure 5.6). Furthermore cells treated with 50μM or 100μM 2-APB after 3μM progesterone first showed a consistent decrease in the $[Ca^{2+}]_i$ response which was not observed when applied

before progesterone stimulation (Figure 5.6). Subsequently sustained $[Ca^{2+}]_i$ levels increased marginally above levels observed before 2-APB treatment. These results suggest a model whereby 2-APB sensitive channels could contribute to the sustained progesterone induced Ca^{2+} influx if 2-APB blocked CatSper channels, as was shown by patch clamp (Lefievre *et al.*, 2012). As a consequence 2-APB sensitive channels would be released from inhibitory regulation by $[Ca^{2+}]_i$ thus enabling Ca^{2+} influx and the $[Ca^{2+}]_i$ recovery observed in Figure 5.5.

In summary we have shown that 2-APB elevates $[Ca^{2+}]_i$ at the PHN in a dose dependent manner which is reliant on extracellular Ca^{2+}. Exposure of cells to 5μM 2-APB enhances both components of the biphasic Ca^{2+} response induced by 3μM progesterone application. However only the increase in $[Ca^{2+}]_i$ during the transient component of the progesterone response is significantly greater than the untreated control . In addition our identification of SOCE proteins STIM and Orai are indicative of intracellular Ca^{2+} store presence and contribution to spatio-temporal regulation in human sperm (Lefievre *et al.*, 2012). Taken together these findings suggest a role for a 2-APB sensitive Ca^{2+} channel at the PHN which enhances the progesterone induced Ca^{2+} response activated through CatSper.

CHAPTER SIX: STORE-OPERATED Ca^{2+} ENTRY MODULATION USING SKF AT THE PHN OF HUMAN SPERM

6.1 Abstract

SKF-96365 (SKF) is a non-specific inhibitor of store-operated Ca^{2+} channels (SOCC). At low concentrations (<40μM) SKF prevents receptor activated Ca^{2+} influx at the plasma membrane (PM), but at higher concentrations (>40μM) SKF can modulate Ca^{2+} release from intracellular storage organelles (Merritt *et al.,* 1990). Previous chapters have highlighted evidence for the existence of SOCE in human sperm and their essential role in the progesterone induced biphasic $[Ca^{2+}]_i$ response. Here we report that Ca^{2+} fluorescence imaging using Oregon Green-BAPTA-1AM shows SKF has complex effects on $[Ca^{2+}]_i$ in human sperm. 3μM & 30μM SKF caused an elevation of resting $[Ca^{2+}]_i$ but pre-treatment of cells with 30μM SKF amplified the $[Ca^{2+}]_i$ transient induced by 3μM progesterone stimulation, whilst significantly reducing the subsequent sustained $[Ca^{2+}]_i$ elevation. These findings support similar observations in other cell types (Merritt *et al.,* 1990) suggesting SOCE contribution to the sustained component of the biphasic progesterone $[Ca^{2+}]_i$ response. Furthermore 30μM SKF reduced the proportion of human sperm cells exhibiting hyperactivated motility (as determined by CASA) both under control conditions and in the presence of 3μM progesterone.

6.2 Introduction

In the preceding chapters we identify a role for SOCE at the PHN in human sperm. 1-(beta-[3-(4-methoxy-phenyl)propoxy]-4-methoxyphenethyl)-1H-imidazole hydrochloride otherwise known as SKF-96365 (SKF) is an inhibitor of store-operated Ca^{2+} channels (SOCC). Identified in 1990, SKF is a hydrophobic compound structurally distinct from traditional Ca^{2+} antagonists conferring selectivity between PM receptor facilitated Ca^{2+} entry (receptor mediated Ca^{2+} entry; RMCE, which includes capacitive Ca^{2+} entry; CCE) and Ca^{2+} release from internal stores (Merritt *et al.,* 1990). Initial observations by Merritt and colleagues revealed that exposure of human platelets, neutrophils or endothelial cells to 10-20μM SKF inhibited a stimulus evoked rise in $[Ca^{2+}]_i$ when the response was dependent on extracellular Ca^{2+}. Fluorescence studies of quin2-loaded platelets showed that treatment with 25μM SKF almost completely inhibited 20μM ADP-evoked Ca^{2+} entry via RMCE. In addition experiments conducted in the absence of extracellular Ca^{2+} showed little effect of SKF treatment on ADP induced internal Ca^{2+} store release suggesting SKF antagonism is selective for PM receptors (Merritt *et al.,* 1990). Furthermore subsequent studies have shown that these PM effects are not SOCE specific (Jenner & Sage, 2000; Marumo *et al.,* 2012; Blackmore, 1993). At higher concentrations (>40μM) SKF was reported to modulate intracellular Ca^{2+} store activity, causing both inhibition and in some cases enhancing release of stored Ca^{2+} (Merritt *et al.,* 1990).

In human platelets thapsigargin induces a biphasic $[Ca^{2+}]_i$ response comprising of an initial transient followed by a sustained peak, suggesting at least two separate Ca^{2+} pathways contribute to the response. Fluorescence imaging and fluorimetry have been used to investigate the effects of tyrosine phosphorylation and SOC inhibitors on the biphasic

thapsigargin induced $[Ca^{2+}]_i$ increase (Vostal & Schafer, 1996; Jenner & Sage, 2000). Platelet pre-treatment with SKF had no observable effects on the initial transient but the sustained Ca^{2+} rise was inhibited, consistent with an initial release of stored Ca^{2+} followed by activation of SOCE (Jenner & Sage, 2000; Marumo *et al.,* 2012). Similarly SKF has been shown to inhibit RMCE in both neutrophils (Davies *et al.,* 1992) and endothelial cells (Kruse *et al.,* 1995). Indeed Davies *et al.,* 1992 confirmed the ability of SKF to disassociate transmembrane Ca^{2+} influx from intracellular Ca^{2+} store release in neutrophils through Mn^{2+} quenching. Krause *et al.,* 1995 used the same methodology to prove that thrombin receptor-activating peptide TRAP14 required external Ca^{2+} influx for $[Ca^{2+}]_i$ increase and cell sensitisation. In all instances SKF has shown non-selective antagonism of PM Ca^{2+} receptors; however it appears to affect multiple RMCE pathways though L and T Type Ca^{2+} channels (Merritt *et al.,* 1990). It is also important to note that SKF appears to have little effect on ATP-gated channels (Merritt *et al.,* 1990) unless they function in conjunction with SOCE (Jantaratnotai *et al.,* 2009).

There are few studies on the effects of SKF on SOCE in human sperm. In 1993 Blackmore was the first to suggest that the $[Ca^{2+}]_i$ increase associated with progesterone metabolite stimulation of human platelets could be associated with the progesterone induced $[Ca^{2+}]_i$ response in human sperm through a SOCE mechanism. Here Blackmore (1993) showed pregnanolone and pregnanedione promoted a rapid rise in human platelet $[Ca^{2+}]_i$ and aggregation similar to the effects of thrombin, which was inhibited by SKF application. In addition it was proposed that progesterone stimulates Ca^{2+} influx through a similar mechanism due to the nature of the Ca^{2+} response and the presence of SOC receptors in the PM. Subsequent studies on sea urchin sperm show correlations between the biphasic $[Ca^{2+}]_i$

response produced by fucose sulfate polymer (FSP) of egg jelly in ascidians and the biphasic progesterone induced $[Ca^{2+}]_i$ response in mammals (Hirohashia &Vacquier, 2003). In experiments measuring $[Ca^{2+}]_i$ of sea urchin sperm using Fura-2, treatment with SKF was sufficient induce inhibitory effects on the sustained $[Ca^{2+}]_i$ response consistent with SOCE inhibition (Hirohashia & Vacquier, 2003). In addition SKF treatment has been shown to antagonise Ca^{2+} influx induced by mitochondrial inhibitors (CCCP) suggesting a role for SOCs in ascidian mitochondrial Ca^{2+} regulation (Ardon *et al.*, 2009). Studies on the effects of SKF on mammalian sperm are limited; however Trevino *et al.,* 1996 demonstrates that SKF inhibits both the increase in $[Ca^{2+}]_i$ and AR associated with Maitotoxin (a potent cation activator) treatment of mammalian spermatogonial cells through SOCs. Furthermore SKF has been shown to significantly reduce the motility of human sperm (Krasznai *et al.,* 2006). SKF is therefore a useful antagonist to determine the effect of SOCE on progesterone induced $[Ca^{2+}]_i$ increase at the PHN of human sperm.

6.3 Aims

The aim of this chapter was to determine the effect of SKF-96365 treatment on $[Ca^{2+}]_i$ at the PHN of human sperm and subsequent effect on the biphasic $[Ca^{2+}]_i$ response induced by progesterone. In addition we wanted to quantify the effects of SKF-96365 on human sperm motility parameters and critically those associated with hyperactivation to correlate changes in $[Ca^{2+}]_i$ with physiological function.

6.4 Material and Methods

6.4.1 Materials

Progesterone and 1-(beta-[3-(4-methoxy-phenyl)propoxy]-4-methoxyphenethyl)-1H-imidazole hydrochloride (SKF-96365) were purchased from Sigma Aldrich Company Ltd. (Dorset) and Merck Millipore (Watford, UK) respectively. For all other materials see chapter 2.1.1.

6.4.2 Methods

6.4.2.1 Cell preparation

Human semen was collected and prepared as in chapter 2.3.

6.4.2.2 Cell incubation and capacitation

Sperm harvested by swim up procedure (chapter 2.4.2.1) were incubated and capacitated as in chapter 2.4.

6.4.2.3 CASA

All CASA experiments for this chapter were conducted as in chapter 2.5. However it should be noted that in experiments treated with SKF and Progesterone both doses were administered simultaneously.

6.4.2.4 Single cell imaging

All imaging experiments for this chapter were conducted with Oregon Green-BAPTA-1AM and followed the methodology outlined in chapter 2.6.1.

6.4.3 Analysis

Calcium imaging with Oregon Green-BAPTA-1AM results were analysed as in chapter 2.6.1.

6.5 Results

6.5.1 SKF elevates resting $[Ca^{2+}]_i$ at the PHN

Figure 6.1 shows typical fluorescence traces of Oregon Green-BAPTA-1AM loaded human sperm cells exposed to SKF at 3μM (A) or 30μM (B) in the presence of extracellular calcium. Treatment of sperm with either 3μM or 30μM SKF induced an increase in $[Ca^{2+}]_i$ in ~70% cells within 100s. At both concentrations SKF induces either a plateau or series of Ca^{2+} transients in subsets of cells stabilizing an increased level within 200s (Figure 6.1). ΔF_{mean} was determined as the average of the 3 highest consecutive points within the 200s period of SKF application and displayed dose dependency (Figure 6.2A). This increase in resting $[Ca^{2+}]_i$ (ΔF_{mean}) was seen in all experiments at both concentrations (3μM (n=9); 30μM (n=13)). However the increase in resting $[Ca^{2+}]_i$ observed with SKF was significantly less than that observed in parallel experiments with 3μM progesterone (3μM SKF P=0.00005, 30μM SKF P=0.03; paired t-test; n=5, n=8 respectively).

Individual cell Ca^{2+} responses to SKF revealed no significant difference between concentrations in the proportion of cells eliciting a significant $[Ca^{2+}]_i$ increase (3μM SKF 74.7±6.5%, 30μM SKF 60.3±8.3%; P=0.2; paired t-test; n=5, n=8 respectively; Figure 6.2B). When compared to the proportion of cells showing a significant increase in $[Ca^{2+}]_i$ in parallel progesterone experiments (89.5±2.1%) the proportion of cells responding to SKF(both concentrations) was significantly lower (P=0.02 & P=0.01 ; paired t-test; n=5, n=8 respectively; Figure 6.2B). SKF concentration had no effect the amplitude distribution of single cell SKF response increments but these differed significantly from the well characterised bell shaped distribution of the progesterone induced $[Ca^{2+}]_i$ response

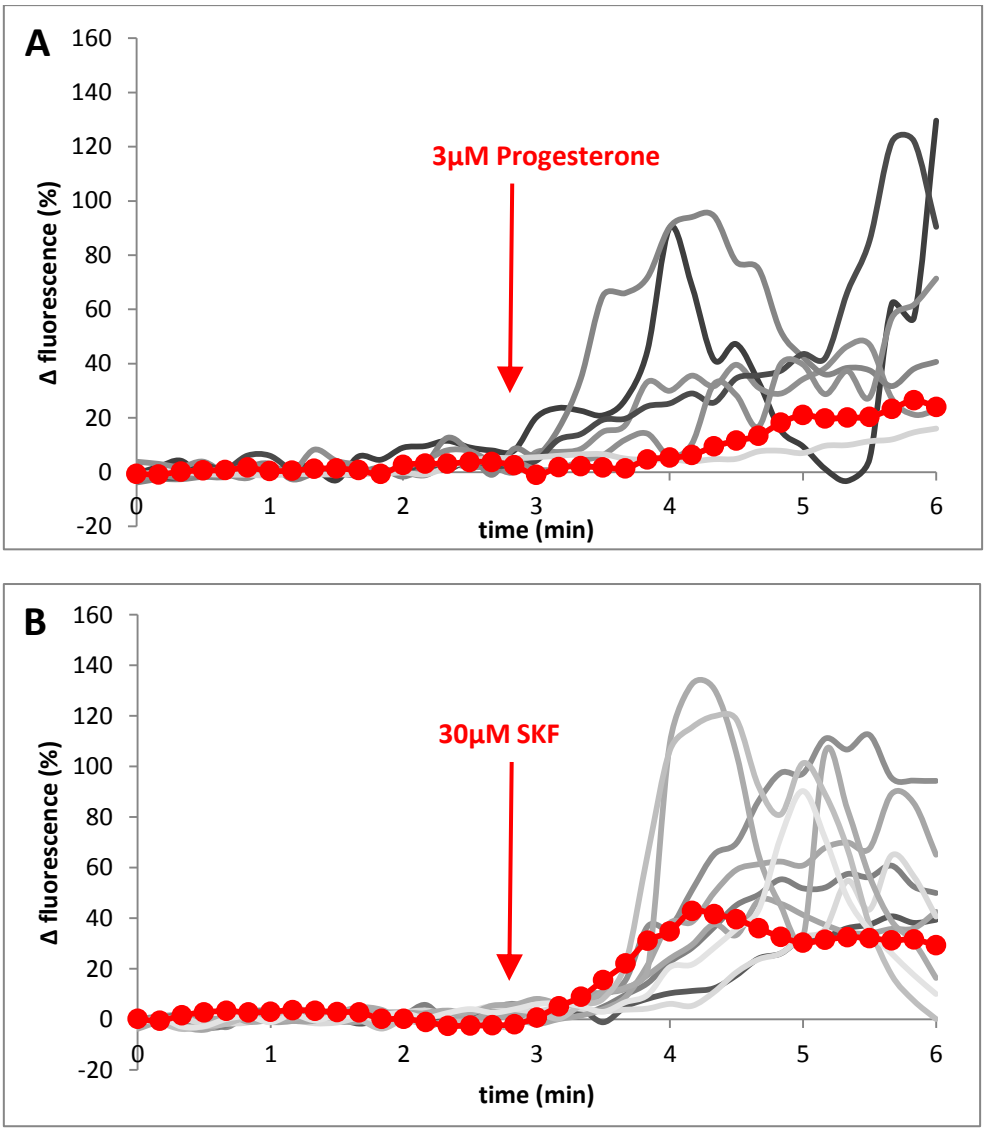

Figure 6.1 SKF elevates resting $[Ca^{2+}]_i$. Capacitated cells were monitored for a minimum of 200seconds before either (A) 3µM or (B) 30µM SKF was applied (red arrow). Each graph shows individual cell responses (grey traces) and ΔF_{mean} (red trace) for all cells in that experiment, (n=134, n=71 respectively).

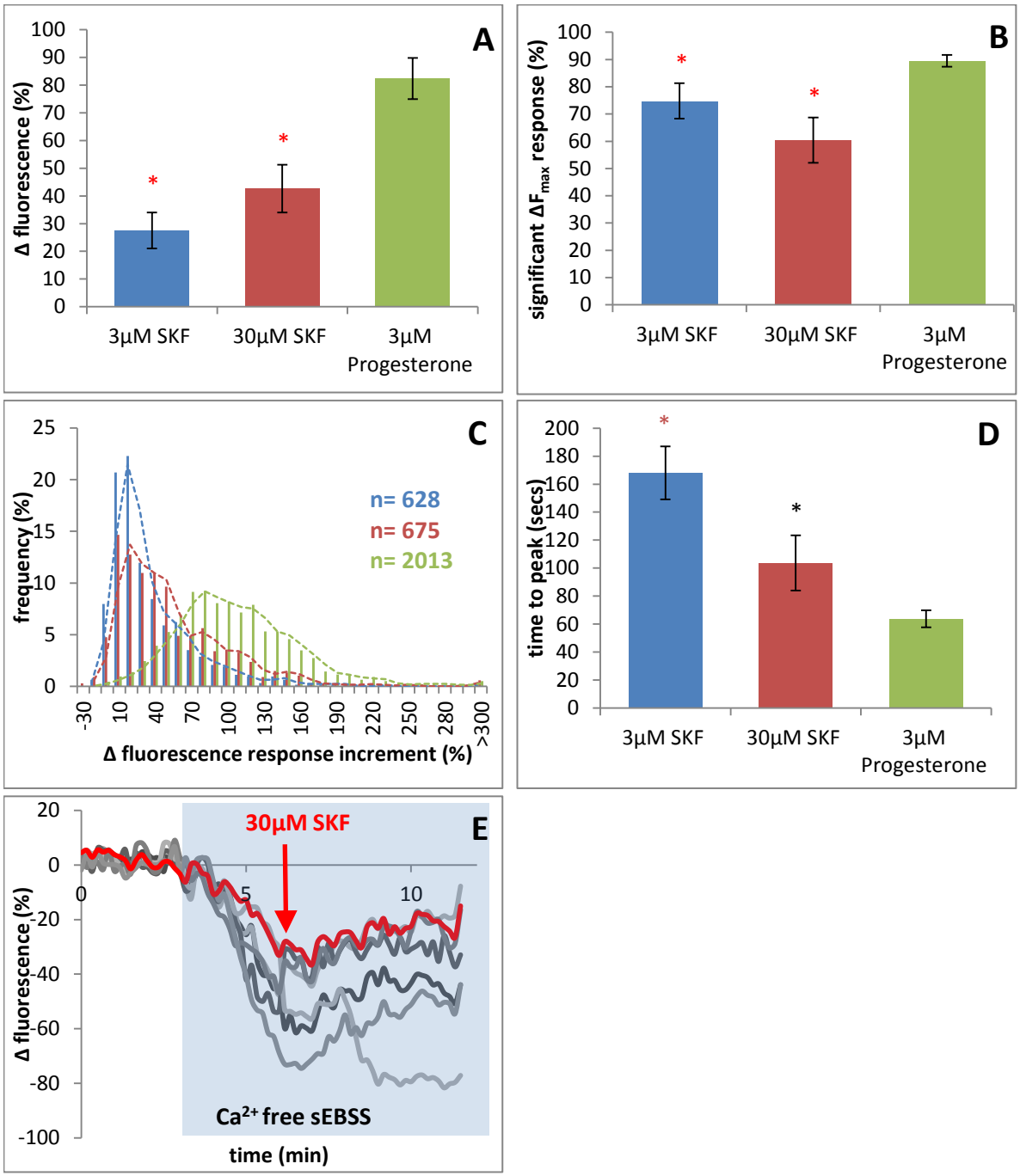

Figure 6.2 Effect of SKF on resting $[Ca^{2+}]_i$ in human sperm. In the following graphs cells were treated with 3μM SKF (blue), 30μM SKF (red) or 3μM progesterone (green). (A) Effect of treatment on $\Delta F_{mean.}$ (B) Percentage of cells producing a significant increase in $[Ca^{2+}]_i$ as a result of treatment application mean ± S.E.M. (C) Effect of treatment on amplitude distribution of changes in $[Ca^{2+}]_i$ (n=number of cells observed) (D) Time taken to achieve ΔF_{mean}. Each bar shows the mean time taken to achieve maximum amplitude ± S.E.M. (E) Effect of 30μM SKF in the absence of extracellular Ca^{2+}. Graph shows individual ΔF cell responses (grey traces) and ΔF_{mean} (red trace) for all cells in that experiment.* $P<0.05$; compared to 3μM SKF; paired t-test. * $P<0.05$; compared to P; paired t-test, n=5 & n=8 respectively.

(Figure 6.2C). In contrast, the time to peak response showed significant concentration effects; cells treated with 30μM SKF demonstrated significantly shorter response times compared to those treated with 3μM SKF (*P*=0.03; paired t-test; n=5, n=8 respectively Figure 6.2D). However both concentrations of SKF took longer to achieve ΔF_{mean} when compared to progesterone response time (*P*=0.001 & *P*=0.06; paired t-test; n=5, n=8 respectively; Figure 6.2D). Superfusion of capacitated cells with EGTA-buffered medium (~$3x10^{-7}$M Ca^{2+}) for 2min caused an initial decrease in $[Ca^{2+}]_i$. Addition of 30μM SKF then caused a small increase in $[Ca^{2+}]_i$ consistent with the release of Ca^{2+} from intracellular stores (Figure 6.2F). This effect was observed in ~70% of the population (69.9±11.2%; n=7). In the remaining proportion of cells $[Ca^{2+}]_i$ continued to decrease and a further fall in $[Ca^{2+}]_i$ also occurred in many responsive cells after Ca^{2+} stores have emptied. To further analyse the effect of SKF on progesterone induced Ca^{2+} influx cells were pre-treated with SKF before 3μM progesterone application and the response observed.

6.5.2 SKF enhances the progesterone induced $[Ca^{2+}]_i$ transient at the PHN

The biphasic effect of progesterone on $[Ca^{2+}]_i$ of human sperm is well established (Kirkman-Brown *et al.*, 2000; Harper *et al.*, 2004) and 3μM progesterone is sufficient to induce this characteristic response. As SKF is an inhibitor of SOCE it is therefore interesting to see if pre-treatment with SKF prior to progesterone application induces any effects on the Ca^{2+} transient. To identify the effect of SKF on the progesterone induced Ca^{2+} transient experiments were conducted in pairs. Cells from the same semen sample were prepared and either pre-treated with SKF for 200s or untreated prior to progesterone stimulation. The untreated control population showed an initial transient increase in $[Ca^{2+}]_i$ followed by a plateau in ~90% of cells within 70s (data not shown) upon stimulation with 3μM

progesterone. Pre-treatment with 3μM SKF or 30μM SKF induced dose dependent $[Ca^{2+}]_i$ responses as described above (Figure 6.3A&B respectively). When progesterone was then applied to cells exposed to 3μM SKF the amplitude of the Ca^{2+} transient (increment in ΔF_{mean}) was enhanced (control/pre-treated ΔF_{mean}; 108.6±7.4%, 127.6±10.8%) but this effect was not statistically significant (*P*=0.18; paired t-test; n=4; day averages of 8 experiments; Figure 6.4A). 30μM SKF pre-treatment acted similarly, but at this concentration the effect was more consistent (11 out of 13 experimental pairs) and robust. Indeed the amplitude of the progesterone Ca^{2+} transient was significantly increased compared to parallel controls (control/pre-treated ΔF_{mean}; 65.9±9.4%, 82.8±6.8%; *P*=0.01; paired t-test; n=8 (day averages) Figure 6.4A&C). In addition 30μM SKF increased the percentage of cells exhibiting a significant transient response to progesterone (control/pre-treated; 84.9±2.3%, 95.4±2.6%; *P*=0.02; paired t-test; n=8 (day averages) Figure 6.4D). Analysis of individual cell Ca^{2+} transient responses revealed no difference in the frequency distribution and time taken to achieve ΔF_{mean} amongst the control and pre-treated populations at both SKF concentrations (Figure 6.4B); furthermore SKF response amplitude showed no correlation with the subsequent progesterone response (Figure 6.4E).

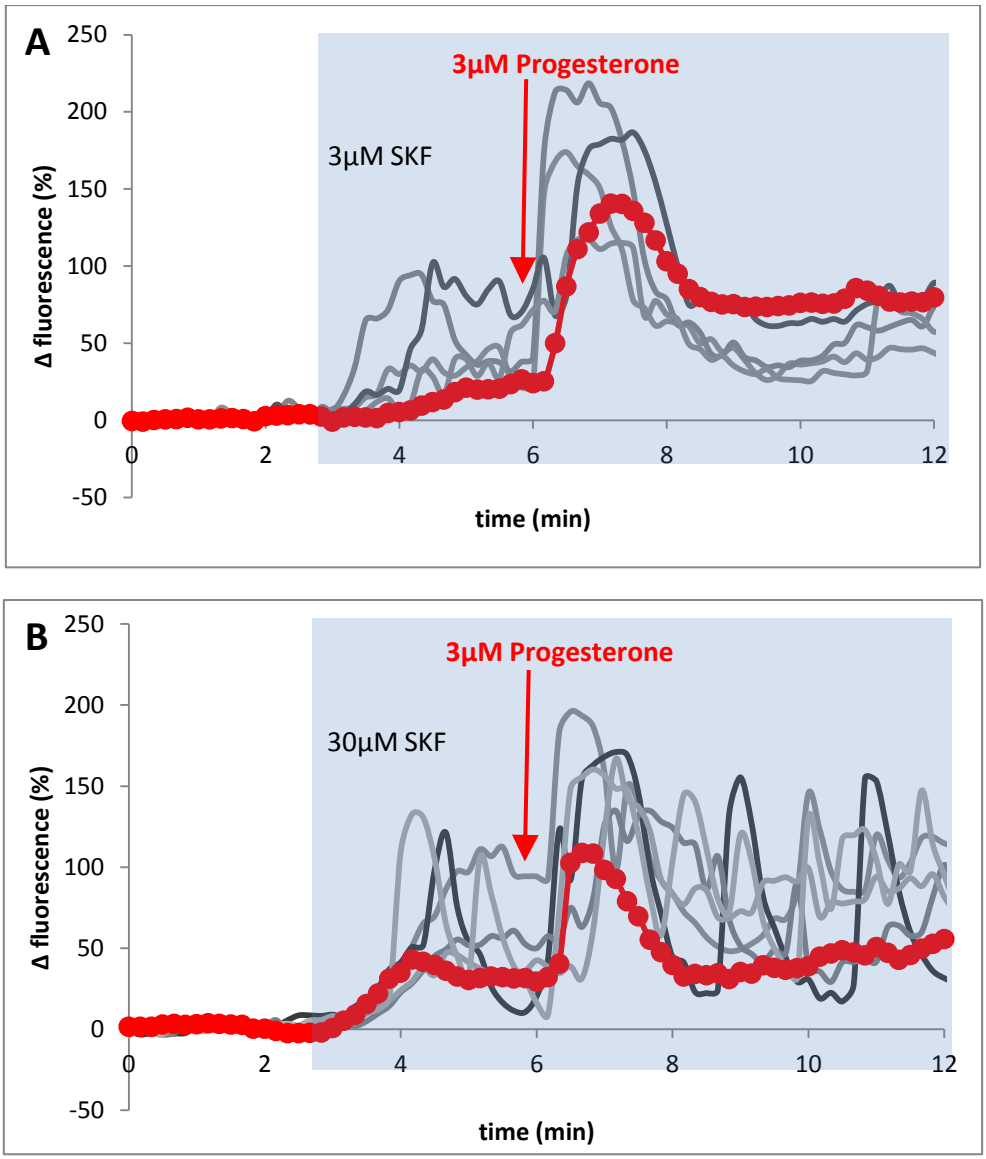

Figure 6.3 SKF pre-treatment modifies the progesterone induced $[Ca^{2+}]_i$ response. Cells were monitored for a minimum of 200s before pre-treatment with either (A) 3µM or (B) 30µM SKF was applied (grey box). After a further 300s 3µM progesterone was applied (red arrow). Each graph shows individual cell responses (grey traces) and ΔF_{mean} (red trace) for all cells in that experiment, (n=134, n=71 respectively).

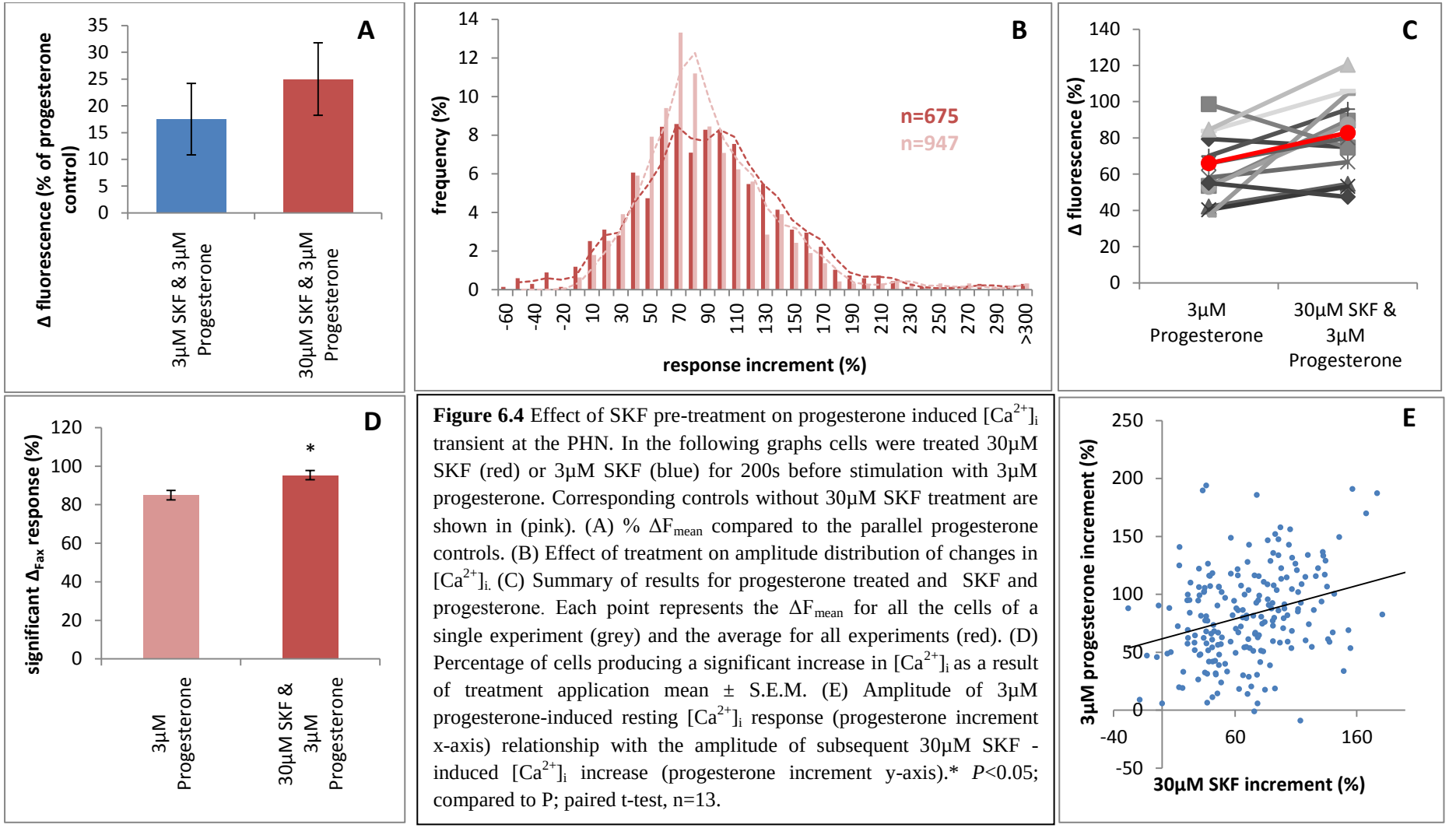

Figure 6.4 Effect of SKF pre-treatment on progesterone induced $[Ca^{2+}]_i$ transient at the PHN. In the following graphs cells were treated 30μM SKF (red) or 3μM SKF (blue) for 200s before stimulation with 3μM progesterone. Corresponding controls without 30μM SKF treatment are shown in (pink). (A) % ΔF_{mean} compared to the parallel progesterone controls. (B) Effect of treatment on amplitude distribution of changes in $[Ca^{2+}]_i$. (C) Summary of results for progesterone treated and SKF and progesterone. Each point represents the ΔF_{mean} for all the cells of a single experiment (grey) and the average for all experiments (red). (D) Percentage of cells producing a significant increase in $[Ca^{2+}]_i$ as a result of treatment application mean ± S.E.M. (E) Amplitude of 3μM progesterone-induced resting $[Ca^{2+}]_i$ response (progesterone increment x-axis) relationship with the amplitude of subsequent 30μM SKF - induced $[Ca^{2+}]_i$ increase (progesterone increment y-axis).* $P<0.05$; compared to P; paired t-test, n=13.

6.5.3 SKF diminishes the sustained $[Ca^{2+}]_i$ response induced by progesterone at the PHN

It has been suggested that in mammalian sperm cells the sustained component of the biphasic $[Ca^{2+}]_i$ response to progesterone involves SOCE (Harper & Publicover, 2005). As an inhibitor of SOCC, SKF should therefore induce a negative effect on the sustained $[Ca^{2+}]_i$ progesterone to implicate SOCE at the PHN. To assess the effect of SKF treatment on the sustained $[Ca^{2+}]_i$ plateau we used the value of ΔF_{mean} recorded 3min after progesterone application (average of 3 consecutive points) comparing these with parallel progesterone controls. SKF pre-treatment reduced the amplitude of the sustained progesterone induced $[Ca^{2+}]_i$ response in a dose dependent manner (Figure 6.5A). 3μM SKF reduced the sustained $[Ca^{2+}]_i$ response by ~17% on average. Pre-treatment with 30μM SKF was more effective, reducing the amplitude of the sustained component in 11 out of 12 samples (Figure 6.5B), with a mean reduction of ~40% (*P*=0.19 & *P*=0.007; paired t-test; n=12 respectively). Frequency distribution of sustained $[Ca^{2+}]_i$ response increments shows a bell shaped curve for both pre-treated and control populations, with a shift to the left observed in pre-treated cells (Figure 6.5C). In addition pre-treatment with 30μM SKF induced a significant reduction in the proportion of cells in which a sustained $[Ca^{2+}]_i$ response occured (*P*=0.011; paired t-test; n=12; Figure 6.5D).

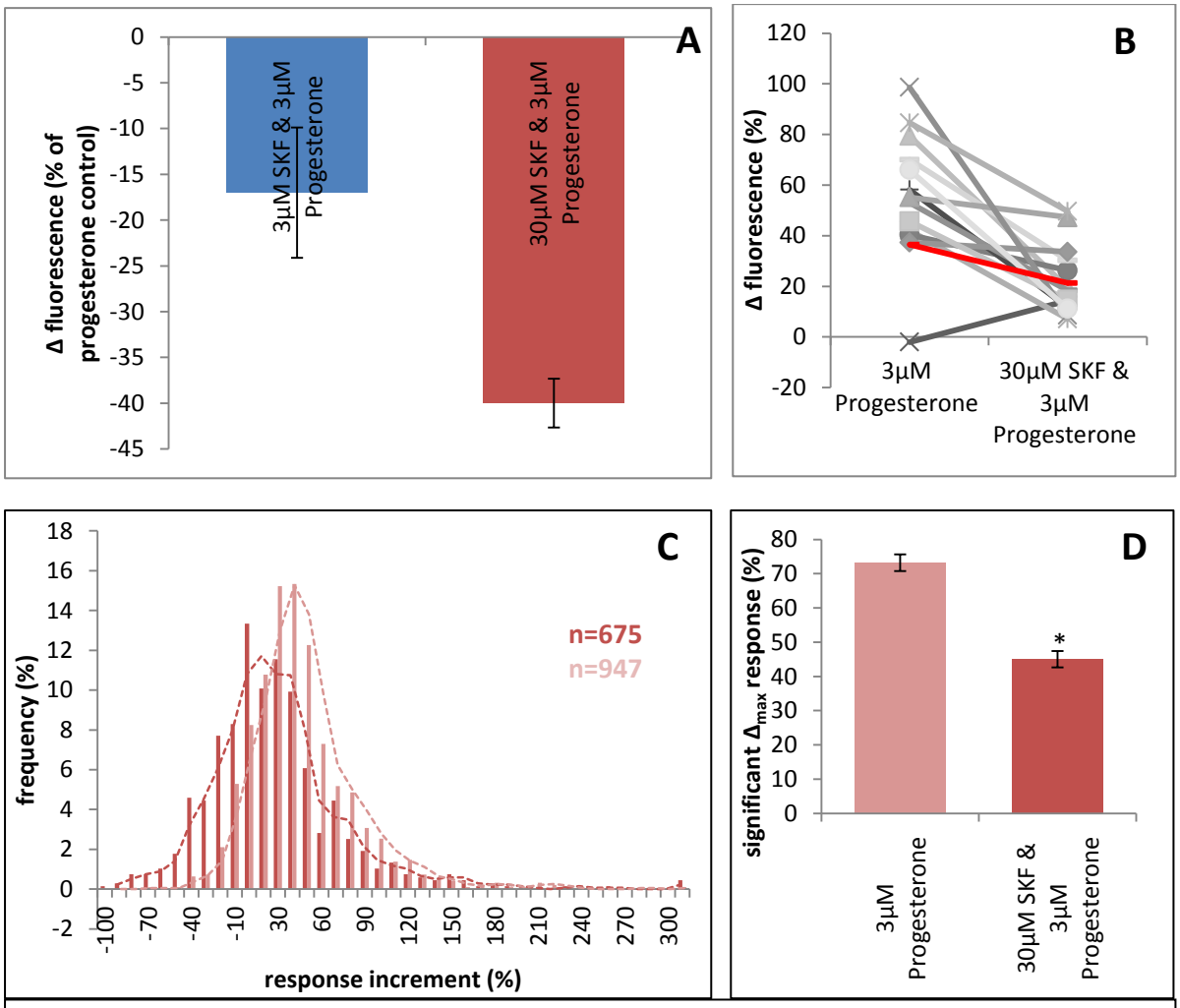

Figure 6.5 Effect of SKF pre-treatment on sustained progesterone $[Ca^{2+}]_i$ response. In the following graphs cells were treated 30μM SKF (red) or 3μM SKF (blue) for 200s before treatment with 3μM progesterone. (A) % increase in ΔF_{mean} compared to parallel controls 3 min after progesterone stimulation. (B) Summary of results for 12 pairs of control (left hand side) and 30μM SKF pre-treated experiments (right hand side). Each point represents the ΔF_{mean} for all the cells of a single experiment. (C) Effect of 30μM SKF pre-treatment on amplitude distribution of 3μM progesterone induced sustained increases in $[Ca^{2+}]_i$ (pink bars show control and red bars show the pre-treated cells, n=total number of cells analysed). (D) Percentage of cells producing a significant increase in $[Ca^{2+}]_i$ as a result of 3μM progesterone application mean ± S.E.M, * P<0.05 compared to control, n=12.

6.5.3.1 Progesterone increases the SKF induced $[Ca^{2+}]_i$ rise at the PHN

To further determine the effect of SKF on the sustained $[Ca^{2+}]_i$ response induced by 3μM progesterone we administered SKF after progesterone treatment. SKF was applied 4-5 after 3μM progesterone treatment, upon cessation of the initial $[Ca^{2+}]_i$ transient. In a manner congruous with the previous experiments, progesterone pre-treated samples were coupled with untreated controls. In 10 out of 12 experimental pairs, application of 30μM SKF to progesterone pre-treated samples induced an increase in ΔF_{mean} at the PHN within 3 min of application (Figure 6.6A). Upon SKF stimulation pre-treated samples showed a transient increase in $[Ca^{2+}]_i$ followed by a plateau or series of oscillations in ~85% cells that exceeded the Δ fluorescence levels observed before SKF application (Figure 6.6A&B), but this was insignificant (52.7±5.4%, 42.6±8.6% respectively; *P*=0.37; paired t-test; n=12; Figure 6.6C). Conversely, progesterone pre-treatment caused a significant increase of 55% in the proportion of the cell population generating a significant $[Ca^{2+}]_i$ response to 30μM SKF (*P*=0.008; paired t-test; n=12; Figure 6.6F&E). Taken together this data indicates that progesterone pre-treatment triggers some of the Ca^{2+} response mechanisms essential to produce the SKF $[Ca^{2+}]_i$ response.

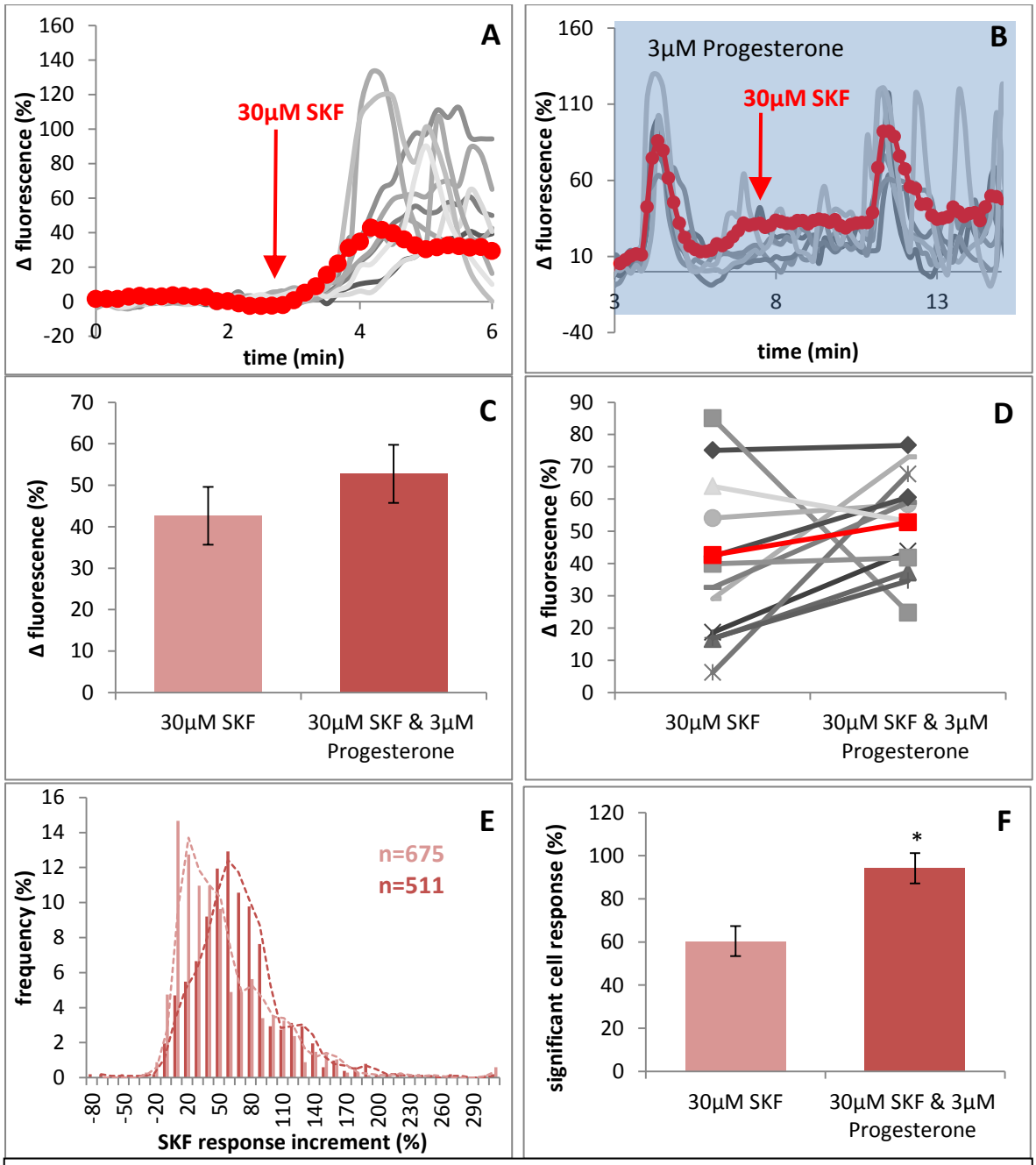

Figure 6.6 Effect of progesterone pre-treatment on SKF induced $[Ca^{2+}]_i$ response. Elevation of $[Ca^{2+}]_i$ at the PHN in response to application of 30µM SKF (red arrow) without pre-treatment (A) and after 300s exposure to 3µM progesterone (B), individual cell responses (grey traces) and average cell response for that experiment (red trace). (C) ΔF_{mean} of the SKF induced increase in $[Ca^{2+}]_i$. Each bar shows the mean amplitude ± S.E.M. for 12 sets of experiments (30-150 cells each). (D) Summary of results for 12 pairs of control (left hand side) and 3µM progesterone pre-treated experiments (right hand side). Each point represents the ΔF_{mean} for all the cells of a single experiment. (E) Effect of 3µM progesterone pre-treatment on amplitude distribution of 30µM induced SKF increases in $[Ca^{2+}]_i$. Pink bars shown control and red bars show the pre-treated cells, n= number of cells analysed. (F) Percentage of cells producing a significant increase in $[Ca^{2+}]_i$ as a result of 30µM SKF application mean ± S.E.M, * $P<0.05$ compared to control.

6.5.4 SKF significantly reduces hyperactivation in human sperm

Analysis of the motility parameters by CASA shows that 30μM SKF significantly reduces the proportion of cells displaying hyperactivated motility compared to the untreated control (*P*=0.03; paired t-test; n=9 (day averages)). In addition the proportion of hyperactivated cells was lower in preparations exposed to 3μM progesterone and 30μM SKF (dual) compared to progesterone alone (*P*=0.01; paired t-test; n=9 (day averages)). CASA also determined a number of significant decreases in both 30μM treatment and dual treatment parameters compared to the untreated control including path velocity, progressive velocity and track speed (Table 6.1). It should be noted that both linearity and straightness were significantly decreased by SKF treatment and linearity was also reduced in dual treated samples compared to progesterone alone. These changes are normally associated with hyperactivated motility and thus suggest SKF increases the complexity of cell paths that are not sufficient to be classified as hyperactivated by CASA parameters. These findings are consistent with Krasznai *et al.*, 2006 suggesting a role for SKF inhibited SOCC's in human sperm motility.

PARAMETER	CONTROL	S.E.M	30µM SKF	S.E.M	Progesterone	S.E.M	30µM SKF & Progesterone	S.E.M	UNITS
Hyperactivation	4.60	0.81	2.7*	2.15	5.90	1.85	3.7*	1.62	%
Path velocity VAP	65.34	3.66	57.22****	3.15	55.26**	4.71	48.1*	3.13	µm/s
Prog. velocity VSL	56.20	3.94	47.40**	3.43	43.19*	4.85	35.32*	3.25	µm/s
Track Speed VCL	107.21	5.18	99.46***	5.33	96.48*	8.02	85.62**	5.87	µm/s
Lateral Amplitude ALH	4.98	0.24	5.01	0.20	5.04	0.24	4.73	0.29	µm
Beat Frequency BCF	25.47	1.00	23.20*	0.87	22.94****	1.67	23.77**	1.63	Hz
Straightness STR	82.55	1.72	77.55**	1.72	75*	2.53	73.70	4.04	%
Linearity LIN	51.72	1.82	46.48****	1.66	44.5*	2.30	42.5*	2.71	%
Elongation	66.43	0.52	66.72	0.87	67.83	1.27	68.2*	0.70	%

Table 6.1 SKF reduces hyperactivation parameters as determined by CASA. Experiments were carried out in pairs, where cells from the same semen sample were analysed by CASA with and without treatment. Cells without treatment were prepared in sEBSS; control no treatment (purple). Treated cells were exposed to either30µM SKF (SKF, turquoise), 3µM progesterone (P, red), 30µM SKF & 3µM progesterone (SKF&P, pale blue). For each condition hyperactivation, path velocity (VCL), progressive velocity (VSL), track speed (VCL), lateral head amplitude (ALH), beat frequency (NCF), straightness (STR), linearity (LIN) and elongation were determined. * P<0.05, ** P<0.02, *** P<0.01, ****P<0.001; compared to CNT; paired t-test; n=3-7. * P<0.05; compared to P; paired t-test; n=10-12.

6.6 Discussion

Ca^{2+} plays an integral role in the regulation of a variety of physiological processes in a plethora of cell types (Berridge, 1997). As a result cells have developed numerous mechanisms for regulating intracellular Ca^{2+} signalling and homeostasis. Despite this evidence of analogous Ca^{2+} mobilisation pathways exist across all cell types and species (Berridge, 2001). Transient increases in cytosolic $[Ca^{2+}]_i$ are just one essential component of intracellular Ca^{2+} regulation. Identified in a diverse range of cell systems, transient rises in $[Ca^{2+}]_i$ result from either Ca^{2+} entry from the extracellular medium and/or Ca^{2+} release from intracellular Ca^{2+} stores (specific to cell type; Jan *et al.,* 1999). In somatic cells store-mediated transient $[Ca^{2+}]_i$ increases often result from activation of PLC leading to production of IP_3 and subsequent activation of intracellular Ca^{2+} stores resulting in an increase in $[Ca^{2+}]_i$ (Berridge, 1993). This store release is often followed by a secondary Ca^{2+} influx through the activation of PM SOCE. This will maintain and elevate $[Ca^{2+}]_i$ and replenish the intracellular Ca^{2+} stores leading to a fall in $[Ca^{2+}]_i$ when the stimulus is withdrawn. In Chapter 5 we demonstrated the potential contribution of SOCE to the biphasic Ca^{2+} response in human sperm through treatment with the bimodal SOCE activator 2-APB. In addition we provided evidence for the presence of two components of SOCE machinery; Ca^{2+} store receptors STIM and PM receptors Orai in human sperm. Here we aimed to investigate the effect of SKF-96365 on Ca^{2+} signalling in human sperm cells and its effect on the biphasic progesterone response, in particular the SOCE contribution to the sustained $[Ca^{2+}]_i$ component.

Initially identified as a selective blocker of RMCE in non-excitable cells (e.g. platelets, neutrophils and Hek cells) SKF-96365 is one of the most widely used inhibitors of CCE (SOCE; Merritt *et al.,* 1990; Jan *et al.,* 1999). In addition to effects on SOCE, SKF has also

been shown to exhibit effects on various other important components or regulators of the Ca^{2+}-signalling machinery including high voltage activated (HVA) Ca^{2+} channels (L-type; Merritt *et al.,* 1990), K^{+} channels (Liu *et al.,* 2007) and sarcoplasmic reticulum Ca^{2+}-ATPase (Mason *et al.,* 1993). However it is the transient receptor potential canonical type channels (TRPC) that are believed to be the principal target of SKF (Singh *et al.,* 2010; Zhu *et al.,* 1998). Indeed micromolar concentrations of SKF (2-100μM) have been shown to inhibit TRPC facilitated Ca^{2+} influx in a number of biological systems (Zhu *et al.,* 1998). In somatic cells TRPC channels have been shown to play a significant role in RMCE, with some contribution to SOCE regulation (Moran *et al.,* 2004 demonstrated TRPC contribution to SOCE in neuronal cells). Therefore it seemed likely that upon the identification of TRPC channels in mature human sperm cells a PM receptor for SOCE had been identified (Trevino *et al.,* 2001; Castellano *et al.,* 2003). Indeed localisation of the TRPC receptors to the sperm flagellum suggested a convincing hypothesis for SOCE involvement in motility.

The discovery of STIM and Orai molecules in 2005 and 2006 respectively (Liou *et al.,* 2005; Feske *et al.,* 2006; Vig *et al.,* 2006; Zhang *et al.,* 2006) as modulators of SOCE, and their subsequent identification in human sperm (Lefievre *et al.,* 2012) has placed less significance on TRPC channels. However it should be noted that upon Ca^{2+} store depletion or agonist stimulation TRPC's have been shown to interact with STIM receptors on the Ca^{2+} store membrane and facilitate SOCE (Liao *et al.,* 2008; Salido *et al.,* 2011). In addition there is mounting evidence suggesting a close relationship between TRPC's and LVA T-type channels (Singh *et al.,* 2010), which maybe expressed in sperm (Arnoult *et al.,* 1996; 1998). This information coupled with experimental evidence that SKF inhibition of LVA T-type channels has a greater potency than that observed with TRPC's when expressed in

heterologous systems, necessitates caution when analysing inhibitory effects of an antagonist (Singh *et al.,* 2010). It should be noted that although the inhibitory effects of SKF on SOCC are well established and several studies have also identified increases in $[Ca^{2+}]_i$ as result of SKF application a mechanism of action remains to be elucidated (Merritt *et al.,* 1990; Jenner & Sage 2000; Jan *et al.,* 1999).

In the present chapter we demonstrate that SKF concentrations 3μM and 30μM both in the inhibitory range (2-100μM) induce a transient increase in $[Ca^{2+}]_i$ at the PHN of human sperm with and without extracellular Ca^{2+} (Figure 6.1, 6.2A&G). However the increase in $[Ca^{2+}]_i$ observed is significantly less than that induced by 3μM progesterone. Although the role of SKF as a CCE inhibitor is well documented there is also increasing evidence for multiple effects on SOCE and on other aspects of Ca^{2+} signalling (see previous). In 1996 Iouzalen *et al.,* discovered that SKF inhibited intracellular Ca^{2+} pumps resulting in increased $[Ca^{2+}]_i$, whilst Thastrup *et al.,* 1990 demonstrated that SKF released Ca^{2+} from thapsigargin sensitive intracellular Ca^{2+} stores in thymic lymphocytes. Leung *et al.,* 1996 even observed an SKF dependent release of intracellular Ca^{2+} with subsequent SOCE upon addition of Ca^{2+} to the extracellular medium in human leukemic cells. Taken together these results are indicative of multiple modes of action of SKF-96365, which can include increasing $[Ca^{2+}]_i$ through activation of SOCE. However it should be noted that SKF has also been found to affect multiple Ca^{2+} channels in somatic cells.

We also investigated the effect of SKF treatment on the biphasic progesterone induced increase in $[Ca^{2+}]_i$. We analysed the effect of 3μM and 30μM SKF exposure on both the progesterone $[Ca^{2+}]_i$ transient and sustained responses. It should be noted that at both

concentrations SKF exhibited similar responses. However 30μM SKF exhibited more potency. When cells were exposed to SKF (30μM) the transient increase in $[Ca^{2+}]_i$ induced by progesterone was enhanced significantly ~25% compared to parallel controls. In contrast SKF exposure significantly reduced the sustained $[Ca^{2+}]_i$ component by ~40%, suggesting dual modes of action of SKF on this response. From our observations with 2-APB (chapter 5 it is likely that the inhibition of the sustained progesterone $[Ca^{2+}]_i$ is the result of SOCE inhibition at the PM; however the transient $[Ca^{2+}]_i$ elevation is likely due to SKF effects on other Ca^{2+} channels. Similar effects have also been observed with SKF pre-treatment in neutrophils and endothelium; typically histidine induces a biphasic increase in $[Ca^{2+}]_i$ similar to that observed in sperm by progesterone (Merritt *et al.,* 1999; Jenner & Sage, 2000). Cells treated with SKF prior to histidine stimulation had elevated transient phases and reduced sustained $[Ca^{2+}]_i$ responses (Merritt *et al.,* 1999; Jenner & Sage, 2000). Together these data indicate a specific method of action for SKF in agonist induced biphasic $[Ca^{2+}]_i$ responses, which may not be specific to sperm or progesterone.

Collectively we have found that SKF elevates $[Ca^{2+}]_i$ at the PHN in a dose dependent manner which is independent of extracellular Ca^{2+}. Pre-treatment of cells with 3μM and 30μM SKF enhances the transient Ca^{2+} response induced by 3μM progesterone application whilst the sustained response is inhibited. However only the changes in $[Ca^{2+}]_i$ induced by 30μM SKF significantly differ from the parallel progesterone controls. Taken together these findings suggest SKF acts to enhance activity of a Ca^{2+} channel at the PHN and/or release of stored Ca^{2+} during the transient component of the progesterone response through an SKF sensitive channel, but inhibits the subsequent sustained $[Ca^{2+}]_i$ increase via inhibition of SOCE.

CHAPTER SEVEN: STORE-OPERATED Ca^{2+} ENTRY MANIPULATION USING NOVEL ORAI TARGETED BIOPORTIDES

7.1 Abstract

Store Operated Ca^{2+} Entry (SOCE) facilitates replenishment of intracellular Ca^{2+} stores from extracellular Ca^{2+} influx. This process requires communication between Ca^{2+} stores and plasma membrane CRAC channels. In somatic cells stromal interaction molecules (STIM) have been identified as the Ca^{2+} sensor present in the ER (Liou *et al.*, 2005), which interact with the PM CRAC channel Orai (Feske *et al.*, 2006; Vig *et al.*, 2006; Zhang *et al.*, 2006). Recently we reported the presence of SOCE receptors STIM and Orai in human sperm (Lefievre *et al.*, 2012). Mammalian STIM and Orai isoforms displayed regional localisation but all were expressed at the PHN and midpiece of mature sperm; where evidence from previous chapters suggests a second Ca^{2+} store is located (Figure 7.2). Due to the absence of PM machinery required for endocytotic uptake, to date SOCE manipulation in human sperm has been limited to cell permeable biochemical modulators. Recent identification of cell penetrating peptides (CPPs) has provided a novel new approach. In bovine sperm these peptides have been shown to deliver bioactive agents (bioportides) into intracellular compartments through translocation of the cell membrane. Here we report the effects of recently developed KIKKK CPPs on basal $[Ca^{2+}]_i$ and the biphasic progesterone induced $[Ca^{2+}]_i$. Single cell Ca^{2+} imaging revealed differential effects of CPPs on basal $[Ca^{2+}]_i$, however KIKKK containing CPPs increased the number of cells in which a monophasic, maintained $[Ca^{2+}]_i$ increase occurred and significantly decreased the number of cells that produced a biphasic $[Ca^{2+}]_i$ profile in response to 3μM progesterone stimulation. Inability of a scrambled CPP control to replicate this inhibition indicates the observed response is the result of CPP effects on STIM/Orai interaction and not a result of CPP PM translocation, implicating SOCE in $[Ca^{2+}]_i$ elevations associated with progesterone.

7.2 Introduction

Traditionally patch-clamp studies have been used to detect the biophysically specific I_{CRAC} current associated with SOCE in somatic cells (chapter 1.6.3; Feske *et al.,* 2006; Prakriya *et al.,* 2006; Yeromin *et al.,* 2006). At present this method has detected only a handful of channels in human sperm, including a single Ca^{2+} permeable channel, CatSper (Ren *et al.,* 2001; Strunker *et al.,* 2011). As discussed previously CatSper is a pHi-regulated channel expressed solely in the sperm flagellum. Sensitive to pHi, membrane potential and a range of small organic molecules, CatSper acts as a polymodal chemosensor (Brenker *et al.,* 2012). Recent studies have identified a role for CatSper in the progesterone induced Ca^{2+} response in human sperm (Lishko *et al.,* 2011; Strunker *et al.,* 2011). However blockage of CatSper mediated Ca^{2+} entry with NNC-55-0396 is insufficient to inhibit all components of progesterone induced biphasic Ca^{2+} response, suggesting alternative methods of Ca^{2+} mobilisation are present in human sperm.

In mammalian systems sperm are deposited in the female tract which they must first navigate to locate and fertilise the oocyte. External cues from both the tract and cumulus-oocyte complex are essential in regulating a variety of sperm activities in particular hyperactivated motility through Ca^{2+} signalling (Publicover *et al.,* 2007). We have recently shown that CatSper activation through pHi and progesterone, which induce sustained elevations in $[Ca^{2+}]_i$ did not induce significant hyperactivation, the asymmetrical flagella beat required for both progression down the oviduct and penetration of the ZP (Alasmari *et al.,* 2013). Treatment of cells with 5μM thimerosal (a known mobiliser of stored Ca^{2+}) induced both sustained elevations in $[Ca^{2+}]_i$ and hyperactivation which was insensitive to treatment with CatSper current blocker NNC-55-0336 (Alasmari *et al.,* 2013; chapter 4).

Blackmore (1993) originally identified a role for CCE (SOCE) in human sperm, while investigating the effects of thapsigargin (SERCA inhibitor) he observed a sustained $[Ca^{2+}]_i$ increase due to Ca^{2+} entry from the extracellular environment; abolished when performed in EGTA-buffered media (Blackmore, 1993). Studies by other groups have also identified Ca^{2+} release from intracellular stores under 'Ca^{2+}-free' conditions when treated with thapsigargin or the SPCA inhibitor bisphenol (Harper *et al.,* 2005; Rossato *et al.,* 2001; Williams & Ford, 2003). These results corroborate the hypothesis that intracellular Ca^{2+} stores occur in human sperm though they are small and apparently depleted in Ca^{2+} buffered media. However this Ca^{2+} mobilisation is apparently sufficient to induce SOCE and possibly contribute to the action of progesterone. SOCE has currently been detected most notably in mouse (O'Toole *et al.,* 2000), sheep (Dragileva *et al.,* 1999), and sea urchin sperm (Gonzalez-Martinez *et al.,* 2004; Ardón *et al.,* 2009).

SOCE requires both a membrane Ca^{2+} permeable channel and a mechanism to monitor stored $[Ca^{2+}]_i$. In somatic cells TRPCs were initially thought to facilitate SOCE but identification of STIM and Orai in 2005 and 2006 respectively gave a new mechanism of action (Liou *et al.,* 2005; Feske *et al.,* 2006). STIM proteins act as stored Ca^{2+} sensor on the ER and Orai proteins form a Ca^{2+} sensitive CRAC channel in the PM discussed previously (chapter 1.6.3). Since discovery there has been rapid progress in mapping domains and functional interaction between STIM and Orai. Under basal conditions STIM proteins reside in the ER membrane, upon Ca^{2+} store depletion Ca^{2+} molecules dissociate from the EF-hand of STIM1 causing a conformational rearrangement in EF-hand-SAM triggering oligomerization (Figure 7.1; Muik *et al.,* 2012). The subsequent translocation of STIM1 dimers adjacent to the PM brings them

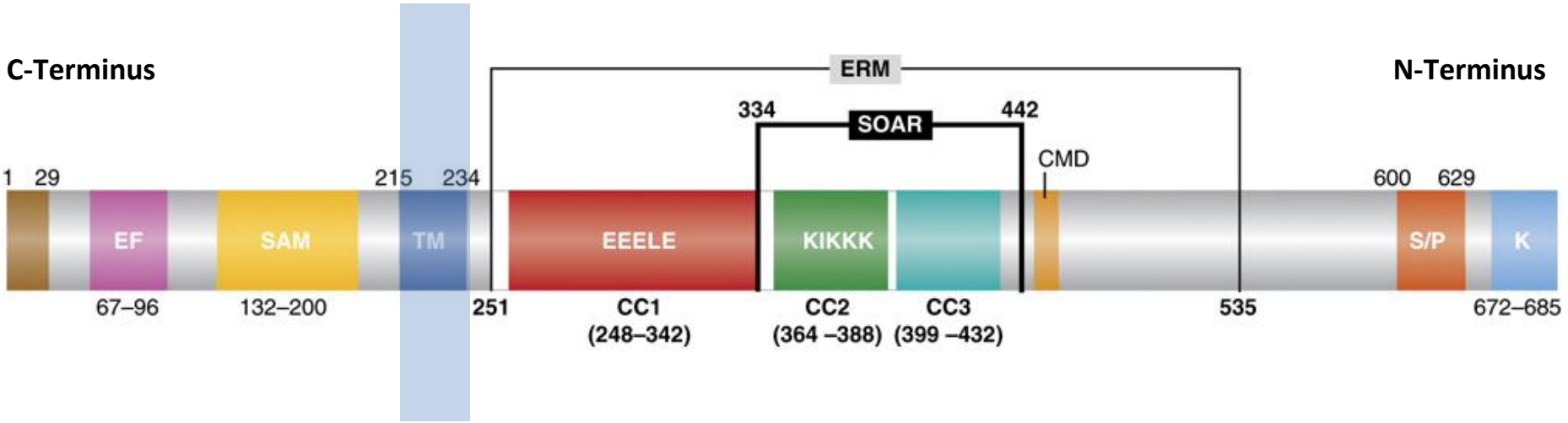

Figure 7.1 Diagrammatic representation of STIM1 domains and potential mechanism for SOAR activation of Orai, adapted from Kim & Muallem, 2011. STIM molecules are ~685 amino acids in length comprising of; K, lysine-rich domain; S/P, proline and serine rich segment; ERM, Ezrin/radixin/moesin; CMD, CRAC modulatory domain; SOAR, STIM1-Orai1 activating region; cc, coiled-coil (1,2&3); CC2, contains the conserved polybasic sequence KIKKK; TM, transmembrane portion; SAM, sterile α motif and EF hand involved in Ca^{2+} binding.

into close proximity with Orai tetramers (Penna *et al.,* 2008). There is a continuing debate on the resting conformation of Orai, but biochemical analysis show a tetrameric structure in its activated state (Ji *et al.,* 2008; Penna *et al.,* 2008). Studies have shown that STIM1 is obligatory for Orai function, in particular the SOAR domain (amino acids 344-442) encompassing CC2 and CC3 appears to be the minimum sequence required to induce fully activated Orai (Yuan *et al.,* 2009). SOAR regions of both STIM1 dimer molecules bind to either Orai's cytoplasmic N or C terminus to induce CRAC channel activation (Figure 7.1). Within the SOAR region there is a highly conserved polybasic region (amino acids 382-387; KIKKKR) which may electrostatically interact with the amphipathically coiled acidic Orai domains (Calloway *et al.,* 2010; Soboloff *et al.,* 2012).

Recently we have detected the SOCE proteins STIM and Orai in human sperm and shown variability in isoform distribution at the acrosome, PHN and midpiece (Lefievre *et al.,* 2012). Studies of the intracellular Ca^{2+} signalling cascade involved in sperm SOCE have been restricted due to the static nature of the membrane. Unlike somatic cells the PM of sperm is unable to actively recycle lipids thus endocytosis of modulatory peptides is inhibited (Gadella & Evans, 2011). To date studies have been limited to either demembranated models or observing the effects of cell permeable biochemical modulators on $[Ca^{2+}]_i$. Demembranated models facilitate direct accessibility to intracellular targets, removal of the PM by detergents such as triton X-100 can be detrimental to protein function (Jones *et al.,* 2013). Our own Ca^{2+} imaging experiments revealed low doses of 2-APB (<10μM) potentiate CCE through STIM: SOC interaction, while simultaneously inhibiting CatSper current (Lefievre *et al.,* 2012). Recent development of cell penetrating peptides (CPPs) has provided an alternative investigative tool to directly interact with STIM channels themselves.

CPPs are small water-soluble peptide sequences typically 30-35 amino acid residues in length with the ability to penetrate cells without damaging the PM (Madani *et al.,* 2011). Furthermore in somatic cells CPPs enable transport of large protein cargos across the PM as non-covalent complexes (Lukanowska *et al.,* 2013). In human sperm chemically heterogeneous CPPs have been shown to penetrate the PM and accumulate within distinct intracellular compartments without having any detrimental effects on motility (Jones *et al.,* 2013). However when compared to somatic cells the uptake of protein cargos associated with CPPs is less successful in human sperm (Jones *et al.,* 2013), which is likely the result of differences in PM composition. Unlike somatic cells the PM of mammalian sperm contains a significant concentration of polyunsaturated fatty acids and plasmalogen, which contributes to the cells inability to endocytose CPPs (Lenzi *et al.,* 1996). Jones *et al.,* (2013) concluded that without clathrin-mediated endocytosis the primary mechanism of CPP uptake across the PM in mammalian sperm is direct translocation of cationic CPPs. Translocation is a rapid process dependent on the CPP sequence used, with certain sequences targeted towards specific intracellular organelles. Here we describe the effects on $[Ca^{2+}]_i$ and the biphasic progesterone response of CPP's targeted to the Orai binding region of the STIM1 protein in human sperm including **KQLLVAKEGAEKIKKKRNTLFG,** which encompasses the polybasic CC2 domain of SOAR (amino acids 370-392).

7.3 Chapter aims

The aims of this chapter were to observe the effects of KIKKK domain containing CPPs on basal $[Ca^{2+}]_i$ in capacitated human sperm. Following this we wanted to determine if pre-treatment and continued exposure to KIKKK domain containing CPPs modified the characteristic biphasic $[Ca^{2+}]_i$ progesterone response.

7.4 Materials and Methods

7.4.1 Materials

The basic STIM peptide KIKKK(STIM1$^{371-392}$), an α-aminoisobutyric acid (Aib) containing analogue (*D*Arg, Aib^{10} STIM1$^{371-392}$) and a scrambled control peptide were developed by Pantechnia (University of Wolverhampton). The basic KIKKK(STIM1$^{371-392}$) peptide is composed of the amino acid sequence **KQLLVAKEGAEKIKKKRNTLF** but in the analogue the alanine at position 10 was substituted with an an α-aminoisobutyric acid (Aib) to enhance helicity (***D*-ArgKQLLVAKEGAibEKIKKKRNTLF**). The scrambled control peptide contained the amino acids of the original peptide in a scrambled sequence **LKNKFKGVKLAEIEKQALKGTR**. For all other materials see chapter 2.1.

7.4.2 Methods

7.4.2.1 Cell preparation

Human semen was collected and prepared as in chapter 2.3, however for this chapter BSA was not added to the sEBSS as it was found to inhibit peptide translocation.

7.4.2.2 Cell incubation and capacitation

Sperm harvested by swim up procedure were incubated and capacitated as in chapter 2.4 in the absence of BSA.

7.4.2.3 Single cell Imaging

Cells were left to capacitate for 6 hours at 6 x10^{6}cells/ml in sEBSS containing no BSA, the human sperm cell preparation was then diluted to 3x10^{6}cells/ml with sEBSS containing no BSA prior to single cell imaging. All imaging experiments for this chapter were conducted as

per chapter 2.6.1 calcium imaging with Oregon Green-BAPTA-1AM with the single exception that no BSA was added to the sEBSS.

7.4.3 Analysis

All calcium imaging data was initially normalised as in chapter 2.6.1.2.

7.4.3.1 Statistical analysis of agonist response

Peak amplitude and individual cell response significance were calculated as in chapter 2.6. Time to peak amplitude was calculated using the same formula as peak amplitude, time of agonist addition was subtracted from time at peak amplitude, where a second treatment was applied a second 'control' period was identified as the 4 frames prior to second treatment addition. All categories were deemed statistically significant if $P<0.5$ in a paired t-test.

7.4.3.2 Assessment of the CPP effects on the biphasic Ca^{2+} response

Initial attempts to use excel logical analysis as an objective method to determine the percentage of cells that produce a biphasic $[Ca^{2+}]_i$ response to progesterone application were ineffective due to irregularity in the transient size and duration. As a result we characterised the cells displaying biphasic $[Ca^{2+}]_i$ by eye, using the time fluorescence intensity plots. Cell responses were grouped into two categories; the well characterised biphasic response (Figure 7.2A) or a steady increase in $[Ca^{2+}]_i$ that plateaus at a level above that of the control period (monophasic Ca^{2+} response; Figure 7.2B). Only cells where a defined transient element is not clearly definable were categorised as sustained elevators. In these cells we calculated the peak Ca^{2+} response as we would the typical Ca^{2+} transient as this was achieved within the same time-frame. Sustained response levels were also determined 3min post progesterone application as with other experiments.

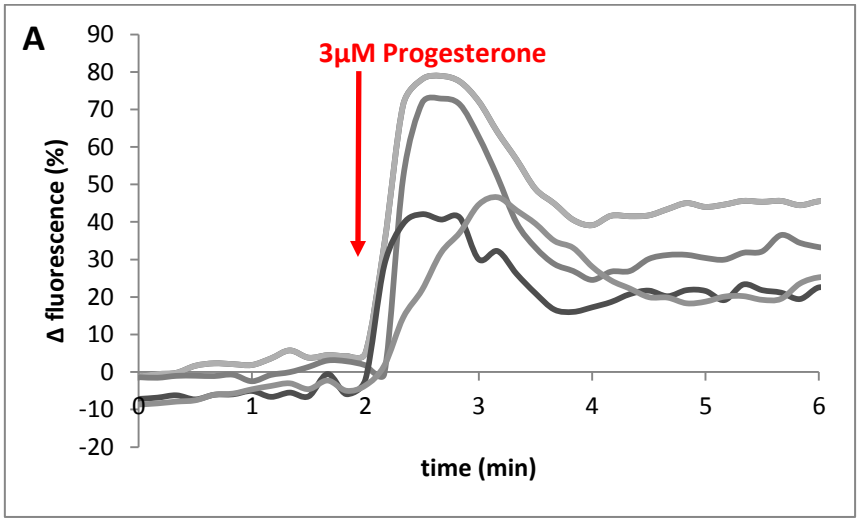

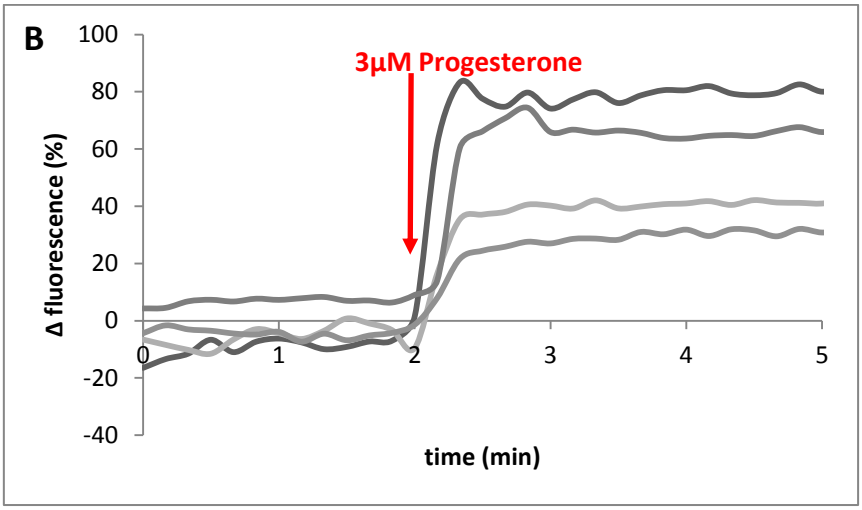

7.2 Characterisation of progesterone induced $[Ca^{2+}]_i$ responses. The $[Ca^{2+}]_i$ responses of all cells treated with 3µM progesterone were characterised as either (A) biphasic or (B) sustained elevations. Each grey trace represents the $[Ca^{2+}]_i$ trace for an individual cell.

7.5 Results

In mammalian sperm evidence indicates absence of endocytotic machinery and inability to form lysosomes to internalise CPPs (Jones *et al.,* 2013; Gadella & Evans, 2011). To date CPP effects and import mechanisms have been reported in bovine sperm; where direct membrane translocation facilitates CPP uptake that enables CCP interaction with intracellular organelles (Jones *et al.,* 2013). In human sperm STIM 1 and STIM 2 have been localised to the acrosomal and anterior midpiece/neck regions (Lefievre *et al.,* 2012). Manipulation of SOCE has been limited to cell permeable Ca^{2+} modulators until the recent development of two STIM1 targeting cell penetrating peptides. *KIKKK(STIM1$^{371-392}$)* and it's more stable analogue (*D*Arg, Aib^{10} STIM1$^{371-392}$) both contain 20 amino acids of the CC2 region of STIM1 implicated in Orai binding and CRAC channel activation. A scrambled control peptide contains the same amino acids in a jumbled sequence to observe whether Ca^{2+} effects seen are CC2 binding specificity or the result of CPP translocation.

7.5.1 $[Ca^{2+}]_i$ responses to Cell Penetrating Peptides (CPP)

Application of 5μM STIM1 CPP *KIKKK(STIM$^{371-392}$)* or 5μM of the scrambled control to resting sperm populations induced a small decrease in $[Ca^{2+}]_i$ which appeared to return to basal control level within approximately 120 seconds (Figure 7.3A&B; 7.4A). This response was visible as a transient decrease in ~ 60% (n=533) and ~70% (n=548) of single cell traces of STIM1 peptide *KIKKK(STIM$^{371-392}$)* and the scrambled control respectively (Figure 7.4A&B). In contrast when cells were treated with 5μM of the STIM1 analogue CPP a small increase in resting $[Ca^{2+}]_i$ was observed within ~70 seconds, which remained elevated above basal levels (Figure 7.3C). Figure 7.3 shows individual cell response traces which clearly

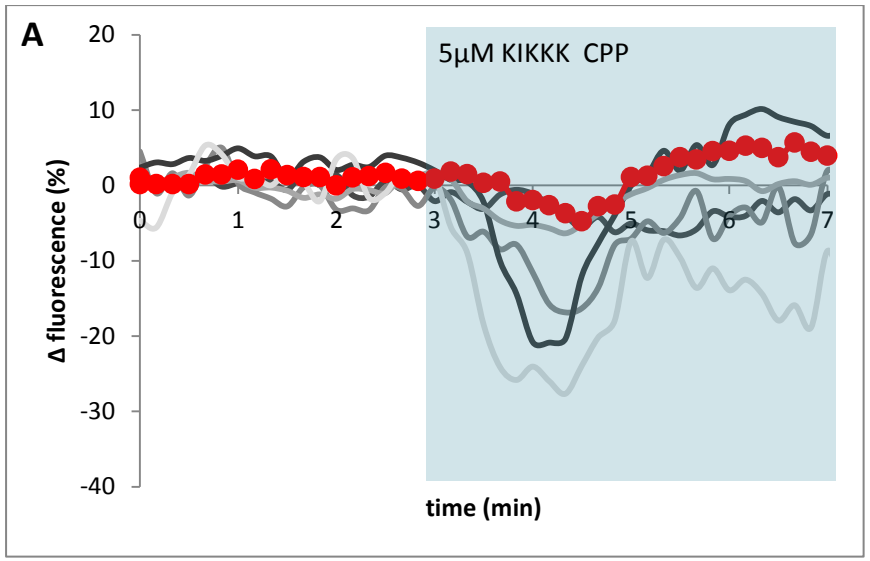

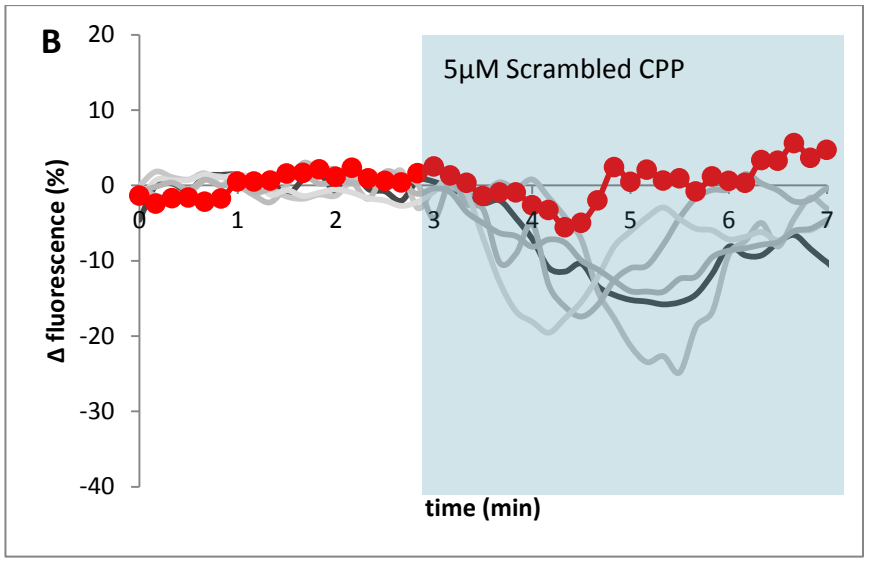

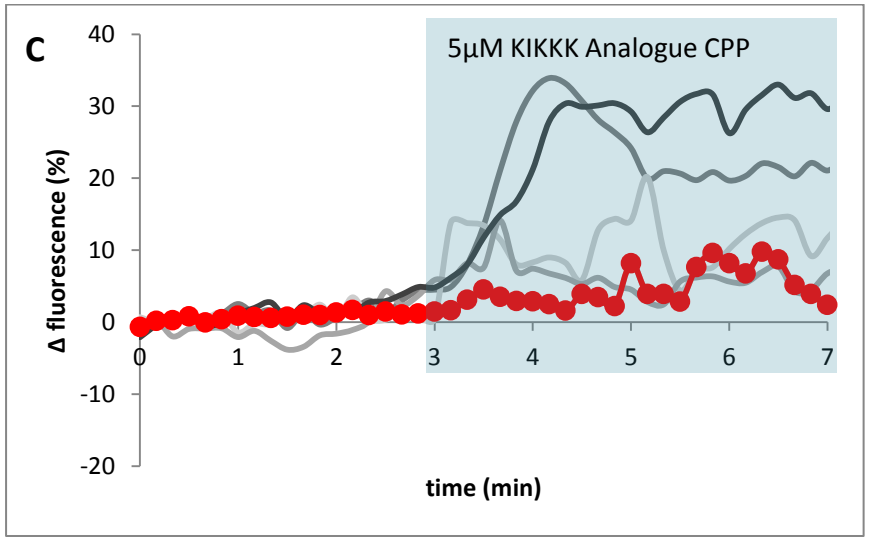

Figure 7.3 $[Ca^{2+}]_i$ responses of individual cells to CPPs. Each graph shows a single experiment R_{tot} (red trace) and individual cell traces (grey traces). Capacitated sperm were first perfused with sEBSS, then (**A**) 5µM KIKKK CPP ($STIM1^{371-392}$) (**B**) 5µM scrambled CPP or (**C**) 5µM KIKKK analogue CPP (*D*Arg, Aib^{10} $STIM1^{371-392}$) were added to the perfusion media at 220 seconds (grey box).

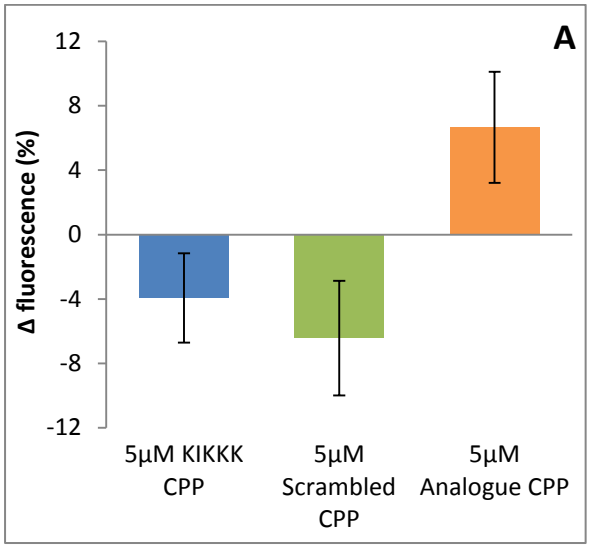

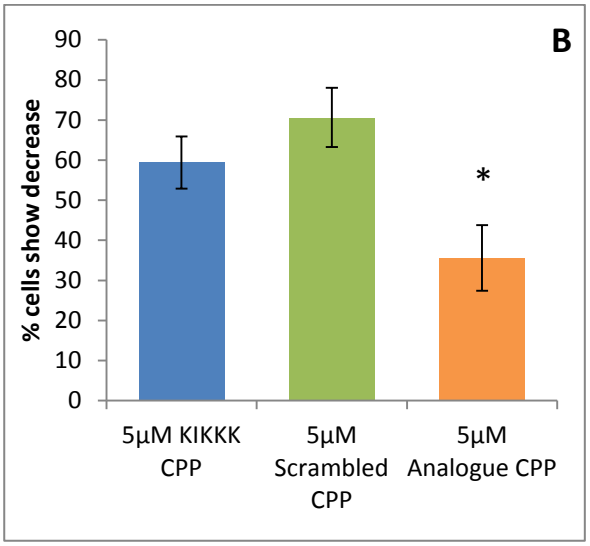

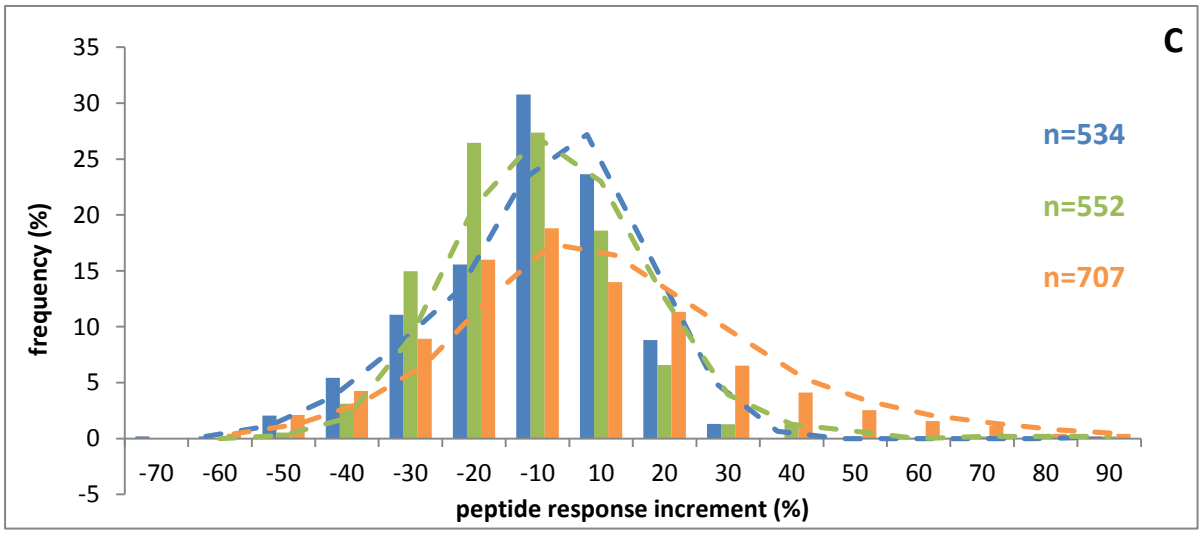

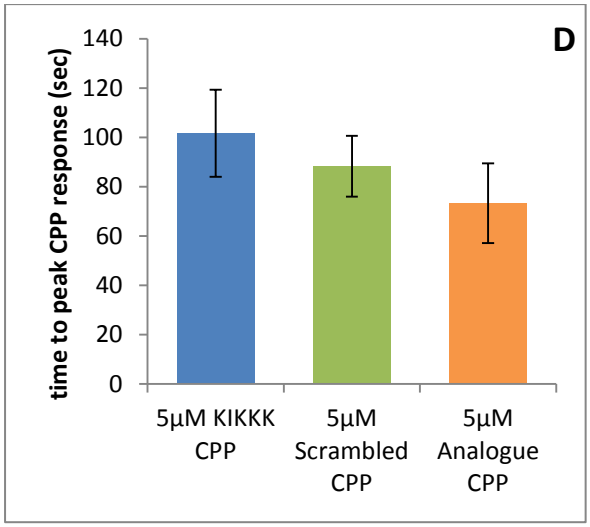

Figure 7.4 Effects of CPPs on resting $[Ca^{2+}]_i$. In the following graphs 5μM KIKKK CPP (blue), 5μM scrambled CPP (green) & 5μM KIKKK analogue CPP (orange) are plotted. (A) Maximum CCP ΔF_{mean} response increment. (B) Proportion of individual cell traces where a decrease below control is observed. (C) Frequency of CCP ΔF_{mean} response increment, (n= number of cells analysed) (D) Time to peak CCP ΔF_{mean} response. * $P<0.05$; paired t-test; compared to scrambled CPP control; n=12 experiments.

identify CPP induced $[Ca^{2+}]_i$ effects. Average traces are representative of the $[Ca^{2+}]_i$ response of the population.

Despite observable CPP effects on $[Ca^{2+}]_i$ at the PHN, treatment with either 5μM STIM1 KIKKK*(STIM$^{371-392}$)*, KIKKK analogue or the scrambled CPP did not induce a significant $[Ca^{2+}]_i$ response when compared with the control period (Figure 7.4A, P>0.5; paired t-test, n=6). The frequency distribution of single cell responses revealed a wider distribution of 5μM STIM1 KIKKK analogue CPP responses (Figure 7.4C), with a greater proportion of the cells displaying an increase in $[Ca^{2+}]_i$ in response to the CPP. Cells treated with the scrambled CPP display the greatest decreases in $[Ca^{2+}]_i$ in response to treatment; ~70% of the cells observed displayed a clearly discernable decrease, which exceeded cells treated with KIKKK CPP and KIKKK analogue CPP (P=0.06 & P=0.004 respectively; paired t-test; unpaired t-test respectively; n=12). In addition the mean time from CPP application to peak $[Ca^{2+}]_i$ response differed between treatments (Figure 7.4D). Cells treated with STIM1 KIKKK analogue reach ΔF_{mean} the quickest followed by cells exposed to the scrambled CPP and finally KIKKK CPP treated populations (Figure 7.4D). This may be due to different membrane translocation times amongst the CPPs, however this difference was statistically insignificant (Figure 7.4D; P>0.5; paired t-test, n=6).

7.5.2 STIM1 targeted CPPs inhibit the biphasic progesterone $[Ca^{2+}]_i$ response

The biphasic $[Ca^{2+}]_i$ response of human sperm to 3μM progesterone is well established. Kirkman Brown *et al.,* 2000 reported that >90% of cells in a population generated an initial transient peak in $[Ca^{2+}]_i$ followed by a second smaller sustained $[Ca^{2+}]_i$ rise. Treatment of

cells with 5μM CPP *KIKKK(STIM$^{371-392}$)* and scrambled control have already shown an initial transient decrease in $[Ca^{2+}]_{i,}$ whilst conversely treatment with 5μM of the KIKKK analogue CPP showed a sustained elevation of $[Ca^{2+}]_i$ at the PHN of human sperm (chapter 7.5.1). When CPP treated cells were then exposed to 3μM progesterone there was a consistent reduction in the percentage of cells displaying a biphasic $[Ca^{2+}]_i$ response (Figure 7.6A&B). Application of 5μM KIKKK CPP or 5μM KIKKK analogue CPP prior to stimulation with 3μM progesterone did not affect the proportion responsive cells; however pre-treatment did significantly increase the proportion of cells producing the monophasic $[Ca^{2+}]_i$ response outlined in Figure 7.2B (*P*=0.05 & *P*=0.04 respectively; paired t-test; n=12; compared to progesterone control; Figure 7.6) by ~10% compared to parallel controls (Figure 7.6C) although this was not observable in the average ΔF_{mean} trace (Figure 7.5). Individual cell responses were categorised as either biphasic if an initial transient $[Ca^{2+}]_i$ increase followed by a slower sustained elevation was present (Figure 7.2A), or sustained elevators with no distinguishable transient and a sustained elevated plateau was observed (Figure 7.2B). In these cells $[Ca^{2+}]_i$ responses were ~20-30 seconds slower (Figure 7.5B&C). Conversely application of the scrambled STIM1 CPP control had no effect on the proportion of cells displaying a biphasic $[Ca^{2+}]_i$ progesterone response (*P*=0.99; paired t-test; n=12; compared to progesterone; Figure 7.6C). This suggests that the differences in progesterone response profile are the result of KIKKK containing CPP interactions with STIM1 receptors and not the result of CPP translocation and cytoplasmic presence.

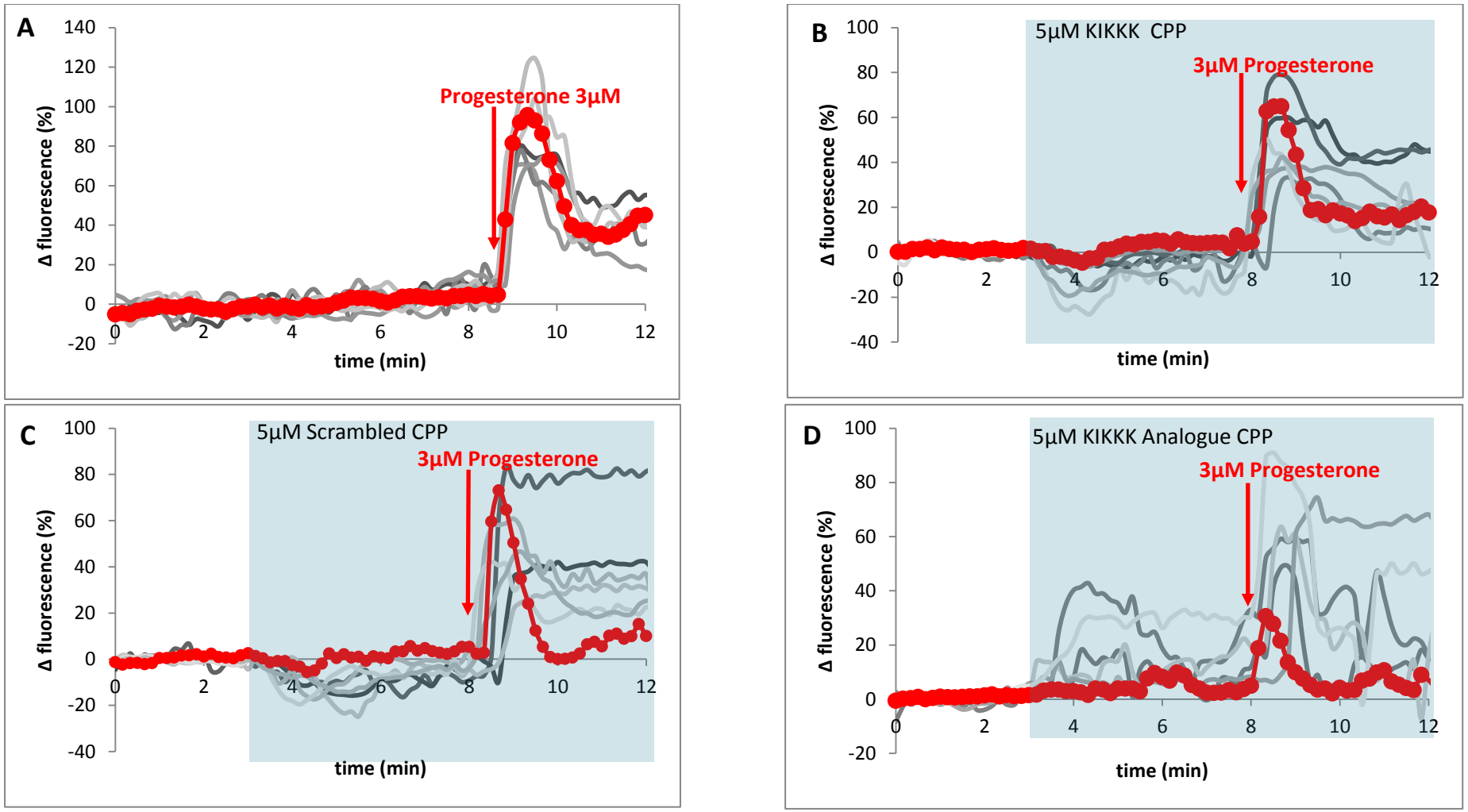

Figure 7.5 Effects of CPPs on $[Ca^{2+}]_i$ to Progesterone. Each graph shows a single experiment R_{tot} (red trace) and individual cell traces (grey traces). Capacitated sperm were first perfused with sEBSS (A) then (**B**) 5µM KIKKK CPP (STIM1$^{371-392}$) (**C**) 5µM scrambled CPP or (**D**) 5µM KIKKK analogue CPP (*D*Arg, Aib^{10} STIM1$^{371-392}$) were added to the perfusion media at 220 seconds (grey box) before 3µM progesterone is added (red arrow).

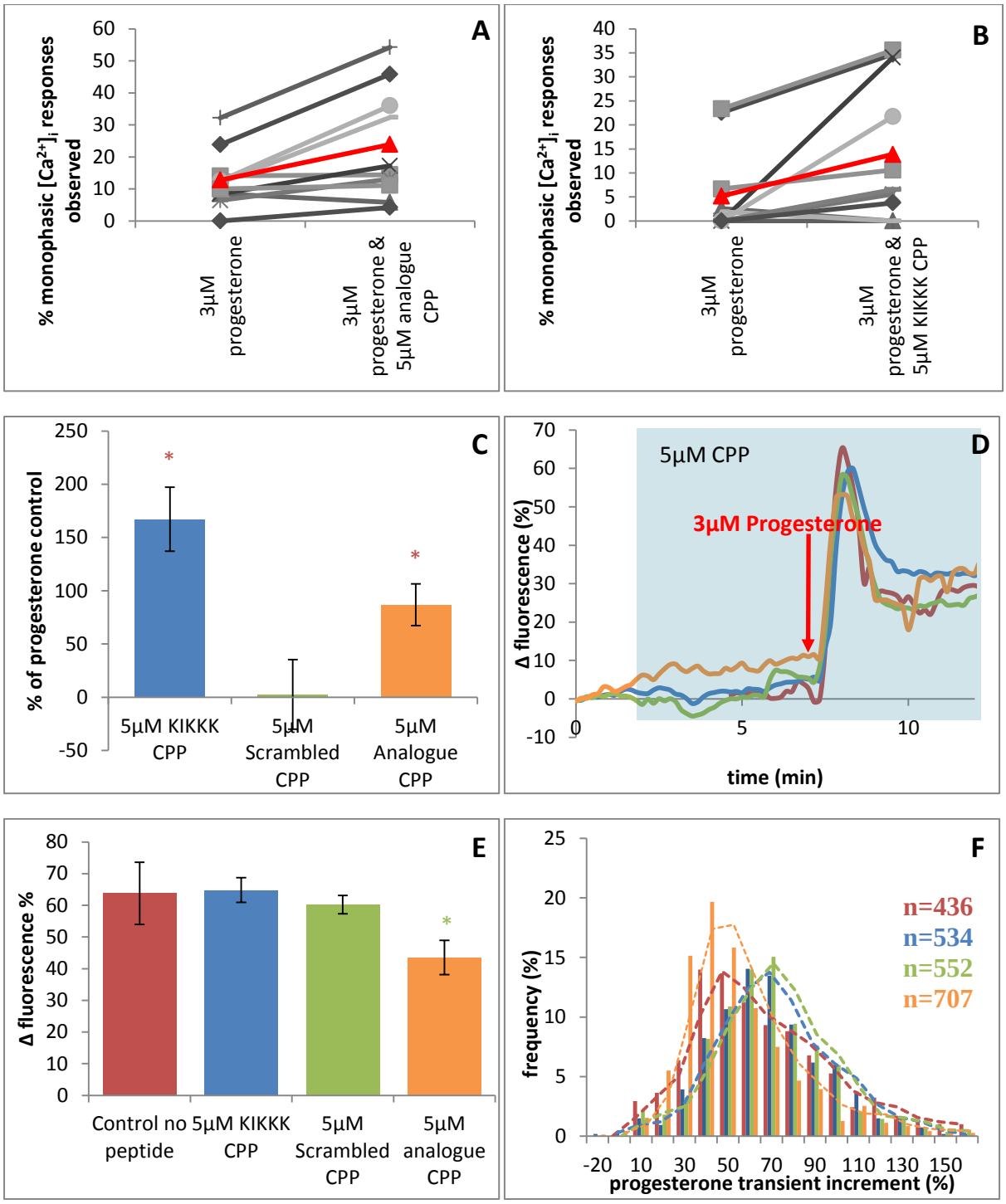

Figure 7.6 CPP effects on the $[Ca^{2+}]_i$ progesterone transient. Summary of results for control % monophasic $[Ca^{2+}]_i$ responses (left hand side) and CPP induced changes in the proportion of cells producing a monophasic $[Ca^{2+}]_i$ response. Each point represents the percentage of cells treated with 5µM analogue CPP (A) or 5µM KIKKK CPP (B). The red trace is the average of all experiments. For each subsequent graph cells the values for with no pre-treatment (Red), 5µM STIM1 KIKKK CPP (Blue), 5µM STIM1 KIKKK analogue CPP & 5µM Scrambled CPP (Green) are plotted. (C)Increase in the proportion of cells displaying a sustained $[Ca^{2+}]_i$ elevation (with no clear transient) in response to progesterone; expressed as a percentage of parallel progesterone control experiments. (D) R_{tot} traces for all treatments. (E) ΔF_{mean} for 3µM progesterone transient amplitude. (F) Frequency of transient progesterone response increment, (n= number of cells analysed). * $P<0.05$; paired t-test; compared to progesterone; * $P<0.05$; paired t-test; compared to scrambled CPP; n=12 experiments.

7.5.2.1 CPP effects on the progesterone induced $[Ca^{2+}]_i$ transient

A transient $[Ca^{2+}]_i$ increase of ~65% is observed in ~95% of cells stimulated with 3µM progesterone under control conditions. Pre-treatment of cells with 5µM of any one of the three CPPs defined here prior to 3µM progesterone exposure caused a consistent observable but non-significant decrease in progesterone transient amplitude compared to parallel controls (for representative Rtot's see Figure 7.6D; KIKKK: *P*=0.90, Analogue: *P*=0.27 & scrambled: *P*=0.57 ; paired t-test; compared to progesterone control; n=12). Cells treated with 5µM KIKKK analogue CPP display the greatest transient amplitude decrease of ~20% in ~80% of cells (n=707) compared to parallel controls, which is significantly less than cells treated with the scrambled CPP control (*P*= 0.044; paired t-test; compared to scrambled control; n=12, Figure 7.6E). Progesterone transient amplitude distribution (Figure 7.6F) showed that the proportion of progesterone transient amplitudes ≥110% ΔF was lower in cells pre-treated with the *KIKKK* CPP and scrambled CPP treated cells.

7.5.2.2 CPP effects on the sustained progesterone induced $[Ca^{2+}]_i$ response

In control populations treated with 3µM progesterone typically there is a sustained elevation of $[Ca^{2+}]_i$ above resting levels that succeeds the initial transient. To assess the effect of pre-treatment with CPPs on this $[Ca^{2+}]_i$ plateau we used the value of ΔF_{mean} recorded 4min after progesterone application. Pre-treatment with CPPs induced no significant changes in the progesterone induced sustained $[Ca^{2+}]_i$ component at the PHN compared to parallel untreated controls (KIKKK *P*=0.70, analogue *P*=0.23, scrambled *P*=0.68; paired t-test; compared to progesterone; n=12; Figure 7.7A). However pre-treatment with 5µM KIKKK CPP significantly elevated the sustained progesterone $[Ca^{2+}]_i$ increase ~10% and 15% more than scrambled and KIKKK analogue CPPs respectively (*P*=0.022 & *P*=0.015; paired t-test;

compared to KIKKK; n=12; Figure 7.7A), but this did not correlate with the initial $[Ca^{2+}]_i$ response to CPP alone (*P*=0.99). This is also observed in the distribution of the sustained $[Ca^{2+}]_i$ responses, where an increased proportion of smaller sustained amplitudes is evident in populations pre-treated with CCP's (Figure 7.7B). Here we show that there are significant differences between the KIKKK, KIKKK analogue and scrambled CPP effects on sustained $[Ca^{2+}]_i$ responses and suggest that these are the result of different interactions with STIM1 at the PHN of human sperm.

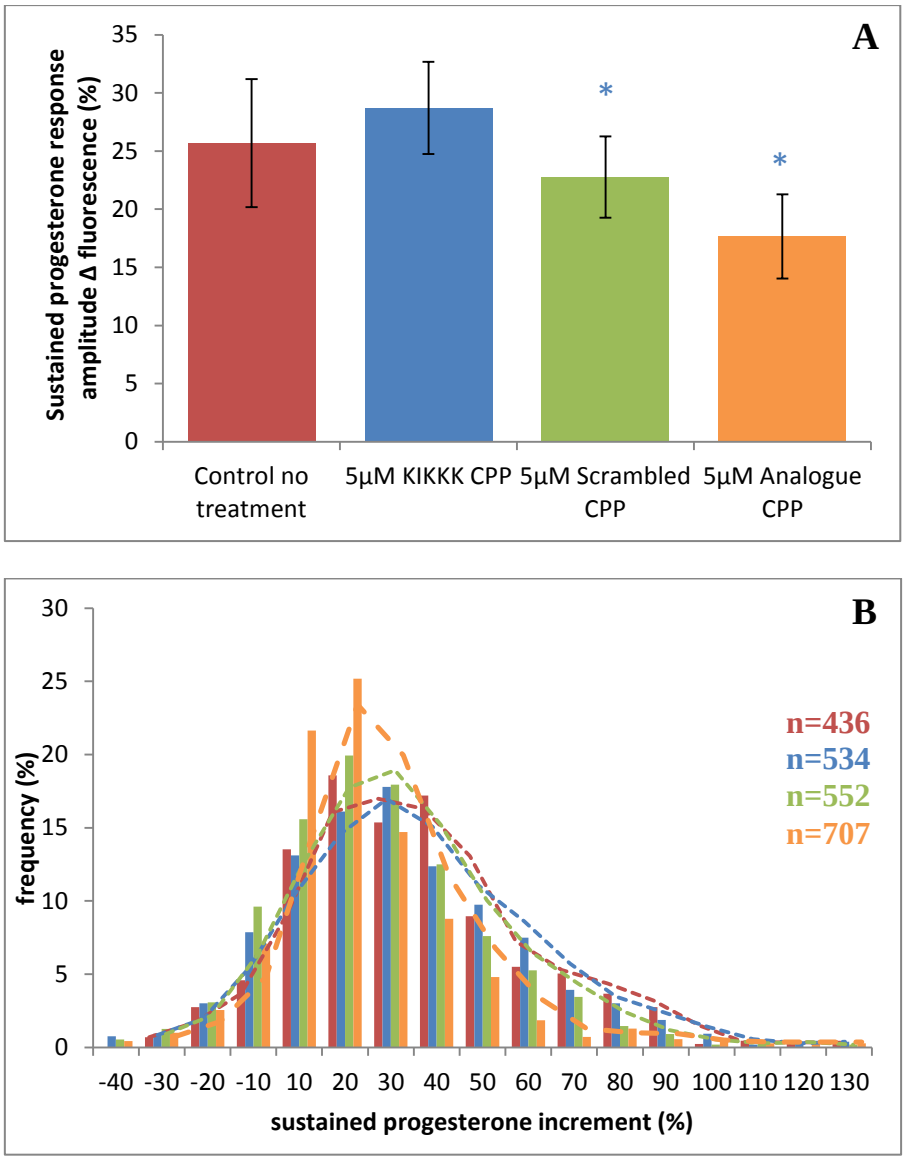

Figure 7.7 The effects of CPPs on the sustained $[Ca^{2+}]_i$ progesterone response. In the following graphs cells were treated with either 5µM KIKKK CPP (blue), 5µM scrambled CPP (green), 5µM KIKKK analogue CPP (orange) or control no treatment (red) for 300s prior to 3µM progesterone treatment. (A) ΔF_{mean} 240 seconds after progesterone application. (B) Frequency of sustained progesterone response increment, (n= number of cells analysed). * $P<0.05$; paired t-test; compared to KIKKK CPP; n=12 experiments.

7.6 Discussion

The plasma membrane (PM) composition of mammalian sperm has historically been a barrier to the study of intracellular signalling processes. Highly specialised, the PM of sperm differs significantly from the typical passive phospholipid bilayer observed in somatic cells (Lenzi *et al.,* 1996). In fact successful fertilisation is dependent on the unique PM structure which is integral in capacitation, AR and sperm-oocyte fusion. Capacitation itself is an important regulator of PM conformation, as PM lipid maturation is only achieved after epididymal passage (Salvolini *et al.,* 2013; Gadella & Evans, 2011). Studies on the lipid composition of mammalian sperm have identified an unusually high concentration of polyunsaturated fatty acids (PUFA) and a sperm specific phospholipid plasmalogen (Lenzi *et al.,* 1996). In addition sperm PM lack the cellular machinery to undergo endocytosis of extracellular molecules observed in somatic cells (Jones *et al.,* 2013). Hence it was uncertain whether CPPs, effective bioactive delivery agents in somatic cells could penetrate the PM of mammalian sperm.

CPPs have been shown to penetrate the PM of somatic cells *in vivo* and *in vitro* at low micromolar concentrations without inducing any permanent damage, but mechanisms of PM uptake are still unresolved (Madani *et al.,* 2011; Jones *et al.,* 2013). In cells capable of endocytosis this is the favoured CPP entry route proposed, conversely in cells incapable of endocytosis direct translocation is supported (Duchardt *et al.,* 2007; Johnsson *et al.,* 2011; Madani *et al.,* 2011). In studies of CCP uptake in bovine sperm cytochemical investigations confirmed absence of lysosomes and endocytotic machinery for both macropinocytosis and clathrin-mediated endocytosis; indicating direct translocation as the primary mechanism for CPP uptake (Jones *et al.,* 2013). Furthermore PM translocation was rapid, saturable and ultimately dependent on the CPP sequence used. Of the six CPPs used by Jones *et al.,* (2013)

C105Y was the most efficient delivery vector in bovine sperm; assumed due to a favourable incorporation into the specialised lipid membrane (Rhee & Davis, 2006). Jones and colleagues' further studies on the effects of CPPs on human and bovine cell viability and motility showed no negative effect of CPP direct translocation on sperm function. Indeed penetratin, another protein derived CPP tested, increased cell viability (Madani *et al.,* 2011; Derossi *et al.,* 1994). Their observations highlighted sperm as a good model system for investigating direct translocation of CPPs due to the absence of an alternative PM entry mechanism.

The specialised PM of human sperm provides an effective barrier against the extracellular environment (Madani *et al.,* 2011). Absence of endocytic machinery restricts the size of molecular compounds able to penetrate the cell under normal physiological conditions. As a result the study of intracellular $[Ca^{2+}]_i$ signalling cascades has until recently been limited to available cell permeable modulators of Ca^{2+} function or removal of the cell membrane (Howl *et al.,* 2012). CPPs provide an alternative mechanism of vector delivery; in somatic cells they facilitate the uptake of large hydrophilic molecules (Linberg *et al.,* 2011; Madani *et al.,* 2011). In bovine sperm when coupled to large peptides CPP uptake was inhibited, likely the result of PM direct translocation limitations (Jones *et al.,* 2013). However CPPs coupled to small peptides were not only taken up by bovine sperm but also displayed targeted organelle localisation.

Prior to the studies reported here it was uncertain whether CPPs delivering targeted peptide sequences (bioportides) would readily translocate the PM of human sperm and influence $[Ca^{2+}]_i$. Under basal conditions we demonstrated that application of CPPs coupled to targeted

peptide sequences (otherwise PM impermeable) had differential effects on $[Ca^{2+}]_i$ (Lukanowska *et al.,* 2013). As the CPP component (penetratin) was the same for all three peptides tested, the differences in $[Ca^{2+}]_i$ responses observed must be the result of the different peptide sequences attached. The two peptides which induced a decrease in $[Ca^{2+}]_i$ (KIKKK CPP and scrambled CPP) were both composed of the same amino acids. As the decrease in $[Ca^{2+}]_i$ observed was transient and returned to basal control levels it could be the result of cytoplasmic Ca^{2+} loss during peptide translocation across the membrane or a temporary effect on pHi. One current model for direct PM translocation implies the formation of PM pores (Alves *et al.,* 2011). In contrast the KIKKK analogue CPP induced an increase in $[Ca^{2+}]_i$ which remained elevated above basal levels. Unlike the other two CPPs used the KIKKK analogue contained α-aminoisobutyric acid and an extended *D*Arg N-terminal to enhance helicity, stability and cellular penetration. There are three potential explanations for the increase in $[Ca^{2+}]_i$ observed; firstly an influx in extracellular Ca^{2+} during the translocation, secondly the CPP could induce Ca^{2+} entry through Orai at the PM or finally the CPP could activate Ca^{2+} release from intracellular stores. Induced Ca^{2+} entry through Orai activation appears the most likely explanation since the main difference between the other two CPPs used in this study is that stabilisation of helical structure in this peptide should enhance interaction with the binding domain on Orai. Furthermore, the sustained effect of the KIKKK analogue is not consistent with an effect exerted during translocation. At present there is insufficient evidence to ultimately determine the mechanism responsible.

The biphasic $[Ca^{2+}]_i$ increase associated with progesterone stimulation is well characterised (Kirkman-Brown *et al.,* 2000; 2003), however the mechanisms underlying the response appear complicated and remain to be clarified. Identification of the PM progesterone receptor CatSper by Strunker *et al.,* (2011) finally provided a mechanism for external Ca^{2+} influx;

however the CatSper current blocker NNC-55-0396 failed to abolish the signal entirely (Jensen & Publicover, 2012; Strunker *et al.,* 2011; Sagare-Patil *et al.* 2012). The inability of CatSper channels to account for the biphasic $[Ca^{2+}]_i$ response suggests participation of other components of Ca^{2+} signalling, including release of intracellular stored Ca^{2+} (chapters 3, 4&5; Lefievre *et al.,* 2012; Alasmari *et al.,* 2013) and a mechanism for Ca^{2+} store replenishment.

In previous chapters we provide evidence for the existence of a Ca^{2+} channel at the PHN of human sperm that is distinct from the mitochondria of the midpiece. Here we report that KIKKK containing CPPs have a significant effect on the distinctive biphasic progesterone induced $[Ca^{2+}]_i$ profile. Application of both KIKKK containing CPPs (KIKKK CPP and analogue CPP) caused a significant increase in the proportion of cells in which the response to progesterone consisted of a rapid rise followed by a monophasic $[Ca^{2+}]_i$ plateau (Figure 7.4B) instead of the well-characterised biphasic response (Figure 7.3A). Thus it appears that in a subset of cells, KIKKK analogue CPP can bind and constitutively activate Orai PM SOCE influx and both KIKKK containing STIM1 CPPs can maintain SOCE following agonist-induced store mobilisation. It should be noted that a similar response is not observed in those cells treated with the scrambled CPP which does not contain the intact KIKKK sequence, indicating that the response is not the result of the CPP but of the KIKKK containing peptides.

In summary our findings demonstrate that KIKKK containing CPPs induce differential effects on basal $[Ca^{2+}]_i$. It is likely that these effects are the result of CPP direct translocation across the PM but further study needs to be undertaken in human sperm. CPP effects on the

biphasic progesterone response indicate a role for SOCE in the formation of the progesterone transient, STIM and Orai interaction are fundamental and modulation with engineered bioportides can significantly alter $[Ca^{2+}]_i$ (Lukanowska *et al.*, 2013). Thus bioportides are an effective vector for delivery of small otherwise impermeable bioactive peptides, which could be utilised for modulation of other intracellular signalling pathways (Howl *et al.*, 2012; Costello *et al.*, 2009).

CHAPTER EIGHT: EFFECTS OF $[Ca^{2+}]_i$ AGONISTS ON MITOCHONDRIAL MEMBRANE POTENTIAL

8.1 Abstract

The Ca^{2+} storage potential of mitochondria is well established in somatic cells. At resting physiological conditions mitochondrial Ca^{2+} contribution is minimal, but when the system is stressed under pathological conditions or due to pharmacological inhibition of Ca^{2+} pumps mitochondrial Ca^{2+} uptake increases, leading to shaping of the $[Ca^{2+}]_i$ signal (Duchen, 2000; Scorziello *et al.,* 2013). The contribution of mitochondrial Ca^{2+} to homeostasis in somatic cells is acknowledged, but we wanted to identify the potential mitochondrial Ca^{2+} input to the $[Ca^{2+}]_i$ signals at the PHN induced by these agonists. Mitochondrial membrane potential (MMP; $\Delta\Psi_m$) reflects Ca^{2+} accumulation by these organelles, at low MMP the mitochondria take up cytoplasmic Ca^{2+} whilst at high MMP mitochondria Ca^{2+} is released (Duchen, 2000). Here we utilise the dual emission mitochondrial potential sensitive probe JC-1 to report two different effects of Ca^{2+} agonists on MMP. 3μM progesterone and 5μM 2-APB both induce MMP hyperpolarisation whilst conversely 5μM thimerosal and 2mM 4AP induce significant MMP depolarisation in resting cells. These results suggest that if MMP is indicative of mitochondrial Ca^{2+} contribution to $[Ca^{2+}]_i$ then their input is variable and unable to account for all increases in $[Ca^{2+}]_i$ observed at the PHN. Therefore it is likely that another Ca^{2+} store is present at the PHN which provides a greater Ca^{2+} contribution to the increases in $[Ca^{2+}]_i$ observed with thimerosal and 4AP treatment.

8.2 Introduction

Sperm are minimalist cells, as such they lack organelles required for genomic regulation of cellular function. $[Ca^{2+}]_i$ signalling is therefore integral in regulating all biochemical and physiological processes required for successful fertilisation. Numerous Ca^{2+} channels have been identified in human sperm, including those associated with intracellular Ca^{2+} stores of somatic cells (Costello *et al.,* 2009). IP_3Rs, the Ca^{2+}-ATPase SPCA1, RyRs and calreticulin (a Ca^{2+}-buffering protein associated with somatic stores) have all been localised to the anterior acrosome and PHN/midpiece regions of mammalian sperm (Naaby-Hansen *et al.,* 2001; Harper *et al.,* 2005; 2004). Phospholipase-C (PLC) and G-proteins associated with the IP_3 signalling cascade have also been detected (Walensky & Snyder, 1995; Kuroda *et al.,* 1999). In 2005, Herrick and colleagues provided evidence for the Ca^{2+} storage ability of the acrosome; however the identity of a Ca^{2+} store at the PHN remains controversial. Potential candidates include; RNE, cytoplasmic droplet and mitochondria (Ho & Suarez, 2003).

Mitochondria of mammalian sperm are localised to the midpiece where they are wrapped around the axoneme, connected via multiple disulphide bridges. In somatic cells these organelles are fundamentally important in the production of ATP required to maintain cellular function. Oxidative phosphorylation requires both the respiratory chain and ATP-synthase enzymes located in the inner mitochondrial membrane to generate ATP from an electron donor. Though there is evidence for an important contribution of glycolysis for generation of ATP in mammalian sperm (Miki *et al.,* 2004), abnormalities of mitochondrial structure or organisation have been shown to be associated with severe asthenozoospermia, apparently due to inadequate ATP production and maintenance of the mitochondrial membrane potential (MMP/$\Delta\Psi_m$; Piasecka & Kawiak, 2003; Piomboni *et al.,* 2012). A

relationship between $\Delta\Psi_m$ and sperm motility was first identified by Evenson and colleagues in 1982, they demonstrated that MMP of fertile men exceeded those of men with reduced sperm motility parameters. Subsequent confirmation of these results by a number of groups has also identified that high mitochondrial functionality is indicative of increased fertilisation potential (Marchetti *et al.,* 2002; Gallon *et al.,* 2006; Sousa *et al.,* 2011). As a result mitochondrial contribution to motility regulation is of particular interest, if found to be fundamental in the facilitation of hyperactivated motility then they present a target for treatment of asthenozoospermic patients and conversely contraceptive agents.

Mitochondria are also implicated in a number of intracellular homeostatic mechanisms, fatty acid β-oxidation, amino acid metabolism and Ca^{2+} storage have all been reported (Piomboni *et al.,* 2012). Significantly, modest Ca^{2+} uptake into the mitochondria stimulates dehydrogenases of the TCA cycle, leading to increased mitochondrial respiration, potentially providing increased ATP generation during periods of high cellular activity (Duchen, 2000). In mammalian sperm mitochondrial uptake of Ca^{2+} has been observed *in situ* (Vijayaraghavan & Hoskins, 1990; Wennemuth *et al.,* 2003); however contribution of mitochondrial Ca^{2+} stores was dependent on the physiological stresses on the system. At rest mitochondrial Ca^{2+} flux was minimal, but when the cells were exposed to pharmacological agents that elicited an increase in $[Ca^{2+}]_i$ mitochondrial Ca^{2+} uptake increased accordingly (Wennemuth *et al.,* 2003; Scorziello *et al.,* 2013). These observations have also been made in somatic cells, where increased $[Ca^{2+}]_i$ activates the mitochondrial Ca^{2+} uniporter (MCU) to drive Ca^{2+} uptake into mitochondria (Murgia *et al.,* 2009), which has been shown to cause depolarisation of the MMP (Duchen, 2000). Furthermore MMP ($\Delta\Psi$) is associated with ATP produced by respiration and oxidative phosphorylation (Rizzuto & Brini, 2004). On this note

Ho and colleagues have identified that bull sperm immotility induced by mitochondrial disruption can be restored (including hyperactivation potential) by addition of Ca^{2+} and ATP (Ho *et al.*, 2002), suggesting an integral role for ATP production in hyperactivated motility. However treatment with the Ca^{2+} store mobilising agonist thapsigargin induced hyperactivation without associated increases in NADH or ATP (Ho & Suarez, 2003). Taken together these results present a complex relationship between storage of intracellular Ca^{2+} and ATP production. Current data propose that multiple mechanisms for Ca^{2+} mobilisation and ATP production could facilitate hyperactivated motility dependent on the signalling cascade induced by the agonist (Piomboni *et al.*, 2012).

In chapter 3 we observed that the mitochondrial uncouplers DNP and CCCP decreased motility parameters and elevated $[Ca^{2+}]_i$ at the PHN in the presence of extracellular Ca^{2+}. To determine whether these effects were the result of mitochondrial uncoupling and release of stored Ca^{2+} from the mitochondria or an alternative Ca^{2+} store in the region we utilised the MMP sensitive dye JC-1. JC-1 is a dual emission potential-sensitive probe, at low MMP JC-1 exists as a fluorescent green monomer (λ_{ex}520nm) in the cytoplasm of cells. High MMP's cause multimerisation of the monomers into red fluorescent 'J-aggregates' that accumulate in the mitochondria (λ_{em}596nm). A ratio of the red-green fluorescence intensities (F_R/F_G) gives a measurement of MMP which is not affected by mitochondrial size, shape or density (chapter 2.7). The subsequent MMP ratio determined offers insight into the Ca^{2+} flux of the mitochondria. This observation lead us to question the effect of inducers of $[Ca^{2+}]_i$ and hyperactivated motility on MMP ($\Delta\Psi_m$) in human sperm. Here we report the effects of 5µM thimerosal, 3µM progesterone, 5µM 2-APB and 2mM 4AP on MMP and the implications of this on the Ca^{2+} storage potential of human sperm mitochondria.

8.3 Aims

The aim of this chapter was to assess the effect of inducers of hyperactivated motility and increased $[Ca^{2+}]_i$ elevation (identified in chapters 4 and 5) on mitochondrial membrane potential in human sperm.

8.4 Material and Methods

8.4.1 Materials

JC-1 mitochondrial dye was purchased from Enzo Life Sciences, (Exeter). For all other materials see chapter 2.1.1.

8.4.2 Methods

8.4.2.1 Cell preparation

Human semen was collected and prepared as in chapter 2.3.

8.4.2.2 Cell incubation and capacitation

Sperm were incubated and capacitated for a minimum of 5 hours as in chapter 2.4.

8.4.2.3 Mitochondrial imaging with JC-1

All mitochondrial imaging experiments were conducted following the protocol outlined in chapter 2.7. After an initial control period of 20 frames (200secs) cells were exposed to 3µM Progesterone, 5µM Thimerosal, 5µM 2-APB or 2mM 4AP for 30 frames. In addition cells exposed to 5µM Thimerosal, 5µM 2-APB or 2mM 4AP were then treated with 3µM progesterone for a further 30 frames and MMP response observed.

8.4.3 Analysis

Effects of agonists on mitochondrial membrane potential were analysed as in chapter 2.7.

8.5 Results

Fluorescence imaging of loosely tethered cells showed that human sperm labelled effectively with the dual emission dye JC-1. As anticipated, at rest sperm of fertile donors displayed high levels of red fluorescence in the midpiece (corresponding to mitochondrial presence) and low levels of green fluorescence throughout the cytoplasm (Figure 8.1B).

8.5.1The mitochondrial membrane potential of resting cells oscillates in human sperm.

At rest MMP ($\Delta\Psi_m$) of the majority of human sperm cells were subject to a number of oscillations (Figure 8.1D). Initial observations showed high levels of red fluorescence in the midpiece and low levels of green cytoplasmic fluorescence; indicative of healthy cells with functional mitochondria (Sousa *et al.,* 2011; Figure 8.1B). $\Delta\Psi_m$ was assessed for each frame of a given experiment upon completion of the time-lapse protocol by ratioing the red/green fluorescence intensities (Figure 8.1C). Upon initiation of fluorescence imaging cells were monitored for a minimum of 20 frames (200s) to establish an adequate representation of the $\Delta\Psi_m$ at rest. During this 'control period' we observed numerous small $\Delta\Psi_m$ oscillations in ~90% of the cells observed (Figure 8.1D & 8.2), which due to the variation in frequency and amplitude amongst the population was not usually visible in the average $\Delta\Psi_m$ trace. To establish a baseline on which to determine subsequent agonist induced $\Delta\Psi_m$ changes the control period was averaged for each individual cell and subtracted from the max agonist induced $\Delta\Psi_m$ response.

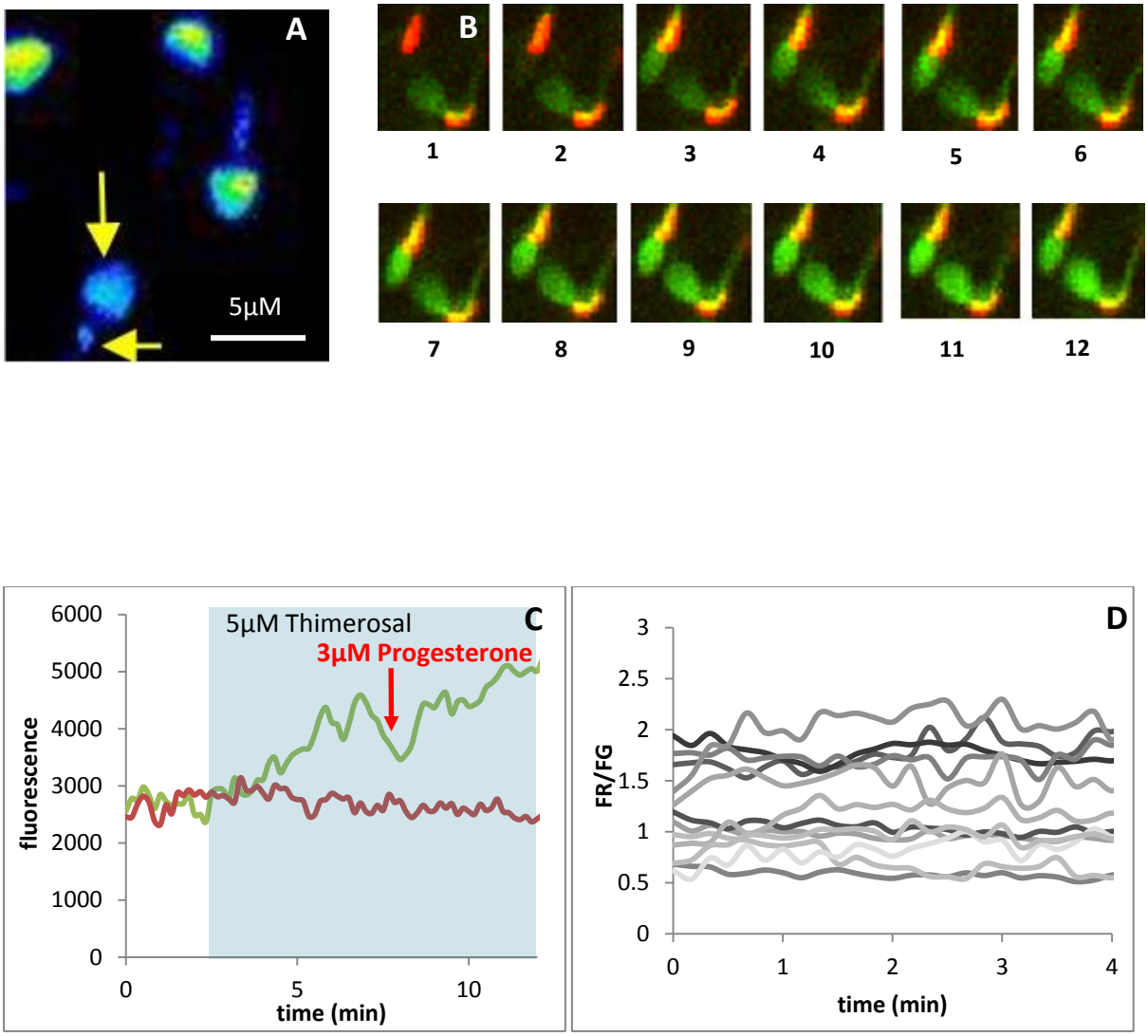

Figure 8.1 MMP effects in human sperm. (A) Pseudo colour image of sperm loaded with the low affinity Ca^{2+} dye Mag-Fluo-4AM (warm colours indicate areas of high Ca^{2+} concentration including the Ca^{2+} stores at the acrosome and PHN highlighted by the yellow arrows). (B) Image series of 2 sperm cells loaded with the MMP sensitive dye JC-1, green fluorescence corresponds to the monomeric dye structure and red fluorescence corresponds to the dye tetramers. (C) Individual cell MMP response to 5µM thimerosal stimulation, red trace corresponds to mitochondrial JC-1 fluorescence and green trace corresponds to cytoplasmic JC-1 fluorescence. (D) Each grey trace represents the MMP response for an individual cell during the 20 frame control period, determined by the ratio of red: green fluorescence with the mitochondrial potential sensitive dye (JC-1).

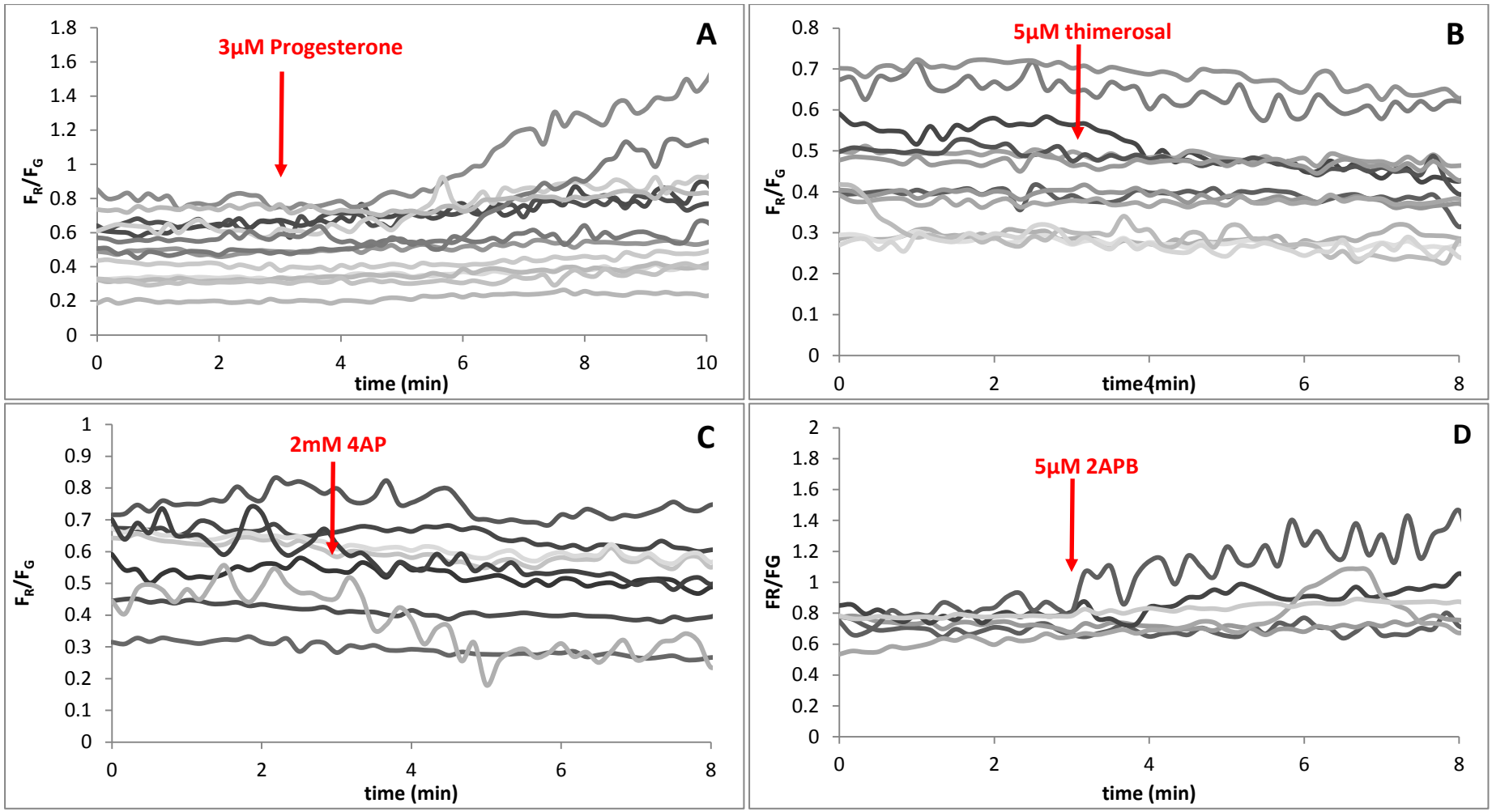

Figure 8.2 MMP response of individual cells to inducers of increased $[Ca^{2+}]_i$. All cells were treated with JC-1 and their MMP monitored for a period of 20 frames (200s) before stimulation with (A) 3µM progesterone, (B) 5µM thimerosal, (C) 2mM 4AP or (D) 5µM 2-APB (red arrow). Each grey trace represents the MMP response for an individual cell, determined by the ratio of red: green fluorescence with the mitochondrial potential sensitive dye (JC-1).

8.5.2 Mitochondrial membrane potential response to Ca^{2+} store agonists.

In chapters 4 and 5 we reported increases in $[Ca^{2+}]_i$ at the PHN associated with progesterone, thimerosal, 4AP and 2-APB stimulation. Here we have assessed the possible contribution of mitochondrial Ca^{2+} buffering to these $[Ca^{2+}]_i$ responses by monitoring the MMP.

8.5.2.1 MMP $\Delta\Psi_m$ response to progesterone.

The biphasic $[Ca^{2+}]_i$ progesterone response at the PHN is well documented (Kirkman-Brown *et al.,* 2000; 2003), but potential mitochondrial Ca^{2+} contribution remains to be elucidated. In cells stimulated with 3µM progesterone significant hyperpolarisation of the mitochondrial membrane potential was observed (Figure 8.2A, 8.3A) in ~ 40% of cells (Figure 8.3C). Elevation of $\Delta\Psi_m$ began ~1minute after progesterone application and peaked after ~100 seconds (Figure 8.3D) then plateaued or induced a series of oscillations. This response was seen in the majority of cells in all experiments with analysis of individual cell responses revealing ~65% of cells induce an increase in the $\Delta\Psi_m$ associated with progesterone application and potentially mitochondrial Ca^{2+} uptake into the mitochondria.

8.5.2.2 MMP $\Delta\Psi_m$ response to known inducers of hyperactivation.

Thimerosal and 4AP have been shown to induce hyperactivated motility in human sperm through increasing $[Ca^{2+}]_i$ at the PHN (Alasmari *et al.,* 2013; Costello *et al.,* 2009; chapter 4); however their impact on $\Delta\Psi_m$ has not been recorded. In cells treated with JC-1, stimulation with either 2mM 4AP or 5µM thimerosal induced significant $\Delta\Psi_m$ depolarisation compared to the control period (P=0.04 & P=0.01 respectively; paired t-test, n=8, n=14; Figure 8.2B&C, 8.3A).

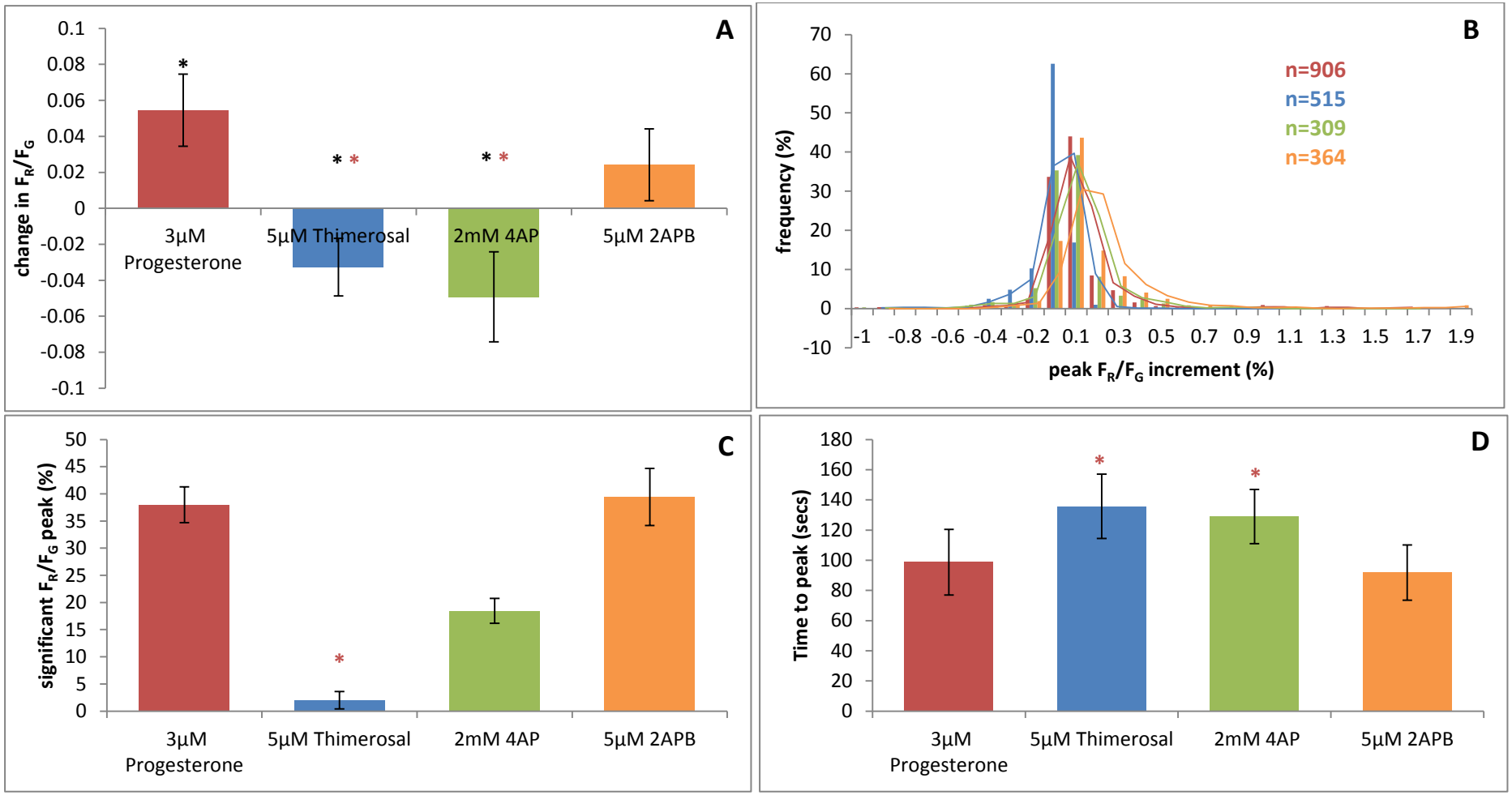

Figure 8.3 Effect of inducers of $[Ca^{2+}]_i$ on mitochondrial membrane potential. (A) Maximum MMP response within 3min of agonist application. (B) Frequency distribution of MMP response amongst the cell population. n= total number of cells analysed. Colours indicate the 4 different stimuli as in panel A. (C) Proportion of cells displaying significant MMP response. (D) Time taken to reach peak MMP ($\Delta\Psi_m$). Results are mean ± S.E.M. for 24, 14, 9 and 11 experiments respectively. * $P<0.05$; paired t-test; compared to control period. * $P<0.05$; paired t-test; compared to progesterone response.

Analysis of peak F_R/F_G increment distribution shows the highest proportion of thimerosal responses to be between 0.1-0.2 F_R/F_G (Figure 8.3B) with <5% of cells producing a significant hyperpolarisation response (Figure 8.3C). In addition ~80% of cells exposed to 2mM 4AP did not produce a significant increase in $\Delta\Psi_m$.

It is interesting to note that both 4AP and thimerosal responses were lower than those seen with progesterone stimulation (*P*=0.001 & *P*=0.016 respectively; paired t-test, n=8, n=14; Figure 8.3A). As with Ca^{2+} response observations progesterone mitochondrial hyperpolarisation occurs rapidly, in comparison both 4AP and thimerosal responses are significantly slower (*P*=0.04 & *P*=0.02 respectively; paired t-test, n=8, n=14; Figure 8.3D). Clearly the effects of these agents on mitochondrial Ca^{2+} accumulation are not the same.

8.5.2.3 MMP $\Delta\Psi_m$ response to SOCE activator 2-APB.

Upon addition of 5µM 2-APB to the perfusion medium ~40% of sperm showed a significant response compared to the parallel control periods (n=11; Figure 8.2D, 8.3B&C). An average increase of 0.07 $\Delta\Psi_m$ was observed, caused by an increase in mitochondrial red fluorescence and a decrease in green cytoplasmic fluorescence however this was statistically insignificant (*P*=0.50, paired t-test, n=11; Figure 8.3A). Elevation of $\Delta\Psi_m$ began within 2-3 frames (20-30seconds) and peaked ~90 seconds after application. Amplitude of the 2-APB induced increase in $\Delta\Psi_m$ and associated response kinetics has great similarity to that observed with application of 3µM progesterone (section 2.5.2.1). Furthermore in chapter 5 we showed that 5µM 2-APB treatment amplifies the transient increase in $[Ca^{2+}]_i$ induced by progesterone (Lefievre *et al.*, 2012).

8.5.3 Effect of Ca^{2+} store agonists on the progesterone induced increase in MMP

To investigate possible effects of 5µM thimerosal, 2mM 4AP or 5µM 2-APB pre-treatment on the mitochondrial hyperpolarisation caused by 3µM progesterone, experiments were carried out in pairs. Cells from the same semen sample were exposed to 3µM progesterone with or without pre-treatment with 5µM thimerosal, 2mM 4AP or 5µM 2-APB (Figure 8.4). In 5 out of 7 experimental pairs, pre-treatment with 5µM thimerosal (300s) significantly reduced the mitochondrial hyperpolarisation induced by 3µM progesterone compared to the non-pre-treated parallel experiment, inhibiting both $\Delta\Psi_m$ and the proportion of cells exhibiting a significant response to treatment (*P*=0.03 & *P*=0.0005 respectively; paired t-test; n=7; Figure 8.5A&C). In contrast there was no significant difference between the progesterone induced $\Delta\Psi_m$ with or without pre-treatment with 2-APB or 4AP which correlated with analysis of individual cell responses (Figure 8.5B&C). Furthermore all pre-treated cell populations displayed no significant difference in time taken to achieve maximum progesterone induced $\Delta\Psi_m$ (thimerosal: *P*=0.11, 4AP: *P*=0.45, *2-APB P*=0.46; paired t-test; n=7, n=8 & n=14 respectively; Figure 8.5D).

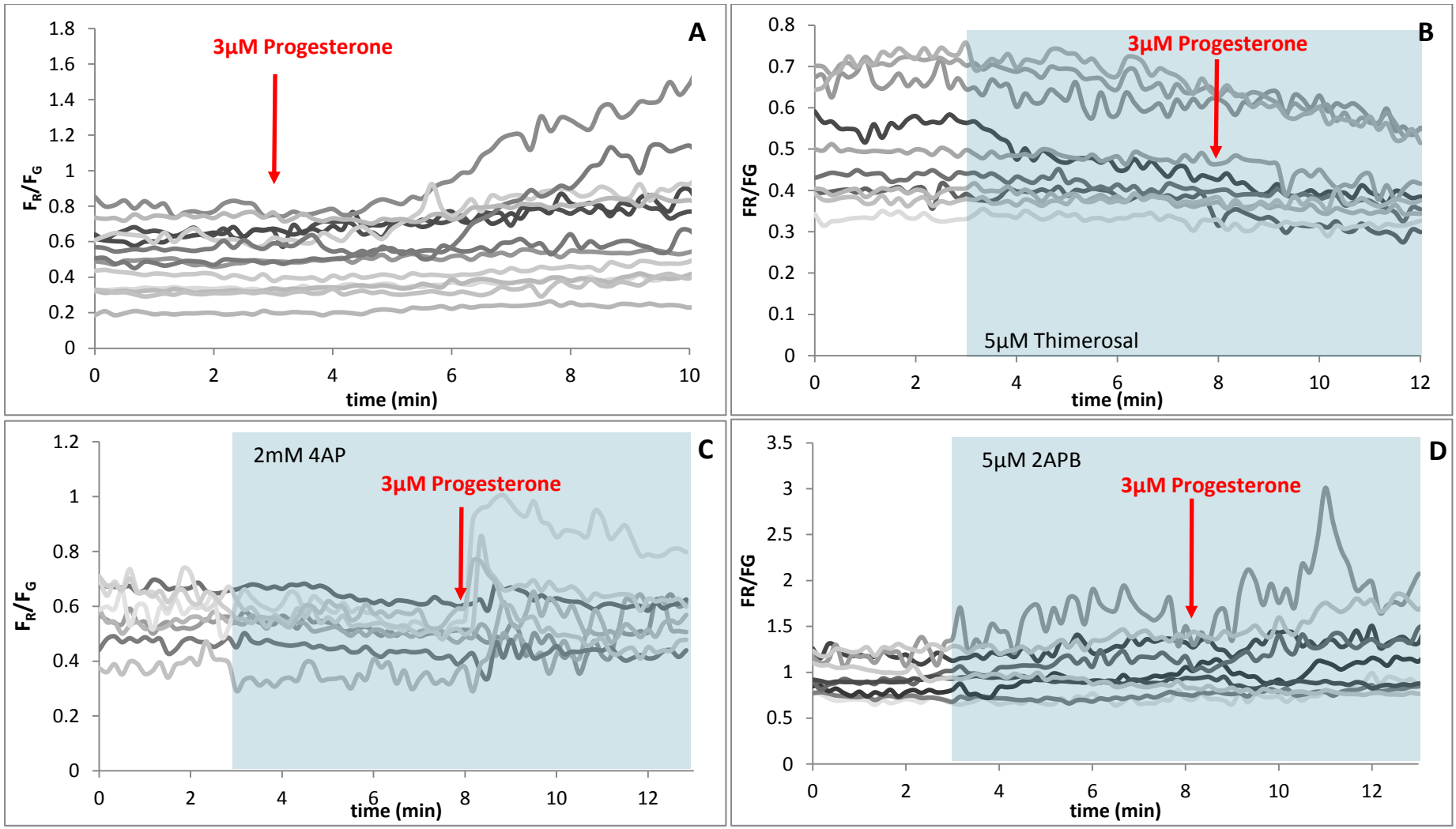

Figure 8.4 Individual cell MMP responses to Ca^{2+} agonist pre-treatment on progesterone induced hyperpolarisation. All cells were treated with JC-1 and their MMP monitored for a period of 20 frames (200s) before stimulation with 3µM progesterone without pre-treatment (A) or pre-treated with (B) 5µM thimerosal, (C) 2mM 4AP or (D) 5µM 2-APB (red arrow). Each grey trace represents the MMP response for an individual cell, determined by the ratio of red: green fluorescence with the mitochondrial potential sensitive dye (JC-1).

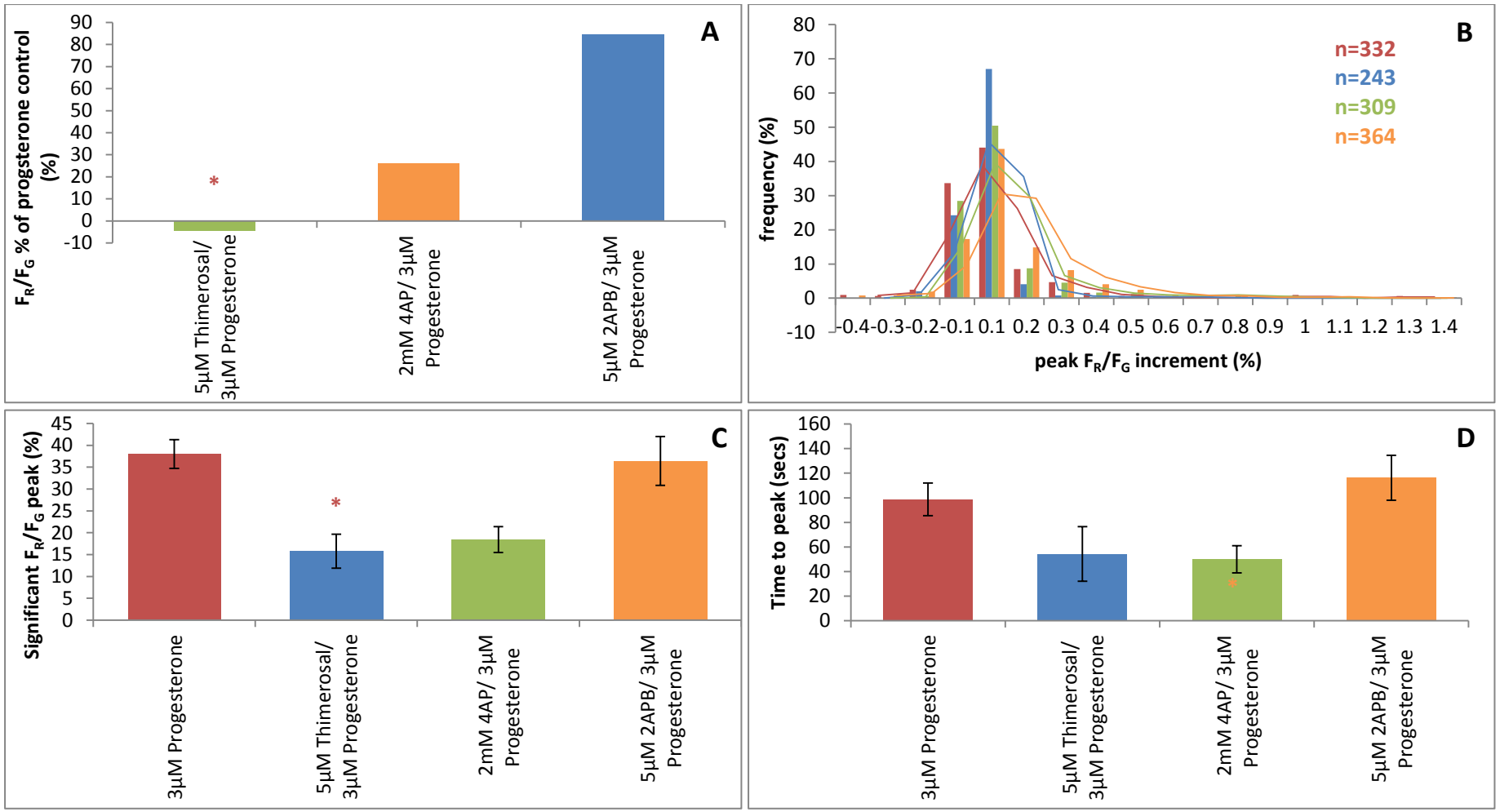

Figure 8.5 Effect of Ca^{2+} agonists on progesterone induced MMP hyperpolarisation. (A) Maximum MMP response after agonist stimulation expressed as a percentage of the parallel progesterone controls. (B) Frequency distribution of progesterone induced MMP response amongst the cell population. n= total number of cells analysed. (C) Proportion of cells displaying significant progesterone induced MMP response. (D) Time taken to reach progesterone induced MMP ($\Delta\Psi_m$) peak. Results are mean ± S.E.M. for 7, 9 and 11 experiments respectively. * $P<0.05$; paired t-test; compared to progesterone response.

8.6 Discussion

To date two candidates have been acknowledged as potential Ca^{2+} stores at the PHN/midpiece of human sperm. The RNE was proposed by Suarez and colleagues in 2003. Nevertheless mitochondria are established Ca^{2+} storage organelles in somatic cells and have been shown to accumulate Ca^{2+} in mammalian sperm of rabbit (Storey & Keyhani, 1973; 1974), rat (Babcock *et al.,* 1976), bovine (Vijayaraghavan & Hoskins, 1990) and murine (Wennemuth *et al.,* 2003) models *in situ*.

Mitochondria are the "powerhouses" of the cell, responsible for the oxidative phosphorylation of glycolytic products to produce the ATP required for numerous intracellular processes. In human sperm the contribution of glycolysis (throughout the tail) and oxidative phosphorylation (restricted to the mitochondria of the midpiece) to ATP production and sperm motility is topical. Miki *et al.,* 2004 observed that Glyceraldehyde-3-phosphate dehydrogenase-S (GAPDS; a glycolytic enzyme) was essential for fertility in murine sperm. Gapds knock-out sperm exhibited reduced ATP production and profound motility defects, however mitochondrial oxygen consumption was unaffected. More recently several authors have utilised mitochondrial membrane potential sensitive dyes to emphasise the importance of oxidative phosphorylation in motility and fertilisation (Evenson *et al.,* 1982; Gallon *et al.,* 2006; Espinoza *et al.,* 2009; Sousa *et al.,* 2011). Indeed $\Delta\Psi_m$ has been proposed as an accurate indicator of sperm fertilising potential (Evenson *et al.,* 1982; Espinoza *et al.,* 2009; Sousa *et al.,* 2011).

Evenson *et al.,* first identified a correlation between $\Delta\Psi_m$ and sperm motility in 1982, where they used the $\Delta\Psi_m$ sensitive fluorochrome Rhodamine 123 to compare the ejaculates of fertile and asthenozoospermic men. Subsequently several groups have utilised alternative $\Delta\Psi_m$ sensitive dyes to report that high $\Delta\Psi_m$ are indicative of both ability to undergo successful hyperactivation and oocyte fusion (Marchetti *et al.,* 2002; Gallon *et al.,* 2006; Sousa *et al.,* 2011). Our own observations in chapter 3 confirm this, in cells treated with the $\Delta\Psi_m$ dye JC-1 stimulation with either 10µM DNP or 10µM CCCP (mitochondrial uncouplers) significantly decreased $\Delta\Psi_m$ and the percentage of cells displaying hyperactivated motility as determined by CASA. Conversely here we demonstrate that 2mM 4AP and 5µM thimerosal both known inducers of hyperactivated motility (chapter 4, Costello *et al.,* 2009; Alasmari *et al.,* 2013), significantly depolarise the $\Delta\Psi_m$ indicating the complexity of the factors that determine occurrence of hyperactivated motility (Figure 8.3A&C).

In somatic cells regulation of mitochondrial Ca^{2+} accumulation is dependent on an electrochemical gradient $\Delta\Psi_m$ and $[Ca^{2+}]_i$, negative $\Delta\Psi_m$ and high $[Ca^{2+}]_i$ induce mitochondrial Ca^{2+} uptake via the mitochondrial uniporter (MCU; Zhao *et al.,* 2013; Murgia *et al.,* 2009). In mammalian sperm, mitochondrial MCU facilitated Ca^{2+} uptake has shown variability at different developmental stages and is believed to contribute to motility regulation due to its association with ATP production (Piomboni *et al.,* 2012). Several studies have questioned the importance of oxidative phosphorylation and glycolysis in the production of ATP required for motility. Miki *et al.,* 2004 concluded that glycolytic ATP has greater significance on murine sperm motility, whilst Ho and Suarez have demonstrated induction of hyperactivated motility with thapsigargin treatment without associated increases in NADH or ATP in bovine sperm (Ho & Suarez, 2003). The later study emphasises the importance of

$[Ca^{2+}]_i$ regulation and provides evidence for a Ca^{2+} storage organelle in addition to the mitochondria at the PHN of mammalian sperm.

In resting (unstimulated) sperm we observed a stable $\Delta\Psi_m$ (F_R/F_G) upon which many cells showed small oscillations, typically with a period of 1-2min, which were enhanced when the cells were stimulated (Figure 8.2A&D). This may well reflect cyclic mitochondrial $[Ca^{2+}]_i$ accumulation and release occurring in response agonist-induced $[Ca^{2+}]_i$ oscillations (Harper *et al.,* 2004).

In chapter 4 we demonstrated that 5μM thimerosal was sufficient to induce a consistent increase in $[Ca^{2+}]_i$ at the PHN, which has also been observed in cells treated with 2mM 4AP (Alasmari *et al.,* 2013; Costello *et al.,* 2009). Interestingly in cardiomyocytes $\Delta\Psi_m$ depolarisation, subsequently induced activation of PTPs at high mitochondrial $[Ca^{2+}]_i$, suggesting activation of mitochondrial Ca^{2+} efflux when the store reaches Ca^{2+} capacity (Zhao *et al.,* 2013). An initial $\Delta\Psi_m$ depolarisation followed by hyperpolarisation was also observed in astrocytes, where depolarisation was linked to mitochondrial Ca^{2+} accumulation (Duchen *et al.,* 2000). Our observation of $\Delta\Psi_m$ depolarisation associated with thimerosal and 4AP stimulation indicates mitochondrial Ca^{2+} accumulation, since $\Delta\Psi_m$ is required for Ca^{2+} uptake. When $[Ca^{2+}]_i$ is elevated, NCX facilitated Ca^{2+} efflux might contribute to the increases in $[Ca^{2+}]_i$ observed at the PHN. Under non-pathological conditions little Ca^{2+} is normally present within the mitochondrial matrix (Duchen, 2000) and thus it is likely that an alternative Ca^{2+} store at the PHN is primarily responsible for the thimerosal and 4AP associated increases in $[Ca^{2+}]_i$ that facilitate hyperactivated motility. Nevertheless this

additional store could have numerous close contacts <80nm with the mitochondria and be influenced by mitochondrial $[Ca^{2+}]_i$ (Murgia *et al.,* 2009), but further analysis of NCX facilitated Ca^{2+} efflux is required in human sperm to understand this process.

In contrast we show that treatment with 3μM progesterone and 5μM 2-APB induce hyperpolarisation of the $\Delta\Psi_m$ (Figure 8.2A&D; Lefievre *et al.,* 2012) which is consistent with secondary release of Ca^{2+} and consequent stimulation of mitochondrial respiration. Previous studies by our research group have shown that homeostatic mitochondrial uptake and release plays no significant role in the store-mediated oscillations observed at the PHN in cells treated with progesterone (Machado-Oliveira *et al.,* 2008). Furthermore in chapter 3 we show that neither DNP or CCCP pre-treatment has an inhibitory effect on the biphasic progesterone induced $[Ca^{2+}]_i$ response. Thus though this physiological stimulus apparently leads to Ca^{2+} release by the mitochondria, this does not significantly contribute to the amplitude or kinetics of the $[Ca^{2+}]_i$ signal at the PHN.

SPCA1, Ca^{2+}-ATPases have been localised to both the PHN and anterior midpiece of human sperm, they could potentially utilise glycolytically generated ATP to transport Ca^{2+} into the inner mitochondrial membrane when MCU is inhibited, thus restoring mitochondrial Ca^{2+} contribution to $[Ca^{2+}]_i$ responses (Harper *et al.,* 2004). However evidence suggests that mitochondrial contribution to agonist induced Ca^{2+} responses is limited, it is more likely they play a key role in maintaining resting $[Ca^{2+}]_i$ homeostasis and mitochondrial respiration under physiological conditions (Jimenez-Gonzalez *et al.,* 2006).

In summary these results indicate potential for mitochondrial Ca^{2+} contribution to $[Ca^{2+}]_{i,}$ buffering in human sperm but the mechanisms are complex and dependent on a number of factors. Contradiction between $\Delta\Psi_m$ observations and hyperactivated motility parameters in cells treated with thimerosal and 4AP suggest an alternative Ca^{2+} store at the PHN is responsible for the increase in $[Ca^{2+}]_i$ and percentage hyperactivation in chapter 4. Furthermore the reduction in the $\Delta\Psi_m$ associated with 2-APB pre-treatment prior to progesterone stimulation does not implicate mitochondrial Ca^{2+} in the increase in the progesterone induced $[Ca^{2+}]_i$ transient observed in chapter 5. It is therefore apparent that mitochondrial Ca^{2+} contribution to $[Ca^{2+}]_i$ appears minimal and complex, but it is likely another Ca^{2+} store is also present in the PHN of human sperm that is involved in the regulation of hyperactivated motility and is closely associated with the mitochondria.

CHAPTER NINE: GENERAL DISCUSSION

9.1 General discussion

Ca^{2+} is a versatile ubiquitous second messenger implicated in the regulation of numerous intracellular processes in a plethora of cell types. Spatial and temporal Ca^{2+} regulation is crucial to facilitate discrete cellular signalling responses over a wide dynamic range (Berridge, 2006). Versatility is achieved through sophisticated regulation of stored intracellular Ca^{2+} by a diverse Ca^{2+} toolkit (Publicover *et al.,* 2007; chapter 1.10). Indeed, alteration in Ca^{2+} regulation components can induce disease aetiology (Berridge *et al.,* 2012).

We have confirmed that human sperm possess two discrete areas of high Ca^{2+} concentration indicative of Ca^{2+} store localisation. Cells labelled with the low affinity Ca^{2+} dye Mag-Fluo-4AM to visualise the Ca^{2+} stores, showed fluorescence was localised to the acrosome and PHN/midpiece regions of mature sperm (Figure 9.1; Costello *et al.,* 2009). To date mitochondria and the RNE (or an alternative membranous organelle in the vicinity) have been proposed Ca^{2+} store candidates at the PHN. The main aim of this study was to characterise mobilisation of stored Ca^{2+} at the PHN of human sperm, to identify the Ca^{2+} storage capability of the two identified candidates (mitochondria and an IP_3 sensitive sperm specific store, potentially the RNE) to determine the potential contribution of these Ca^{2+} stores to shaping the biphasic progesterone $[Ca^{2+}]_i$ response.

We identified that human sperm mitochondria sequester and release Ca^{2+} as is reported in sea urchin (Ardon *et al.,* 2009), bovine (Vijayaraghavan & Hoskins, 1990), murine (Wennemuth *et al.,* 2003) sperm and a number of somatic cell types (Duchen, 2000). In bovine and murine models mitochondrial contribution to cytoplasmic Ca^{2+} clearance increased when other mechanisms of uptake were inhibited (Vijayaraghavan & Hoskins, 1990; Wennemuth *et al.,*

2003). Treatment with mitochondrial inhibitors disrupts the electrical driving force across the inner mitochondrial membrane that facilitates MCU Ca^{2+} uptake and ATP production required for motility. Here we report that CCCP and DNP induced an increase in $[Ca^{2+}]_i$ at the PHN in the presence of extracellular Ca^{2+} which indicates store mobilisation and replenishment. The increase in $[Ca^{2+}]_i$ is likely the result of inhibited mitochondrial Ca^{2+} uptake mechanisms, and spontaneous leakage of mitochondrial Ca^{2+}. We show that pre-treatment with the Ca^{2+}-ATPase inhibitor bisphenol (15µM) significantly reduced the proportion of cells exhibiting significant $[Ca^{2+}]_i$ increases associated with both mitochondrial uncouplers. Interpretation of this observation is not simple but it seems most likely that bisphenol, which will mobilise Ca^{2+} from non-mitochondrial stores, saturates SOCE. Thus human sperm mitochondria may play a role similar to that in sea urchin sperm where uncoupling induces a biphasic $[Ca^{2+}]_i$ rise due to initial mitochondrial Ca^{2+} mobilisation followed by activation of store-operated Ca^{2+} channels (Ardon *et al.*, 2009).

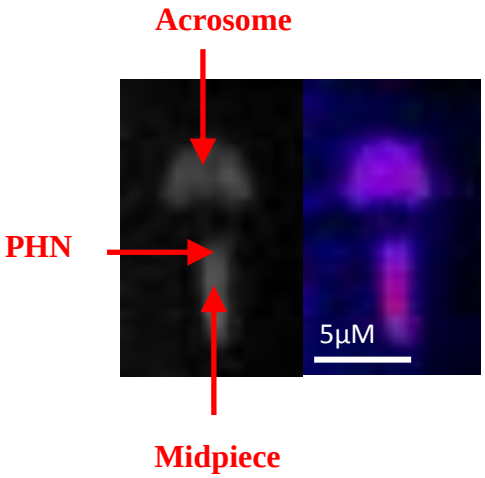

Figure 9.1 Location of Ca^{2+} stores in human sperm. Grey scale and pseudo-colour images (respectively) of a single human sperm cell treated with Mag-Fluo-4AM. Treatment clearly identifies two discrete Ca^{2+} stores where areas of white or warm colours (respectively) show areas of high Ca^{2+} concentration.

$[Ca^{2+}]_i$ elevation induced by mitochondrial inhibitors CCCP and DNP showed similarities to the biphasic $[Ca^{2+}]_i$ response induced by 3µM progesterone. Despite being intensively studied the underlying mechanisms of Ca^{2+} progesterone-induced mobilisation are still debated. It has been suggested that the initial transient increase in $[Ca^{2+}]_i$ and subsequent sustained increase in $[Ca^{2+}]_i$ are the result of multiple intracellular signalling pathways. The plasma membrane progesterone receptor CatSper, located at the principal piece of the flagellum, is believed to be the primary mediator of the rapid increase in $[Ca^{2+}]_i$ associated with the transient phase (Strunker *et al.,* 2011). Nanomolar progesterone concentrations activate CatSper channels resulting in a rapid Ca^{2+} influx across the PM. NNC-55-0396 abolished the CatSper current and inhibited the biphasic progesterone $[Ca^{2+}]_i$ response, but the response was not eliminated entirely (Jensen & Publicover *et al.,* 2012; Sagare-Patil *et al.,* 2012). It is therefore likely that an intracellular Ca^{2+} store is responsible for the additional increase in $[Ca^{2+}]_i$ observed at the PHN.

Investigation of the effect of mitochondrial inhibitor pre-treatment on the biphasic $[Ca^{2+}]_i$ response induced by 3µM progesterone showed no significant modulation of the $[Ca^{2+}]_i$ response at the PHN and acrosome when compared to parallel controls. CCCP and DNP induced clear increases in the progesterone Ca^{2+} transient at the midpiece. Since mitochondrial uncoupling will disrupt normal mechanisms of mitochondrial Ca^{2+} uptake, this effect could be independent of the MMP and the response observed with JC-1. These results confirm a functional significance for mitochondrial Ca^{2+} accumulation in human sperm. Contribution to generation of the progesterone-induced $[Ca^{2+}]_i$ transient at the PHN is insignificant, suggesting that a different (additional) Ca^{2+} store at the PHN is involved, consistent with other studies (Naaby-Hansen *et al,* 2001; Ho & Suarez, 2001; 2003).

IP_3R are synonymous with the ER of somatic cells, where they release stored Ca^{2+} in response to IP_3 mediation (Berridge, 2003; Michelangeli *et al.,* 1995). Mature sperm lack ER but a number of studies have localised IP_3R to the PHN of mammalian sperm (including human; Naaby-Hansen *et al.,* 2001; Bovine: Ho & Suarez, 2002; Murine: Ho & Suarez, 2003). We have determined using single cell fluorescence imaging and pharmacological manipulation of IP_3Rs that an IP_3 sensitive store (distinct from the mitochondria) at the PHN contributes to the sustained component of the progesterone $[Ca^{2+}]_i$ response observed in the region independent of CatSper channels. Thimerosal (at IP_3R activating concentrations) induces a sustained increase in $[Ca^{2+}]_i$ at the PHN that is resistant to the CatSper channel blocker NNC 55-0396, which confirms thimerosal induced effects are the initiated by stored $[Ca^{2+}]_i$ release and not PM Ca^{2+} influx (Alasmari *et al.,* 2013). The associated decrease in the sustained component of the $[Ca^{2+}]_i$ response induced by progesterone supports a model for at least two separate Ca^{2+} signalling components and presence of a Ca^{2+} store at the PHN associated with motility regulation. Indeed Ca^{2+} oscillations during the sustained progesterone plateau phase have been associated with flagellar bending and lateral head displacement in human sperm (Harper *et al.,* 2004). Furthermore our analysis of sperm motility parameters using CASA indicates a significant contribution of an IP_3 sensitive store at the PHN of human sperm in the regulation of hyperactivated motility previously reported in bovine sperm (Ho & Suarez, 2001).

We have recently published evidence for the presence of store operated Ca^{2+} entry (SOCE) in human sperm (Lefievre *et al.,* 2012) which has also been identified in several other species (sea urchin: Ardon *et al.,* 2009; Murine: O'Toole *et al.,* 2000). We confirmed that at low

doses (5μM) of the bimodal SOCE modulator 2-APB, SOCE was enhanced in human sperm as in somatic cells (Goto *et al.,* 2010; DeHaven *et al.,* 2008; Zhang *et al.,* 2008). We observed similar effects on SOCE with SKF-96365 (30μM), another bimodal SOCE modulator (Merritt *et al.,* 1990). Although SKF treatment induced an increase in $[Ca^{2+}]_i$ at the PHN like 2-APB, the incidence of hyperactivated motility was reduced compared to parallel controls as determined by CASA. Although this may be due to the kinetics of the response. 3μM progesterone treatment does not induce a significant increase in hyperactivation measured by CASA but during live cell imaging it is clear that there is a brief (60-90 s) burst of increased flagellar activity during the $[Ca^{2+}]_i$ transient (Harper *et al.,* 2004; Machado-Oliveira *et al.,* 2008).

Subsequent investigations into the stimulatory effects of these pharmacological SOCE modulators (SKF and 2-APB) on the biphasic $[Ca^{2+}]_i$ progesterone response, demonstrated a significant potentiation of the transient $[Ca^{2+}]_i$ response. We observed that in cells treated with 2-APB or SKF SOCE contribution was increased sufficiently as to elevate the transient $[Ca^{2+}]_i$ progesterone response at the PHN greater than that observed in parallel controls. SKF may have complex effects, being able both to release Ca^{2+} from intracellular storage organelles and inhibit SOCE (chapter 6). Taken together these results are consistent with a role for 2-APB sensitive SOC channels at the PHN in the formation and amplification of the progesterone $[Ca^{2+}]_i$ transient initiated by Ca^{2+} influx through PM CatSper channels (Strunker *et al*., 2011). Interestingly, pre-treatment with 2-APB and SKF exhibited opposing effects on the sustained component of the progesterone induced $[Ca^{2+}]_i$ response. In cells treated with 2-APB we observed an increase in $[Ca^{2+}]_i$ at the PHN that was inconsistent and insignificant. 2-APB was shown to enhance that occurrence of a late, secondary Ca^{2+} mobilisation 10-20s

after the initial transient, which may contribute to hyperactivated motility (Lefievre *et al.*, 2012; Harper *et al.*, 2004). Conversely in cells treated with SKF a decrease in the sustained $[Ca^{2+}]_i$ progesterone response was observed, consistent with similar responses in other cell types (Jenner & Sage, 2000). It should be noted that SKF has also demonstrated effects on other Ca^{2+} channels which may be contributing to the response observed here (Merritt *et al.*, 1990). These results implicate SKF and 2-APB sensitive Ca^{2+} channels in the regulation of the progesterone induced $[Ca^{2+}]_i$ transient with potential contribution of 2-APB sensitive stores to the sustained Ca^{2+} response (Figure 9.2).

Identification of the SOCE receptors STIM and Orai in 2005 (Roos *et al.*, 2005; Liou *et al.*, 2005) and 2006 (Feske *et al.*, 2006; Vig *et al.*, 2006; Zhang *et al.*, 2006) respectively provided the first complete mechanism for SOCE in somatic cells. We recently reported expression of both STIM (1&2) and Orai (1-3) isoforms in human sperm through a combination of protein expression and immunofluorescence (Lefievre *et al.*, 2012). All isoforms exhibited specific localised expression throughout the cell; however all were detected at the PHN indicative of at least one Ca^{2+} store in the region. SOCE facilitates replenishment of intracellular Ca^{2+} stores, upon Ca^{2+} store depletion STIM molecules on the Ca^{2+} store oligomerise and relocate to induce Ca^{2+} influx through PM Orai channels (Feske *et al.*, 2009). Recent studies have identified that STIM is essential for Orai function, in particular a ~98amino acid SOAR domain containing a conserved polybasic KIKKK sequence (Kim & Muallem, 2011). Recent advances in the use of cell penetrating peptides (CPPs or bioportides) provided an alternative mechanism for studying SOCE in human sperm (Jones *et al.*, 2013).

We observed that CPPs developed to include the KIKKK sequence essential to STIM and Orai interaction penetrated the human sperm cells in the absence of BSA (Jones *et al.*, 2013). In the presence of BSA CPP uptake was reduced which is potentially the result of membrane fluidity effects but the mechanism is unknown (data not included). The CPPs themselves exhibited inconsistent effects on basal $[Ca^{2+}]_i$ thought to be the combination of membrane translocation effects and SOCE activation, however after 5min the $[Ca^{2+}]_i$ effect established a sustained plateau. It should be noted that the original STIM KIKKK peptide and scrambled control peptide exhibited similar $[Ca^{2+}]_i$ effects however the KIKKK analogue which contained a more stabilised structure differed, most likely due to structural differences.

Our investigation of SOCE targeted CPPs on the biphasic $[Ca^{2+}]_i$ response at the PHN induced by 3μM progesterone substantiated our pharmacological modulation studies. In cells pre-treated with either of the KIKKK containing CPPs there was a significant increase in the proportion of cells that responded to progesterone with a rapid rise in $[Ca^{2+}]_i$ that was maintained for an extended period (monophasic $[Ca^{2+}]_i$ response; Figure 7.3B). This is likely the result of tonic activation of Orai through STIM KIKKK containing CPP interaction. Taken together these results indicate a role for SOCE in both potentiation and definition of the progesterone $[Ca^{2+}]_i$ transient at a Ca^{2+} store other than the mitochondria at the PHN.

The observations reported here indicate the existence of at least two discrete Ca^{2+} stores at the PHN of human sperm, each with discrete mechanisms of mobilisation and replenishment. Mitochondria demonstrate Ca^{2+} uptake and storage ability similar to that observed in somatic cells (Scorziello *et al.*, 2013), nevertheless contribution to the biphasic $[Ca^{2+}]_i$ progesterone response at the PHN is unable to fully account for the $[Ca^{2+}]_i$ response observed during

CatSper inhibition. Furthermore Ca^{2+} channels and proteins associated with intracellular Ca^{2+} storage organelles of somatic cells (SPCA1, RyR, IP_3R, STIM and calreticulin) and localised to the PHN do not typically associate with mitochondria (Harper *et al.*, 2004; Lefievre *et al.*, 2012; Naaby-Hansen *et al.*, 2001). Our investigations indicate the presence of an additional sperm specific Ca^{2+} store at the PHN sensitive to IP_3, 2-APB and SKF which is modulated by STIM and Orai facilitated SOCE. We propose that this store would amplify and propagate the progesterone induced $[Ca^{2+}]_i$ response at the PHN initiated by CatSper and has a potential role in regulation of motility (Figure 9.2).

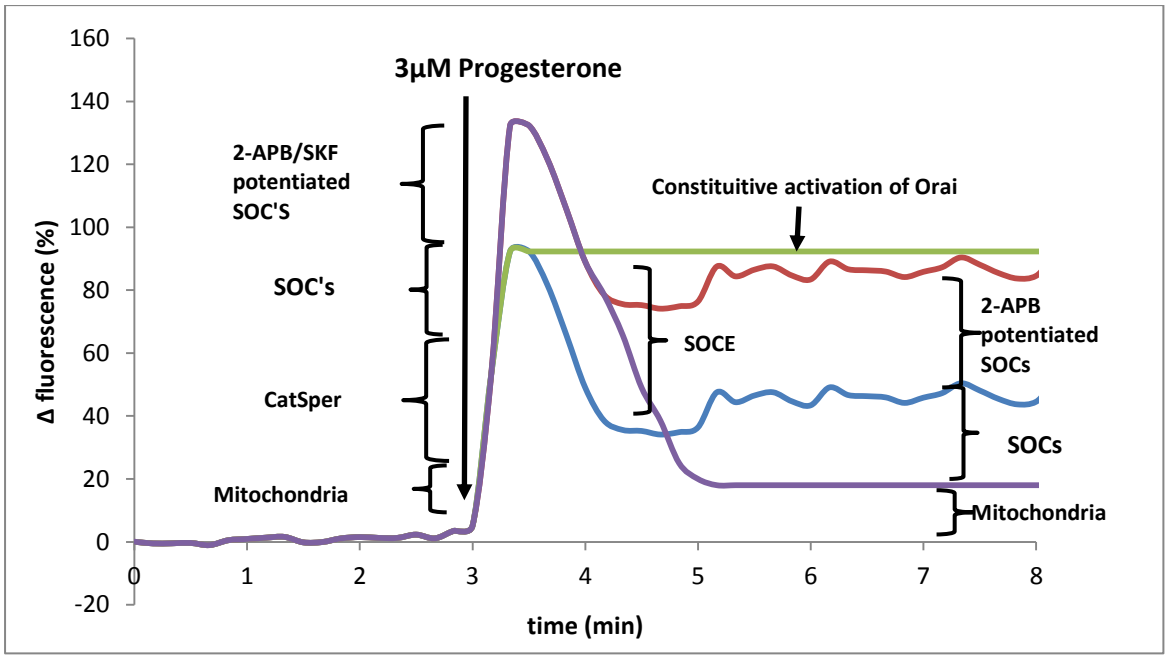

Figure 9.2 Ca^{2+} mechanisms responsible for the increases in $[Ca^{2+}]_i$ associated with progesterone. 3µM progesterone was added at 3 min (black arrow). The blue trace represents control cells responses in cells exposed to 3µM progesterone alone. The red trace represents cells treated with 5µM 2-APB prior to progesterone stimulation where potentiation is observed due to SOCs. The Purple trace represents cells treated with 30µM SKF. The green trace represents monophasic progesterone $[Ca^{2+}]_i$ increases associated with application of KIKKK containing STIM CPPs prior to progesterone, which demonstrates constitutive SOCE activation.

9.2 Future Work

Development of cell penetrating peptides (CPPs) or bioportides present numerous opportunities for elucidating intracellular signalling cascades in human sperm. To date the study of intracellular signalling cascades in intact human sperm has been hindered by the absence of clathrin mediated endocytosis. Manipulation of intracellular Ca^{2+} stores and the signalling pathways associated with them has been restricted to the use of cell permeable pharmacological modulators or studies of demembranated cells, whose responses may differ from those observed under normal physiological conditions. Here we have shown that sequence targeted CPPs are able to both penetrate and manipulate $[Ca^{2+}]_i$ in human sperm. Furthermore there is potential to develop new CPPs targeted to other Ca^{2+} channels associated with both intracellular Ca^{2+} storage organelles and the mitochondria. Indeed Jones *et al.,* 2013 demonstrated the innate predisposition of some CPPs to target intracellular organelles such as the mitochondria in bovine sperm. Future studies could utilise CPPs to determine the extent of mitochondrial Ca^{2+} accumulation through MCU and Ca^{2+}-ATPase targeted peptides. In addition CPPs could be developed to target IP_3R, to observe the effects on motility and the acrosome reaction. In conclusion CPPs provide a new mechanism for the study of intracellular Ca^{2+} signalling in sperm with the potential to elucidate a number of mechanisms responsible for cellular function. These peptides could potentially be utilised to treat sub-fertile individuals where SOCE and Ca^{2+} signalling pathways are impaired (Baldi *et al,* 1999; Espino *et al,* 2009). It would be interesting to observe the effects of both pharmacological modulators of SOCE 2-APB, SKF in conjunction with SOCE targeted CPPs in patients with pathological sub-fertility, to determine potential targets for personalised patient treatment.

CHAPTER TEN: REFERENCES

10.0 References

Alasmari, W., Costello, S., Correia, J., Oxenham, S.K., Morris, J., Fernandes, L., Ramalho-Santos, J., Kirkman-Brown, J., Michelangeli, F., Publicover, S. and Barratt, C.L. (2013). Ca2+ signals generated by CatSper and Ca2+ stores regulate different behaviours in human sperm. *J Biol Chem* **288**, 6248-58.

Alves, M.G., Rato, L., Carvalho, R.A., Moreira, P.I., Socorro, S. and Oliveira, P.F. (2013). Hormonal control of Sertoli cell metabolism regulates spermatogenesis. *Cell Mol Life Sci* **70**, 777-93.

Amaral, A., Lourenço, B., Marques, M. and Ramalho-Santos, J. (2013). Mitochondria functionality and sperm quality. *Reproduction* **146**, 163-74.

Anderson, A.N., Gianaroli, L., Felberbaum, R., Mouzon, J. & Nygren, K.G. (2002). Assisted reproductive technology in Europe, 2002. Results generated from European registers by ESHRE. *Reproduction* **21**, 1680-1697.

Ardon, F., Rodriguez-Miranda, E., Beltran, C., Hernandez-Cruz, A. and Darszon, A. (2009). Mitochondrial inhibitors activate influx of external Ca^{2+} in sea urchin sperm. *Biochim Biophys Acta* **1787**, 15–24.

Arienti, G., Carlini, E. and Palmerini, C.A. (1997). Fusion of human sperm to prostasomes at acidic pH. *J Membr Biol* **155**, 89–94.

Arienti, G., Carlini, E., Nicolucci, A., Cosmi, E.V., Santi, F. and Palmerini, C.A. (1999). The motility of human sperm as influenced by prostasomes at various pH levels. *Biol Cell* **91**, 51–54.

Arienti, G., Carlini, E., Saccardi, C. and Palmerini, C.A. (2004). Role of human prostasomes in the activation of sperm. *J Cell Mol Med* **8**, 77-84.

Arnheim, N. and Calabrese, P. (2009). Understanding what determines the frequency and pattern of human germline mutations. *Nature Reviews Genetics* **10**, 478-488.

Arnoult, C., Cardullo, R.A., Lemos, J.R. and Florman, H.M. (1996). Activation of mouse sperm T-type Ca^{2+} channels by adhesion to the egg zona pellucida. *Proc Natl Acad Sci USA* **93**, 13004–13009.

Arnoult, C., Villaz, M. and Florman, H.M. (1998). Pharmacological properties of the T-type Ca2+ current of mouse spermatogenic cells. *Mol Pharmacol* **53**, 1104-11.

Arnoult, C., Pierre, V. and Ray, P.F. (2011). [Chemotaxis of sperm is regulated by progesterone binding on calcium channel CATSPER]. *Med Sci* **27**, 702-4.

Austin, C.R. (1951). Observations on the penetration of sperm into the mammalian egg. *Aust J Sci* **4**, 581–596.

Austin, C.R. (1952). The "capacitation" of mammalian sperm. *Nature* **170**, 326.

Avella, M.A., Xiong, B. and Dean, J. (2013). The molecular basis of gamete recognition in mice and humans. *Mol Hum Reprod* **19**, 279-89.

Avidan, N., Tamary, H., Dgany, O., Cattan, D., Pariente, A., Thulliez, M., Borot, N., Moati, L. And Beckman, J.S. (2003). CATSPER2, a human autosomal nonsyndromic male infertility gene. *Eur J Hum Genet* **11**, 497-502.

Baba, Y., Hayashi, K., Fujii, Y., Mizushima, A., Watarai, H., Wakamori, M., Numaga, T., Mori, Y., Lino, M., Hikida, M. and Kurosaki, T. (2006). Coupling of STIM1 to store-operated Ca^{2+} entry through its constitutive and inducible movement in the endoplasmic reticulum. *Proc Natl Acad U S A* **103**, 16704-16709.

Babcock, D.F., First, N.L. and Lardy, H.A. (1976). Action of ionophore A23187 at the cellular level. Separation of effects at the plasma and mitochondrial membranes. *The Journal of Biological Chemistry* **251**, 3881–3886.

Babcock, D.F. and Pfeiffer, D.R. (1987). Independent elevation of cytosolic [Ca2+] and pH of mammalian sperm by voltage-dependent and pH-sensitive mechanisms. *J Biol Chem* **262**, 15041-7.

Bailey, J.L. (2010). Factors regulating sperm capacitation. *Syst Biol Reprod Med* **56**, 334-48.

Bailey, J.L. and Storey, B.T. (1994). Calcium influx into mouse sperm activated by solubilized mouse zona pellucida, monitored with the calcium fluorescent indicator, fluo-3. Inhibition of the influx by three inhibitors of the zona pellucida induced acrosome reaction: tyrphostin A48, pertussis toxin, and 3-quinuclidinyl benzilate. *Mol Reprod Dev* **39**, 297–308.

Baker, M.A., Hetherington, L. and Aitken, R.J. (2006). Identification of SRC as a key PKA-stimulated tyrosine kinase involved in the capacitation-associated hyperactivation of murine sperm. *J Cell Sci* **119**, 3182–92.

Baldi, E., Luconi, M., Bonaccorsi, L., Maggi, M., Francavilla, S., Gabriele, A., Properzi, G. and Forti, G. (1999). Nongenomic progesterone receptor on human sperm: biochemical aspects and clinical implications. *Steroids* **64**, 143-8.

Barratt, C.L. and Cooke, I.D. (1988). Sperm loss in the urine of sexually rested men. *Int J Androl* **11**, 201-207.

Barratt, C.L., Kay, V. & Oxenham, S.K. (2009). The human spermatozoon – a stripped down but refined machine. *J. Biol* **8**, 63.

Barratt, C.L.R and Publicover, S.J. (2001). Interaction between sperm and zona pellucida in male infertility. *Lancet* **358**, 1660-1662.

Barratt, C.L.R. and Publicover, S.J. (2012). Sperm are promiscuous and CatSper is to blame… *EMBO Journal* **31**, 1624–1626.

Baughman, J.M., Perocchi, F., Girgis, H.S., Plovanich, M., Belcher-Timme, C.A., Sancak, Y., Bao, X.R., Strittmatter, L., Goldberger, O., Bogorad, R.L., Koteliansky, V. and Mootha, V.K. (2011). Integrative genomics identifies MCU as an essential component of the mitochondrial calcium uniporter. *Nature* **476**, 341-5.

Bedu-Addo, K., Barratt, C.L.R., Kirkman-Brown, J.C. and Publicover, S.J. (2007). Patterns of $[Ca^{2+}]_i$ mobilization and cell response in human sperm exposed to progesterone. *Developmental Biology* **302**, 324-332.

Bello, A. (2012). Golden ratio discovered in uterus. *The Guardian* 14 August, p.10.

Bellve, A.R. & O'Brien, D.A. (1983).The Mammalian Spermatozoon: Structure and Temporal Assembly. Mechanism and control of animal fertilization. 1st Edition, London: Academic Press.

Benaroya, R.O., Orvieto, R., Gakamsky, A., Pinchasov, M. and Eisenbach, M. (2008). The sperm chemoattractant secreted from human cumulus cells is progesterone**.** *Hum. Reprod* **23**, 2339-2345.

Benoff, S., Cooper, G.W., Hurley, I., Mandel, F.S. and Rosenfeld, D.L. (1993). Antisperm antibody binding to human sperm inhibits capacitation induced changes in the levels of plasma membrane sterols. *Am J Reprod Immunol* **30**, 113-30.

Bercegeay S, Jean M, Lucas H, Barriere P. (1995). Composition of human zona pellucida as revealed by SDS-PAGE after silver staining. *Mol Reprod Dev* **41**, 355-9.

Berridge, M.J. (2000). The versatility and universality of calcium signalling. *Nature Reviews Molecular Cell Biology* **1**, 11-21.

Berridge, M.J. (2006). Calcium microdomains: organization and function. *Cell Calcium* **40**, 405-12.

Berridge, M.J. (2009). Inositol trisphosphate and calcium signalling mechanisms. *Biochim Biophys Acta* **1793**, 933-40.

Berridge, M.J. (2012). Calcium signalling remodelling and disease. *Biochem Soc Trans* **40**, 297-309.

Berridge, M.J., Bootman, M.D and Roderick, H.L. (2003). Calcium signalling: dynamics, homeostasis and remodelling. *Nat Rev Mol Cell Biol* **4**, 517-29.

Biel, M. (2009). Cyclic Nucleotide-regulated Cation Channels. *J Biol Chem* **284**, 9017–9021.

Biel, M. and Michalakis, S. (2007). Function and dysfunction of CNG channels: insights from channelopathies and mouse models. *Mol Neurobiol* **35**, 266-277.

Biel, M. and Michalakis, S. (2009). Cyclic Nucleotide-Gated Channels. *Handbook of Experimental Pharmacology* **191**, 111-136.

Blackmore, P.F. (1993). Rapid non-genomic actions of progesterone stimulate Ca2+ influx and the acrosome reaction in human sperm. *Cell Signal* **5**, 531-8.

Bleil, J.D. and Wassarman, P.M. (1980). Structure and function of the zona pellucida: identification and characterization of the proteins of the mouse oocyte's zona pellucida. *Dev Biol* **76**, 185-202.

Bogeski, I., Kilch, T. and Niemeyer, B.A. (2012). ROS and SOCE: recent advances and controversies in the regulation of STIM and Orai. *J Physiol* **590**, 4193-4200.

Bosanac, I., Alattia, J.R., Mal, T.K., Chan, J., Talarico, S., Tong, F.K., Tong, K.I., Yoshikawa, F., Furuichi, T., Iwai, M., Michikawa, T., Mikoshiba, K. and Ikura, M. (2002). Structure of the inositol 1,4,5-trisphosphate receptor binding core in complex with its ligand. *Nature* **420**, 696–700.

Brenker, C., Goodwin, N., Weyand, I., Kashikar, N.D., Naruse, M., Krähling, M., Müller, A., Kaupp, U.B. and Strünker, T. (2012). The CatSper channel: a polymodal chemosensor in human sperm. *EMBO J* **31**, 1654-65.

Brewer, L. R., Corzett, M., Lau, E. Y. and Balhorn, R. (2003). Dynamics of protamine 1 binding to single DNA molecules. *J. Biol. Chem* **278**, 42403- 42408.

Brini, M. (2004). Ryanodine receptor defects in muscle genetic diseases. *Biochem Biophys Res Commun* **322**, 1245–1255.

Brini, M. and Carafoli, E. (2009). Review Calcium pumps in health and disease. *Physiol Rev* **89**, 1341-78.

Brini, M. and Carafoli, E. (2011). The Plasma Membrane Ca2+ ATPase and the Plasma Membrane Sodium Calcium Exchanger Cooperate in the Regulation of Cell Calcium. *Cold Spring Harb Perspect Biol* **3**, a004168.

Bronson, R. (2011). Biology of the male reproductive tract: its cellular and morphological considerations. *Am J Reprod Immunol* **65**, 212-219.

Bultynck, G., Sienaert, I., Parys, J.B., Callewaert, G., De Smedt, H., Boens, N., Dehaen, W. and Missiaen, L. (2003). Pharmacology of inositol trisphosphate receptors. *Pflugers Arch* **445**, 629–642.

Bunch, D.O., Welch, J.E., Magyar, P.L., Eddy, E.M. and O'Brien, D.A. (1998). Glyceraldehyde 3-phosphate dehydrogenase-S protein distribution during mouse spermatogenesis. *Biol Reprod* **58**, 834-41.

Burden, H.P., Holmes, C.H., Persad, R. and Whittington, K. (2006). Prostasomes--their effects on human male reproduction and fertility. *Hum Reprod Update* **12**, 283-92.

Burkman, L.J. (1984). Characterization of hyperactivated motility by human sperm during capacitation: comparison of fertile and oligozoospermic sperm populations. *Arch Androl* **13**, 153-65.

Butler, D.M., Allen, K.M., Garrett, F.E., Lauzon, L.L., Lotfizadeh, A. and Koch, R.A. (1999). Release of Ca(2+) from intracellular stores and entry of extracellular Ca(2+) are involved in sea squirt sperm activation. *Dev Biol* **215**, 453-64.

Cahalan, M. (2009). STIMulating store-operated Ca^{2+} entry. *Nat Cell Biol* **11**, 669-677.

Cahalan, M.D., Zhang, S.L., Yeromin, A.V., Ohlsen, K., Roos, J. and Stauderman, K.A. (2012). Molecular basis of the CRAC channel. *Cell Calcium* **42**, 133-144.

Cai, X. (2007). Molecular Evolution and Structural Analysis of the Ca^{2+} Release-Activated Ca^{2+} Channel Subunit, Orai. *Journal of Molecular Biology* **368**, 1284–1291.

Calloway, N., Vig, M., Kinet, J. P., Holowka, D. and Baird, B. (2009). Molecular clustering of STIM1 with Orai1/CRACM1 at the plasma membrane depends dynamically on depletion of Ca^{2+} stores and on electrostatic interactions. *Mol Biol Cell* **20**, 389-399.

Calloway, N., Holowka, D. and Baird, B. (2010). A basic sequence in STIM1 promotes Ca2+ influx by interacting with the C-terminal acidic coiled-coil of Orai. *Biochemistry* **49**, 1067-1071.

Calogero, A.E., Burrello, N., Barone, N., Palermo, I., Grasso, U. and D'Agata, R. (2000). Effects of progesterone on sperm function: mechanisms of action. *Hum Reprod* **15**, 28-45.

Campbell, N. and Reece, J. (2004). Biology. 2nd Edition, London: *Pearson publishing inc.*

Carafoli, E. and Brini, M.R. (2000). Calcium pumps: structural basis for and mechanism of calcium transmembrane transport. *Curr Opin Chem Biol* **4**, 152–161.

Carlson, A.E., Westenbroek, R.E., Quill, T., Ren, D., Clapham, D.E., Hille, B., Garbers, D.L. and Babcock, D.F. (2003). CatSper1 required for evoked Ca2+ entry and control of flagellar function in sperm. *Proc Natl Acad Sci U S A* **100**, 14864-8.

Carlson, A.E., Hille, B. and Babcock, D.F. (2007). External Ca2+ acts upstream of adenylyl cyclase SACY in the bicarbonate signaled activation of sperm motility. *Dev Biol* **312**, 183-92.

Carrera, A., Gerton, G.L. and Moss, S.B. (1994). The major fibrous sheath polypeptide of mouse sperm: structural and functional similarities to the A-Kinase anchoring proteins. *Developmental Biology* **165**, 272-284.

Castellano, L.E., Treviño, C.L., Rodríguez, D., Serrano, C.J., Pacheco, J., Tsutsumi, V., Felix, R. and Darszon, A. (2003). Transient receptor potential (TRPC) channels in human **sperm**: expression, cellular localization and involvement in the regulation of flagellar motility. *FEBS Lett* **541**, 69-74.

Cataldo, L., Baig, K., Oko, R., Mastrangelo, M.A. and Kleene, K.C. (1996). Developmental expression, intracellular localization, and selenium content of the cysteine-rich protein associated with the mitochondrial capsules of mouse sperm. *Mol Reprod Dev* **45**, 320-31.

Catterall, W.A. (2000). Structure and regulation of voltage-gated Ca2+ channels. *Annu Rev Cell Dev Biol* **16**, 521–555.

Chakravarty, S., Kadunganattil, S., Bansal, P., Sharma, R.K. and Gupta, S.K. (2008). Relevance of glycosylation of human zona pellucida glycoproteins for their binding to capacitated human sperm and subsequent induction of acrosomal exocytosis. *Mol Reprod Dev* **75**, 75–88.

Chakravarty, S., Suraj, K. and Gupta, S.K. (2005). Baculovirus-expressed recombinant human zona pellucida glycoprotein-B induces acrosomal exocytosis in capacitated sperm in addition to zona pellucida glycoprotein-C. *Mol Hum Reprod* **11**, 365–72.

Chamberlin, M.E. and Dean, J. (1990). Human homolog of the mouse sperm receptor. *Proc Natl Acad Sci U S A* **87**, 6014-8.

Chang, M.C. (1951). Fertilizing capacity of sperm deposited into the fallopian tubes. *Nature* **168**, 697–698.

Chen, W.Y., Xu, W.M., Chen, Z.H., Ni, Y., Yuan, Y.Y., Zhou, S.C., Zhou, W.W., Tsang, L.L., Chung, Y.W., Höglund, P., Chan, H.C. and Shi, Q.X. (2009). Cl- is required for HCO3- entry necessary for sperm capacitation in guinea pig: involvement of a Cl-/HCO3- exchanger (SLC26A3) and CFTR. *Biol Reprod* **80**, 115-23.

Cheng, C.Y. and Mruk, D.D. (2012). The blood-testis barrier and its implications for male contraception. *Pharmacol Rev* **64**, 16-64.

Chiarella, P., Puglisi, R., Sorrentino, V., Boitani, C. and Stefanini, M. (2004). Ryanodine receptors are expressed and functionally active in mouse spermatogenic cells and their inhibition interferes with spermatogonial differentiation. *J Cell Sci* **117**, 4127-34.

Chocu, S., Calvel, P., Rolland, A.D. and Pineau, C. (2012). Spermatogenesis in mammals: proteomic insights. *Syst Biol Reprod Med* **58,**179-90.

Chung, J.J., Navarro, B., Krapivinsky, G., Krapivinsky, L. and Clapham, D.E. (2011). A novel gene required for male fertility and functional CATSPER channel formation in sperm. *Nat Commun* **2**, 153.

Cisneros-Mejorado, A. and Sánchez, D. (2011). A role for cyclic nucleotide-gated channels in the capacitation of mammalian sperm. *Proc West Pharmacol Soc* **54**, 27-29.

Conner, S.J., Lefièvre, L., Hughes, D.C. and Barratt, C.L. (2005). Cracking the egg: increased complexity in the zona pellucida. *Hum Reprod* **20**,1148-52.

Cooper, T.G. (2011). The epididymis, cytoplasmic droplets and male fertility. *Asian J Androl* **13**, 130-8.

Cooper, T.G. and Woolley, D.M. (1982). Stroboscopic illumination for the assessment of hyperactivated motility of mouse sperm. *J Exp Zool* **223**, 291-294.

Cooper, T.G. and Yeung, C.H. (2006). Computer-aided evaluation of assessment of "grade a" sperm by experienced technicians. *Fertil Steril* **85**, 220-4.

Cornwall, G.A. (2009). New insights into epididymal biology and function. *Hum Reprod Update* **15**, 213–227.

Costello, S, Michelangeli, F., Nash, K., Lefievre, L., Morris, J., Machado-Oliveira, G., Barratt, C., Kirkman-Brown, J. and Publicover, S. (2009). Ca2+-stores in sperm: their identities and functions. *Reprod* **138**, 425-437.

Cross, N.L. (2004). Reorganization of lipid rafts during capacitation of human sperm. *Biol Reprod* **71**, 1367-73.

Cross, N.L., Morales, P., Overstreet, J.W. and Hanson, F.W. (1988). Induction of acrosome reaction by the human zona pellucida. *Biol Reprod* **38**, 235–44.

Cummins, J.M. and Woodall, P.F. (1985). On mammalian sperm dimensions. *J. Reprod. Fertil* **75**, 153-175.

Dacheux, J.L., Belleannée, C., Guyonnet, B., Labas, V., Teixeira-Gomes, A.P., Ecroyd, H., Druart, X., Gatti, J.L. and Dacheux, F. (2012). The contribution of proteomics to understanding epididymal maturation of mammalian sperm. *Syst Biol Reprod Med* **58**, 197-210.

da Fonseca, P.C., Morris, S.A., Nerou, E.P., Taylor, C.W. and Morris, E.P. (2003). Domain organization of the type 1 inositol 1,4,5-trisphosphate receptor as revealed by single-particle analysis. *Proc Natl Acad Sci USA* **100**, 3936–3941.

Darszon, A., Acevedo, J.J., Galindo, B.E., Hernández-González, E.O., Nishigaki, T., Treviño, C.L., Wood, C. and Beltrán, C. (2006). Sperm channel diversity and functional multiplicity. *Reproduction* **131**, 977-988.

Darszon, A., Nishigaki, T., Beltran, C. and Trevino, C.L. (2011). Calcium Channels in the Development, Maturation, and Function of Sperm. *Physiol Rev* **91**, 1305-1355.

DasGupta, S., O'Toole, C., Mills, C.L. and Fraser, L.R. (1994). Effect of pentoxifylline and progesterone on human sperm capacitation and acrosomal exocytosis. *Hum Reprod* **9**, 2103-9.

Davies, E.V., Campbell, A.K. and Hallett, M.B. (1992). Dissociation of store release from transmembrane influx of calcium in human neutrophils. *FEBS Lett* **313**, 121-125.

D'Cruz, O.J., Wang, B-L. and Haas, G.G. Jr. (1992). Phagocytosis of immunoglobulin G and C3-bound human sperm by human polymorphonuclear leukocytes is not associated with the release of oxidative radicals. *Biol Reprod* **46**, 721–732.

DeHaven, W.I., Smyth, J.T., Boyles, R.R., Bird, G. S. and Putney, Jr J.W. (2008). Complex actions of 2-aminoethyldiphenyl borate on store operated Ca^{2+} entry. *J. Biol. Chem* **283**, 19265-19273.

De Jonge, C. (2005). Biological basis for human capacitation. *Hum Reprod Update* **11**, 205-14.

Demarco, I.A., Espinosa, F., Edwards, J., Sosnik, J., De La Vega-Beltran, J.L., Hockensmith, J.W., Kopf, G.S., Darszon, A. and Visconti, P.E. (2003). Involvement of a Na+/HCO-3 cotransporter in mouse sperm capacitation. *J Biol Chem* **278**, 7001-9.

Derossi, D., Joliot, A.H., Chassaing, G. and Prochiantz, A. (1994). The third helix of the Antennapedia homeodomain translocates through biological membranes. *J Biol Chem* **269**, 10444-50.

Diaz, A., Dominguez, I., Fornes, M.W., Burgos, M.H. and Mayorga, L.S. (1996). Acrosome content release in streptolysin O permeabilized mouse sperm. *Andrologia* **28**, 21–26.

Dragileva, E., Rubinstein, S. and Breitbart, H. (1999). Intracellular Ca(2+)-Mg(2+)-ATPase regulates calcium influx and acrosomal exocytosis in bull and ram sperm. *Biol Reprod* **61**, 1226-34.

Duchardt, F., Fotin-Mleczek, M., Schwarz, H., Fischer, R. and Brock, R. (2007). A comprehensive model for the cellular uptake of cationic cell-penetrating peptides. *Traffic* **8**, 848-66.

Duchen, M.R. (1999). Contributions of mitochondria to animal physiology: from homeostatic sensor to calcium signalling and cell death. *The Journal of Physiology* **516**, 1-17.

Duchen, M.R. (2000) Mitochondria and calcium: from cell signalling to cell death. *J Physiol* **529**, 57-68.

Dyer, J.L. and Michelangeli, F. (2001). Inositol 1,4,5-trisphosphate receptor isoforms show similar Ca^{2+} release kinetics. *Cell Calcium* **30**, 245–250.

Eddy, E.M., Toshimori, K. and O'Brien, D.A. (2003). Fibrous sheath of mammalian sperm. *Microsc Res Tech* **61**, 103–115.

Erkkila, K., Kyttanen, S., Wikstrom, M., Taari, K., Hikim, A.P., Swerdloff, R.S. and Dunkel, L. (2006). Regulation of human male germ cell death by modulators of ATP production. *Am J Physiol Endocrinol Metab* **290**, 1145-54.

Espino, J., Mediero, M., Lozano, G.M., Bejarano, I., Ortiz, A., García, J.F., Pariente, J.A. and Rodríguez, A.B. (2009). Reduced levels of intracellular calcium releasing in sperm from asthenozoospermic patients. *Reprod Biol Endocrinol* **6**, 7-11.

Evans, J.P. (2002). The molecular basis of sperm-oocyte membrane interactions during mammalian fertilization. *Human reproduction update* **8,** 297-311.

Evenson, D.P., Darzynkiewicz, Z. and Melamed, M.R. (1982). Simultaneous measurement by flow cytometry of sperm cell viability and mitochondrial membrane potential related to cell motility. *J Histochem Cytochem* **30**, 279-80.

Fawcett, D.W. and Porter, K.R. (1954). A study of the fine structure of ciliated epithelia. *J. Morph* **94**, 221-282.

Feske, S., Gwack, Y., Prakriya, M., Srikanth, S., Puppel, S.H., Tanasa, B., Hogan, P.G., Lewis, R.S., Daly, M. and Rao, A. (2006). A mutation in Orai1 causes immune deficiency by abrogating CRAC channel function. *Nature* **441**, 179.

Feske, S. (2009). ORAI1 and STIM1 deficiency in human and mice: roles of store-operated Ca2+ entry in the immune system and beyond. *Immunol Rev* **231**, 189-209.

Ford, W.C.L. (2006). Glycolysis and sperm motility: does a spoonful of sugar help the flagellum go round? *Human Reproduction Update* **12**, 269-274.

Ford, W.C. and Harrison, A. (1981). The role of oxidative phosphorylation in the generation of ATP in human sperm. *J Reprod Fertil* **63**, 271-8.

Franca, L.R., Parreira, G.G., Gates, R.J. and Russell, L.D. (1998). Hormonal regulation of spermatogenesis in the hypophysectomised rat: quantitation of Germ-cell population and effect of testosterone after long-term hypophysectomy. *Journal of Andrology* **19**, 335-342.

Franken, D.R., Bastiaan, H.S. and Oehninger, S.C. (2000). Physiological induction of the acrosome reaction in human sperm: validation of a microassay using minimal volumes of solubilized, homologous zona pellucida. *J Assist Reprod Genet* **17**, 374–8.

Fraser, L.R., Adeoya-Osiguwa, S.A., Baxendale, R.W. and Gibbons, R. (2006). Regulation of mammalian sperm capacitation by endogenous molecules. *Front Biosci* **11**, 1636-45.

Frischauf, I., Schindl, R., Derler, I., Bergsmann, J., Fahrner, M. and Romanin, C. (2008). The STIM/Orai coupling machinery. *Channels* **2**, 261-8.

Fukuda, M.N. and Sugihara, K. (2012). Trophinin in cell adhesion and signal transduction. *Front Biosci* **4,** 342-350.

Gadella, B.M. and Evans, J.P. (2011). Membrane fusions during mammalian fertilization. *Adv Exp Med Biol* **713**, 65–80.

Gadella, B.M and Visconti, P.E. (2006). Regulation of capacitation. *The Sperm Cell* (ed. C. DeJonge and C. Barratt), 1st Edition, Cambridge: Cambridge University Press.

Gagnon, C. and de Lamirande, E. (2006).Regulation of capacitation. *The Sperm Cell* (ed. C. DeJonge and C. Barratt), 1st Edition, Cambridge: Cambridge University Press.

Galione, A., Jones, K.T., Lai, F.A., and Swann, K. (1997). A cytosolic sperm protein factor mobilizes Ca2+ from intracellular stores by activating multiple Ca2+ release mechanisms independently of low molecular weight messengers. *J Biol Chem* **272**, 28901-5.

Gallon, F., Marchetti, C., Jouy, N. and Marchetti, P. (2006). The functionality of mitochondria differentiates human sperm with high and low fertilizing capability. *Fertil Steril* **86**, 1526-30.

Gamlin, L. &Vane, G. (1987).The evolution of Life. 1st Edition, New York: Oxford University Press.

Ghazal, S. (2013). Oogonial stem cells: do they exist and may they have an impact on future fertility treatment? *Curr Opin Obstet Gynecol* **25**, 223-8.

Giacomello, M., Drago, I., Pizzo, P. and Pozzan, T. (2007). Mitochondrial Ca2+ as a key regulator of cell life and death. *Cell Death Differ* **14**, 1267-74.

Giannini, G., Conti, A., Mammarella, S., Scrobogna, M. and Sorrentino, V. (1995). The ryanodine receptor/calcium channel genes are widely and differentially expressed in murine brain and peripheral tissues. *J Cell Biol* **128**, 893–904.

Gilbert, S.F. (2004). Developmental Biology, 2nd Edition, London: Pearson publishing inc.

Giuliano, F. and Clément, P. (2005). Physiology of ejaculation: emphasis on serotonergic control. *Eur Urol* **48**, 408-17.

Gonzalez-Martinez, M.T., Bonilla-Hernandez, M.A. and Guzman-Grenfell, A.M. (2002). Stimulation of Voltage dependent calcium channels during capacitation and by progesterone in human sperm. *Arch Biochem Biophys* **408**, 205-210.

Goodwin, L.O., Karabinus, D.S., Pergolizzi, R.G. and Benoff, S. (2000) L-type voltage-dependent calcium channel α1C subunit mRNA is present in ejaculated human sperm. *Mol Hum Reprod* **6**, 127–136.

Goto, J.I., Suzuki, A.Z., Ozaki, S., Matsumoto, N., Nakamura, T., Ebisui, E., Fleig, A., Penner, R. and Mikoshiba, K. (2010). Two novel 2-aminoethyl diphenylborinate (2-APB) analogues differentially activate and inhibit store-operated Ca^{2+} entry via STIM proteins. *Cell Calcium* **47**, 1–10.

Greve, J.M. and Wassarman, P.M. (1985). Mouse egg extracellular coat is a matrix of interconnected filaments possessing a structural repeat. *J Mol Biol* **181**, 253–264.

Griswold, M.D. and Oatley, J.M. (2013). Concise review: Defining characteristics of mammalian spermatogenic stem cells. *Stem Cells* **31,** 8-11.

Gunaratne, H.J. and Vacquier, V.D. (2006). Evidence for a secretory pathway Ca2+-ATPase in sea urchin sperm. *FEBS Lett* **580**, 3900-4.

Gunteski-Hamblin, A.M., Clarke, D.M. and Shull, G.E. (1992). Molecular cloning and tissue distribution of alternatively spliced mRNAs encoding possible mammalian homologues of the yeast secretory pathway calcium pump. *Biochemistry* **31**, 7600–7608.

Gupta, S.K. and Bhandari, B. (2011). Acrosome reaction: relevance of zona pellucida glycoproteins. *Asian Journal of Andrology* **13,** 97–105.

Gupta, S.K., Bhandari, B., Shrestha, A., Biswal, B.K., Palaniappan, C., Malhotra, S.S. and Gupta, N. (2012). Mammalian zona pellucida glycoproteins: structure and function during fertilization. *Cell Tissue Res* **349**, 665-78.

Guzmán-Grenfell, A.M., Bonilla-Hernández, M.A. and González-Martínez, M.T. (2000). Glucose induces a Na(+),K(+)-ATPase-dependent transient hyperpolarization in human sperm. I. Induction of changes in plasma membrane potential by the proton ionophore CCCP. *Biochim Biophys Acta* **1464**, 188-98.

Gwack, Y., Srikanth, S., Feske, S., Cruz-Guiloty, F., Oh-hora, M., Neems, D.S, Hogan, P.G, Rao, A. (2007). Biochemical and functional characterization of Orai proteins. *J Biol Chem* **282**, 1623-1643.

Hamilton, D.W. and Waites, G.M. (1990). Cellular and molecular events in spermiogenesis, 1st Edition, New York: Cambridge University Press.

Harper, C.V., Barratt, C.L.R., Publicover, S.J. (2004). Stimulation of Human Sperm with progesterone gradients to stimulate approach to the oocyte. *J Biol Chem* **279**, 46315-46325.

Harper, C.V., Cummerson, J.A., White, M.R., Publicover, S.J. and Johnson, P.M. (2008). Dynamic resolution of acrosomal exocytosis in human sperm. *J Cell Sci* **121**, 2130-5.

Harper, C.V., Kirkman- Brown, J.C., Barratt, C.L.R. and Publicover, S.J. (2003). Encoding of progesterone stimulus intensity by intracellular calcium in human sperm. *Biochem. J* **372**, 407-417.

Harper, C.V. and Publicover, S.J. (2005). Reassessing the role of progesterone in fertilization – compartmentalized calcium signalling in human sperm? *Human Reproduction* **20,** 2675-2680.

Harper, C., Wootton, L., Michelangeli, F., Lefievre, L., Barratt, C. and Publicover, S. (2005). Secretory pathway Ca^{2+}-ATPase (SPCA1) Ca^{2+} pumps, not SERCAs, regulate complex $[Ca^{2+}]_i$ signals in human sperm. *J Cell Sci* **118**, 1673–1185.

Harrison, R.A. and Miller, N.G. (2000). cAMP-dependent protein kinase control of plasma membrane lipid architecture in boar sperm. *Mol Reprod Dev* **55**, 220-8.

Hasegawa, A., Koyama, K. and Isojima, S. (1991). Isolation of four major glycoprotein families (ZP1, ZP2, ZP3, ZP4) of porcine zona pellucida and characterization of antisera raised to each glycoprotein family. *Nihon Sanka Fujinka Gakkai Zasshi* **43**, 221-6.

Herrick, S.B., Schweissinger, D.L., Soo-Woo, K., Bayan, K.R., Mann, S. and Cardullo, R.A. (2005). The acrosomal vesicle of mouse sperm is a calcium store. *J Cell Physiol* **202**, 663–671.

Hildebrand, M.S., Avenarius, M.R., Fellous, M., Zhang, Y., Meyer, N.C., Auer, J., Serres, C., Kahrizi, K., Najmabadi, H., Beckmann, J.S. and Smith, R.J. (2010). Genetic male infertility and mutation of CATSPER ion channels. *Eur J Hum Genet* **18**, 1178-84.

Hilge, M. (2012). Ca2+ regulation of ion transport in the Na+/Ca2+ exchanger. *J Biol Chem* **287**, 31641-9.

Hirohashi, N. and Vacquier, V.D. (2003). Store-operated calcium channels trigger exocytosis of the sea urchin sperm acrosomal vesicle. *Biochem Biophys Res Commun* **304**, 285-92.

Ho, H.C., Granish, K.A. and Suarez, S.S. (2002). Hyperactivated motility of bull sperm is triggered at the axoneme by Ca^{2+} and not cAMP. *Dev Biol* **250**, 208-217.

Ho, H.C. and Suarez, S.S. (2001). An inositol 1,4,5-trisphosphate receptor-gated intracellular Ca2+store is involved in regulating sperm hyperactivated motility. *Biol Reprod* **65**, 1606-1615.

Ho, H.C. and Suarez, S.S. (2003). Characterization of the intracellular calcium store at the base of the sperm flagellum that regulates hyperactivated motility. *Biol Reprod* **68**, 1590–1596.

Holstein, A.F., Schulze, W. and Davidoff, M. (2003). Understanding spermatogenesis is a prerequisite for treatment. *Reprod Biol Endocrinol* **1**, 107.

Holt, W.V. and Fazeli, A. (2010). The Oviduct as a Complex Mediator of Mammalian Sperm Function and Selection. *Molecular Reproduction & Development* **77**, 934-943.

Hong, C.Y., Huang, J.J., Chiang, B.N. and Wei, Y.H. (1986). The inhibitory effect of some ionophores on human sperm motility. *Contraception* **33**, 301-6.

Hong, S.J., Lin, W.W. and Chang, C.C. (1994). Inhibition of the Sodium Channel by SK&F 96365, an Inhibitor of the Receptor-Operated Calcium Channel, in Mouse Diaphragm. *J Biomed Sci* **1**, 172-178.

Hoth, M. and Penner, R. (1992). Depletion of intracellular calcium stores activates a calcium current in mast cells. *Nature* **355**, 353–355.

Howl, J., Matou-Nasri, S., West, D.C., Farquhar, M., Slaninová, J., Ostenson, C.G., Zorko, M., Ostlund, P., Kumar, S., Langel, U., McKeating, J. and Jones, S. (2012). Bioportide: an emergent concept of bioactive cell-penetrating peptides. *Cell Mol Life Sci* **69**, 2951-66.

Huang, L., Keyser, B.M., Tagmose, T.M., Hansen, J.B., Taylor, J.T., Zhuang, H., Zhang, M., Ragsdale, D.S. and Li, M. (2004). NNC 55-0396 [(1S,2S)-2-(2-(N-[(3-benzimidazol-2-yl)propyl]-N-methylamino)ethyl)-6-fluoro-1,2,3,4-tetrahydro-1-isopropyl-2-naphtyl cyclopropanecarboxylate dihydrochloride]: a new selective inhibitor of T-type calcium channels. *Journal of Pharmacology and Experimental Therapeutic.* **58**, 78-85.

Huang, G.N., Zeng, W., Kim, J.Y., Yuan, J.P., Han, L., Muallem, S. and Worley, P.F. (2006). STIM1 carboxyl-terminus activates native SOC, I(crac) and TRPC1 channels. *Nat Cell Biol* **8**, 1003-1010.

Hughes, P.J., McLellan, H., Lowes, D.A., Kahn, S.Z., Bilmen, J.G., Tovey, S.C., Godfrey, R.E., Michell, R.H., Kirk, C.J. and Michelangeli, F. (2000). Estrogenic alkylphenols induce cell death by inhibiting testis endoplasmic reticulum Ca(2+) pumps. *Biochem Biophys Res Commun* **277**, 568-74.

Hyne, R.V., Murdoch, R.N. and Boettcher, B. (1978). The metabolism and motility of human sperm in the presence of steroid hormones and synthetic progestagens. *J Reprod Fertil* **53**,315-22.

Ickowicz, D., Finkelstein, M. and Breitbart, H. (2012). Mechanism of sperm capacitation and the acrosome reaction: role of protein kinases. *Asian J Androl* **14**, 816-21.

Ikemoto, T., Iino, M. and Endo, M. (1995). Enhancing effect of calmodulin on Ca^{2+}-induced Ca^{2+} release in the sarcoplasmic reticulum of rabbit skeletal muscle fibers. *J. Physiol* **487**, 573–582.

Ilio, K.Y. and Hess, R.A. (1994). Structure and function of the ductuli efferentes: a review. *Microsc Res Tech* **29**, 432-467.

Ishijima, S. (2011). Dynamics of flagellar force generated by a hyperactivated spermatozoon. *Reproduction September* **142,** 409-415.

Ito, C., Akutsu, H., Yao, R., Kyono, K., Suzuki-Toyota, F., Toyama, Y., Maekawa, M., Noda, T. and Toshimor, K. (2009). Oocyte activation ability correlates with head flatness and presence of perinuclear theca substance in human and mouse sperm. *Human reproduction* **24**, 2588-2595.

Iwasaki, H., Mori, Y., Hara, Y., Uchida, K., Zhou, H. and Mikoshiba, K. (2001). 2-Aminoethoxydiphenyl borate (2-APB) inhibits capacitative calcium entry independently of the function of inositol 1,4,5-trisphosphate receptors. *Receptors Channels* **7**, 429–39.

Jagannathan, S., Punt, E.L., Gu, Y., Arnoult, C., Sakkas, D., Barratt, C.L. and Publicover, S.J. (2002). Identification and localization of T-type voltage-operated calcium channel subunits in human male germ cells. Expression of multiple isoforms. *J Biol Chem* **277**, 8449–8456.

Jan, C.R., Ho, C.M., Wu, S.N. and Tseng, C.J. (1999). Multiple effects of 1-[beta-[3-(4-methoxyphenyl)propoxy]-4-methoxyphenethyl]-1H-imidazole hydrochloride (SKF 96365) on Ca2+ signaling in MDCK cells: depletion of thapsigargin-sensitive Ca2+ store followed by capacitative Ca2+ entry, activation of a direct Ca2+ entry, and inhibition of thapsigargin-induced capacitative Ca2+ entry. *Naunyn Schmiedebergs Arch Pharmacol* **359**, 92-101.

Jantaratnotai, N., Choi, H.B. and McLarnon, J.G. (2009). ATP stimulates chemokine production via a store-operated calcium entry pathway in C6 glioma cells. *BMC Cancer* **9**, 442.

Jensen, M.B. and Publicover, S.J. (2012). Progesterone and CatSper dependency. *J Androl* **35**, 631–632.

Ji, W., Xu, P., Li, Z., Lu, J., Liu, L., Zhan, Y., Chen, Y., Hille, B., Xu, T. and Chen, L. (2008). Functional Stoichiometry of the unitary calcium-release-activated calcium channel. Proc. Natl Acad. Sci. USA **105**, 13668-13673.

Jimenez-Gonzalez, C., Michelangeli, F., Harper, C.V., Barratt, C.L. and Publicover, S.J. (2006). Calcium signaling in human sperm: a specialized 'toolkit' of channels, transporters and stores. **12,** 253-267.

Jin, J., Jin, N., Zheng, H., Ro, S., Tafolla, D., Sanders, K.M., Yan, W. (2007). Catsper3 and Catsper4 are essential for sperm hyperactivated motility and male fertility in the mouse. *Biol Reprod* **77**, 37-44.

Johansson, H.J., Andaloussi, S.E. and Langel, U. (2011). Mimicry of protein function with cell-penetrating peptides. *Methods Mol Biol* **683**, 233-47.

Johnson, M.H. (2013). Essential Reproduction. 7th Edition, West Sussex: Wiley-Blackwell.

Johnson, M.H. and Everitt, B.J. (2000). Essential Reproduction. 5th Edition, London: Blackwell Science Ltd.

Jones, R., James, P.S., Howes, L., Bruckbauer, A. and Klenerman, D. (2007). Supramolecular organization of the sperm plasma membrane during maturation and capacitation. *Asian J Androl* **9**, 438-44.

Jones, S. and Howl, J. (2012). Enantiomer-specific bioactivities of peptidomimetic analogues of mastoparan and mitoparan: characterization of inverso mastoparan as a highly efficient cell penetrating peptide. *Bioconjug Chem* **23**, 47-56.

Jones, S., Lukanowska, M., Suhorutsenko, J., Oxenham, S., Barratt, C., Publicover, S., Copolovici, D.M., Langel, Ü. and Howl, J. (2013). Intracellular translocation and differential accumulation of cell-penetrating peptides in bovine sperm: evaluation of efficient delivery vectors that do not compromise human sperm motility. *Hum Reprod* **28(7)**, 1874-89.

Juyena, N.S. and Stelletta, C. (2012). Seminal plasma: an essential attribute to sperm. *J Androl* **33**, 536-51.

Kaji, K. and Kudo, A. (2004). The mechanism of sperm-oocyte fusion in mammals. *Reproduction* **127**, 423-429.

Kang, J.K., Lee, Y.J., No, K.O., Jung, E.Y., Sung, J.H., Kim, Y.B. and Nam, S.Y. (2002). Ginseng intestinal metabolite-I (GIM-I) reduces doxorubicin toxicity in the mouse testis. *Reproductive Toxicology* **16**, 291-298.

Kerr, C.L., Hanna, W.F., Shaper, J.H. and Wright, W.W. (2002). Characterization of zona pellucida glycoprotein 3 (ZP3) and ZP2 binding sites on acrosome-intact mouse sperm. *Biol Reprod* **6**, 1585-95.

Khattri, A., Reddy, V.P., Pandey, R.K., Sudhakar, D.V., Gupta, N.J., Chakravarty, B.N., Deenadayal, M., Singh, L. and Thangaraj, K. (2012). Novel mutations in

calcium/calmodulin-dependent protein kinase IV (CAMK4) gene in infertile men. *Int J Androl* **35**, 810-8.

Kim, J.Y. and Muallem, S. (2011). Unlocking SOAR releases STIM. *The EMBO Journal* **30**, 1673-1675.

Kimlicka, L. and Van Petegem, F. (2011). The structural biology of ryanodine receptors. *Sci China Life Sci* **54**, 712-24.

Kirichok, Y. and Lishko, P.V. (2011). Rediscovering sperm ion channels with the patch-clamp technique. *Mol Hum Reprod* **17**, 478-99.

Kirkman-Brown, J.C., Bray, C., Stewart, P.M., Barratt, C.L. and Publicover, S.J. (2000). Biphasic elevation of $[Ca^{(2+)}](i)$ in individual human sperm exposed to progesterone. *Dev Biol* **222**, 326-35.

Kohlhaas, M. and Maack, C. (2013). Calcium release microdomains and mitochondria. *Cardiovasc Res.* [Epub ahead of print]

Kopera, I.A., Bilinska, B., Cheng, C.Y. and Mruk. D.D. (2010). Sertoli–germ cell junctions in the testis: a review of recent data. *Philos Trans R Soc Lond B Biol Sci* **365**, 1593–1605.

Kraev, A., Quednau, B.D., Leach, S., Li, X.F., Dong, H., Winkfein, R., Perizzolo, M., Cai, X., Yang, R., Philipson, K.D. et al. (2001). Molecular cloning of a third member of the potassium-dependent sodium-calcium exchanger gene family, NCKX3. *J Biol Chem* **276**, 23161–23172.

Krapf, D., Arcelay, E., Wertheimer, E.V., Sanjay, A., Pilder, S.H. *et al*. (2010). Inhibition of Ser/Thr phosphatases induces capacitation-associated signaling in the presence of Src kinase inhibitors. *J Biol Chem* **285**, 7977–85.

Krasznai, Z., Krasznai, Z.T., Morisawa, M., Bazsáné, Z.K., Hernádi, Z., Fazekas, Z., Trón, L., Goda, K. and Márián, T. (2006). Role of the Na+/Ca2+ exchanger in calcium homeostasis and human sperm motility regulation. *Cell Motil Cytoskeleton* **63**, 66-76.

Kruse HJ, Mayerhofer C, Siess W, Weber PC. (1995). Thrombin receptor-activating peptide sensitizes the human endothelial thrombin receptor. *Am J Physiol* **268**, 36-44.

Kumar, P.G. and Shoeb, M. (2011). The Role of TRP Ion Channels in Testicular Function. *Advances in Experimental Medicine and Biology* **704**, 881-908

Kuroda, Y., Kaneko, S., Yoshimura, Y., Nozawa, S. and Mikoshiba, K. (1999). Are there inositol 1,4,5-triphosphate (IP3) receptors in human sperm? *Life Sci* **65**,135–143.

Lanner, J.T. (2012). Ryanodine receptor physiology and its role in disease. *Adv Exp Med Biol* **740**, 217-34.

Lawson, C., Dorval, V., Goupil, S. and Leclerc, P. (2007). Identification and localisation of SERCA 2 isoforms in mammalian sperm. *Mol Hum Reprod* **13**, 307-16.

Lawson, C., Goupil, S. and Leclerc, P. (2008). Increased activity of the human sperm tyrosine kinase SRC by the cAMP-dependent pathway in the presence of calcium. *Biol Reprod* **79**, 657–66.

Lefievre, L., De Lamirande, E., Gagnon, C. (2000). The cyclic GMP-specific phosphodiesterase inhibitor, sildenafil, stimulates human sperm motility and capacitation but not acrosome reaction. *J Androl* **21**, 929-937.

Lefièvre, L., Conner, S.J., Salpekar, A., Olufowobi, O., Ashton, P., Pavlovic, B., Lenton, W., Afnan, M., Brewis, I.A., Monk, M., Hughes, D.C. and Barratt, C.L. (2004). Four zona pellucida glycoproteins are expressed in the human. *Hum Reprod* **19**, 1580-6.

Lefievre, L., Chen, Y., Conner, S. J., Scott, J., Publicover, S., Ford, W., Barratt, C.L.R. (2007). Human Sperm Contain multiple Targets for Protein S-Nitrosylation: An alternative Mechanism of the Modulation of Sperm Function by Nitric Oxide? *Proteomics* **7,** 3066-3084.

Lefièvre, L., Nash, K., Mansell, S., Costello, S., Punt, E., Correia, J., Morris, J., Kirkman-Brown, J., Wilson, S.M., Barratt, C.L.R. and Publicover, S. (2012). 2-APB-potentiated channels amplify CatSper-induced Ca^{2+} signals in human sperm. *Biochem. J* **448,** 189–200.

Lencesova, L. & Krizanova, O. (2012). IP(3) receptors, stress and apoptosis. *Gen Physiol Biophys* **31**, 119-30.

Lenzi, A., Picardo, M., Gandini, L. and Dondero, F. (1996). Lipids of the sperm plasma membrane: from polyunsaturated fatty acids considered as markers of sperm function to possible scavenger therapy. *Hum Reprod Update* **2**, 246–256.

Leung, A., Shapiro, B. and Brown, M. (1996). I-131 localization in acute megakaryocytic leukemia. *Clin Nucl Med* **21**, 950-2.

Lewis, R.S. *(*2011*).* Store-operated calcium channels: new perspectives on mechanism and function. *Cold Spring Harb Perspect Biol* **3**, pii: a003970.

Li, C. and Zhou, X. (2012). Gene transcripts in sperm: markers of male infertility. *Clin Chim Acta* **413**, 1035-8.

Li, L. and Moore, P.K. (2007). An overview of the biological significance of endogenous gases: new roles for old molecules. *Biochem Soc Trans* **35**, 1138-1141.

Li, R. and Albertini, D.F. (2013). The road to maturation: somatic cell interaction and self-organization of the mammalian oocyte. *Nat Rev Mol Cell Biol* **14**, 141-52.

Liao, Y., Erxleben, C., Abramowitz, J., Flockerzi, V., Zhu, M.X., Armstrong, D.L. and Birnbaumer, L. (2008). Functional interactions among Orai1, TRPCs, and STIM1 suggest a STIM-regulated heteromeric Orai/TRPC model for SOCE/Icrac channels. *Proc Natl Acad Sci U S A* **105**, 2895-900.

Liao, Y., Plummer, N. W., George, M. D., Abramowitz, J., Zhu, M. X. and Birnbaumer, L. (2009). A role for Orai in TRPC-mediated Ca^{2+} entry suggests that a TRPC:Orai complex may mediate store and receptor operated Ca^{2+} entry. *Proc. Natl. Acad. Sci. U.S.A.* **106**, 3202–3206.

Lievano, A., Santi, C.M., Serrano, C.J., Trevino, C.L., Bellve, A.R., Hernandez-Cruz, A. and Darszon, A. (1996). T-type Ca2+ channels and alpha1E expression in spermatogenic cells, and their possible relevance to the sperm acrosome reaction. *FEBS Lett* **388**, 150–154.

Lindberg, S., Copolovici, D.M. and Langel, U. (2011). Therapeutic delivery opportunities, obstacles and applications for cell-penetrating peptides. *Ther Deliv* **2**, 71-82.

Liou, J., Kim, M.L., Heo, W.D., Jones, J.T., Myers, J.W., Ferrell, J.E. and Meyer, T. (2005). STIM is a Ca^{2+} sensor essential for Ca^{2+} store depletion triggered Ca^{2+} influx. *Curr Biol* **15**, 1235.

Liou, J., Fivaz, M., Inoue, T and Meyer, T. (2007). Live-cell imaging reveals sequential oligomerization and local plasma membrane targeting of stromal interaction molecule 1 after Ca^{2+} store depletion. *Proc Natl Acad Sci U S A* **104**, 9301-9306.

Lis, A., Peinelt, C., Beck, A., Parvez, S., Monteilh-Zoller, M., Fleig, A. and Penner, R. (2007). CRACM1, CRACM2, and CRACM3 are store-operated Ca2+ channels with distinct functional properties. *Curr Biol* **17**, 794–800.

Lishko, P.V., Botchkina, I.L. and Kirichok, Y. (2011). Progesterone activates the principal Ca2+ channel of human sperm. *Nature* **471**, 387-391.

Lishko, P.V., Kirichok, Y., Ren, D., Navarro, B., Chung, J.J. and Clapham, D.E. (2012). The control of male fertility by spermn ion channels. *Annu Rev Physiol* **74**, 453-75.

Liu, X., Wang, W., Singh, B.B., Lockwich, T., Jadlowiec, J., O'Connell, B., Wellner, R., Zhu, M.X. and Ambudkar, I.S. (2000) Trp1, a candidate protein for the store-operated Ca^{2+} influx mechanism in salivary gland cells. *J Biol Chem* **275**, 3403–3411.

Lobley, A., Pierron, V., Reynolds, L., Allen, L. and Michalovich, D. (2003). Identification of human and mouse CatSper3 and CatSper4 genes: characterisation of a common interaction domain and evidence for expression in testis. *Reprod Biol Endocrinol* **1**, *53.*

Luik, R.M., Wang, B., Prakriya, M., Wu, M.M. and Lewis, R.S. (2008). Oligomerization of STIM1 couples ER calcium depletion to CRAC channel activation. *Nature* **454**, 538-542.

Lukanowska, M., Howl, J. and Jones S. (2013). Bioportides: bioactive cell-penetrating peptides that modulate cellular dynamics. *Biotechnol J* **8**, 918-30.

Machado-Oliveira, G., Lefievre, L., Ford, C., Herrero, M.B., Barratt, C., Connolly, T.J., Nash, K., Morales-Garcia, A., Kirkman-Brown, J. and Publicover, S.J. (2008). Mobilisation of Ca2+ stores and flagellar regulation in human sperm by S-nitrosylation: a role for NO synthesised in the female reproductive tract. *Development* **135**, 3677-3686.

Madani, F., Lindberg, S., Langel, U., Futaki, S. and Gräslund, A. (2011). Mechanisms of cellular uptake of cell-penetrating peptides. *J Biophy* **20**, 414729.

Maher, E.R. (2005). Imprinting and assisted reproductive technology. *Human molecular genetics* **14**, 133-138.

Mallilankaraman, K., Doonan, P., Cárdenas, C., Chandramoorthy, H.C., Müller, M., Miller, M., Hoffman, N.E., Gandhirajan, R.K., Molgó, J., Birnbaum, M.J., Rothberg, B.S., Mak, D.O.D., Foskett, J.K. and Madesh, M. (2012). MICU1 Is an Essential Gatekeeper for MCU-Mediated Mitochondrial Ca^{2+} Uptake that Regulates Cell Survival. *Cell* **151**, 630-644.

Marchetti, C., Obert, G., Deffosez, A., Formstecher, P. and Marchetti, P. (2002). Study of mitochondrial membrane potential, reactive oxygen species, DNA fragmentation and cell viability by flow cytometry in human sperm. *Hum Reprod* **17**, 1257-65.

Marquez, B., Ignotz, G. and Suarez, S.S. (2007). Contributions of extracellular and intracellular Ca^{2+} to regulation of sperm motility. Release of intracellular stores can hyperactivate CatSper1 and CatSper2 null sperm. *Dev. Biol* **303**, 214-221.

Marumo, M., Nakano, T., Takeda, Y., Goto, K. and Wakabayashi, I. (2012). Inhibition of thrombin-induced Ca^{2+} influx in platelets by R59949, an inhibitor of diacylglycerol kinase. *J Pharm Pharmacol* **64**, 855-61.

Maruyama, T., Kanaji, T., Nakade, S., Kanno, T. and Mikoshiba, K. (1997). 2APB, 2-aminoethoxydiphenyl borate, a membrane-penetrable modulator of Ins(1,4,5)P3-induced Ca2+ release. *J Biochem* **122**, 498–505.

Maruyama, Y., Ogura, T., Mio, K., Kato, K., Kaneko, T., Kiyonaka, S., Mori, Y. and Sato, C. (2009). Tetrameric Orai1 is a teardrop-shaped molecule with a long, tapered cytoplasmic domain. *J. Biol. Chem* **284**, 13676-85.

Mason, M.J., Mayer, B. and Hymel, L.J. (1993). Inhibition of Ca2+ transport pathways in thymic lymphocytes by econazole, miconazole, and SKF 96365. *Am J Physiol* **264**, 654-62.

Matsumoto, M., Hirose, A. and Ema, M. (2008). Review of testicular toxicity of dinitrophenolic compounds, 2-sec-butyl-4,6-dinitrophenol, 4,6-dinitro-o-cresol and 2,4-dinitrophenol. *Reprod Toxicol* **26**, 185-90.

Mclachan, R.I. (2000). The endocrine control of spermatogenesis. *Ballieres Best Prac Res Clin Endocrinol Metab* **14**, 345-362.

McLaren, A. (2003). Primordial germcells in the mouse. *Dev. Biol* **262**, 1–15.

McLaren, A., Simpson, E., Tomonari, K., Chandler, P. and Hogg, H. (1984). Male sexual differentiation in mice lacking H-Y antigen. *Nature* **312**, 552-555.

McNally, B.A. and Prakriya, M. (2012). Permeation, selectivity and gating in store-operated CRAC channels. *Journal of Physiology* **590**, 4179–4191.

Meikar, O., Da Ros, M., Korhonen, H. and Kotaja, N. (2011). Chromatoid body and small RNAs in male germ cells. *Reproduction* **142**, 195-209.

Meizel, S. and Turner, K.O. (1991). Progesterone acts at the plasma membrane of human sperm. *Mol Cell Endocrinol* **77**, R1-5.

Mercer, J.C., DeHaven, W.I., Smyth, J.T., Wedel, B., Boyles, R.R., Bird, G.S. and Putney, J.W. (2006). Large Store-operated Calcium Selective Currents Due to Co-expression of Orai1 or Orai2 with the Intracellular Calcium Sensor, Stim1. *The Journal of Biological Chemistry* **281**, 24979-24990.

Merritt, J.E., Armstrong, W.P., Benham, C.D., Hallam, T.J., Jacob, R., Jaxa-Chamiec, A., Leigh, B.K., McCarthy, S.A., Moores, K.E. and Rink, T.J. (1990). SK&F 96365, a novel inhibitor of receptor-mediated calcium entry. *Biochem J* **271**, 515-22.

Michelangeli, F., Mezna, M., Tovey, S. and Sayers, L.G. (1995). Pharmacological modulators of the inositol 1,4,5-trisphosphate receptor. *Neuropharmacology* **34**, 1111–1122.

Michelangeli, F., Ogunbayo, O.A. and Wootton, L.L. (2005). A plethora of interacting organellar Ca^{2+} stores. *Curr Opin Cell Biol* **17**, 135–140.

Miki, K., Qu, W., Goulding, E.H., Willis, W.D., Bunch, D.O., Strader, L.F., Perreault, S.D., Eddy, E.M. and O'Brien, D.A. (2004). Glyceraldehyde 3-phosphate dehydrogenase-S, a sperm-specific glycolytic enzyme, is required for sperm motility and male fertility. *Proc Natl Acad Sci U S A* **101**, 16501-6.

Minelli, A., Allegrucci, C., Rosati, R. and Mezzasoma, I. (2000). Molecular and binding characteristics of IP_3 receptors in bovine sperm. *Mol Reprod Dev* **56**, 527–533.

Mitchell, L.A., Nixon, B., Baker, M.A. and Aitken, R.J. (2008). Investigation of the role of SRC in capacitation-associated tyrosine phosphorylation of human sperm. *Mol Hum Reprod* **14**, 235–43.

Monné, M. and Jovine, L. (2011). A structural view of egg coat architecture and function in fertilization. *Biol Reprod* **85**, 661-9.

Morales, P. and Llanos, M. (1996). Interaction of human sperm with the zona pellucida of oocyte: development of the acrosome reaction. *Front Biosci* **1**, 146-60.

Moran, M.M., Xu, H. and Clapham, D.E. (2004). TRP ion channels in the nervous system. *Curr Opin Neurobiol* **14**, 362-9.

Morisawa, M. (1994). Cell signaling mechanisms for sperm motility. *Zoolog Sci* **11**, 647-62.

Mortimer, S.T., Swan, M.A. and Mortimer, D. (1998). Effect of seminal plasma on capacitation and hyperactivation in human sperm. *Hum Reprod* **13**, 2139-46.

Moseley, F.L., Jha, K.N., Björndahl, L., Brewis, I.A., Publicover, S.J., Barratt, C.L. and Lefièvre, L. (2005). Protein tyrosine phosphorylation, hyperactivation and progesterone-

induced acrosome reaction are enhanced in IVF media: an effect that is not associated with an increase in protein kinase A activation. *Mol Hum Reprod* **11**, 523-9.

Moss, S.B. and Gerton, G.L. (2001). A-Kinase anchor proteins in endocrine systems and reproduction. Trends in endocrinology and metabolism **12**, 434-440.

Muik, M., Frischauf, I., Derler, I., Fahrner, M., Bergsmann, J., Eder, P., Schindl, R., Hesch, C., Polzinger, B., Fritsch, R., Kahr, H., Madl, J., Gruber, H., Groschner, K. and Romanin, C. (2008). Dynamic coupling of the putative coiled-coil domain of Orai1 with STIM1 mediates Orai1 channel activation. *J Biol Chem* **283**, 8014-8022.

Muik, M., Schindl, R., Fahrner, M. and Romanin, C. (2012). Ca2+ release-activated Ca2+ (CRAC) current, structure, and function. *Cell Mol Life Sci* **69**, 4163-4176.

Munire, M., Shimizu, Y., Sakata, Y., Minaguchi, R. and Aso, T. (2004). Impaired hyperactivation of human sperm in patients with infertility. *J Med Dent Sci* **51**, 99-104.

Murgia, M., Giorgi, C., Pinton, P. and Rizzuto, R. (2009). Controlling metabolism and cell death: at the heart of mitochondrial calcium signalling. *J Mol Cell Cardiol* **46**, 781-8.

Naaby-Hansen, S., Diekman, A., Shetty, J., Flickinger, C.J., Westbrook, A. and Herr, J.C. (2010). Identification of calcium-binding proteins associated with the human sperm plasma membrane. *Reprod Biol Endocrinol* **15**, 8-6.

Naaby-Hansen, S., Wolkowicz, M.J., Klotz, K., Bush, L.A., Westbrook, V.A., Shibahara, H., Shetty, J., Coonrod, S.A., Reddi, P.P., Shannon, J. et al. (2001). Co-localization of the inositol 1,4,5-trisphosphate receptor and calreticulin in the equatorial segment and in membrane bounded vesicles in the cytoplasmic droplet of human sperm. *Mol Hum Reprod* **10**, 923–933.

Nash, K.L., Lefievre, L., Peralta-Arias, R., Morris, J., Morales-Garcia, A., Connolly, T., Costello, S., Kirkman-Brown, J. and Publicover, S.J. (2010). Techniques for imaging Ca^{2+} signaling in human sperm. *J Vis Exp* **16.**

Navarro-Borelly, L., Somasundaram, A., Yamashita, M., Ren, D., Miller, R.J. and Prakriya M. (2008). STIM1-Orai1 interactions and Orai1 conformational changes revealed by live-cell FRET microscopy. *J. Physiol* **586**, 5383-5401.

Nicholls, D. G. and Crompton, M. (1980). Mitochondrial calcium transport. *FEBS Letters* **111**, 261—268.

Nicholls, D.G., and Ferguson S.J. (2002). Bioenergetics 3, London: Academic Press.

Nomikos, M., Elgmati, K., Theodoridou, M., Calver, B.L., Cumbes, B., Nounesis, G., Swann, K. and Lai, F.A. (2011). Male infertility-linked point mutation disrupts the Ca2+ oscillation-inducing and PIP(2) hydrolysis activity of sperm PLCζ. *Biochem J* **434**, 211-7.

Oatley, J. and Hunt, P.A. (2012). Of mice and (wo)men: purified oogonial stem cells from mouse and human ovaries. *Biol Reprod* **86**, 196.

O'Flaherty, C., de Lamirande, E. and Gagnon, C. (2006). Positive role of reactive oxygen species in mammalian sperm capacitation: triggering and modulation of phosphorylation events. *Free Radic Biol Med* **41**, 528-40.

Ohmuro, J. and Ishijima, S. (2006). Hyperactivation is the mode conversion from constant-curvature beating to constant-frequency beating under a constant rate of microtubule sliding. *Molecular Reproduction and Development* **73**, 1412-1421.

Okunade, G.W., Miller, M.L., Pyne, G.J., Sutliff, R.L., O'Connor, K.T., Neumann, J.C., Andringa, A., Miller, D.A., Prasad, V., Doetschman, T. et al. (2004) Targeted ablation of plasma membrane Ca^{2+}-Atpase (PMCA) 1 and 4 indicates a major housekeeping function for PMCA1 and a critical role in hyperactivated sperm motility and male fertility for PMCA4. *J Biol Chem* **279**, 33742–33750.

Oren-Benaroya, R., Orvieto, R., Gakamsky, A., Pinchasov, M. and Eisenbach, M. (2008). The sperm chemoattractant secreted from human cumulus cells is progesterone. *Hum Reprod* **23**, 2339-45.

O'Toole, C.M.B., Arnoult, C., Darszon, A., Steinhardt, R.A. and Florman, H.M. (2000). Ca^{2+} entry through store-operated channels in mouse sperm is initiated by egg ZP3 and drives the acrosome reaction. *Mol Biol Cell* **11**, 1571–1584.

Pacey, A.A., Hill, C.J., Scudamore, I.W., Warren, M.A., Barratt, C.L.R. and Cooke, I.D. (1995). The interaction in vitro of human sperm with epithelial cells from the human uterine (fallopian) tube. *Hum Reprod* **10**, 360–366.

Palty, R., Hershfinkel, M. and Sekler, I. (2012). Molecular identity and functional properties of the mitochondrial Na+/Ca2+ exchanger. *J Biol Chem* **287**, 31650-7.

Palty, R. and Sekler, I. (2012). The mitochondrial Na(+)/Ca(2+) exchanger. *Cell Calcium* **52**, 9-15**.**

Parekh, A.B., and Putney, J.W. (2005). Store-operated calcium channels. *Physiol Rev* **85**, 757–810.

Parinaud, J., Labal, B. and Vieitez, G. (1992). High progesterone concentrations induce acrosome reaction with a low cytotoxic effect. *Fertil Steril* **58**, 599-602.

Park, C.Y., Hoover, P.J., Mullins, F.M., Bachhawat, P., Covington, E.D., Raunser, S., Walz, T., Garcia, K.C., Dolmetsch, R.E. and Lewis, R.S. (2009). STIM1 clusters and activates CRAC channels via direct binding of a cytosolic domain to Orai1. *Cell* **136**, 876-890.

Park, K.H., Kim, B.J., Kang, J., Nam, T.S., Lim, J.M., Kim, H.T., Park, J.K., Kim, Y.G., Chae, S.W. and Kim, U.H. (2011). Ca2+ signaling tools acquired from prostasomes are required for progesterone-induced sperm motility. *Sci Signal* **4,** 445-450.

Parys, J.B. and De Smedt, H. (2012). Inositol 1,4,5-Trisphosphate and Its Receptors. *Advances in Experimental Medicine and Biology* **740**, 255-279.

Patrat, C., Auer, J., Fauque, P., Leandri, R.L., Jouannet, P. and Serres, C. (2006). Zona pellucida from fertilised human oocytes induces a voltage-dependent calcium influx and the acrosome reaction in sperm, but cannot be penetrated by sperm. *BMC Dev Biol* **6**, 59.

Patrat, C., Serres, C. and Jouannet, P. (2000). The acrosome reaction in human sperm. *Biol Cell* **92**, 255-66.

Patron, M., Raffaello, A., Granatiero, V., Tosatto, A., Merli, G., De Stefani, D., Wright, L., Pallafacchina, G., Terrin, A., Mammucari, C. and Rizzuto, R. (2013). The mitochondrial calcium uniporter (MCU): molecular identity and physiological roles. *J Biol Chem* **288**, 10750-8.

Peeters, M. and Giuliano, F. (2008). Central neurophysiology and dopaminergic control of ejaculation. *Neurosci Biobehav Rev* **32**, 438-53.

Penna, A., Demuro, A., Yeromin, A.V., Zhang, S.L, Safina, O., Parker, I., Cahalan, M.D. (2008). The CRAC channel consists of a tetramer formed by Stim-induced dimerization of Orai dimers. *Nature* **456**, 116-120.

Piasecka, M. and Kawiak, J. (2003). Sperm mitochondria of patients with normal sperm motility and with asthenozoospermia: morphological and functional study. *Folia Histochem Cytobiol* **41**, 125-39.

Piomboni, P., Focarelli, R., Stendardi, A., Ferramosca, A. and Zara, V. (2012). The role of mitochondria in energy production for human sperm motility. *Int J Androl* **35**, 109-24.

Prakriya, M., Feske, S., Gwack, Y., Srikanth, S., Rao, A. and Hogan, P.G. (2006) Orai1 is an essential pore subunit of the CRAC channel. *Nature* **443**, 230-233.

Publicover, S.J., Harper, C.V. and Barratt, C. (2007). $[Ca^{2+}]_i$ signalling in sperm – making the most of what you've got. *Nat Cell Biol* **9**, 235-242.

Putney, J.W. (2011). The Physiological Function of Store-operated Calcium Entry. *Neurochem Res* **36**, 1157-1165.

Quednau, B.D., Nicoll, D.A. and Philipson, K.D. (1997). Tissue specificity and alternative splicing of the Na^+/Ca^{2+} exchanger isoforms NCX1, NCX2, and NCX3 in rat. *Am J Physiol.* **272**, C1250–C1261.

Qi, H., Moran, M.M, Navarro, B., Chong, J.A., Krapivinsky, G., Krapivinsky, L., Kirichok, Y., Ramsey, I.S., Quill, T.A., Clapham, D.E. (2007). All four CatSper ion channels proteins are required for male fertility and sperm cell hyperactivated motility. *Proc Natl Acad U S A* **104**, 1219-1223.

Quill, T.A., Ren, D., Clapham, D.E. and Garbers, D.L. (2001). A voltage-gated ion channel expressed specifically in sperm. *Proc Natl Acad Sci U S A* **23**, 12527–12531.

Quill, T.A., Sugden, S.A., Rossi, K.L., Doolittle, L.K., Hammer, R.E. and Garbers, D.L. (2003). Hyperactivated sperm motility driven by CatSper2 is required for fertilization. *Proc. Natl. Acad. Sci. U.S.A.* **100**, 14869-14874.

Raffaello, A., De Stefani, D. and Rizzuto, R. (2012). The mitochondrial Ca(2+) uniporter. *Cell Calcium* **52**, 16-21.

Rankin, T. and Dean, J. (1996). The molecular genetics of the zona pellucida: mouse mutations and infertility. *Mol Hum Reprod* **2**, 889-94.

Rankin, T., Familari, M., Lee, E., Ginsberg, A., Dwyer, N., Blanchette-Mackie, J., Drago, J., Westphal, H. and Dean, J. (1996). Mice homozygous for an insertional mutation in the Zp3 gene lack a zona pellucida and are infertile. *Development* **122**, 2903-10.

Rankin, T.L., Tong, Z.B., Castle, P.E., Lee, E., Gore-Langton, R., Nelson, L.M. and Dean, J. (1998). Human ZP3 restores fertility in Zp3 null mice without affecting order-specific sperm binding. *Development* **125**, 2415-24.

Rath, D., Schuberth, H.J., Coy, P. and Taylor, U. (2008). Sperm interactions from insemination to fertilization. *Reprod Domest Anim* **43**, 2-11.

Ren, D., Navarro, B., Perez, G., Jackson, A.C., Hsu, S., Shi, Q., Tilly, J.L. and Clapham, D.E. (2001). A sperm ion channel required for sperm motility and male fertility. *Nature* **413**, 603-9.

Rhee, M. and Davis, P. (2006). Mechanism of uptake of C105Y, a novel cell-penetrating peptide. *J Biol Chem* **281**, 1233-40.

Rienzi, L., Balaban, B., Ebner, T. and Mandelbaum, J. (2012). The oocyte. *Hum Reprod.* **27**, 2-21.

Rizzuto, R. and Brini, M. (2004). Calcium Transport in Mitochondria. *Encyclopedia of Biological Chemistry* **2**, 261-266.

Rizzuto, R. and Pozzan, T. (2006). Microdomains of intracellular Ca2+: molecular determinants and functional consequences. *Physiol Rev* **86**, 369-408.

Roberts-Thomson, S.J., Peters, A.A., Grice, D.M. and Monteith, G.R. (2010). ORAI-mediated calcium entry: Mechanism and roles, diseases and pharmacology. *Pharmacology & Therapeutics* **127**, 121-130.

Rockwell, P.L. and Storey, B.T. (2000). Kinetics of onset of mouse sperm acrosome reaction induced by solubilized zona pellucida: fluorimetric determination of loss of pH gradient between acrosomal lumen and medium monitored by dapoxyl (2-aminoethyl) sulfonamide and of intracellular Ca(2+) changes monitored by fluo-3. *Mol Reprod Dev* **55,** 335-349.

Rodriguez-Peña, M.J., Castillo-Bennett, J.V., Soler, O.M., Mayorga, L.S. and Michaut, M.A. (2013). MARCKS protein is phosphorylated and regulates calcium mobilization during human acrosomal exocytosis. *PLoS One* **8**, e64551.

Roldan, E.R. and Shi, Q.X. (2007). Sperm phospholipases and acrosomal exocytosis. *Front Biosci* **1**, 89-104.

Ronquist, G. (2012). Prostasomes are mediators of intercellular communication: from basic research to clinical implications. *J Intern Med* **271,** 400-13.

Ronquist, G., Brody, I., Gottfries, A. and Stegmayr, B. (1978a). An Mg^{2+} and Ca^{2+} stimulated adenosine triphosphate in human prostatic fluid – part I. *Andrologia* **10**, 261–272.

Ronquist, G., Brody, I., Gottfries, A. and Stegmayr, B. (1978b). An Mg^{2+} and Ca^{2+} stimulated adenosine triphosphatase in human prostatic fluid – part II. *Andrologia* **10**, 427–433.

Roos, J., DiGregorio, P.J., Yeromin, A.V., Ohlsen, K., Lioudyno, M., Zhang, S., Safrina, O., Kozak, J.A., Wagner, S.L., Cahalan, M.D., Veliçelebi, G. and Stauderman, K.A. (2005). STIM1, an essential and conserved component of store-operated Ca^{2+} channel function. *J Cell Biol* **169**, 435–445.

Rosado, J.A. and Sage, S.O. (2000). Coupling between inositol 1,4,5-trisphosphate receptors and human transient receptor potential channel 1 when intracellular Ca^{2+} stores are depleted. *Biochem J* **350**, 631–635.

Rossato, M., Di Virgilio F., Rizzuto R., Galeazzi C. and Foresta C. (2001). Intracellular calcium store depletion and acrosome reaction in human sperm: role of calcium and plasma membrane potential. *Mol Hum Repro* **7,** 119-128.

Rossi, A.M., Tovey, S.C., Rahman, T., Prole, D.L. & Taylor, C.W. (2012). Analysis of IP3 receptors in and out of cells. *Biochim Biophys Acta* **1820**, 1214-27.

Russell, L.D., Ettin, R.A., Hitkim, A.P.S. and Clegg, E.D. (1990). Histological pathological evaluation of the testis, Clear water FL: Cache River Press.

Saez, F., Ouvrier, A. and Drevet, J.R. (2011). Epididymis cholesterol homeostasis and sperm fertilizing ability. *Asian J Androl* **13**, 11-7.

Sagare-Patil, V., Galvankar, M., Satiya, M., Bhandari, B., Gupta, S.K. and Modi, D. (2012). Differential concentration and time dependent effects of progesterone on kinase activity, hyperactivation and acrosome reaction in human sperm. *Int J Androl* **35**, 633-44.

Salicioni, A.M., Platt, M.D., Wertheimer, E.V., Arcelay, E., Allaire, A., Sosnik, J. and Visconti, P.E. (2007). Signalling pathways involved in sperm capacitation. *Soc Reprod Fertil* **65**, 245-59.

Salido, G.M., Jardín, I. and Rosado, J.A. (2011). The TRPC ion channels: association with Orai1 and STIM1 proteins and participation in capacitative and non-capacitative calcium entry. *Adv Exp Med Biol* **704**, 413-33.

Salvolini, E., Buldreghini, E., Lucarini, G., Vignini, A., Lenzi, A., Di Primio, R. and Balercia, G. (2011). Involvement of sperm plasma membrane and cytoskeletal proteins in human male infertility. *Ther Deliv* **2**, 71-82.

Sánchez, F. and Smitz, J. (2012). Molecular control of oogenesis. *Biochim Biophys Acta* **1822**, 1896-912.

Sayers, L.G., Brown, G.R., Michell, R.H. and Michelangeli, F. (1993). The effects of thimerosal on calcium uptake and inositol 1,4,5-trisphosphate induced calcium release in cerebellar microsomes. *Biochem. J* **289**, 883-887.

Scarpa, A. and Azzone, G.F. (1970). The mechanism of ion translocation in mitochondria. 4. Coupling of K+ efflux with Ca2+ uptake. *Eur J Biochem* **12**, 328-35.

Schatzmann, H.J. (1966). ATP-dependent Ca++-extrusion from human red cells. *Experientia* **22**, 364-5.

Schindl, R., Bergsmann, J., Frischauf, I., Derler, I., Farner, M., Muik, M., Fritsch, R., Groschner, K. and Romanin, C. (2008). 2-aminoethoxydiphenyl borate alters selectivity of Orai3 channels by increasing their pore size. *J Biol.Chem* **283**, 20261-20267.

Schoff, P.K. (1995). Mitochondrial calcium uptake stimulated by Cibacron blue F3GA in bovine sperm. *Arch Biochem Biophys* **318**, 349–355.

Schuh, K., Cartwright, E.J., Jankevics, E., Bundschu, K., Liebermann, J., Williams, J.C., Armesilla, A.L., Emerson, M., Oceandy, D., Knobeloch, K.P. and Neyses, L. (2004). Plasma membrane Ca^{2+} ATPase 4 is required for sperm motility and male fertility. *J Biol Chem* **279**, 28220–28226.

Scorziello, A., Savoia, C., Secondo, A., Boscia, F., Sisalli, M.J., Esposito, A., Carlucci, A., Molinaro, P., Lignitto, L., Di Renzo, G., Feliciello, A. and Annunziato, L. (2013). New Insights in Mitochondrial Calcium Handling by Sodium/Calcium Exchanger. *Advances in Experimental Medicine and Biology* **961**, 203-209.

Sedo, C.A., Oko, R., Sutovsky, P., Chemes, H. & Rawe, V.Y. (2009). Biogenesis of the sperm head perinuclear theca during human spermiogenesis. *Fertil Steril* **92**, 1472-3.

Serrano, C.J., Trevino, C.L., Felix, R. and Darszon, A. (1999). Voltage-dependent Ca(2+) channel subunit expression and immunolocalization in mouse spermatogenic cells and sperm. *FEBS Lett* **462**, 171–176.

Shabanowitz, R.B. and O'Rand, M.G. (1988). Characterization of the human zona pellucida from fertilized and unfertilized eggs. *J Reprod Fertil* **82**, 151-61.

Shalet, S.M. (2009). Normal testicular function and spermatogenesis. *Pediatric Blood & Cancer* **53**, 285–288.

Shaman, J.A. and Ward, W.S. (2006).Sperm chromatin stability and susceptibility to damage in relation to its structure. The sperm cell. 1st Edition, New York: Cambridge University Press.

Shao, M., Ghosh, A., Cooke, V.G., Naik, U.P. and Martin-DeLeon, P.A. (2008). JAM-A is present in Mammalian Sperm where it is Essential for Normal Motility. *Dev Biol* **313**, 246–255.

Shirakawa, H. and Miyazaki, S. (1999). Spatiotemporal characterization of intracellular Ca2+ rise during the acrosome reaction of mammalian sperm induced by zona pellucida. *Dev Biol* **208**, 70-8.

Shivaji, S., Kumar, V., Mitra, K. and Jha, K.N. (2007). Mammalian sperm capacitation: role of phosphotyrosine proteins. *Soc Reprod Fertil Suppl* **63**, 295-312.

Shukla, K.K., Mahdi, A.A. and Rajender, S. (2001). Ion channels in sperm physiology and male fertility and infertility. *Nature* **413**, 603-9.

Shukla, K.K., Mahdi, A.A. and Rajender, S. (2012). Ion channels in sperm physiology and male fertility and infertility. *J Androl* **33**, 777-88.

Signorelli, J., Diaz, E.S. and Morales, P. (2012). Kinases, phosphatases and proteases during sperm capacitation. *Cell Tissue Res* **349**, 765-82.

Silber, S.J. (1997). The use of epididymal sperm for the treatment of male infertility. *Baillieres Clin Obstet Gynaecol* **1911**, 739-52.

Singh, A., Hildebrand, M.E., Garcia, E. and Snutch, T.P. (2010). The transient receptor potential channel antagonist SKF96365 is a potent blocker of low-voltage-activated T-type calcium channels. *Br J Pharmacol* **160**, 1464-75.

Singh, J.P., Babcock, D.F. and Lardy, H.A. (1978). Increased calcium-ion influx is a component of capacitation of sperm. *Biochem J* **172**, 549-56.

Smith, D.J., Gaffney, E.A., Gadelha, H. and Kirkman-Brown, J.C. (2008). Radical effects of viscosity on sperm motility. *Human Reproduction* **23**, 265-272.

Smyth, J.T., Dehaven W.I., Jones, B.F., Mercer, J.C., Trebak, M., Vazquez, G. and Putney, J.W. (2006). Emerging perspectives in store-operated Ca2+ entry: roles of Orai, Stim and TRP. *Biochim Biophys Acta* **11**, 1147-1160.

Soboloff, J., Spassova, M. and Hewavitharana, T. (2006) STIM2 is an inhibitor of STIM1-mediated store-operated Ca2+ entry. *Curr Biol* **16**, 1465-1470.

Soboloff, J., Rothberg, B.S., Madesh, M. and Gill, D.L. (2012) STIM proteins: dynamic calcium signal trasducers. *Nat. Rev. Mol. Cell Biol* **13**, 549-565.

Sobrero, A.J. and MacLeod, J. (1962). The immediate postcoital test. *Fertil Steril **13**,*184–189.

Sousa, A.P., Amaral, A., Baptista, M., Tavares, R., Caballero, P., Campo. P., Freitas, A., Paiva, A., Almeida-Santos, T. and Ramalho-Santos, J. (2011). Not all sperm are equal: functional mitochondria characterize a subpopulation of human sperm with better fertilization potential. *PLoS One* **6**, e18112.

Stathopulos, P.B., Li, G., Plevin, M.J., Ames, J.B. and Ikura, M. (2006). Stored Ca^{2+} Depletion-induced Oligomerization of Stromal Interaction Molecule 1 (STIM1) via the EF-SAM Region: AN INITIATION MECHANISM FOR CAPACITIVE Ca^{2+}ENTRY. *Journal of Biological Chemistry* **281**, 35855-35862.

Stathopulos, P.B., Zheng, L. and Ikura, M. (2009). Stromal interaction molecule (STIM) 1 and STIM2 calcium sensing regions exhibit distinct unfolding and oligomerization kinetics. *J Biol Chem* **284**, 728-732.

Stathopulos, P.B., Zheng, L. Li, G.Y., Plevin, M.J. and Ikura, M. (2008). Structural and mechanistic insights into STIM1-mediated initiation of store-operated calcium entry. *Cell* **135**, 110-122.

Stauderman, K.A. And Cahalan, M.D. (2006). Genome-wide RNAi screen of Ca(2+) influx identifies genes that regulate Ca(2+) release-activated Ca(2+) channel activity. *Proc Natl Acad Sci U S A* **24**, 9357-9362.

Stetson, I., Izquierdo-Rico, M.J., Moros, C., Chevret, P., Lorenzo, P.L., Ballesta, J., Rebollar, P.G., Gutiérrez-Gallego, R. and Avilés, M. (2012). Rabbit zona pellucida composition: a molecular, proteomic and phylogenetic approach. *J Proteomics* **75**, 5920-35.

Stoop, H., Honecker, F., Cools, M., de Krijger, R., Bokemeyer, C. and Looijenga, L.H. (2005). Differentiation and development of human female germ cells during prenatal gonadogenesis: an immunohistochemical study. *Hum Reprod* **20**,1466-76.

Storey, B.T. and Keyhani, E. (1973). Interaction of calcium ion with the mitochondria of rabbit sperm. *FEBS Lett* **37**, 33-6.

Storey, B.T. and Keyhani, E. (1974). Energy metabolism of sperm: III. Energy-linked uptake of calcium ion by the mitochondria of rabbit epididymal sperm. *Fertil Steril* **25**, 976-84.

Storey, B.T. and Keyhani, F.J. (1975). Energy metabolism of sperm. V. The Embden-Myerhof pathway of glycolysis: activities of pathway enzymes in hypotonically treated rabbit epididymal sperm. *Fertil Steril* **26**, 1257–1265.

Strünker, T., Goodwin, N., Brenker, C., Kashikar, N.D., Weyand, I., Seifert, R. and Kaupp, U.B. (2011). The CatSper channel mediates progesterone-induced Ca2+ influx in human sperm. *Nature* **471,** 382-6.

Su, Y.H. and Vacquier, V.D. (2002). A flagellar K^+-dependent Na^+/Ca^{2+} exchanger keeps Ca^{2+} low in sea urchin sperm. *Proc Natl Acad Sci USA* **99**, 6743–6748.

Suarez, S.S. (2007). Interactions of sperm with the female reproductive tract: inspiration for assisted reproduction. *Reprod Fertil Dev* **19**, 103-10.

Suarez, S.S. (2008). Control of hyperactivation in sperm. *Hum Reprod Update* **14**, 647-57.

Suarez, S.S. and Ho, H.C. (2003). Hyperactivated motility in sperm. *Reprod Domest Anim* **38**, 119-24.

Suarez, S.S. and Pacey, A.A. (2006). Sperm transport in the female reproductive tract. *Hum Reprod Update* **12**, 23-37.

Sutovsky, P. & Manandhar, G. (2006). Mammalian spermatogenesis and sperm structure: anatomical and compartmental analysis. The sperm cell. 1st Edition, New York: Cambridge University Press.

Suzuki, A.Z., Ozaki, S., Goto, J.I. and Mikoshiba, K. (2010). Synthesis of bisboron compounds and their strong inhibitory activity on store-operated calcium entry. *Bioorganic & Medicinal Chemistry Letters* **20**, 1395-1398.

Tajima, Y., Okamura, N. and Sugita, Y. (1987). The activating effects of bicarbonate on sperm motility and respiration at ejaculation. *Biochim Biophys Acta* **924**, 519-29.

Tanaka, Y. and Tashjian A.H. Jr. (1994). Thimerosal potentiates Ca2+ release mediated by both the inositol 1,4,5-trisphosphate and the ryanodine receptors in sea urchin eggs. Implications for mechanistic studies on Ca^{2+} signalling. *J. Biol. Chem* **269**, 11247-11253.

Taylor, C.W., Genazzani, A.A. and Morris, S.A. (1999). Expression of inositol trisphosphate receptors. *Cell Calcium* **26**, 237–251.

Thastrup, O., Cullen, P.J., Drøbak, B.K., Hanley, M.R. and Dawson, A.P. (1990). Thapsigargin, a tumor promoter, discharges intracellular Ca2+ stores by specific inhibition of the endoplasmic reticulum Ca2(+)-ATPase. *Proc Natl Acad Sci U S A* **87**, 2466-70.

Tjioe, S., Bianchi, C. and Haugaard, N. (1970). The function of ATP in Ca2+ uptake by rat brain mitochondria. *Biochim Biophys Acta* **216**, 270-3.

Travis, A.J., Foster, J.A., Rosenbaum, N.A., Visconti, P.E., Gerton, G.L., Kopf, G.S. and Moss, S.B. (1998). Targeting of a germ cell–specific type 1 hexokinase lacking a porin-binding domain to the mitochondria as well as to the head and fibrous sheath of murine sperm. *Mol Biol Cell* **9**, 263–276.

Trevino, C.L., Santi, C.M., Beltran, C., Hernandez-Cruz, A., Darszon, A. and Lomeli, H. (1998). Localisation of inositol trisphosphate and ryanodine receptors during mouse spermatogenesis: possible functional implications. *Zygote* **6**, 159–172.

Toshimori, K. and Ito, C. (2003). Formation and organization of the mammalian sperm head. *Arch Histol Cytol* **66**, 383-396.

Toshimori, K., Tanii, I., Araki, S. and Oura, C. (1992). Characterization of the antigen recognized by a monoclonal antibody MN9: unique transport pathway to the equatorial segment of sperm head during spermiogenesis. *Cell Tissue Res* **270**, 459-468.

Toyoshima, C. (2009). How Ca^{2+}-ATPase pumps ions across the sarcoplasmic reticulum membrane. *Biochim Biophys Acta* **1793**, 941–946.

Trevino, C.L., Felix, R., Castellano, L.E., Gutierrez, C., Rodriguez, D., Pacheco, J., Lopez-Gonzalez, I., Gomora, J.C., Tsutsumi, V., Hernandez-Cruz, A. et al. (2004). Expression and differential cell distribution of low-threshold Ca^{2+} channels in mammalian male germ cells and sperm. *FEBS Lett* **563**, 87–92.

Tulsiani, D.R. and Abou-Haila, A. (2011). Molecular events that regulate mammalian fertilization. *Minerva Ginecol* **63,**103-18.

Turner, R.M. (2003). Tales from the tail: What do we really know about sperm motility? *Journal of Andrology* **24**, 790-803.

Turner, K.O., Garcia, M.A. and Meizel, S. (1994).Progesterone initiation of the human sperm acrosome reaction: the obligatory increase in intracellular calcium is independent of the chloride requirement. *Mol Cell Endocrinol* **101**, 221-5.

Utleg, A.G., Yi, E.C., Xie, T., Shannon, P., White, J.T., Goodlett, D.R., Hood, L. and Lin, B. (2003). Proteomic analysis of human prostasomes. *Prostate* **56**, 150–161.

Vandecaetsbeek, I., Vangheluwe, P., Raeymaekers, L., Wuytack, F. and Vanoevelen, J. (2011). The Ca2+ pumps of the endoplasmic reticulum and Golgi apparatus. *Cold Spring Harb Perspect Biol* **3**, a004184.

Van Petegem, F. (2012). Ryanodine receptors: structure and function. *J Biol Chem* **287**, 31624-32.

Vemuganti, S.A., Bell, T.A., Scarlett, C.O., Parker, C.E., de Villena, F.P. and O'Brien, D.A. (2007). Three male germline-specific aldolase A isozymes are generated by alternative splicing and retrotransposition. *Dev Biol* **309**, 18-31.

Vig, M., Peinelt, C., Beck, A., Koomoa, D.L., Rabah, D., Koblan-Huberson, M., Kraft, S., Turner, H., Fleig, A., Penner, R. and Kinet, J.P. (2006). CRACM1 is a plasma membrane protein essential for store-operated Ca2+ entry. *Science* **312**, 1220-1223.

Vijayaraghavan, S. and Hoskins, D.D. (1990). Changes in the mitochondrial calcium influx and efflux properties are responsible for the decline in sperm calcium during epididymal maturation. *Mol Reprod Dev* **25**, 186–194.

Visconti, P.E. (2009). Understanding the molecular basis of **sperm** capacitation through kinase design. *Proc Natl Acad Sci U S A* **106**, 667-8.

Visconti, P.E., Krapf, D., de la Vega-Beltrán, J.L., Acevedo, J.J. and Darszon, A. (2011). Related citationsIon channels, phosphorylation and mammalian sperm capacitation. *Asian J Androl* **13**, 395-405.

Visconti, P.E., Ning, X., Fornés, M.W., Alvarez, J.G., Stein, P., Connors, S.A. and Kopf, G.S. (1999). Cholesterol efflux-mediated signal transduction in mammalian sperm: cholesterol release signals an increase in protein tyrosine phosphorylation during mouse sperm capacitation. *Dev Biol*. **214**, 429-43.

Vostal, J.G. and Shafer, B. (1996). Thapsigargin-induced calcium influx in the absence of detectable tyrosine phosphorylation in human platelets. *J Biol Chem* **271**, 19524-9.

Walensky, L.D. and Snyder, S.H. (1995). Inositol 1,4,5-trisphosphate receptors selectively localized to the acrosomes of mammalian sperm. *J Cell Biol* **130**, 857–869.

Wang. Y., Deng, X., Zhou, Y., Hendron, E., Mancarella, S., Richie, M.F., Tang, X.D., Baba, Y., Kurosaki, T., Mori, Y. et al. (2009). STIM protein coupling in the activatiob of Orai channels. Proc. *Natl.Acad.Sci. U.S.A.* **106**, 7391-7396.

Wang, Z., Jiang, Y., Lu, L., Huang, R., Hou, Q. and Shi, F. (2007). Molecular mechanisms of cyclic nucleotide-gated ion channel gating. *J Genet Genomics* **34**, 477-85.

Wassarman, P.M., Jovine, L. and Litscher, E.S. (2004). Mouse zona pellucida genes and glycoproteins. *Cytogenet Genome Res* **105**, 228-34.

Wassarman, P.M. and Litscher, E.S. (2008). Mammalian fertilization:the egg's multifunctional zona pellucida. *Int. J. Dev. Biol* **52**, 665 – 676.

Wassarman, P.M. and Litscher, E.S. (2013). Biogenesis of the mouse egg's extracellular coat, the zona pellucida. *Curr Top Dev Biol* **102**, 243-66.

Wennemuth, G., Westenbroek, R.E., Xu, T., Hille, B. and Babcock, D.F. (2000). $Ca_V2.2$ and $Ca_V2.3$ (N- and R-type) Ca^{2+} channels in depolarization-evoked entry of Ca^{2+} into mouse sperm. *J Biol Chem* **275**, 21210–21217.

Wennemuth, G., Babcock, D.F. and Hille, B. (2003). Calcium clearance mechanisms of mouse sperm. *J Gen Physiol* **122**, 115–128.

Weyand, I., Godde, M., Frings, S., Weiner, J., Müller, F., Altenhofen, W., Hatt, H. and Kaupp, U.B. (2004). Cloning and functional expression of a cyclic-nucleotide-gated channel from mammalian sperm. *Nature*. **368**, 859-63.

Williams, K.M. and Ford, W.C. (2003). Effects of Ca-ATPase inhibitors on the intracellular calcium activity and motility of human sperm. *Int J Androl* **26**, 366–375.

Williams, R.T., Manji, S.S., Parker, N.J., Hancock, M.S., Van Stekelenburg, L., Eid, J.P., Senior, P.V., Kazenwadel, J.S., Shandala, T., Saint, R., Smith P.J. and Dziadek, M.A. (2001). Identification and characterisation of the STIM gene family: coding for a novel class of gene proteins. *Biochem J* **357**, 673–685.

Wojcikiewicz, R.J. and Luo, S.G. (1998). Differences among type I, II, and III inositol-1,4,5-trisphosphate receptors in ligand-binding affinity influence the sensitivity of calcium stores to inositol-1,4,5-trisphosphate. *Mol Pharmacol* **53**, 656–662.

Wolf, D.E., Hagopian, S.S. and Ishijima, S. (1986). Changes in sperm plasma membrane lipid diffusibility after hyperactivation during in vitro capacitation in the mouse. *J Cell Biol* **102**, 1372-7.

Wuytack, F., Raemaekers, L. and Missiaen, L. (2002). Molecular physiology of the SERCA and SPCA pumps. *Cell Calcium* **32**, 279-305.

Xie, F., Garcia, M.A., Carlson, A.E., Schuh, S.M., Babcock, D.F., Jaiswal, B.S., Gossen, J.A., Esposito, G., van Duin, M. & Conti, M. (2006). Soluble adenylyl cyclase (sAC) is indispensable for sperm function and fertilization. *Developmental Biology* **296**, 353-362.

Yanagimachi, R. (1970). The movement of golden hamster sperm before and after capacitation. *J Reprod Fertil* **23**, 193-196.

Yeromin, A.V., Zhang, S.L., Jiang, W., Yu, Y., Safrina, O. and Cahalan, M.D. (2006). Molecular identification of the CRAC channel by altered ion selectivity in a mutant of Orai. *Nature* **443**, 226-9.

Yoshida, M. and Yoshida, K. (2011). Sperm chemotaxis and regulation of flagellar movement by Ca2+. *Mol Hum Reprod* **17,** 457-65.

Yuan, J.P., Zeng, W., Dorwart, M.R., Choi, Y.J., Worley, P.F. and Muallem, S. (2009). SOAR and the polybasic STIM1 domains gate and regulate Orai channels. *Nat Cell Biol* **11,** 337-343.

Yuan, J.P., Zeng, W., Huang, G.N., Worley, P.F. and Muallem, S. (2007). STIM1 heteromultimerises TRPC channels to determine their function as store-operated channels. *Nat Cell Biol* **9,** 636-645.

Yunes, R., Michaut, M., Tomes, C. and Mayorga, L.S. (2000). Rab3A triggers the acrosome reaction in permeabilized human sperm. *Biol. Reprod* **62**, 1084–1089.

Zalk, R., Lehnart, S.E. and Marks, A.R. (2007). Modulation of the ryanodine receptor and intracellular calcium. *Annu Rev Biochem* **76**, 367-85.

Zeng, Y., Clark, E.N. and Florman, H.M. (1995). Sperm membrane potential: hyperpolarization during capacitation regulates zona pellucida-dependent acrosomal secretion. *Dev Biol* **171**, 554-63.

Zhang, S.L., Kozak, J.A., Jiang, W., Yeromin, A.V., Chen, J., Yu, Y., Penna, A., Shen, W., Chi, V. and Cahalan, M.D. (2008) Store-dependent and independent modes regulating Ca2+ release-activated Ca2+ channel activity of human Orai1 and Orai3. *J.Biol.Chem* **283**, 17662-17671.

Zhang, S.L., Yu, Y., Roos, J., et al. (2005). STIM1 is a Ca^{2+} sensor that activates CRAC channels and migrates from the Ca^{2+} store to the plasma membrane. *Nature* **437**, 902-905.

Zhang, S.L., Yeromin, A.V., Zhang, X.H., Yu, Y., Safrina, O., Penna, A., Roos, J., Stauderman, K.A. And Cahalan, M.D. (2006). Genome-wide RNAi screen of Ca(2+)

influx identifies genes that regulate Ca(2+) release-activated Ca(2+) channel activity. *Proc Natl Acad Sci U S A* **24**, 9357-9362

Zhao, L., Reim, K. and Miller D.J. (2008). Complexin-1-deficient sperm are subfertile due to a defect in zona pellucida penetration. *Reproduction* **136**, 323-334.

Zhao, Z., Gordan, R., Wen, H., Fefelova, N., Zang, W.J. and Xie, L.H. (2013). Modulation of intracellular calcium waves and triggered activities by mitochondrial ca flux in mouse cardiomyocytes. *PLoS One* **8**, e80574.

Zhou, H., Iwasaki, H., Nakamura, T., Nakamura, K., Maruyama, T., Hamano, S., Ozaki, S., Mizutani, A. and Mikoshiba, K. (2007). 2-Aminoethyl diphenylborinate analogues: Selective inhibition for store-operated Ca^{2+} entry. *Biochemical and Biophysical Research Communications* **352**, 277-282.

Zhu, X., Jiang, M. and Birnbaumer, L. (1998). Receptor-activated Ca2+ influx via human Trp3 stably expressed in human embryonic kidney (HEK)293 cells. Evidence for a non-capacitative Ca2+ entry. *J Biol Chem* **273**, 133-42.

CHAPTER ELEVEN: APPENDIX

11.1Appendix I - List of Suppliers

Alpha Laboratories
40 Parham Drive
Eastleigh
Hampshire
UK

BD Biosciences
Edmund Halley Road
Oxford Science Park
Oxford
UK

Cairn Research Ltd
Graveney Road
Faversham
Kent
UK

Calbiochem
Distributed by Merck Biosciences,
Beeston,
Nottingham,
UK

Corning Inc.
See Starlabs UK Ltd

Enzo Life Sciences
Palatine House
Hatford Court
Exeter
UK

Falcon Products
See Starlabs UK Ltd

Hamilton Thorne, Inc.
100 Cummings Center
Beverly
MA
USA

Institute of Medical Microbiology and Hygiene
Johannes Gutenberg-University
Hochhaus am Augustusplatz
55101 Mainz
Germany

Invitrogen Life Technologies Ltd
3 Fountain Drive
Inchinnan Business Park
Paisley
UK

Fisher Scientific UK Ltd
Bishop Meadow Road
Loughborough
UK

Merck Millipore
Building 6
Croxley Green Business Park
Watford
UK

Nikon Instruments UK
380 Richmond Road
Kingston Upon Thames
Surrey
UK

Patechnia
University of Wolverhampton
Wulfruna Street
Wolverhampton
UK

SAFC Biosciences Inc
Smeeton Road
West Portway
Anderes
Hampshire
UK

Sigma- Aldrich Company Ltd
The Old Brickyard
New Road
Gillingham
Dorset
UK

Scientific Laboratory Supplies
Wilford Industrial Estate
Ruddington Lane
Wilford
Nottingham
UK

Starlabs UK Ltd
4 Tannors Drive
Blakelands
Milton Keynes
UK

Stratech Scientific Limited
Oaks Drive
Newmarket
Suffolk
UK

United States Biological
PO Box 261
Swampscott
MA 01907
USA

Warner Instruments from Harvard Apparatus
Firecroft Way
Edenbridge
Kent
UK

11.2 Appendix II – Media Preparation

Formula for the preparation of experimental media based on supplemented Earle's Balanced Salt Solution

Chemical	Formula	M.W	mM	g/l
Sodium Phosphate Monobasic	NaH_2PO_4	119.98	1.02	0.122
Potassium Chloride	KCl	74.55	5.4	0.4
Magnesium Sulphate Heptahydrate	$MgSO_4.7H_2O$	246.48	0.81	0.2
Glucose	$C_6H_{12}O_6$	180.16	5.5	1.0
Sodium Pyruvate	$C_3H_3NaO_3$	110	2.5	0.3
Sodium Lactate-LD	$C_3H_5NaO_3$.	112.06 in 60% W/W	19.0	4.68
Calcium Chloride	$CaCl_2.2H_2O$	147	1.8	0.265
Sodium Bicarbonate		84.01	52.4	2.2
HEPEs		238.31	15	3.57

sEBSS pH was adjusted to 7.3-7.35 and then NaCl (MW 58.44) was added to achieve osmolarity of 285-295 mOSM, approximately 5g (118.4mM).

Experimental media was sterile filtered into 100ml aliquots before storing at 4^oC until required.

Media was supplemented with 0.3% (w/v) fatty acid free BSA immediately before use.

Formula for the preparation of Calcium (Ca^{2+}) free experimental media based on supplemented Earle's Balanced Salt Solution

Chemical	Formula	M.W	mM	g/l
Sodium Phosphate Monobasic	NaH_2PO_4	119.98	1.02	0.122
Potassium Chloride	KCl	74.55	5.4	0.4
Magnesium Sulphate Heptahydrate	$MgSO_4.7H_2O$	246.48	0.81	0.2
Glucose	$C_6H_{12}O_6$	180.16	5.5	1.0
Sodium Pyruvate	$C_3H_3NaO_3$	110	2.5	0.3
Sodium Lactate-LD	$C_3H_5NaO_3$.	112.06 in 60% W/W	19.0	4.68
Calcium Chloride	$CaCl_2.2H_2O$	147	4.966	0.735
Sodium Bicarbonate	$NaHCO_3$	84.01	26.19	1.1
Sodium Chloride	NaCl	58.44	85	6.92
HEPEs		238.31	15	3.57
EGTA			5.994	2.28

Ca^{2+} free sEBSS pH was adjusted to 7.3-7.35 and then NaCl (MW 58.44) was added to achieve osmolarity of 285-295 mOSM, approximately 5g (118.4mM).

Ca^{2+} free media was sterile filtered into 100ml aliquots before storing at 4^{o}C until required.

All media was supplemented with 0.3% (w/v) fatty acid free BSA immediately before use.

Formula for the preparation of sucrose buffer used in the Streptolysin O Permeabilization process:

Chemical	M.W	mM	g/l
Sucrose	342.3	250	85.58
EGTA	380.35	0.5	0.19
$MgCl_2$	203.31	1.5	0.30
KCl	74.55	50	3.72
HEPES	238.31	20	4.77

Sucrose buffer pH was adjusted to 7 using 1M KOH

Sucrose buffer was sterile filtered into 100ml aliquots before storing at 4^{o}C until required.